GABA, glutamate and beyond: *In vivo* measures and models of neurochemistry and network dynamics in healthy subjects and clinical populations

Alexander D Shaw

Supervisors: K.D. Singh, P.A. Keedwell & S.D. Muthukumaraswamy

A thesis submitted to Cardiff University for the degree of
Doctor of Philosophy

September 2014

Summary & Rationale

Major depressive disorder (MDD) is a chronic, recurrent mood disorder (Kendler, Thornton, & Gardner, 2000; Kumar, Harmer, & Dourish, 2013) with an estimated lifetime prevalence of 16.2% (Kessler *et al*., 2003) which affects more than 350 million people globally (WHO, 2013).

MDD has a complicated and multifarious neuropathology, a result of which is largely ineffective and out-dated pharmacological treatments (Skolnick, 1999). Typical antidepressants are either serotonin re-uptake inhibitors (SRI) or tri-cyclic antidepressants (TCA), both of which target the monoamine system (serotonin and/or dopamine). However, research has suggested a myriad of distinct hypotheses for depression through localisation of functionally distinct neuroanatomical structures, identification of neurotransmitter modulation and receptor subunit alterations as well as genetic, environmental and behavioural observations that could all be targets for antidepressant therapy.

Alterations of the GABAergic and glutamatergic neurotransmitter systems have been reported in major depressive disorder (MDD), both post-mortem *in-vitro* and ante-mortem *in-vivo*. Evidence from magnetic resonance spectroscopy (MRS) studies reported lower bulk concentrations of GABA in currently depressed participants as compared with healthy controls, which may reflect a neurobiological pathology, serve as a biomarker, and guide development of new pharmacological therapies.

If this area of research is to see translation to a clinical setting, the roles of GABA (and glutamate) in depression need to be fully elucidated. Some of the questions that arise are: Do alterations in GABA concentration reflect state or trait markers of depression? Does the GABA deficit observed in depression reflect '*functional'* GABA? Does an existing pharmacological compound with antidepressant efficacy act on the GABA system? This thesis addresses these questions primarily utilizing multimodal neuroimaging techniques, along with computational neuronal modelling and pharmacological manipulation.

Acknowledgements

I would like to thank my supervisory team: Professor Krish Singh, Dr Paul Keedwell and Dr Suresh Muthukumaraswamy, without all 3 of whom my PhD would not have been so interesting.

I thank Dr Paul Keedwell for his copious time and guidance early on, Prof David Linden for initial discussions and Dr C John Evans for his help in MRS pipeline analysis. The help of Prof Krish Singh and Dr Suresh Muthukumaraswamy has been invaluable – from discussions about MEG analysis to dynamic causal modelling, both of which are genuinely fascinating.

Thanks to the MRC Centre for Neuropsychiatric Genetics & Genomics for organising an interesting and intellectually rigorous introductory *rotation year,* and for funding my PhD.

I also thank my colleagues at Cardiff University Brain Research Imaging Centre, and fellow PhD friends for helpful discussions and sharing beers in mutual times of despair. I am particularly thankful to Hannah Robinson for her help and support over the past 2 years.

Publications

A number of experiments in this thesis have been published in the form of a journal article or as an abstract publication of conference proceedings.

Conference proceedings:

GABA, Glutamate & Gamma in Remitted Depression

Shaw A, Muthukumaraswamy S, Singh KD, Keedwell PA

Biological Psychiatry 73 (9), 92S-92S

Society of Biological Psychiatry, San Francisco 2013 (Chapter 3)

Effects of intravenous ketamine on V1 & M1: A pharmaco-MEG & DCM study.

Shaw A, Saxena N, Jackson L, Singh KD, Muthukumaraswamy S

Biological Psychiatry 75 (9S) 1S-426S

Society of Biological Psychiatry, New York 2014 (Chapter 7)

Journal article:

Marked Reductions in Visual Evoked Responses But Not γ-Aminobutyric Acid Concentrations or γ-Band Measures in Remitted Depression

Alexander Shaw, Jennifer Brealy, Heather Richardson, Suresh D. Muthukumaraswamy, Richard A. Edden, C. John Evans, Nicolaas A.J. Puts, Krishna D. Singh, Paul A. Keedwell

Biological Psychiatry, Volume 73, Issue 7, 1 April 2013, Pages 691–698 (Chapter 3)

Submitted:

Ketamine increases gamma frequency oscillations in motor and visual cortices: support for preclinical models of cortical disinhibition and possible relevance to antidepressant mechanism

Alexander Shaw, Neeraj Saxena, Laura Jackson, Krishna D Singh, Judith Hall, Suresh D Muthukumaraswamy

European Neuropsychopharmacology (Chapter 7)

Abbreviations

The following abbreviations and acronyms are utilised throughout the chapters of this thesis.

AMPA	Alpha-amino-3-hydroxy-5-methyl-4-isoxazolepropionic acid
DCM	Dynamic causal modelling
EEAT	Excitatory amino acid transporter
ERD	Event related desynchronisation
ERP / ERF	Event-related potential / field
ERS	Event related synchronisation
GABA	Gamma-aminobutyric acid
GLX	Glutamate + glutamine composite
IGF	Induced gamma frequency
LGN	Lateral geniculate nucleus
MDD	Major depressive disorder
MEG	Magnetoencephalography
MRBD	Movement related beta desynchrony
MRGS	Movement related gamma synchrony
MRS	Magnetic resonance spectroscopy
NMDA	N-methyl-D-aspartate
PIGF	Peak induced gamma frequency
PING	Pyramidal-interneuron gamma
PMBR	Post movement beta rebound
SAM	Synthetic Aperture Magnetometry
VEP / VEF	Visual evoked potential / field

CHAPTER 1. BACKGROUND & LITERATURE 1

1.1 DEPRESSION STATISTICS AND BIOMARKERS 1

1.2 NEUROCHEMICAL HYPOTHESES OF DEPRESSION 2

1.2.1 GABA AND GLUTAMATE RECEPTORS 2

1.2.2 THE GABAERGIC HYPOTHESIS OF DEPRESSION 7

1.2.3 THE GLUTAMATERGIC HYPOTHESIS OF DEPRESSION 13

1.2.4 THE NEUROTROPHIC HYPOTHESIS OF DEPRESSION (THE NMDAR) 15

1.2.5 PROPOSED MECHANISMS OF KETAMINE 16

1.3 VISUALLY EVOKED FIELDS AND INDUCED OSCILLATIONS: BIOGENIC AND THEORETICAL AETIOLOGY 20

1.3.1 RETINOGENICULOSTRIATE PATHWAY & VISUAL CORTEX ANATOMY 21

1.3.2 PRIMARY VISUAL CORTEX HIERARCHICAL MODELS 25

1.3.3 NEUROBIOLOGICAL MECHANISMS OF EVENT RELATED POTENTIAL / FIELD STUDIES 30

1.3.4 NEUROBIOLOGICAL MECHANISMS OF INDUCED, HIGH-FREQUENCY OSCILLATIONS 33

1.4 EVENT-RELATED POTENTIALS, NEUROPHYSIOLOGY AND FUNCTIONAL IMAGING STUDIES IN PSYCHIATRIC DISORDERS. 39

1.4.1 IMAGING BIOMARKERS 39

1.4.2 INTRODUCTION TO EVENT RELATED POTENTIALS 39

1.4.3 EARLY AUDITORY AND VISUAL EVOKED RESPONSES IN PSYCHIATRIC DISORDERS: <100MS 40

1.4.4 LATE EVENT RELATED POTENTIALS IN PSYCHIATRIC DISORDERS: THE P300 43

1.4.5 COMMON ERPS IN DEPRESSION 43

1.4.6 NEUROIMAGING (MRI) & NEUROCHEMICAL IMAGING (PET, MRS) STUDIES OF DEPRESSION 45

1.4.7 NEUROCHEMICAL IMAGING AND TOXICOLOGY (PET, MRS, BLOOD PLASMA) 47

1.5 PREDICTIVE CODING AND NEURONAL MODELLING 52

1.5.1. BIOLOGICAL EVIDENCE AND PLAUSIBILITY OF PREDICTIVE CODING UNDER THE FREE ENERGY PRINCIPAL: CANONICAL MICROCIRCUITS. 54

1.5.2. DYNAMIC CAUSAL MODELLING. 63

1.6 AIMS & HYPOTHESES 65

CHAPTER 2. METHODS 66

2.1 MAGNETOENCEPHALOGRAPHY (MEG) 66

2.1.1 MEG SIGNAL & HARDWARE 66

2.1.2 MEG SIGNAL ANALYSIS 69

2.2 MAGNETIC-RESONANCE IMAGING AND SPECTROSCOPY **74**
2.2.1 MRI SIGNAL & HARDWARE 74
2.2.2 MRS SIGNAL & ANALYSIS 76

CHAPTER 3. VISUALLY EVOKED AND INDUCED OSCILLATORY DYNAMICS AND NEUROCHEMISTRY IN REMITTED DEPRESSION **78**

3.1. ABSTRACT **78**
3.2 BACKGROUND **79**
3.3 EXPERIMENT: PEAK Γ-FREQUENCY AND GABA MEASURES IN REMITTED DEPRESSED SUBJECTS COMPARED WITH HEALTHY CONTROLS **81**
3.3.1 RATIONALE 81
3.3.2 METHODS 81
3.3.3 RESULTS 88
3.3.4 DISCUSSION 92
3.4 EXPERIMENT: MARKED REDUCTIONS IN EARLY VISUAL EVOKED RESPONSE IN REMITTED DEPRESSED SUBJECTS COMPARED WITH HEALTHY, NEVER DEPRESSED CONTROLS. **93**
3.4.1 RATIONALE 93
3.4.2 METHODS 94
3.4.3 RESULTS 94
3.4.4 DISCUSSION 97
3.6 GENERAL DISCUSSION **97**

CHAPTER 4. OSCILLATORY DYNAMICS OF FACE PROCESSING IN REMITTED DEPRESSION **99**

4.1 ABSTRACT **99**
4.2 BACKGROUND **99**
4.3 EXPERIMENT: EXPLICIT AND IMPLICIT EMOTIONAL FACE PROCESSING TASKS. **102**
4.3.1 RATIONALE 102
4.3.2 METHODS 103
4.3.3 RESULTS 106
4.4 RESULTS: INCREASED LEFT INSULA GAMMA POWER IN RESPONSE TO FEARFUL FACES IN FORMERLY DEPRESSED SUBJECTS DURING AN EXPLICIT FACE-PROCESSING TASK **107**
4.5 RESULTS: REDUCED M300 ERF AMPLITUDE IN FORMERLY DEPRESSED SUBJECTS DURING IMPLICIT FACE PROCESSING AS COMPARED WITH HEALTHY, NEVER DEPRESSED CONTROLS **109**

4.6 DISCUSSION **115**

CHAPTER 5. VISUAL OSCILLATORY DYNAMICS AND NEUROCHEMISTRY IN CURRENT EPISODE MDD AND THOSE WITH A FAMILY HISTORY OF MDD **119**

5.1 ABSTRACT **119**

5.2. BACKGROUND **119**

5.3 EXPERIMENT: MEASURES OF VISUAL CORTEX Γ OSCILLATIONS AND GABA ACROSS CURRENT EPISODE, REMITTANCE AND A FAMILY HISTORY OF MAJOR DEPRESSION. **122**

5.3.1 RATIONALE 122

5.4 METHODS **122**

5.5 RESULTS **127**

5.6 DISCUSSION **133**

CHAPTER 6. DYNAMIC CAUSAL MODELLING OF CANONICAL MICRO CIRCUITRY UNDER THE FREE ENERGY PRINCIPAL: PREDICTORS OF IMAGING MEASURES AND INFERENCE ON THE DEPRESSED BRAIN. **137**

6.1 RATIONALE **137**

6.2 BACKGROUND **138**

6.3 METHODS **138**

6.3.1 SUBJECT CHARACTERISTICS 138

6.3.2 DCM & CANONICAL MICROCIRCUIT MODEL 138

6.3.3 MODEL PARAMETER SELECTION PROCEDURE 142

6.4 RESULTS **145**

6.5 DISCUSSION **147**

CHAPTER 7. EFFECT OF A NMDA RECEPTOR ANTAGONIST KETAMINE ON OSCILLATIONS IN PRIMARY VISUAL AND MOTOR CORTICES AND DYNAMIC CAUSAL MODELLING **149**

7.1. ABSTRACT. **149**

7.2 BACKGROUND **149**

7.3 EXPERIMENT: EFFECTS OF SUB-ANAESTHETIC, INTRAVENOUS KETAMINE ON VISUAL AND MOTOR CORTEX RESPONSES **150**

7.3.1 RATIONALE 150

7.3.2 METHODS 150

7.3.2.1 Sample characteristics 153

7.3.2.2 Experimental Procedure, Recordings & Analysis 153
7.3.3 Results 157
7.3.2 Discussion 172
7.4 Experiment: Ketamine affects microcircuit effective connectivity in V1: a DCM pilot study. 175
7.4.1 Rationale 175
7.4.2 Methods 176
7.4.3 Results 177
7.4.4 Discussion 181
7.5 General Discussion 184

CHAPTER 8. GENERAL DISCUSSION 187

8.1 Summary of findings 187
8.2 Interpretation and future research 189
8.2.1 No difference in V1 GABA+ or gamma band responses in remitted depression but markedly reduced pattern-onset M80 amplitude 189
8.2.2 No difference in V1 GABA+, gamma band responses or spectral DCM microcircuit connectivity between currently depressed subjects, formerly depressed subjects, family-history positive healthy subjects and healthy controls 190
8.2.3 Increased gamma band amplitude in the left insula of formerly depressed subjects in response to fearful faces during an explicit emotion recognition face paradigm, and reduced M300 amplitude irrespective of face emotion during implicit emotion recognition task 192
8.2.4 Ketamine significantly increases beta and gamma oscillation amplitudes in primary motor and visual cortices and reduced peak gamma frequency to 100% contrast stimuli. 194
8.3 Research impact 195

REFERENCES 197

APPENDIX 1 225

APPENDIX 2. 243

APPENDIX 3. 248

Chapter 1. Background & Literature

1.1 Depression statistics and biomarkers

Depression is a debilitating and recurring mood disorder, characterised by depressed mood, anhedonia, impaired function of everyday social, occupational and educational tasks, insomnia, fatigue, and a range of other symptoms. Beyond the diagnostic criteria, depression has been shown to be multi-causal in nature. Those who suffer depression are at higher risk of a range of diseases including cancer and diabetes, as well as brain-related conditions such as epilepsy and neurodegenerative disorders, which may also trigger depression. Furthermore, depression is assumed to have a substantial genetic component, due to the high probability of offspring and siblings of sufferers being diagnosed with depression (estimated 40-50% heritability: WHO, 2013).

Producing greater abatement in health than diabetes, asthma or arthritis (Kumar *et al*., 2013), and affecting more than 350 million people worldwide, it is arguably the most inadequately understood widespread disorder. Current estimates of remission rates suggest 1/3 respond to first prescribed medication by 6 weeks, however the World Health Organization estimates that 1 million MDD sufferers die by suicide each year.

Better understanding of the neurobiology of depression will be key to developing better treatments, however research to date has demonstrated that the underlying biology is complex and multifaceted.

The aim of psychiatric neuroimaging, and indeed this thesis, is to utilise brain-imaging techniques to probe the neurochemistry and physiology of disorders in living patients. Using these tools to ask questions about the neuroscience of disorders, based on theories from preclinical models and pharmacology, will allow development of biological markers (that is, measures which aid understanding,

prediction or monitoring of disease) which lead to new hypotheses about the aetiology of disorders (causes) and new therapeutic targets (development of new medications.

1.2 Neurochemical Hypotheses of Depression

Within the neurobiology literature there exist a myriad theories of depression and mood disorder neuro-aetiology. Three of the most pertinent to this thesis are the mutually inclusive GABAergic, glutamatergic and neurotrophic hypotheses of depression. These are outlined below, while an introduction to the techniques, which allow testing of them, follows in the subsequent chapter. Preceding this, GABA and glutamate synthesis, transamination and their major receptor pharmacology are introduced.

1.2.1 GABA and Glutamate Receptors

The human cortex is broadly considered as consisting of local circuit neurons (including pyramidal, stellate and interneurons) and projection neurons (predominantly pyramidal cells). Inhibitory interneurons use the neurotransmitter GABA. Conversely, excitatory interneurons, stellate and pyramidal neurons are excitatory and use the neurotransmitter glutamate (Letinic, Zoncu, & Rakic, 2002).

Across the brain, glutamate and GABA are the most abundant excitatory and inhibitory neurotransmitters, respectively. In specific regions they are known to regulate other neurotransmitters, such as the regulatory effect of GABA on dopamine in limbic structures. GABA is exclusively found in the nervous system and in concentrations 1000 times that of any monoamine transmitter (Croarkin, Levinson, & Daskalakis, 2011).

As well as being an excitatory neurotransmitter, glutamate is also the precursor to GABA. Despite this, the cycles synthesizing and metabolizing GABA and glutamate are complex; due to neurons lacking pyruvate carboxylase, they are incapable of *de novo* synthesis (Bak, Schousboe, & Waagepetersen, 2006).

Instead, GABA is formed from L-glutamate by the enzyme glutamic-acid decarboxylase (GAD). Once GABA is released, both GABAergic neurons and astrocytes clear extrasynaptic GABA via transporters. GABA is destroyed by a transamination reaction, which occurs endogenously by the enzyme GABA-transaminase, which is predominantly found in astrocytes. Transamination produces (via tricarboxylic acid, TCA) succinic semialdehyde and then succinic acid as well as α-Ketoglutarate and then glutamate. Glutamate is further converted to glutamine via glutamine synthetase (GS). (Rang, Dale, Ritter, & Flower, 2003, Bak *et al*., 2006, reaction figure 1.1.1, cycle figure 1.1.2).

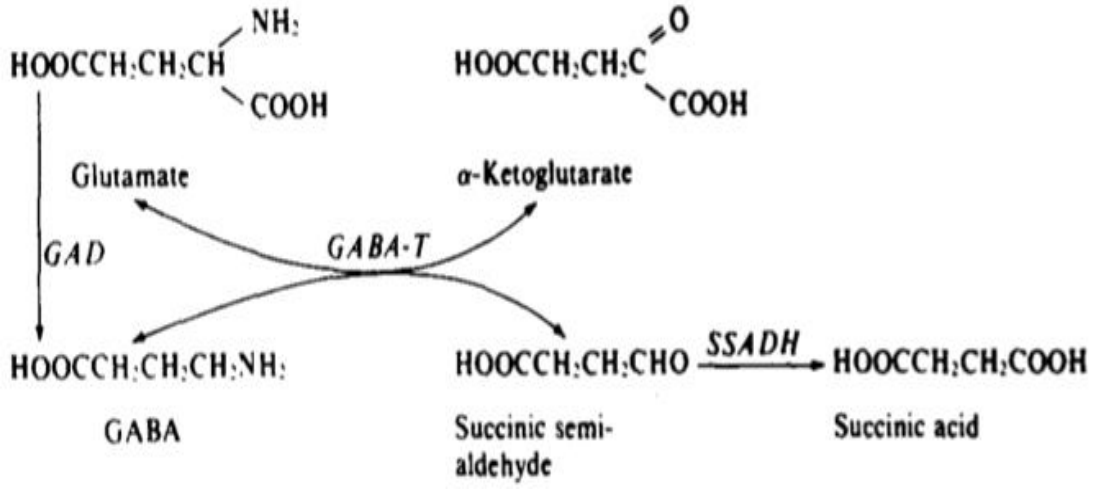

Figure 1.1.1 From Erlander and Tobin (1991). Demonstrating the '*GABA shunt*'. (GAD = glutamatic acid decarboxylase, GABA-T = GABA transaminase, SSADH = succinic semi-aldehyde dehydrogenase).

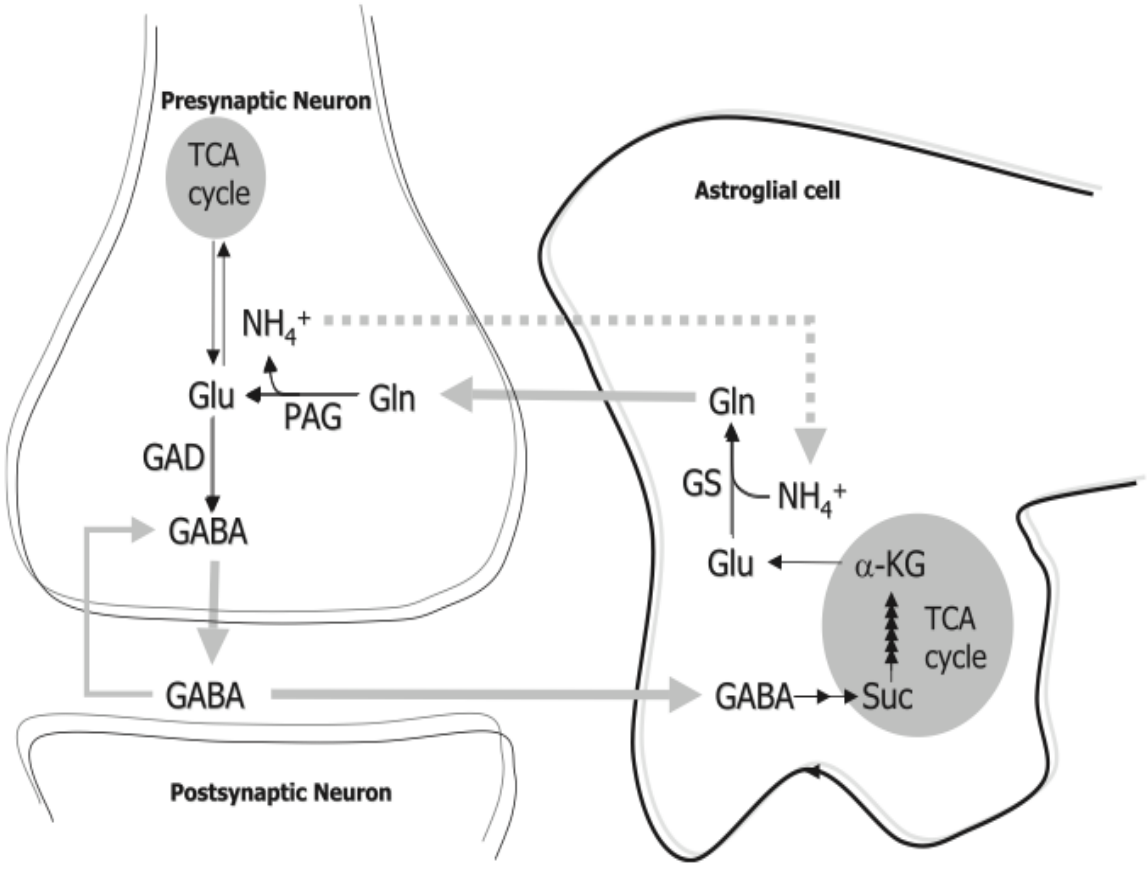

Figure 1.1.2 from Bak (2006). Demonstrating GABA cycle (Suc = succinic acid, TCA cycle = tricarboxylic acid, NH4 = ammonia, α-KG = α-Ketoglutarate to glutamate to glutamine via GS=glutamine synthetase)

Once released, neurotransmitters bind to specific receptors on the postsynaptic neuron. These receptors differ in numerous ways and only the main classes are introduced here. Almost all receptor types fall into the category of metabotropic or ionotropic. Metabotropic receptors are G-protein coupled receptors, which can trigger a range of intracellular mechanisms and are considered slow compared to ionotropic. Ionotropic receptors are ligand-gated ion channels in the cell membrane, which allow particular ions to flow into or out of the cell in order to hyper- or de-polarise the cell. These receptors have fast, direct effects. Table 1 demonstrates the GABAergic and glutamatergic receptor types. Ionotropic receptors comprise permutations of subunits in specific configurations.

Receptor	Shape	Common configuration	Class	Endogenous ligand
$GABA^A$	pentameric	1xα 2xβ 2x γ	Ion	GABA
$GABA^B$	heptahelical		GPC	GABA
AMPA	tetramer	GluA1/Glu2 GluA2/GluA3	Ion	Glutamate
NMDA	tetramer		Ion	Glutamate
Kainate	tetramer		Ion	Glutamate
mGluR 1, 5	--		GPC	Glutamate
mGluR 2, 3	--		GPC	Glutamate
mGluR 4, 6-8	--		GPC	Glutamate

Table 1. Summary of GABAergic and Glutamatergic receptors, including ionotropic and metabotropic receptors.

Neurochemicals can bind at a number of sites on the receptor. For example, at a $GABA_A$ receptor containing the most common subunit composition (1xα 2xβ 2x γ), GABA binds between the α and β subunits (figure 1.1.3). Other chemicals bind at other specific sites, which usually affect the receptor function in some way. The most common of these are agonists, antagonists and allosteric modulators. Agonists bind at the receptor and promote the action of the endogenous (or otherwise) ligand by increasing the permeability of the central pore. Antagonists, through a number of mechanisms reduce the affect of the receptor, and other modulators can have positive or negative functional affects on specific aspects of receptor function. In the context of the $GABA_A$ receptor, benzodiazepines have a binding site between α and γ subunits, but only bind when the subunit comprises a specific configuration of alpha subunits. Their effect is to potentiate the effect of GABA at the $GABA_A$ receptor (Nutt & Malizia, 2001). Interestingly, it is unknown whether the benzodiazepine site has an endogenous ligand (since benzodiazepine drugs do not exist organically within the brain). Some chemicals are more likely to bind to a certain site than others. Once bound, these then are more or less likely to activate the receptor. These functions properties are termed receptor affinity and efficacy (thus antagonists demonstrate 0% efficacy).

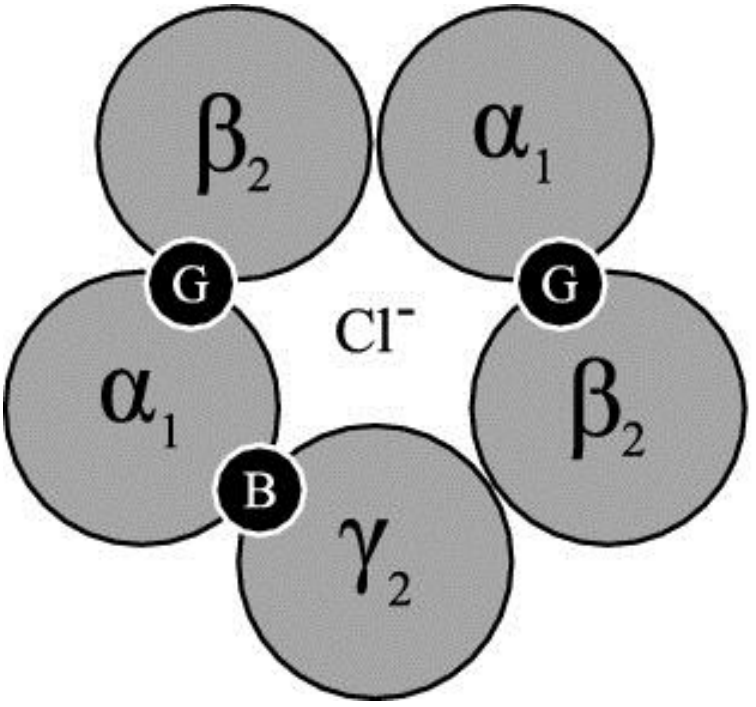

Figure 1.1.3 from Foster (2008). Depicting most common subunit composition of $GABA^A$ receptors (1xα 2xβ 2x γ) with G (GABA) and B (Benzodiazepine) binding sites shown

When binding occurs at GABAergic or glutamatergic receptors, signalling occurs. At inhibitory (e.g. GABAergic) synapses, receptor activation allows the cell to hyperpolarise by permitting chloride flow, which reduces its ability to produce action potentials and produces inhibitory post-synaptic currents (IPSC). Conversely, glutamatergic receptors, depending on subunit composition, are sensitive to calcium, as well as sodium and potassium (AMPA and NMDA) and are voltage dependent (NMDA) (Rang *et al*., 2003).

Depending upon the brain region studied, approximately 20 – 30% (Markram *et al*., 2004) of synapses use fast $GABA_A$ receptors. The balance between excitatory and inhibitory synapses has been shown to be delicate; accession of the GABA system results in amnesia and sedation, while mild debilitation of the GABA system results in anxiety, insomnia and excessive reactivity. This brain-wide, generalised behavioural consequence of altered excitatory-inhibitory balance may have been the starting point for the hypotheses of GABAergic dysfunction in psychiatric disorders such as depression.

Besides the common synaptic $GABA_A$ configurations, an extrasynaptic form has been recently described. Extrasynaptic $GABA_A$ receptors are associated with maintenance of tonic inhibition. Their configurations prominently feature subunits considered rare in synaptic $GABA_A$ receptors; namely the α4, α6 and δ subunits. The pharmacology of these extra-receptors is subsequently unusual in that they do not have a binding site for benzodiazepines (and are insensitive to benzodiazepines) but are sensitive to the experimental sleep drug gaboxadol (THIP), which is thought to bind at the alpha1-beta2 interface and function as a GABA agonist (Belelli *et al*., 2009).

1.2.2 The GABAergic hypothesis of depression

Evidence for a GABAergic deficit in major depression comes from numerous areas of neuroscientific research. Post-mortem studies have revealed that the brains of those who had MDD show reduced size and density of GABAergic interneurons in dorsolateral-prefrontal cortex, compared to those who did not have MDD (Rajkowska *et al*., 2006) and work in animal models demonstrates that chronic stress alters the GABAergic system (Acosta & Rubio, 1994). Neuroimaging and pharmacological studies, however, provide the most compelling evidence of a GABAergic deficit in MDD. These are reviewed extensively before introducing the compatible glutamatergic and neurotrophic hypotheses of depression.

Kalueff and Nutt (2007) reviewed all available evidence of the effects of compounds targeting different aspects of the GABAergic system on depression and anxiety. This demonstrated that gabapentin (a GABA analogue), sodium valproate and vigabatrin (GABA-transaminase inhibitors), tiagabine (presynaptic GABA uptake inhibitor), muscimol (selective $GABA_A$ agonist) and benzodiazepines all reduce depressive symptoms. These findings would suggest both that increasing GABAergic inhibition reduced depressive symptoms, and also that the $GABA_A$ receptor may specifically be involved in depression due to both muscimol and benzodiazepines being $GABA_A$ specific, although this does not rule out any role for $GABA_B$ receptors since it may be that the effect of manipulating $GABA_A$

receptors upon GABA has a knock-on effect on $GABA_B$ receptors via altered availability, or via intracellular processes.

Benzodiazepines were utilised for their antianxiety and antidepressant effects as far back as 1950, nearly 30 years before their binding properties (and thus GABAergic effect) were understood. Subsequently the benzodiazepine receptor complex has been studied extensively, demonstrating subtle difference is the effects of benzodiazepines drugs depending on the subunit composition of the $GABA_A$ receptor. The α1 subunit containing receptor seems to mediate sedative effects, but not anxiolytic. Meanwhile, α2 and α3 subunits mediate anxiolytic effects (Rang *et al*., 2003). Moreover, pharmacologically modulating the benzodiazepine receptor complex (BRC) directly reveals a spectrum of effects. As summarised in figure 1.1.4, agonizing the BRC produces anxiolytic, sedative and anticonvulsant effects in an efficacy-dependence manner as assumed by the effect of full and partial agonism. While antagonists of the BRC have little effect (because antagonizing the BRC simply stops it from potentiating GABA at its binding site, thus having zero efficacy), inverse agonists, defined by agonist-equivalent affinity but negative efficacy, produce anxiogenic, stimulatory and preconvulsive effects in a similar efficacy-dependent manner (i.e. using partial and full inverse agonists) to the agonist.

Research into the functional neuroanatomy of depression has focused largely on brain regions associated with emotion perception and targeting brain structures associated with hallmark features of MDD such as anhedonia. This includes regions such as the dorsolateral/medial prefrontal cortices and the hippocampus which are thought to regulate emotion, while the amygdala, insula, thalamus, orbitofrontal cortex, nucleus accumbens and ventral striatum have also been implicated in aspects of emotion recognition, processing and regulation (Phillips, Drevets, Rauch, & Lane, 2003). Most of these structures are considered part of the limbic system or are within the mesolimbic and mesocortical pathways, which consist of dopamine and serotonin projections. Both serotonin and dopamine have

previously been implicated in MDD; serotonin because of the SSRI class of antidepressant, and dopamine because of its role in reward seeking and hedonic tone, a hallmark of MDD.

While the importance of serotonin and dopamine transmission in MDD is unequivocal, it should be noted that both pathways are interconnected with GABAergic and glutamatergic neurons. It has also been shown that dopamine is inhibited by $GABA_B$ receptors (Bowery *et al*., 1980) and serotonin is inhibited by $GABA_A$, $GABA_B$ and glutamate (Tao & Auerbach, 2000). Figure 1.1.5 demonstrates how dopaminergic projections from the VTA to the NAcc and frontal regions also feature reciprocal GABAergic connections and the VTA receives glutamatergic input from the frontal cortex. Additionally, the aforementioned amygdala, hippocampus, hypothalamus and prefrontal regions have all demonstrated 'rich' GABAergic projections (Croarkin *et al*., 2011).

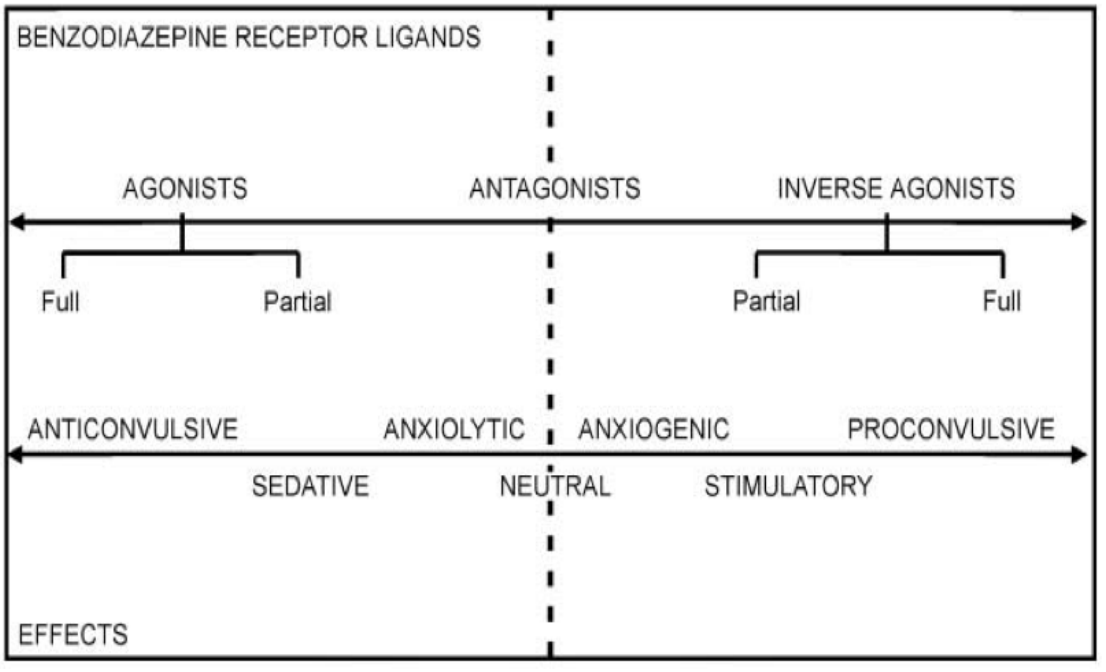

Figure 1.1.4 from Nutt (2001). Demonstrates the spectrum of benzodiazepine efficacy effects.

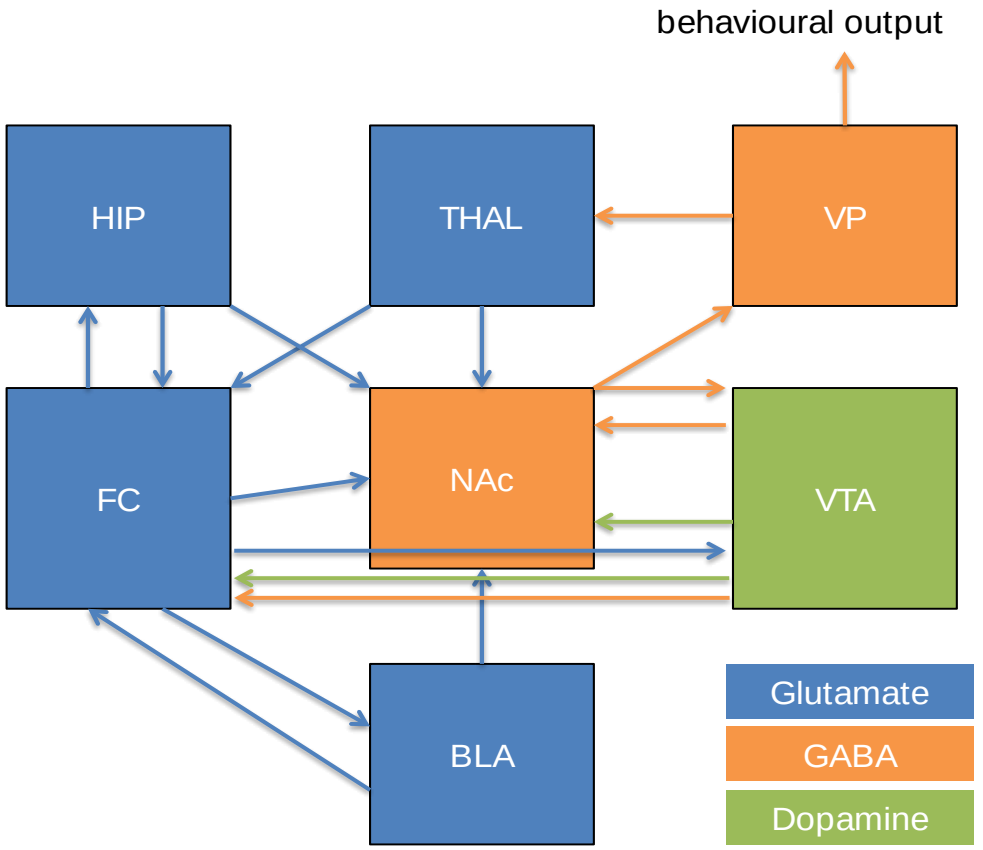

Figure 1.1.5. Adapted from Bailey, C, 2013. (http://www.pa2online.org). HIP, hippocampus; THAL, thalamus; VP, ventral pallidum; FC, frontal cortex; NAc, nucleus accumbens; VTA, ventral tegmental area; BLA, basolateral amygdala.

Neuroimaging studies utilizing nuclear-magnetic resonance spectroscopy (NMR-Spectroscopy or ^{1H}MRS) have demonstrated reduced concentration of GABA in occipital (Sanacora *et al*., 1999) and prefrontal (Hasler *et al*., 2007) cortical regions. Furthermore, this GABA concentration deficit has been shown to normalise with successful SSRI (Sanacora, Mason, Rothman, & Krystal, 2002, Bhagwagar *et al*., 2004), CBT (Sanacora *et al*., 2006) and ECT treatments (Sanacora *et al*., 2003). More recently one group demonstrated that treatment refractory MDD (TRD) subjects demonstrated significantly lower occipital GABA concentration than non-treatment refractory MDD subjects, suggesting that the GABA concentration deficit in MDD could be severity-dependent, or perhaps serve as a marker of treatment resistance. Reports are conflicting as to whether remitted-MDD subjects demonstrate reduced GABA (Hasler *et al*., 2005,

Bhagwagar *et al*., 2007) and therefore whether the observed concentration difference represents a state or trait biomarker.

One study examining GABA in adolescent MDD found that, while adolescents with MDD did indeed show reduced anterior cingulate GABA concentration compared to their psychiatrically healthy counterparts; further stratification revealed that only anhedonic-MDD subjects drove the difference in GABA, whereas non-anhedonic MDD subjects did not differ from controls (Gabbay *et al*., 2012). Although evidence suggests that the GABA concentration reduction in MDD might be brain-wide, the local effects of this deficit will change depending on the region or structures (and their local computations) studied. In this case, the low GABA concentration in the ACC may be driving the anhedonia phenotype via the aforementioned modulatory effects of GABA and inhibitory-excitatory balance on dopamine transmission in reward processing.

One limitation of GABA-MRS is that the technique is not sensitive to the condition of GABA (i.e. whether it is located pre or post-synaptically, in astrocytes, or is extracellular); it is a bulk-measure. Besides in-vivo spectroscopy, plasma-GABA levels have been shown to be reduced in currently depressed subjects (Petty, Kramer, Gullion, & Rush, 1992). This finding supports the idea that GABA is reduced globally in the depressed brain, however plasma concentration is a similarly bulk measure to MRS in that it does not provide any information on functional GABA.

Based on the studies described above, evidence of a GABA deficit, or possible GABAergic dysfunction in MDD is compelling. However an important consideration of any GABAergic deficit in MDD should be the possible mechanisms underlying it. The field of neurogenetics utilises the concept of an intermediate phenotype to elucidate gene functions, for example the mechanism leading from a particular gene to an observed behaviour. It may be that the GABAergic deficit in MDD is an intermediate phenotype between alteration of a set of genes and the symptoms composing MDD.

Using the GABA deficit in MDD as an intermediate phenotype, Choudary *et al* (2005) investigated the molecular mechanisms that may underlie abnormal GABAergic function in the brains of MDD patients who died by suicide. Comparing brains from MDD suicide (n= 9) to non-MDD non-suicide (n= 7) using microarray analysis allowed identification of differentially expressed genes across the cortex. Results demonstrated that a number of genes falling into three distinct categories were dysfunctional in MDD; those which encode glutamate aspartate transporters (excitatory amino-acid transporters, EAATs), glutamate-ammonia ligase (glutamate synthetase) and subunits of ionotropic glutamate and $GABA_A$ receptors. In total four glutamate receptor-related genes were down regulated in anterior cingulate cortex in MDD while two glutamate-receptor genes were up regulated and three down-regulated in DLPFC in MDD. Furthermore, in DLPFC, three $GABA_A$ receptor encoding genes were up-regulated (specifically the $GABA_A$ β3, δ and γ2 subunits) (Choudary, 2005). These results provide a mechanism, which could explain, altered glutamatergic and GABAergic receptor function, which are likely to, in turn, underlie the widely reported GABA concentration deficit of MDD. The exact effect of up-regulating and down-regulating expression of genes encoding receptor subunits (proteins) is not known, beyond that it may alter the receptor function somehow.

Depression is not the only psychiatric disorder in which altered GABAergic activity has been noted. A range of disorders have been reported to demonstrate alterations in GABA (Brambilla, Perez, Barale, Schettini, & Soares, 2003; Petty, 1995), which has led some to propose that GABAergic compounds might be critical to treating a variety of CNS disorders (Whiting 2003). Notably, both anxiety and depression, which demonstrate many overlapping clinical features, have been reported to demonstrate reduced GABA levels, suggesting some neurobiological overlap in these disorders (Kalueff & Nutt, 2007). While this overlap may be important, it should not impede on-going research investigating GABA in either depression or anxiety – much as the clinical overlap between the disorders doesn't preclude a patient from being diagnosed with one of other of the disorders. The

significance of the clinical and GABAergic overlap between anxiety and depression is largely outside the hypotheses of this thesis, however it is an on-going debate among researchers; a review of recent evidence can be found in Mohler (2012) .

1.2.3 The glutamatergic hypothesis of depression

While the evidence for a GABAergic deficit in MDD is compelling, this does not preclude a role for glutamate in MDD. As the brains' major excitatory and inhibitory neurotransmitters, glutamate and GABA have to be, conceptually, balanced, or inversely correlated. In this case, alterations of GABA in MDD will either de-correlate from glutamate or equally alter glutamate, depending upon the mechanism altering GABA. Glutamate is synthesised either from glucose via the Krebs cycle, or from glutamine (see figure 1.2). Glutamate is stored in synaptic vesicles by glutamate transporters and presynaptically released via calcium influx. Glutamate is taken up post-synaptically or cleared extracellularly by glial EAATs. Glutamate is also the immediate precursor to GABA synthesis.

Similarly to GABA, alterations of glutamate concentration have been described in MDD. Increased plasma glutamate has been reported in MDD (Altamura, Maes, Dai, & Meltzer, 1995) and several pharmacological antidepressant therapies target glutamate via ionotropic receptors, notably D-cycloserine and ketamine, both antagonists of the NMDA receptor (the former only in high doses), and lamotrigine, a mood stabiliser which reduces presynaptic glutamate release (Crane, 1959, Zarate *et al*., 2006, Bhagwagar & Goodwin, 2005.

To date, eleven published MR spectroscopy studies quantified glutamate (Glu) or the peak corresponding to glutamate + glutamine, denoted glutamix or Glx (and which additionally includes a small amount of GABA and macro-molecules) in depressed subjects. Somewhat surprisingly, 9 of these studies demonstrated reductions in glutamate, particularly in the ACC and VM/DLPFC (Yüksel & Öngür, 2010) while 2 studies found no difference in glutamate in the ACC, or occipital cortex and one found increased glutamate in occipital cortex (Auer *et al*., 2000, Walter *et al*., 2009, Binesh, Kumar, Hwang, & Mintz, 2004, Sanacora *et al*., 2004,

Pfleiderer *et al*., 2003, Michel *et al*., 2003, Hasler *et al*., 2007, Michael *et al*., 2003, Block *et al*., 2009, Milne, MacQueen, Yucel, Soreni, & Hall, 2009). The voxels tested; along with the number of studies reporting the finding, is depicted in figure 1.1.6.

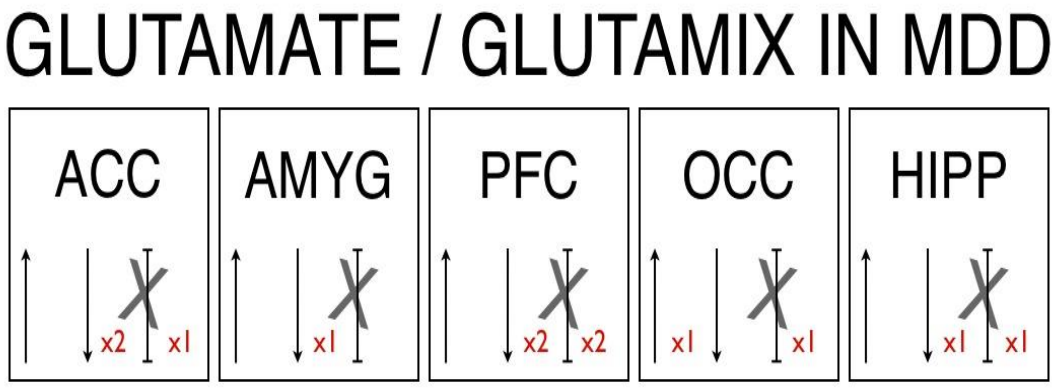

Figure 1.1.6. Summary of MR spectroscopy of glutamate, and glutamate + glutamine, in MDD. Arrow up signifies increased glutamate / Glx in MDD, arrow down signifies decreases and 'X' means studies reported no differences between MDD and controls. Red number illustrates the number of published studies reporting this finding.

An interesting deviation in the trend of reduced glutamate is the reported increase in concentration in occipital cortex. This is the same voxel that most MRS GABA studies have used to demonstrate reduced GABA in MDD, usually chosen because of its good signal-to-noise ratio and generalisable nature (to the whole cortex). No study to date has demonstrated, in MDD, occipital GABA reductions coupled with glutamate increases, despite this being an obvious assumption based on the complementary roles of these neurotransmitters. This may be because, as suggested by the general increase in glutamate concentration in several areas of cortex, both GABA and glutamate are reduced in MDD.

Imaging findings reporting increased glutamate concentration challenge assumptions made based on the actions of glutamate-acting antidepressants. The simplest explanation for this is that antagonism of NMDA receptors (D-cycloserine, ketamine) and inhibiting presynaptic glutamate release (lamotrigine) can both increase global glutamate by decreasing the amount metabolised extracellularly

and post-synaptically (because there is less available to be metabolised) while increasing the (intra+extracellular) concentration via 'storage' (in synaptic vesicles). However ketamine has been shown to increase presynaptic release of glutamate, suggesting that the mechanism is more complex, (Moghaddam, Adams, Verma, & Daly, 1997). This has been suggested to occur as a consequence of disinhibition of GABAergic inputs (Sanacora *et al*., 2008).

The rapid and marked efficacy of ketamine as an antidepressant (Zarate *et al*., 2006), yet its complicated mechanism of action, has led to several novel hypotheses regarding its action, and potential aetiologies of depressive symptoms.

1.2.4 The neurotrophic hypothesis of depression (the NMDAR)

A less comprehensively studied hypothesis, resulting from the finding of ketamine's antidepressant action, is the neurotrophic-synaptogenic mechanism, formalised by Duman (2012) as the 'neurotrophic hypothesis of depression'.

Preclinical studies demonstrated that repeated stress tasks (e.g. forced swim) result in atrophy and decreased density of neurons and glia in the hippocampus and prefrontal cortex, (Duman & Monteggia, 2006, Duman & Li, 2012, Krishnan & Nestler, 2008) which led some researchers to hypothesise that depression is a degenerative (Lang & Borgwardt, 2013) or neurotrophic disorder (Duman & Li, 2012). Subsequent studies revealed that stress exposure decreased levels of brain-derived neurotrophic factor (BDNF) (Duman & Monteggia, 2006), a growth-factor protein found predominantly in the hippocampus and involved in synaptogenesis and differentiation of new neurons. Post-mortem examination of depressed subjects' brains has also demonstrated reduced BDNF, while more recent studies have employed toxicology of blood plasma and serum to assess BNDF blood plasma levels in living subjects. These studies report reductions in serum BDNF in depressed subjects which normalises with successful (chronic) antidepressant therapy (Bocchio-Chiavetto *et al*., 2010, Sen, Duman, & Sanacora, 2008).

It has been suggested that, partially through its NMDAR antagonism, ketamine increases synaptogenesis and neuronal spine density, off-setting the atrophy observed through chronic stress (and depression). This increased synaptogenesis could be a result of increased synaptic plasticity, a mechanism associated with NMDA receptors (Li *et al*., 2010). Most importantly, a study by Haile *et al* (2014) has recently linked the proposed relationship between ketamine and BDNF levels in a randomised control trial of ketamine (with midazolam used as an active placebo) in individuals with treatment resistant depression (n = 22). The study evaluated blood plasma BDNF levels and found that ketamine-responders had increased BDNF plasma levels 240 minutes post infusion. Furthermore, BNDF levels at 240 minutes post infusion correlated negatively with Montgomery-Asberg Depression Rating Scale (MADRS) score. No relationship between BDNF or depression questionnaire score was found in the midazolam group.

1.2.5 Proposed mechanisms of Ketamine

The mechanism of ketamine responsible for its antidepressant action is unknown. It is assumed that the predominant binding affinity is for the N-methyl-D-aspartate (NMDA) ionotropic glutamate receptor, for which endogenous ligands include glutamate, NMDA, glycine and D-serine. However, ketamine is also known to affect the activity of BDNF, a mechanism that has recently received much attention. While an important consideration in the role of ketamine's mechanism of action, the BDNF-related synaptogenic mechanism of ketamine is outside the remit of this experiment.

Numerous studies have demonstrated alterations of cortical inhibition (Brambilla *et al*., 2003; Luscher *et al*., 2010) and excitation (Auer *et al*., 2000; Hasler *et al*., 2007; Luykx *et al*., 2011; Sanacora *et al*., 2008) in major depression. Since cortical inhibition and excitation are functionally directly linked, it has been recently postulated that alterations in cortical excitation-inhibition balance underlie some aspects of the depressive syndrome (Wierońska, Pałucha-Poniewiera, Nowak, & Pilic, 2012).

Although ketamine's primary binding affinity is for the excitatory N-methyl-D-aspartate (NMDA) ionotropic glutamate receptors, where it elicits a direct antagonism, its efficacy as a dissociative anaesthetic suggests that a possible inhibitory GABAergic mechanism of action may additionally be involved in the mediation of its antidepressant effect. Indeed, ketamine has been shown to modulate and directly activate $GABA_A$ receptors; specifically the α6β3δ and α6β2δ subtypes (Hevers *et al*., 2008). Furthermore, early preclinical evidence in mice demonstrated that ketamine (0.8 mmol/kg) significantly increases whole-brain GABA levels via inhibited re-uptake of synaptic GABA by glia and neuronal soma (Wood & Hertz, 1980). Although global GABA may increase following NMDA receptor (NMDAR) blockade (Wood & Hertz, 1980), more recent work has shown that the activity of GABAergic interneurons decreases, whilst pyramidal cell firing increases, resulting in a net effect of excitation caused by disinhibition of pyramidal cells (Homayoun & Moghaddam, 2007).

According to the pyramidal-interneuron gamma (PING) model, the local interaction of superficial pyramidal cells and inhibitory interneuron populations underlie oscillations in the gamma-frequency band (30+ Hz), a theory supported by computational, optogenetic and preclinical studies (Brunel, 2003; Sohal, 2012; Xing, Yeh, Burns, & Shapley, 2012), making assessment of gamma oscillations a useful tool for understanding alterations in cortical excitation-inhibition balance. More specifically, fast oscillations likely reflect reciprocal interactions of fast ionotropic excitatory and inhibitory receptors, such as $GABA_A$ and AMPA (see Buzsaki, 2012, for review). Although AMPA receptors are implicated in PING because of their speed, the slower NMDAR type has also been shown to play a role in gamma rhythm induction (Carlén *et al*., 2011). This may be, in part, due to the fact that AMPA and NMDA receptors are co-localised (Bekkers & Stevens, 1989) and share an endogenous ligand (glutamate). Thus, modulation of the function of one of these receptors will have immediate effects on the function of the other.

Under the PING model, ketamine-induced pyramidal cell disinhibition (Homayoun & Moghaddam, 2007) would result in increased gamma amplitude via increased pyramidal cell excitation while concurrently decreasing peak gamma frequency via altered cortical excitation-inhibition balance.

Consistent with model predictions, Oke and colleagues (2010) demonstrated *in vitro* that APV-induced NMDAR antagonism significantly increased low (20-45 Hz) and high (46-80 Hz) gamma amplitude (by 293 and 295 %, respectively) while significantly reducing the peak frequency of high gamma (mean reduction 13.2 Hz ± 0.6) recorded from rat dorsal neocortex. Similar findings have been reported in rat visual cortex *in vitro*, where a 10 uM dose of ketamine showed a trend towards increasing both layer 3 high (~54 Hz) and layer 5 low (~34 Hz) gamma power, and significantly decreased the frequency of layer 3 gamma (by 22 Hz (18.8 % ± 3.2)) to match that of layer 5 'low' gamma, resulting in cross-layer phase coupling (Anver, Ward, Magony, & Vreugdenhil, 2010). Similar effects of NMDAR hypo-function have been reported *in vivo* when using APV in macaque V1 (Herrero, Gieselmann, Sanayei, & Thiele, 2013) and MK801 in the anterior cingulate cortex (ACC) but not orbital frontal cortex (OFC) of rats (Wood, Kim, & Moghaddam, 2012).

In a further study, Perrine *et al* (2014) utilised 11.7T MRS to assess GABA levels *ex-vivo* in CUS (chronic unpredictable stress) rats before and after ketamine infusion. CUS is a rodent model of depression, which utilises the forced-swim task at unpredictable intervals for 10 days. The day following a 40mg/kg infusion of ketamine, behavioural assessments were administered before euthanizing animals to remove brains for scanning. In keeping with human findings, ketamine significantly reversed stress-induced behaviours while also increasing anterior cingulate cortex GABA levels. Together, these results suggest that, in rodents, NMDA receptor blockade increases cortical excitability via disinhibition of pyramidal cells while also increasing global GABA concentration through inhibited re-uptake by both neurons and glia.

Recent studies investigating neurochemical effects of ketamine in humans have demonstrated that ketamine administration increases glutamate levels in the anterior cingulate cortex, but not GABA levels (administration protocol computed to achieve 150ng/ml^{-1}). The study further reported a correlation between post-ketamine ACC glutamate levels and symptom severity measured by the Positive and Negative Symptom Scale (PANSS). The finding of increased glutamate levels with no increase in GABA supports the aforementioned *pyramidal-disinhibition* hypothesis of ketamine (increased excitation = increased glutamate, inhibited GABAergic interneurons = no increase in GABA) (Stone *et al*., 2012). Another study, published around the same time (Taylor, Tiangga, Ni Mhuircheartaigh, & Cowen, 2011b), reported no increase in Glx (glutamate + glutamine) in the ACC of healthy subjects after an IV infusion of 0.5mg/kg. These seemingly contradictory results could be due to either the difference in dose administered, or the fact that the latter study did not separate glutamate and glutamine in the MRS spectra. In this case, it is possible that glutamine decreased as glutamate increased, resulting in Glx levels not changing (since glutamine is a precursor to glutamate).

Besides the literature described above, there are several other hypotheses of ketamine's action and binding properties in the brain which could explain its antidepressant effects (e.g. Duman & Li, 2012). Of particular relevance is preliminary evidence, which suggests that NMDAR hypofunction-mediated antidepressant effects could be D-serine related, as well as glutamatergic. Postsynaptic NMDA receptors require dual binding – that is, activation of NMDA receptors requires both glutamate and a co-agonist (Lewis, 2012). D-serine, a neuro- and glial-transmitter, shows high affinity for the co-agonist site of NMDARs (reviewed in Wolosker, 2008). Synaptic glutamate evokes D-serine release, which binds as a co-agonist at NMDARs (Malkesman *et al*., 2012). Ketamine has been reported to both 'block' NMDARs and also increase synaptic glutamate (Taylor, Mannie, Norbury, Near, & Cowen, 2011a), and as such the downstream effects on D-serine are unclear. However, in a preclinical study of D-serine as an antidepressant, a single, acute dose (800mg/kg rats, 300mg/kg mice, *i.p.*) of D-serine significantly reversed forced-swim task induced immobility, increased sexual

reward-seeking (female urine sniffing test) and reversed learned-helplessness, suggesting a similar therapeutic profile to ketamine (Malkesman *et al*., 2012). In a similar vein, Kollmar and colleagues (2008) demonstrated in humans that one dose of ketamine (0.5mg/kg, i.v.) followed by daily oral administration of a different NMDAR antagonising drug, memantine (titrated upward form 5mg/day until response observed) prolonged the effects of ketamine. From a clinical perspective this is beneficial because memantine does not elicit the dissociative effects observed with ketamine. Taken together, these studies strongly suggest that NMDA receptors are a key target for antidepressant treatment, and are therefore likely to be the primary therapeutic target of ketamine.

The three neurochemical hypotheses outlined above are not disparate entities; since each has a wealth of research supporting it, it is likely that they are mechanistically linked. GABA and glutamate are linked metabolically as well as in their inhibitory and excitatory functions, respectively. Furthermore, the neurotrophic hypothesis of depression is largely a consequence of the finding that ketamine has antidepressant effects. NMDA receptor antagonism has direct effects on glutamate release and GABA levels (Perrine *et al*., 2014), as well as the aforementioned effects on growth factor proteins such as BDNF.

1.3 Visually evoked fields and induced oscillations: biogenic and theoretical aetiology

Encephalographic recordings have been used extensively in scientific and medical research in the quest to functionally localise experimentally induced behaviours. While neuroscientific literature is rich with experiments linking behaviour and anatomical loci, understanding of the cellular and synaptic properties giving rise to these phenomenon are regularly overlooked. This chapter aims to provide an overview of the neurobiological and physiological mechanisms giving rise to event related and induced cortical responses, particularly in the visual cortex. The imaging modalities utilised to record these measures are introduced in the methods chapter.

While the visual system might not, at first, seem the most suitable area of cortex to study in identifying differences in neural function between psychiatric and healthy groups, it is widely used for such experiments because it is generalisable in its neuronal architecture and function to many other areas of cortex (see *canonical microcircuits*, Douglas & Martin, 1991; Haeusler & Maass, 2007), provides greater signal-to-noise for most imaging techniques than most other areas of cortex and elicits a reliable and stable response to basic sensory stimulation (Adjamian *et al*., 2004) ideal for exploring experimentally or psychiatrically induced changes without the confounds or processing associated with many subcortical and frontal brain regions.

1.3.1 Retinogeniculostriate pathway & visual cortex anatomy

At the posterior portion of the eye, axons of the ganglion cell layer bundle to form the optic nerve. The optic nerve runs to the optic chiasm, where about 60% of the fibres cross the chiasm and form the optic tract. This is the first point in the pathway that fibres from both eyes are co-localised. The majority of fibres in the optic tract terminate in the dorsal lateral geniculate nucleus (LGN) of the thalamus. From the LGN, fibres pass through the optic radiation, terminating in layer 4 (layers 4Ca and 4Cb) of the primary visual cortex (V1, Broadmann's 17, *striate cortex*). From V1 the visual signal is distributed to >30 visual-signal-sensitive extrastriate regions distributed along occipital-parietal and occipital-temporal pathways (Van Essen, Anderson, & Felleman, 1992).

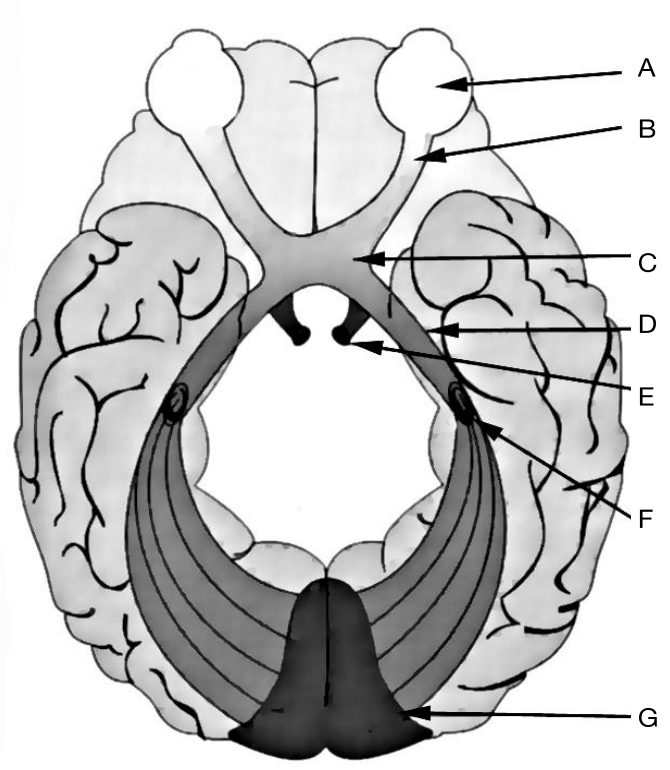

Figure 1.2.1. Retinogeniculostriate pathways from (A) eyes to (B) optic nerve, (C) optic chiasm, (D) optic tract, (E) hypothalamus, pretectum & superior colliculus, (F) dorsal lateral geniculate nucleus, connected via optic radiation to (G) primary visual cortex.

The LGN comprises two ventral *magnocellular* layers (layers 1 & 2) containing large neurons, and several dorsal *parvocellular* layers (layers 4-6), which contain smaller neurons. These layers are sensitive to M- and P-ganglion cells, respectively, which represent different aspects of optic data. M-ganglion cells (M-cells) demonstrate sensitivity to transient visual stimuli whereas P-cells show a slower but sustained response. Furthermore, P-cells are sensitive to differences in light wavelengths and M-cells are not, suggesting that P-cells carry colour information. Damage to the magnocellular layers does not impair visual acuity or colour, but does impair the ability to perceive rapidly changing stimuli; damage to the parvocellular layers does impair colour vision and visual acuity but does not affect motion. These contrasting parvo- and magno-cellular layers follow distinct routes through the optic radiation and terminate in different cortical layers of V1; magnocellular terminating in layer 4Ca and parvocellular in layer 4Cb (Purves, 2008).

The architecture of the visual cortex is predominantly the same as general neocortex in its columnar arrangement and laminar organisation, constituting six cortical layers. The concept of cortical columns stems from observations that specific patterns of neuronal bundling occur throughout cortical regions (e.g. a specific ratio between cells in vertical columns); it was this observation that led to the proposition of cortical microcircuits, discussed in more detail in section 1.5.

A key difference between most cortical laminar and that of visual cortex is the division of layer 4 into 3 subtypes; A, B and C, with C further dividing into C_{alpha} and C_{beta}. Nevertheless, the neuronal architecture of the principal 6 laminar follows that of neocortex. *Deep* pyramidal cells with large apical dendrites occupy layers 6 and 5 (*infragranular layers*), which project both across the cortical layers and also innervate the LGN. Layer 4 (the *granular layer*) constitutes spiny stellate cells and contains the main input layers from LGN. Layers 2 and 3 (*supergranular layers*) comprise *superficial* pyramidal cells, which project to extrastriate cortex (V2, V3, V4, MT) where feature-specific processing occurs. Layer 1 sparsely contains pyramidal cells and GABAergic neurons (Fitzpatrick, Lund, Schmechel, & Towles, 1987), however the density is markedly reduced compared with other layers (figure 1.2.2) and many consider it ‘aneuronal’ (O'Kusky & Colonnier, 1982). Finally, approximately 20% the cortical sheet contains inhibitory interneurons, across layers 2-5, which do not project outside V1. The aforementioned neurons are predominantly excitatory and utilise glutamate via ionotropic receptors for signalling with the exception of inhibitory interneurons, which utilise GABA.

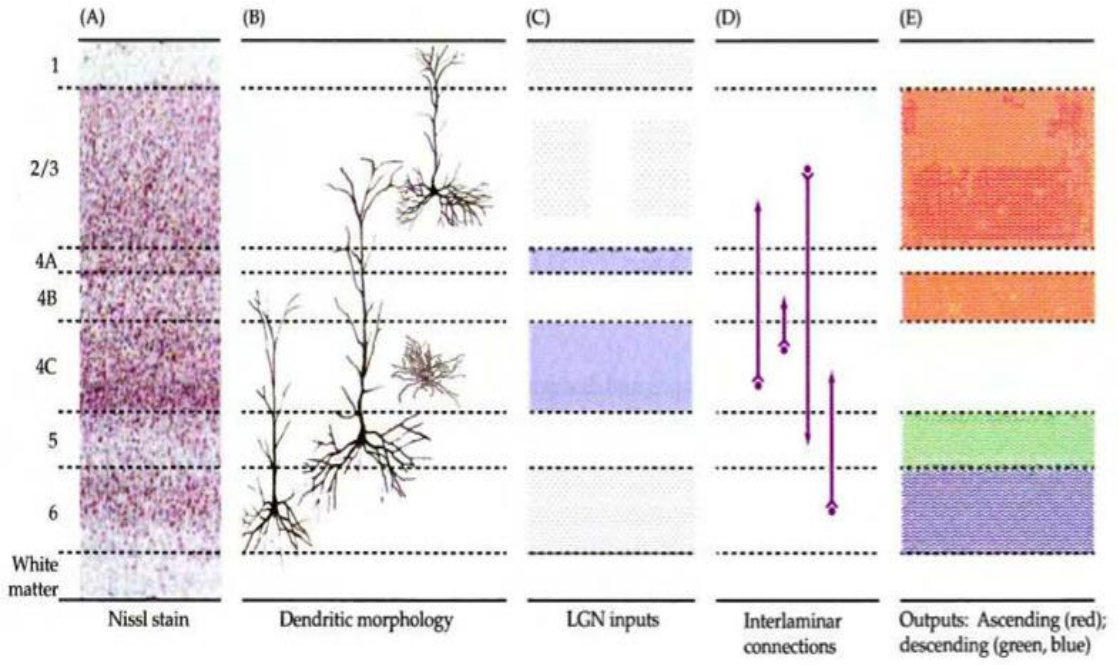

Figure 1.2.2. Purves *et al* 2008. Depicting the 6 layers of visual cortex (a) histologically stained, (b) neuronal constitution excluding inhibitory-interneurons, (c) layers in which LGN inputs terminate, (d) intracortical connections between excitatory neurons, (e) laminar (*output*) connectivity to extrastriate (orange), LGN (blue) and superior colliculus (green).

Eickhoff and colleagues (2007) investigated the laminar distribution and density of 16 receptor types in V1 and extrastriate V2 and V3 in human brain using quantitative receptor autoradiography. Results demonstrated that, averaging across cortical layers, V1 contains a high density of $GABA_A$, $GABA_B$, benzodiazepine (BZ) and NMDA and to a lesser extent, AMPA receptors. Furthermore, they demonstrated that layer-averaged receptor density remains steady across V1, V2 and V3. Layer specific results in V1 demonstrated that significant clustering (possible co-localisation) of receptor types occurs in different layers. Relative to other receptor types, $GABA_A$ and BZ receptor clusters were more prevalent in layers 3, 4a and 4c whereas NMDA, 5-HT2, M3 and M2 receptor clusters were more prevalent in layer 4b. AMPA and $GABA_B$ feature more prevalently in layers 2-4a and less prevalently in layers 4b/c compared with other receptors.

In V2 results demonstrated AMPA and alpha1 clusters showed bi-laminar distributions with the highest concentrations in layers 1, 2, 5 and 6. $GABA_A$ and BZ cluster in layers 3 and 4. $GABA_B$-AMPA clusters observed in V1 are no longer observed and $GABA_B$ show relatively higher expression in layer 3 and lower in layer 5/6. NMDA and D1 (dopamine) also cluster. In V3 $GABA_A$/BZ show the same clustering profile, NMDA/D1 clusters also cluster with $GABA_B$ and show higher concentrations in layer 3 (Eickhoff *et al*., 2007). These results demonstrate that minor variations in receptor clustering occur between V1 and extrastriate regions, however mean receptor prevalences do not change.

	V1		V2		V3	
	Mean	SD	Mean	SD	Mean	SD
5-HT_{1a}	186.3	106.5	260.5	89.6	341.0	126.2
5-HT_2	386.1	165.4	352.4	134.5	331.6	123.9
A1	532.1	403.2	561.3	425.5	552.2	427.1
α1	263.8	43.1	284.0	55.0	298.1	48.7
α2	366.1	128.1	246.2	106.6	219.8	96.5
AMPA	467.9	173.0	412.6	104.1	477.1	133.6
BZ	3630.3	1600.6	3300.3	1528.5	3305.1	1400.8
D1	95.9	25.9	88.3	21.9	84.2	24.6
Nicotinic	51.6	10.5	52.9	12.3	55.8	11.2
$GABA_A$	2618.7	807.3	2193.2	644.5	2192.0	680.3
$GABA_B$	2046.8	525.8	1849.7	401.6	2027.0	238.2
Kainate	272.6	256.5	261.1	232.4	281.7	257.1
M_1	685.3	237.4	547.1	132.2	528.5	98.5
M_2	415.9	56.0	288.3	65.5	235.2	45.7
M_3	447.5	7.9	420.2	6.7	415.4	12.2
NMDA	1361.0	331.5	1207.6	204.8	1172.2	240.0

Figure 1.2.3. From Eickhoff *et al* 2007. Demonstrating concentration of receptor types across V1-3. Highest concentrations are of BZ, $GABA^A$, $GABA^B$ and NMDA receptors.

1.3.2 Primary visual cortex hierarchical models

The neuronal connectivity of the visual system have been relatively well characterised by *in-vivo* rodent and mammal lesion experiments (Van Essen, Newsome, Maunsell, & Bixby, 1986), *in-vitro* human pharmacological studies (Eickhoff *et al*., 2007) and *in-vivo* human functional mapping (Warnking, 2002).

Several studies have proposed hierarchical models of V1 based on the neuronal architecture. Models centre on concept of feedforward, lateral and feedback connections (figures 1.2.2 and 1.2.5). Feedforward connections originate in supragranular layers and terminate in granular layers of another area. Feedback connections originate in infragranular layers and terminate in supra- or infra-granular layers of another area. Lateral connections connect to their own layer and can connect layers from different columns or areas.

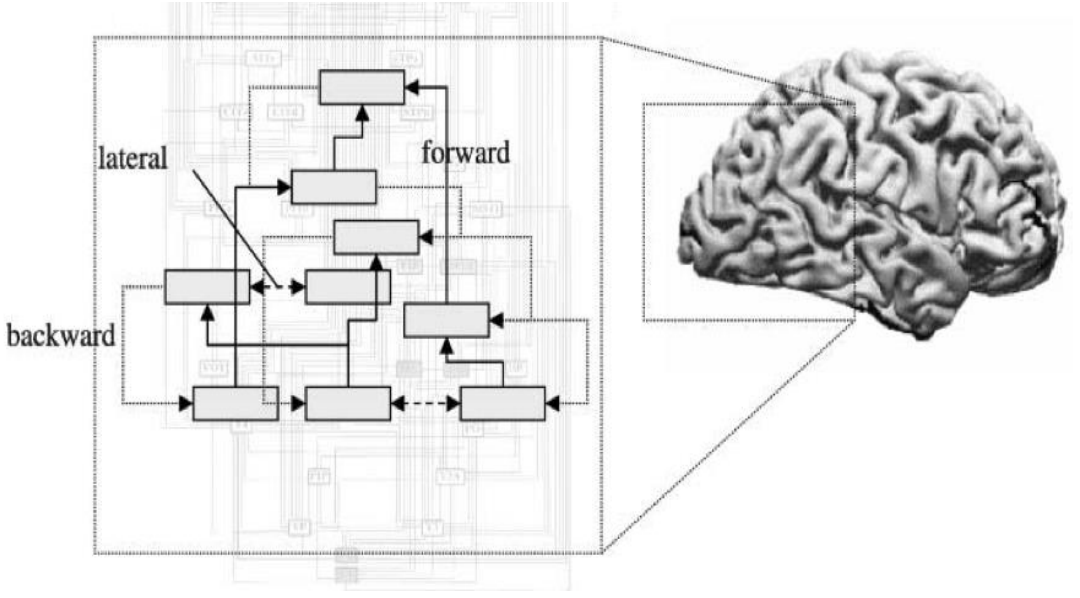

Figure 1.2.4. Friston 2005. Schematic of feedforward, lateral and feedback connections. Feedforward and feedback usually connect different areas or cortical columns. Lateral connections stay within layer.

Coupling the concept of laminar-directional connections with the aforementioned neuronal architecture of the visual cortex suggests that feedforward and feedback connections are excitatory pyramidal neuron projections, while lateral connections are likely to be inhibitory interneurons, however this distinction is not clear. Feedforward connections are considered 'driving' and response eliciting, while feedback connections are 'modulatory'. Furthermore, feedforward projections utilise the fast ionotropic AMPA and $GABA_A$ receptors while modulatory feedback connections utilise the slower voltage-gated NMDA receptors (Friston, 2005).

The primary visual cortex (V1) receives feedforward projections predominantly (Markov *et al*., 2011) from the LGN as well as, to a lesser extent, the pulvinar and other regions (Adams, Hof, Gattass, Webster, & Ungerleider, 2000). There also exist feedback connections from V1 to LGN, pulvinar and other areas, suggesting these areas are reciprocally connected (Graham, 1982). Moving along the visual pathway, V1 exhibits feedforward projections onto extrastriate areas (V2,3,4,5/MT) and receives direct feedback connections from these areas (Barone, Batardiere, Knoblauch, & Kennedy, 2000). Figures 1.2.5 ad 1.2.6 illustrate the connections of the model as described by Friston (2005), with the neuronal types described by Purves (2008).

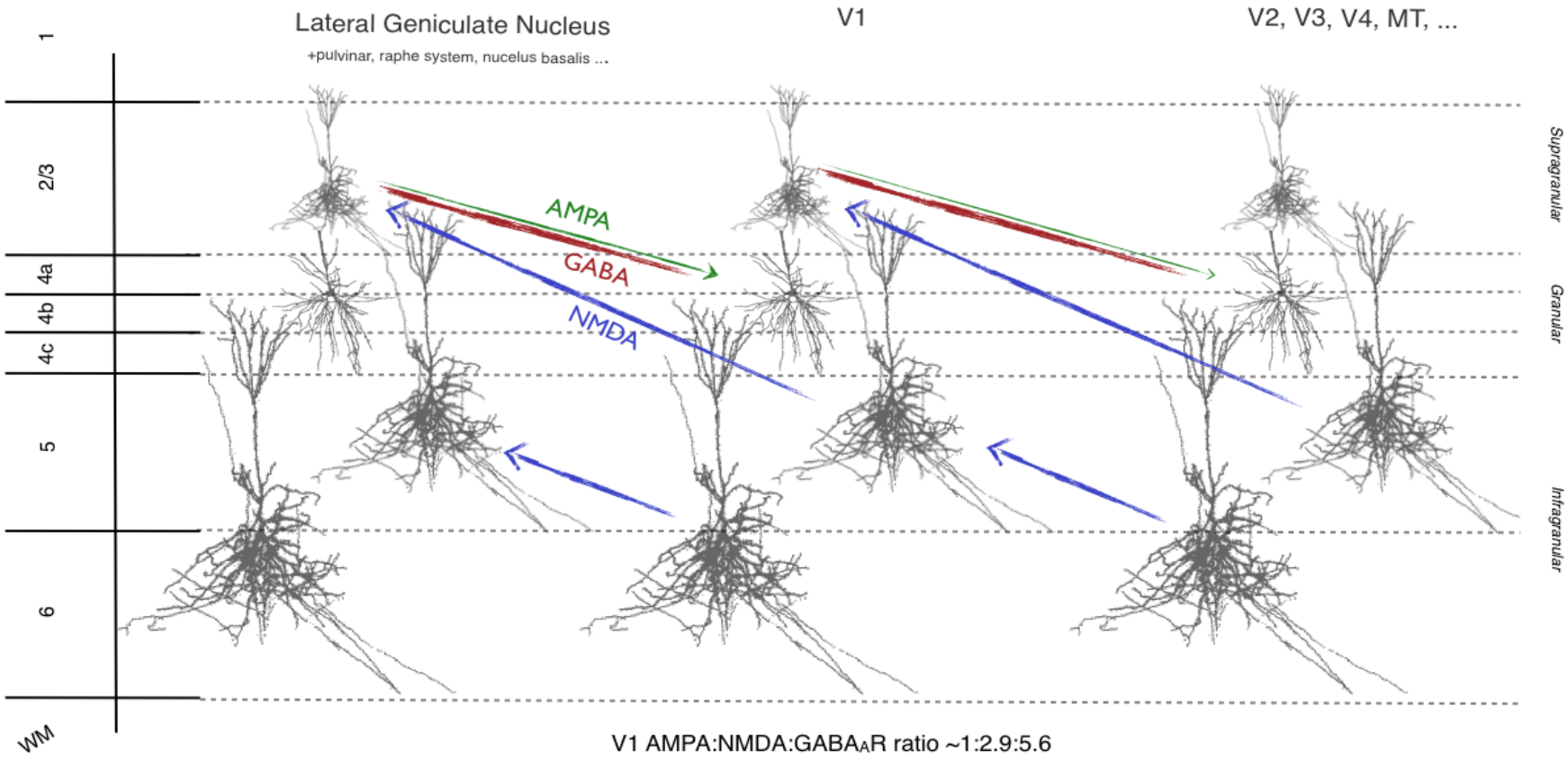

Figure 1.2.5. Illustration of extrinsic forward (arrows pointing down) and backward (arrows pointing up) interlaminar connections between LGN, V1 and extrastriate cortical regions. Green, red and blue lines depict receptor type while line width represents the concentration of receptors in this region. This depiction does not feature intrinsic (interlayer, intracolumn) inhibitory interneurons, which may be a more accurate location of the high $GABA_A$ receptor concentration, rather than on pyramidal cells.

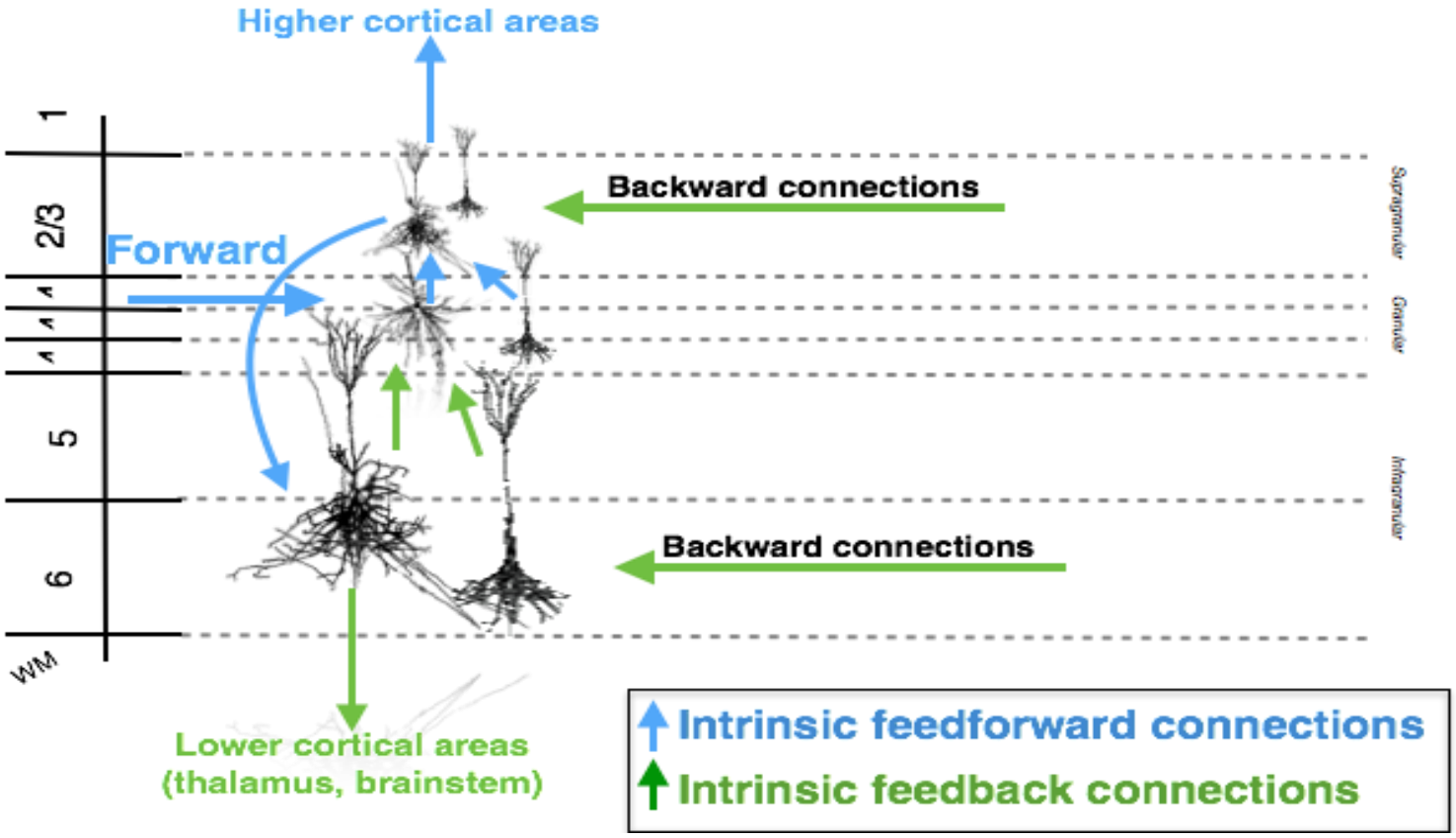

Figure 1.2.6. Demonstrating both intrinsic and extrinsic connections. Amended from Bastos (2012).

1.3.3 Neurobiological mechanisms of Event Related Potential / Field studies

As reviewed in section 1.2, scalp recordings of event related potentials using EEG, or event related fields using MEG, give insight into the function of distinct brain regions in a temporally precise manner. These techniques can be used to test hypotheses about particular cognitive processes or pathologies by presenting specific stimuli or tasks to a subject. The signal measured contains detailed information about neurobiological processes.

The majority of the signal detected by MEG and EEG is made up of the apical dendrites of pyramidal cells in layers 2/3, 5 and 6. This is because, as illustrated in figure 1.2.7, the multiple excitatory postsynaptic potentials sum and, from a distance, resemble a single dipole (Niedermeyer & da Silva, 2005). Furthermore, pyramidal cells parallel (but proximal) apical dendrites sum to magnify this, resulting in a detectable dipole, which can be detected outside the scalp.

The excitatory postsynaptic currents in pyramidal cell dendrites of the primary visual cortex are under the influence of the neurons with which these cells synapse; namely feedforward and feedback projections to LGN and extrastriate regions. Event related scalp recordings are phase-locked to stimulus onset, which in primary sensory areas, such as V1, suggests input to the area. As described previously, this occurs via excitatory feedforward connections from the LGN, in turn suggesting that event related field recordings from V1 are a summation of the excitatory input from the LGN through pyramidal cell connections from superficial layers of LGN to layer 4 of V1. Furthermore, this EPSP is AMPA and $GABA_A$ (Friston, 2005) mediated and is more likely to be magnocellular than parvocellular due to the tendency for magnocellular cells to respond to transient stimuli (Purves, 2008). This model of VEP/VEF generation is supported by results from animal studies.

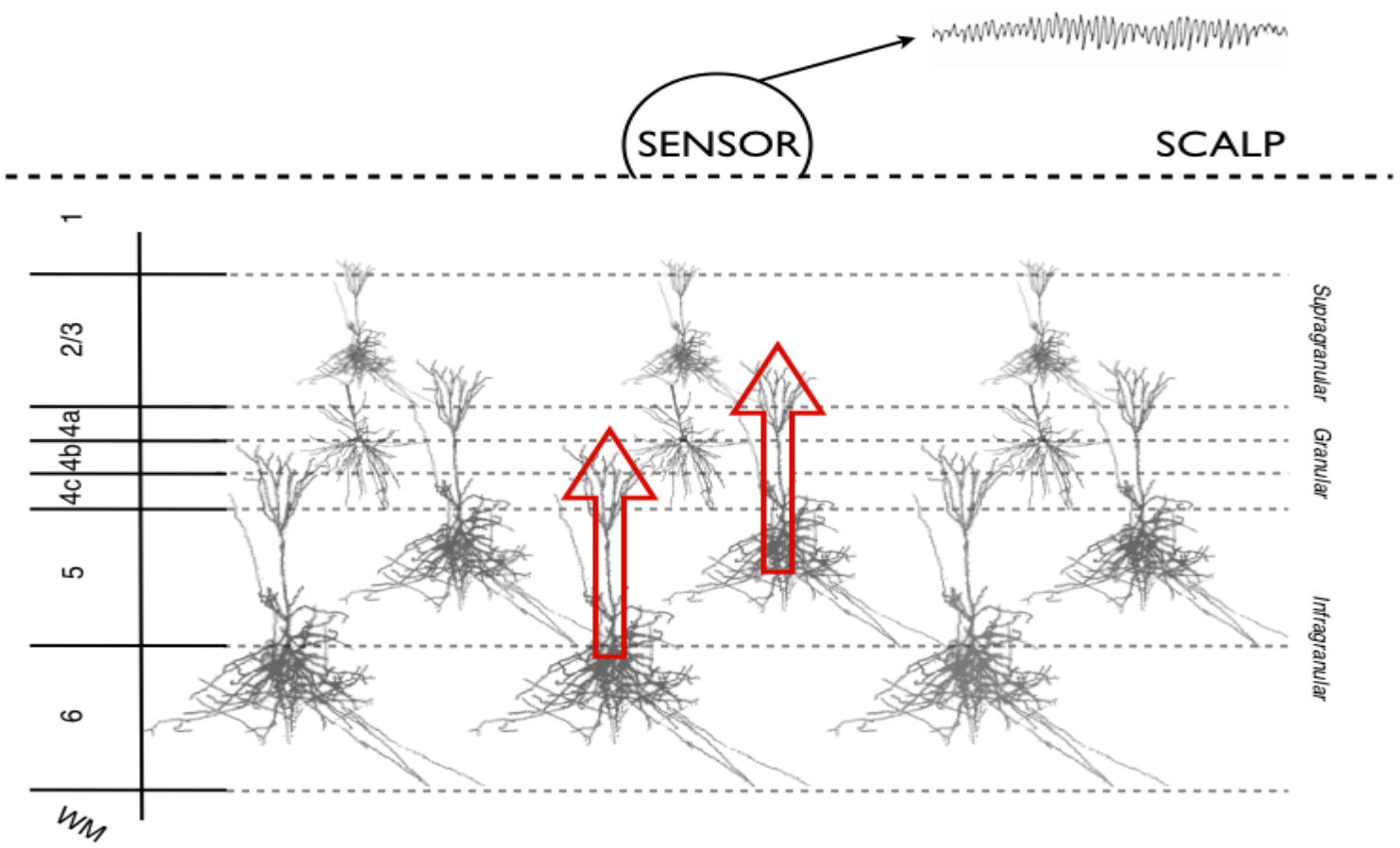

Figure 1.2.7. Laminar specific neuronal architecture. Red arrows illustrate the multiple parallel pyramidal cells apical dendrites carrying postsynaptic potentials, giving rise to a summed dipole detectable at the surface.

Lee *et al* (2012) demonstrated that parvalbumin-containing GABAergic interneurons (PV+) have a role in shaping visually evoked firing rates utilising an optogenetic approach. The light-activated channel rhodopsin ChR2 was expressed in PV+ interneurons, permitting activation of these neurons *in vivo*. Mice viewed a sinusoidal grating while PV+ interneurons were optogenetically driven. Multi-layer V1 spiking was recorded demonstrating that PV+ interneuron activation reduced visually evoked firing rate (Lee *et al*., 2012). While visually evoked firing rate does not translate to ERF *per se*, in the context of visually evoked firing in V1 in response to a grating stimulus, the ERF is likely driven by the same substrate as the EPSC (i.e. AMPAR mediated currents via pyramidal projections from LGN to V1).

One study (Muhammad, 2009) explored the pattern-onset visually evoked response using current source density measures (current sink-peak measurements) across layers of visual cortex while mice viewed a visual grating pattern. Pattern-onset evoked three current sink-peaks; first in layer 4 at 62ms followed by layers 2/3 at 70ms and 5/6 at 81ms. These results likely reflect input from LGN to V1 and subsequent distribution across the cortical layers. Application of a drug combination consisting muscimol and SCH50911 ($GABA_A$ agonist and $GABA_B$ antagonist, respectively) eliminated the later 81ms sink-peak in layers 5/6. This study suggests that elevating $GABA_A$ receptor activity in V1 reduces the visually evoked EPSC to the point that a current sink-peak does not appear. Reduced EPSC in layers 5/6 would result in reduced MEG/EEG ERF amplitude (since EPSCs in pyramidal cells contribute largely to the MEG/EEG signal).

Visually evoked cortical responses in V1 might therefore be considered as the summations of AMPA mediated feedforward EPSCs in layer 2/3 and 5/6 pyramidal cells, but which are under the inhibitory control of $GABA_A$ receptors. Alterations of these cortical responses under pathological (or otherwise) conditions may suggest alteration of one of the aspects discussed here (e.g. AMPA or $GABA_A$ receptor function).

1.3.4 Neurobiological mechanisms of Induced, High-Frequency Oscillations

Induced responses differ from evoked responses in that they are not phase-locked to the stimulus. As a result of this, they often index more sustained neuronal activity. Time-frequency analysis of induced responses permits the signal power to be broken down into frequency bands. This section focuses on high frequency responses.

High-frequency (γ-frequency band, >30Hz) induced oscillatory responses are elicited by a number of stimuli and behavioural tasks, which has resulted in numerous hypotheses regarding their nature including multisensory integration, facilitating working memory (Wang, 2010) and as a mechanism to attention selection (Lakatos, Karmos, Mehta, Ulbert, & Schroeder, 2008). Oscillations are assumed to reference neuronal synchronisation in local and distributed networks (figure 1.2.7) with γ-frequency oscillations proposed as a mechanism for synchronising neuronal assemblies into functional circuits for local computations (Singer, 1999, Spencer, 2009).

Despite the dispute around their function, γ-frequency oscillations (γ-oscillations) have been relatively extensively studied by comparison to ERPs in terms of their biological conception (Mazaheri & Van Diepen, 2014; Whittington, Traub, Kopell, Ermentrout, & Buhl, 2000). γ-oscillations appear throughout the cortex, thus the striate cortical laminar architecture described previously (assumed to be cortex-general) must contain a mechanism for generating high frequency oscillations.

γ-oscillations are thought to arise from an interaction of pyramidal cells and fast-spiking PV+ inhibitory interneurons (Traub *et al*., 1998; Whittington *et al*., 2000; Whittington, Traub, & Jefferys, 1995). In the cortex these neuronal types are reciprocally connected and utilise AMPA and $GABA_A$ receptors because these ionotropic receptors feature time constants fast enough to permit a fast-oscillation.

Modelling studies of reciprocally connected pyramidal neurons have demonstrated that, when adding an external high-frequency excitatory drive to their simulated

network, a sustained oscillation could not establish and firing remained aberrant. However, adding inhibitory interneurons, so that pyramidal neurons and interneurons synapse in an all-to-all fashion (ratio of 4 pyramidal neurons to 1 PV+ interneuron), a sustained oscillation emerges at γ-frequency (Brunel, 2003). Within the physiology nomenclature this network is designated PING (pyramidal-interneuron network gamma). The network parameters constitute 20% connection probability and modelled time constants (latency, rise time and decay time).

The frequency of the PING model is dependent on the ratio of the timescales of the excitatory postsynaptic potentials to inhibitory postsynaptic potentials. In addition, Brunel and Wang's model demonstrates that oscillation frequency reduces with the recurrent excitatory: inhibitory (AMPA: GABA) balance when this is manipulated via pyramidal cells. This decrease is unaffected by the frequency of the external excitatory drive (Brunel, 2003).

A modelling study of PING generators by Wang *et al* revealed that pyramidal cell postsynaptic potentials (PSPs) are phase-locked to the local field gamma rhythm. These phase-locked PSPs reverse polarity close to the equilibrium potential of Cl-, suggestive of a role for $GABA_A$ receptor mediated inhibition in γ-frequency oscillations (Wang & Buzsáki, 1996).

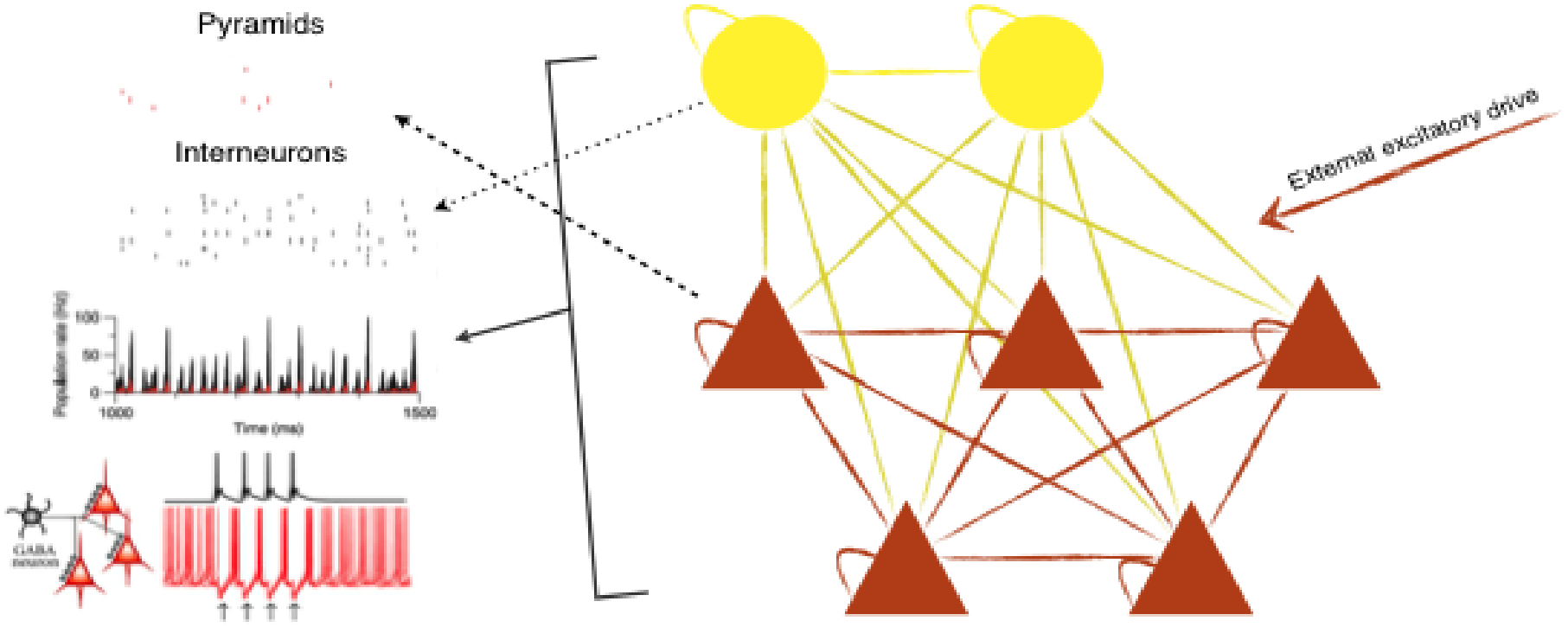

Figure 1.3.1. PING network demonstrating interconnected pyramidal cells and PV+ interneurons, a minimum framework capable of sustained oscillatory activity. Arrows demonstrate sparse, seemingly aberrant firing of each neuronal population separately, but coherent γ-frequency rhythm when measuring total population (LFP) (Brunel, 2003).

The aforementioned computational modelling experiments convincingly implicate GABAergic inhibition in the generation of γ-oscillations. To summarise, Wang *et al* demonstrated that $GABA_A$ mediated GABAergic inhibition (by interneurons) shapes the activity of the EPSP in pyramidal cells (a correlate of local field gamma and the main generator of scalp recorded signals). Furthermore, the recurrent excitatory to inhibitory balance predicts γ-frequency and increasing the ratio of AMPA:GABA activity reduces frequency.

Several studies have suggested that a particular type of fast-spiking inhibitory neuron is required for oscillation maintenance (Bartos, Vida, & Jonas, 2007; Cardin *et al*., 2009). Interneurons expressing the calcium-binding protein parvalbumin, (so called PV+ interneurons) can fire at >200 Hz with little spike-frequency adaptation, meaning they are well suited for a fast-oscillation network. A further link between PV+ interneurons and γ-oscillations comes from the fact that schizophrenic patients present markedly altered γ-oscillations (Spencer *et al*., 2003) and also unusually low levels of GAD67 in their PV+ interneurons (Akbarian & Huang, 2006). A series of optogenetic studies demonstrated that interneurons expressing PV+ coupled with pyramidal neurons can maintain γ-oscillations (Sohal, 2012). Furthermore, rhythmic activation of PV+ interneurons increases local field power in the gamma range, and this entrains firing of pyramidal neurons (summarised in figure 1.3.2) (Carlén *et al*., 2011, Sohal, 2012).

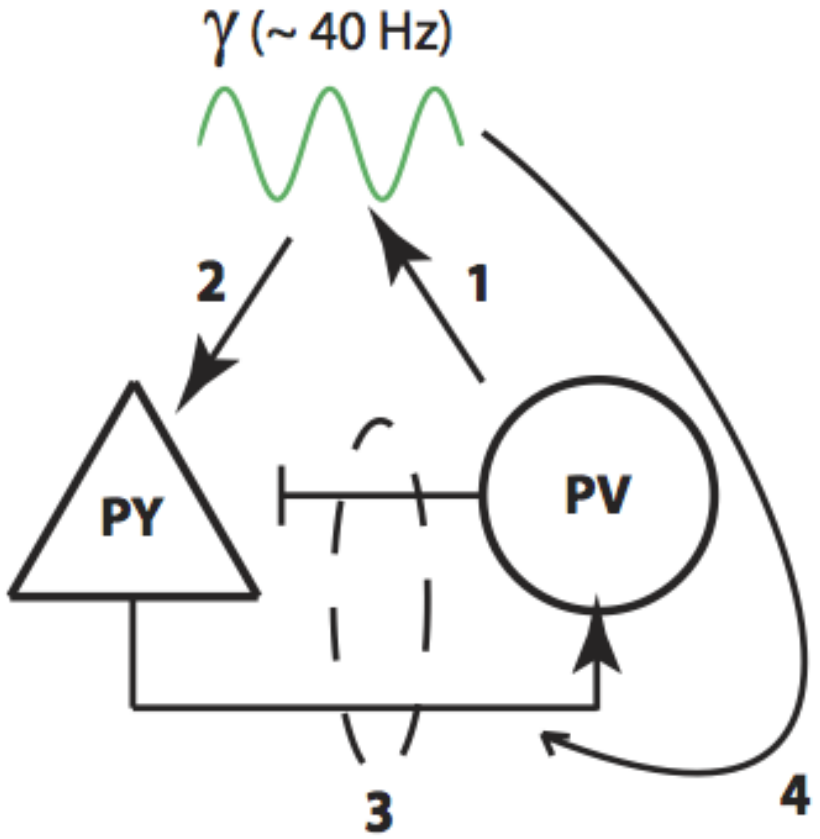

Figure 1.3.2. From Sohal 2012. Oscillation conclusions from optogenetic studies. PV = parvalbumin FSI, PY = pyramidal neurons. (1) PV play a role in generating oscillation, (2) this rhythm entrains pyramidal neurons, (3) interaction between the neuronal populations produces oscillations, (4) Gamma modulated firing in PY enhance flow of information to postsynaptic targets.

Gamma oscillations have been recorded in visual cortex in response to visual stimuli. In the context of visually induced γ-oscillations, V1 contains the PING oscillatory model architecture as previous described (including the external drive in the form of projections from LGN). Theoretically, γ-oscillation frequency in this region, as well as across the cortex, should provide a marker of GABAergic function. In concordance with this, Muthukumaraswamy *et al* (2009) demonstrated that peak γ-oscillation frequency obtained using MEG (while participants viewed a grating stimulus) is positively correlated with the concentration of GABA in the same region in the same participants, as obtained with magnetic resonance spectroscopy. A recent study, however, failed to replicate this finding in a larger sample size (Cousijn *et al*., 2014).

Time-frequency analysis of γ-oscillatory data provides measures of frequency and amplitude. While γ-oscillatory frequency is understood as a marker of GABAergic function and is a highly repeatable measure within individuals (Muthukumaraswamy *et al*., 2010), γ-oscillation amplitude (γ-amplitude) is less well understood and could be less stable within subjects. Despite this, deficits in γ-amplitude have been demonstrated in schizophrenic subjects, and amplitude has been shown to correlate with a number of associated symptoms and behaviours (Uhlhaas, 2013; Uhlhaas & Singer, 2010).

Previous studies have demonstrated that oscillation amplitude reflects synchronisation of spiking in cortical microcircuits (Pfurtscheller & Lopes da Silva, 1999). Spencer (2009) investigated γ-amplitude reductions in schizophrenia in a PING model, based on that of the previously described Brunel & Wang model (2003). This demonstrated that reducing fast-spiking interneuron (FSI; predominantly PV+ interneurons) NMDA input to the 2-population network increased network excitability and increased γ-amplitude (power). The authors suggested that this increase in amplitude occurs as a result of inhibited FSIs disinhibiting excitatory pyramidal neurons, permitting greater network excitability (Spencer, 2009). This study demonstrates both that NMDA receptors may be important in γ-oscillation amplitude, and that network excitability (or increased EPSC) is a correlate of increased amplitude. If amplitude reflects synchronisation of spiking, it may be that increased network excitability results in increased amplitude purely by permitting entrainment of more neurons.

1.4 Event-related potentials, neurophysiology and functional imaging studies in psychiatric disorders.

This section aims to introduce neuroimaging and neurophysiology as tools in investigating psychiatric disorders, with a focus upon biomarkers, major depressive disorder, event-related potential studies and neuroimaging. Neurophysiology and functional neuroimaging findings are reviewed.

1.4.1 Imaging Biomarkers

Biological markers of disease (biomarkers) are needed in psychiatry, and non-invasive brain measurements represent a potential mechanism for discovering and measuring these. Biomarkers are described as either state or trait and include both structural and functional measures. State markers are present while the disease is 'active' and therefore considered to represent only temporary changes, while trait markers present outside of the disease (i.e. at prodromal phase, before onset, in remittance or in genetically at-risk subjects). Imaging biomarkers typically fall into one of three categories: disease characterisation (e.g. for diagnostic utility or exploring pathology), therapeutic characterisation (i.e. drug discovery) or disease progression monitoring (measuring treatment response or stratified medicine) (Kumar *et al*., 2013).

1.4.2 Introduction to Event related Potentials

One of the earliest fields of biomarker research in human psychiatric subjects was electroencephalographic (EEG) studies of event related potentials (Luck, 2005). Event related potentials (ERPs) refer to electrical (or magnetic in magnetoencephalography where referred to as event related fields, ERF) currents recorded from the scalp, which are believed to represent a summation of neuronal postsynaptic potentials in response to a stimulus or task. *In vivo* techniques such as EEG and MEG record a comparable signal to preclinical local field potentials, that is, postsynaptic potentials and currents recorded from populations of neurons, as opposed to multi-unit recordings of single neuron action potentials (more specific biological underpinnings are detailed in 1.4).

Neurophysiological studies may be stimulus driven or record 'resting' function. Resting recordings can be used to compare differences in intrinsic activity between groups, for example between patient and healthy groups. However, this approach does not reveal differences in specific aspects of information processing. Stimulus-driven studies, however, seek to find correlates of a specific aspect of processing or cognition (Haenschel & Linden, 2011). In this context, a stimulus or task is repeated typically fifty or more times during recording and the trials averaged to reveal task-related ERPs.

ERPs are characterised and identified by their latency and amplitude as well as scalp topography. ERPs are denoted by a letter representing their polarity (Positive, P; negative, N; or variable, C), and their average latency in milliseconds (e.g. P300). The meaning of a given ERP depends largely on the stimulus that evokes it, and the sensory and/or cognitive process associated with the stimulus or task. Within the neurophysiology literature, a generally accepted threshold of 100ms differentiates early ($\leq$100ms) and later (~>300ms) ERPs, which are considered to reflect predominantly sensory and cognitive processes, respectively. Thus, particular stimuli will produce stronger effects on the components and location of ERPs across time. For example, a passive task involving a visual checkerboard stimulus is likely to elicit an early (<100ms, sensory) ERP in a brain region associated with vision (a visual evoked potential, VEP). Table 1 demonstrates the most commonly reported ERPs, their latencies, and how these have previously been interpreted. This section will briefly review event-related findings across psychiatric disorders, with a focus on depression and early components (Luck, 2005).

1.4.3 Early auditory and visual evoked responses in psychiatric disorders: <100ms

Early ERPs are considered a reflection of predominantly sensory processes in response to stimuli. Visually evoked waves are a type of early ERP, referred to as visual evoked potentials (VEPs) or visual evoked fields (VEFs). The early

responses P50, N1 and the P100 (P1) have been explored in psychiatric disorders and are briefly reviewed in this section.

The P50 response is considered an index of sensory gating, a gating mechanism thought to prevent sensory overload. A typical sensory gating paradigm involves pairs of auditory clicks, often over a white noise background. The paired clicks appear approximately 500ms apart, eliciting a two-component P50, termed S1 and S2 (a peak for each click). In healthy individuals, the second component, S2, is significantly supressed compared to S1. Sensory suppression is measured as the amplitude of S2/S1, where lower values represent an increase in sensory gating (Cabranes *et al*., 2012).

A meta-analysis of 17 P50-gating studies in schizophrenia (Bramon, Rabe-Hesketh, Sham, Murray, & Frangou, 2004; Cabranes *et al*., 2012; Horner, Ries, Krapcho, & Neyman, 2009; Kessler *et al*., 2003) demonstrated, in a sample of 359 schizophrenics and 340 controls, that the P50 ratio in schizophrenia was significantly higher than in controls, with a pooled standard effect size (Cohen's d) of -1.56 (p=<0.001), indicating less suppression (or sensory gating) in schizophrenia. They found no difference in latency and patients were taking antipsychotics. Furthermore, amplitude was not found to correlate with severity or duration of illness. For this reason, the authors conclude that the P50 gating deficit is a stable trait marker of schizophrenia.

Cabranes *et al* (2012) recently demonstrated that the P50 gating deficit is also apparent in bipolar depressive disorders and exhibits different characteristics across bipolar types 1 and 2 (BP1, BP2). In their sample of 95 healthy controls, 100 euthymic (i.e. medicated but stable) BP1 and 26 BP2, after controlling for confounding variables, BP1 showed a larger deficit in P50 gating compared to controls for S2/S1 (p<=0.001) than BP2 to controls (p=0.031). Furthermore, individuals with a history of psychosis demonstrated poorer sensory gating compared to controls than those without a history of psychosis (however with psychosis vs. without was not reported) and, within the BP2 group, number of

episodes of mania/ hypomania and depression were inversely correlated with S2/S1 ratio (p=<0.01 and 0.05 respectively) suggesting that P50 suppression is worse with an increasing number of episodes.

The common finding of reduced P50 gating across schizophrenia, BP1 and BP2 may indicate a common neurobiological deficit in the disorders. However, as noted by Cabranes *et al* (2012), the amplitude of the S1 response will also alter the S2/S1 ratio and this should be accounted for. In their study, BP2 had marginally higher S1 amplitude, which could account for the difference in S2/S1 ratio compared to BP1. However, besides it's potential use as an endophenotype, an interesting question arises from these reports. Given suggestions from genetic literature that bipolar disorders 1 and 2, and schizophrenia may be seen as a continuum rather than distinct pathological entities (Craddock, O'Donovan, & Owen, 2006; Moller, 2003), a 'disease-dependent' increase in S2/S1 ratio across these disorders may add further support for a common pathophysiology.

The P100 is elicited by any visual stimulus, irrespective of task. Furthermore, the magnitude of the response is dependent on specific properties of the stimulus, including luminance and contrast (Luck, 2005). The P1 VEP has been localised to extrastriate visual cortex (Di Russo, 2002) and middle occipital gyrus (Hall *et al*., 2005) and is sensitive to visual stimuli. It has been associated with spatial attention and filtering of irrelevant stimuli.

A reduction of P1 amplitude in schizophrenia and at-risk of schizophrenia individuals has been reported (Haenschel 2007) and this has been associated with working memory performance. Furthermore, the reduction in P1 amplitude in schizophrenia has been shown to persist regardless of medication, age, illness duration or severity and is not correlated with a specific clinical phenotype.

A reduced P1 VEP amplitude has been demonstrated in euthymic bipolar disorder patients and participants with schizotypy (Yeap, Kelly, Reilly, Thakore, & Foxe, 2009) (Koychev, El-Deredy, Mukherjee, Haenschel, & Deakin, 2012). Further

investigation of the P1 amplitude in psychiatric disorder is warranted, particularly since some have suggested that the common P1 reduction across schizophrenia and bipolar disorder represents a common genetic liability (Yeap *et al*., 2009).

1.4.4 Late Event related potentials in psychiatric disorders: the P300

One of the most commonly used stimuli in evoking the P300 is an auditory or visual *oddball* paradigm. First reported by Squires, Squires and Hillyard (1975), employing a similar design to Sutton *et al* (1965), the odd-ball task involves interrupting strings of identical or matching (congruent) stimuli with unpredictable, or incongruent stimuli. They found that unexpected changes in both loudness and frequency of a string of sounds altered the magnitude of the P300 response. They further identified that instructing participants to either actively listen to the sounds, or ignore them, altered the waveform whereby ignored stimuli had a latency of 220-280ms (referred to as P3a), whereas actively engaged stimuli evoked a larger-magnitude wave with a 310-380ms latency (P3b). The authors suggest that the P3a is probability dependent but independent of task, while the P3b is both probability and task dependent.

Subsequently, alterations of the amplitude, latency and topography of the P300 have been demonstrated in schizophrenia (Morstyn *et al*., 1983), bipolar disorder (Souza *et al*., 1995), major depressive disorder (Diner, Holcomb, & Dykman, 1985), generalised anxiety disorders (Boudarene, 1997), obsessive-compulsive and psychoses (Salisbury & Shenton, 1999), alcohol-related disorders (Cohen *et al* 2006) and at-risk of psychosis and family-history groups (Fromman *et al* 2008). Authors have argued that the lack of specificity of the P300 response suggests that it may have little use in understanding particular psychiatric disorders, and may lack clinical utility as an aid to diagnosis or in monitoring treatment response (Singh, 2000).

1.4.5 Common ERPs in depression

In depression research, the P300 response is most regularly identified as having a reduced amplitude and longer latency than healthy controls, seemingly irrespective of the paradigm utilised (R Singh, 2000). Table 6, taken from Bruder *et al* (2009),

demonstrates P300 auditory odd-ball findings in depression with a clear trend toward depressed participants having lower P300 amplitudes.

Singh *et al* (2000) demonstrated that the auditory odd-ball evoked P300 has a longer latency and lower amplitude in depression compared to non-depressed participants. They further demonstrated that this was absent in medicated depressives, that those >40 years old or with severe depression had significantly greater latency than those <40 years old or without severe depression, and that latency correlated with age and HRSD score while amplitude correlated negatively with age. However, the authors suggest that these findings are unlikely to serve as biological markers due to their lack of specificity and sensitivity to changes in disease state.

Isintas *et al* (2012) attempted to elucidate the sensitivity of the P300 to treatment response in depression. Recording the P300 before and after 12 weeks of 50-200mg sertraline (SSRI) in participants with and without depression, they found no difference in amplitude between responders, non-responders and controls before or after treatment. They did report significantly longer latencies in non-responders compared with responders and controls after treatment, suggesting that P300 latency may be sensitive to antidepressant treatment, however this finding has not seen clinical use. Whether the P300 latency predicts response to other antidepressant treatments, and whether it is sensitive to treatment response in other disorders would help determine its efficacy as a biomarker.

The above literature suggests that, while some ERPs are robustly elicited by specific stimuli, their utility in studying depression is somewhat equivocal. This is partially due to an imbalance in the scientific literature; the number of studies reporting alteration of ERPs in unipolar depression is far less than the number focussing on ERPs in bipolar disorder or schizophrenia.

1.4.6 Neuroimaging (MRI) & neurochemical imaging (PET, MRS) studies of depression

Besides encephalographic studies of the depressed brain, magnetic resonance imaging (MRI) techniques have also been applied to study changes in the brain during depression.

Early MRI studies of psychiatric disorder focussed on comparing structural measures. Since the invention of voxel based morphometry (Ashburner & Friston, 2000), and Freesurfer mesh approaches (Fischl, Sereno, Tootell, & Dale, 1999), permitting easy segmentation of grey matter, this field has seen rapid growth. Numerous studies have reported altered structural findings in depression. Vythilingam (2004) and others reported equivocal results regarding hippocampal volume in depression despite depressed subjects exhibiting reduced performance during working memory paradigms. However, a more recent meta-analysis by Lorenzetti *et al* (2009) suggested robust volumetric reductions of the hippocampus, basal ganglia, orbital frontal cortex and subgenual prefrontal cortex. This study also demonstrated that gender, medication and severity and duration of illness affect volumetric measures, which may explain the discrepancy with some studies.

The Lorenzetti study also highlights the amount of variability in grey matter measures, which could explain why structural measures are not regularly used as biomarkers in psychiatric disease. Some concordance in findings was reported in a series of studies which demonstrated increased amygdala volume in the early stages of depression (Lange & Irle, 2004, Frodl *et al*., 2002) but reductions in volume in later stages (multiple episodes) (Bremner *et al*., 2000, Caetano *et al*., 2004, Hastings, Parsey, Oquendo, Arango, & Mann, 2004, Monkul *et al*., 2007).

The negative-emotion bias observed in depressed subjects has been probed extensively using facial-expression recognition paradigms. These paradigms have been utilised in functional MRI (fMRI) studies with the objective of identifying localised changes in brain activity that occur during facial expression recognition in depressed subjects. Studies of face processing in depression have typically

reported alterations of amygdala, insula and ventral striatum activation (Kumar *et al*., 2013).

In a study Fu and colleagues (2004), subjects with unipolar depression (and matched controls) were recruited to undergo a series of fMRI scans where they completed an affect recognition task discriminating between different intensities of sadness. The scans were completed at baseline and after 2 and 8 weeks into fluoxetine (fluoxetine hydrochloride, 20mg/day) treatment. This enabled both the identification of altered activation patterns in depressed subjects compared with healthy controls (correlates of the negative bias during the face task) and also measurement of any changes in this activation pattern induced by antidepressant treatment. The study demonstrated that, at baseline, patients demonstrated increased amplitude of the BOLD response to sad faces compared with healthy controls. Antidepressant treatment was associated with reduced limbic and subcortical capacity for activations in depressed subjects. Symptomatic improvement correlated with increased anterior cingulate activation, suggesting that the fMRI signal may be sensitive enough to serve as a marker of treatment response. Studies by Sheline *et al* (2001) and Keedwell *et al* (2009) have employed similar methodologies (fMRI, emotional face discrimination, antidepressant treatment). Sheline *et al* (2001) reported increased amygdala activation particularly to fearful faces in patients compared with healthy controls, which was decreased with antidepressant treatment. Keedwell *et al* (2009) reported that depression severity correlated with temporal changes in BOLD signal to sad stimuli in right visual cortex as well as subgenual cingulate and hippocampus. Decreases in symptom scores correlated with decreases in effect size of response in right visual cortex and subgenual cingulate to sad faces. Taken together, these studies demonstrate that the BOLD response is altered in depression specifically to negative stimuli (sad or fearful faces) in both visual cortices and emotional regulation and discrimination associated areas in the limbic system (amygdala, hippocampus) and subgenual / anterior cingulate. These areas also change activation pattern with antidepressant treatment, suggesting fMRI is a powerful tool for monitoring treatment response.

Most studies have used event related experimental design in order to locate activations in a specific region in response to a task. However, recent studies have begun to explore functional connectivity using fMRI. These studies look at temporal correlation in the fluctuations of the BOLD signal in disparate regions of the brain. Using this approach, Anand *et al* (2005) demonstrated differences in cortico-limbic 'activity' and 'connectivity' between depressed patients and healthy controls. During a paradigm that involved viewing negative and neutral valence images, depressed subjects exhibited increased activation of cortical and limbic structures but decreased connectivity was observed between rostral-ACC and amygdala, rACC and dorsomedial thalamus and precuneus and caudate. Thus the patterns of activation typically described in fMRI experiments of depressed subjects are localised effects, with the BOLD signal exhibiting the opposite effect in the connections between regions regularly implicated in altered neural functioning in depressed subjects.

1.4.7 Neurochemical imaging and toxicology (PET, MRS, blood plasma)

While structural and functional MRI studies have demonstrated utility in localizing brain regions involved in specific tasks, and have evidenced sensitivity to drug manipulation suitable for response monitoring, the fMRI BOLD signal does not contain information regarding neurochemistry, and only contains indirect information on the neurophysiology underlying both the signal itself, and task induced alterations (inferred by other measures such as grey matter). To this end, positron emission tomography (PET) and magnetic resonance spectroscopy (MRS) have been employed to measure functional changes and bulk levels of specific chemicals in the brain, respectively. Since the efficacy of pharmacological therapy in mood disorders strongly suggests that neurochemistry is altered in psychiatric disorders, these approaches may be more suitable for probing the neurobiology of depression.

The serotonin system is implicated in the pathophysiology of depression partially because pro-serotonin drugs (e.g. SSRI) alleviate depressive symptoms. In

particular the serotonin 1A receptor, 5HT-1A, is implicated in depression because depressed subjects display blunted responses to 5HT-1A agonists and because post-mortem studies have demonstrated reduced binding at the 5HT-1A receptor in the brains of those who died by suicide as compared with non-suicide. Drevets and colleagues (1999) used PET using the 5HT-1A radioligand [^{11}C]WAY-100635 to identify, spatially, where binding is altered in depressed subjects. Binding potentials were significantly reduced in depressed subjects in the raphe, hippocampus and amygdala, occipital cortex and post-central gyrus. This study confirmed that 5HT-1A receptor binding is altered in depressed subjects compared to controls in a range of brain regions including the amygdala and hippocampus, regions which have been repeated reported to show altered BOLD signal in depressed subjects. Unfortunately the sample consisted of both bipolar and unipolar (MDD) depressed subjects, and as such did not demonstrate reduced binding in an isolated MDD sample. A follow-up study by Sargent *et al* (2000) also demonstrated brain regions where 5HT-1A binding was reduced, and demonstrated that the medication status of the subjects does not affect binding potential, neither does SSRI usage.

PET is a useful tool in probing neurobiological questions about depression, however it is limited by the availability of radioligands, which need to be specifically prepared and designed for experiments, are radioactive and have a very short decay time. Furthermore, PET is both expensive and invasive, making it unsuitable for many studies and as a biomarker. MRS however can be performed without the need for a tracer or radioligand (using ^{1}H) and as such is less invasive and has no time limit.

^{1}H-MRS has been used to investigate the concentration of neurotransmitters in the brain. Because the technique relies on separate chemicals by their resonant frequency, the number of compounds that can be measured is directly proportional to the strength of the MRI magnet, however most scanners are capable of measuring several chemicals of interest to psychiatric research. Notably: choline, creatine, inositol, glucose, N-acetylaspartic acid (NAA) and alanine. Furthermore,

using difference-editing methods (see chapter 2) to suppress the resonances of specific chemicals permits measurement of neurotransmitters such as gamma-aminobutyric acid (GABA) and glutamate and glutamine.

An early study employing this technique demonstrated that choline (referenced to creatine) was elevated compared with matched controls (Binesh *et al*., 2004). Furthermore, NAA/Choline levels increased with successful pharmacotherapy, while choline/creatine levels decreased. Subsequent studies have investigated other compounds in similar experimental designs. A meta-analysis of MRS studies in MDD (Yildiz-Yesiloglu & Ankerst, 2006) demonstrated that, in adult MDD, patients typically exhibit higher levels of choline/creatine in the basal ganglia and reduced Glx (composite glutamate, glutamine and GABA) in frontal regions. This is in contrast with findings in bipolar disorder where Glx is increased (Yildiz-Yesiloglu & Ankerst, 2006). While MRS provides bulk measures, it can be used to investigate hypotheses about specific neurochemical differences or changes in the depressed brain.

	early waves				*late waves*				
COMPONENT	P50 C1	P1/100	N1/100	P2/200	N2/200/N3	P3/300	N400	P600	CNV/MRCP
~LATENCY	40-75	100	90-100	100-250	200	250-400	300-600	600+	Early+Late
INTERPRETATION	Sensory Gating	Unexpected stimuli, Matching process	Sensation-seeking behaviour	Sensitive to physical changes of stimulus		Cognitive processes, discrimination tasks, oddball paradigm	Semantic incongruity, word expectancy	Language processing	Paired-stimuli, movement-related activity
DEPRESSION	Increased amp (Normann 07)	Decreased amp, boosted by SSRI (Normann 07)	Increased amp (Normann 07)			Reduced amp, >latency, no medication effect, positive correlation with age & HRSD (Singh 2000)			
SCHIZOPHRENIA		Reduced amp, P1 strength predicts WM performance (Haenschel 07) Reduced amp, SZ + *at-risk* group (Koychev 12)	Reduced amp, N1, P2, N2 … (O'Donnell 04)			Reduced amp, sensitive to fluctuations in positive symptoms (Mathalon 02)			MMN —> decreased amp in treatment-resistance (Milovan 04)
BIPOLAR DISORDER	P50 suppression + in relatives (Schulze 07)	Reduced VEP amp (Yeap 09)				Increase latency, reduced amp (O'Donnell 04) Amp reduced in manic psychosis (Sailsbury 99)			
ALCOHOLISM			Increased amp & latency (O'Donnell 87)			Reduced amp in 1st-degree relatives (Patrick 06)			

Table 1. Summary of ERP findings in common psychiatric disease.

Table 2: Taken from Bruder *et al* 2009. P300 findings in depression

Table 1. Auditory Oddball Studies Comparing Depressed Patients and Healthy Controls.

Study	Sample [a]	EEG Montage	EEG Reference	P3 Amplitude	Effect Size [b]
Blackwood et al. (1987)	16 MDD (med-free), 59 HC	Cz	Left Ear	MDD < HC	.79
Muir et al. (1991)	46 MDD (35 med-free), 212 HC	Cz	Left Ear	MDD < HC	.52
Gangadhar et al. (1993)	17 MDD (med-free), 22 HC	Cz	Mastoids	MDD < HC	.98
Sara et al. (1994)	14 MDD (med-free), 27 HC	Fz, Cz, Pz	Linked Ears	MDD = HC	.18
	13 MDD (medicated)			MDD = HC	.31
Hansenne et al. (1996)	10 MDDwS (med-free), 20 HC	Cz	Left Ear	MDDwS<HC	1.72
	10 MDDwoS (med-free)			MDDwoS=HC	-.12
Ancy et al. (1996)	17 MDD (15 med-free), 15 HC	Cz	Mastoids	MDD < HC	.85
Yanai et al. (1997)	16 MDD (med-free), 17 HC	Pz	Linked Ears	MDD < HC	2.18
Wagner et al. (1997)	11 MDD (med-free), 10 HC	Fz, Cz	Right Mastoid	MDD < HC	-
Bruder et al. (1998)	40 MDD/DYS (med-free), 22 HC	12 sites	Nose	MDD/DYS = HC	-
Vandoolacghe et al. (1998)	35 MDD (med-free), 11 HC	Cz	Mastoids	MDD = HC	.52
Kaustio et al. (2002)	22 MDD/DYS (med-free), 22 HC	16 sites	Right Mastoid	MDD/DYS = HC	-
Anderer et al. (2002)	60 MDD (med-free), 29 HC	19 sites	Average Mastoids	MDD < HC	-
Röschke & Wagner (2003)	21 MDD (med-free), 21 HC	Cz, Pz	Right Mastoid	MDD < HC	-
Urretavizcaya et al. (2003)	50 MDD (med-free), 31 HC	C3, Cz, C4	Linked Ears	MDD < HC	2.25
Kaiser et al. (2003)	16 MDD (medicated), 16 HC	18 sites	Average	MDD = HC	.11
Karaaslan et al. (2003)	16 MDDwP (med-free), 20 HC	Cz	Linked Mastoids	MDDwP < HC	1.43
	20 MDDwoP (med-free)			MDDwoP = HC	.08
Kawasaki et al. (2004)	22 MDD (med-free), 22 HC	16 sites	Linked Ears	MDD < HC	.90

[a] MDD = major depressive disorder; HC = healthy controls; DYS = dysthymic disorder; MDDwS = MDD with suicide attempt; MDDwoS = MDD without suicide attempt; MDDwP = MDD with psychotic features; MDDwoP = MDD without psychotic features

[b] Cohen's *d* effect size

1.5 Predictive coding and neuronal modelling

Predictive coding describes the brain as a system, whose aim is minimise free energy. According to Friston and colleagues (2009a), minimising free energy is a requirement of all biological agents in order to survive (Friston, Thornton, & Clark, 2012) and provides an account for perception and action. Minimising free energy equates to minimising surprise (*entropy*). Minimising surprise is achieved through changing perceptions, via sensations (*the senses*), which in turn, entails action (e.g. *movement, saccades*). This free energy principal of the brain is a formal assumption of predictive coding.

A key challenge for the brain is to infer the causes of its sensations, an issue first formalised by Helmholtz (1909). How the brain does this is somewhat equivocal, however a key hypothesis is that the brain performs *analysis by synthesis*; that is, it constructs a generative, dynamic model (an *internal model*) of causes (the world) using a form of Bayesian inference, termed inverse-inference (Yuille & Kersten, 2006). This generative model can be considered a hidden Markov model in that it aims to estimate hidden states, or causes, using a Bayesian approach. The Bayesian brain hypothesis is an example of perception as hypothesis testing (Gregory, 1980) whereby the internal model both predicts and explains sensations. This internal model constitutes priors, or hypotheses, about the incoming sensations, while incoming sensations constitute new data. The brain utilises these to perform a Bayesian inference (figures 1.5.1, 1.5.2) technique summarised graphically in figure 6.2. The aim, for the brain, is to calculate the most accurate posterior density, $p(h|d)$, given a likelihood and prior;

$$P(h|d) \propto p(d\ |h)\ p(h) \tag{1}$$

where h = the internal model hypothesis and d = actual sensory data. In a Bayesian interpretation, the probability of the data given the hypothesis, $p(d|h)$, forms the likelihood and the probability of the hypothesis, $p(h)$, forms the prior. The

posterior density updates the internal model (subsequent priors) thus suppressing prediction error. This is the basis of predictive coding schemes (Rao & Ballard, 1999). Prediction error can be expressed numerically either as the difference between input signal and hypothesis signal, or as the distance between the posterior density and prior distributions, illustrated in figure 1.5.2. Predictive coding is a consequence, rather than cause, of surprise minimisation. Free energy is a bound on surprise, where prediction error is a neurobiologically computed measure of free energy. Free energy is, formally, expected energy minus the entropy of predictions (Friston & Stephan, 2007; Friston, Kilner, & Harrison, 2006).

$$F_{max} = ln\ (p(d|h) - D(q(\theta)||p(\theta|d,h))$$
$$F_{max} = \log model\ evidece - divergence \quad (2)$$

where F_{max} is maximal free energy, d = data, h = model (or hypothesis), D = Kullback–Leibler divergence between true and approximate posterior, and $q(\theta)$ is the conditional density.

In a recent discussion article, some authors have questioned the assumptions of predictive coding under the free energy principal; see '*the dark room problem*', Friston *et al* (2012), suggesting that, if the objective were to minimise free energy by minimising surprise, agents would simply find a secure, highly predictable location and stay there indefinitely. Contradictory to this, animals tend to explore, seeking new sensations (Fiorillo, 2010). This issue has subsequently been formalised and labelled *the dark-room problem* (Friston *et al*., 2012). The answer to this issue is somewhat multifarious. Firstly, entropy (average surprise) is a function of both sensations and the internal model, $H(s|m)$, whereas the entropy minimised by the dark-room is a function only of sensations $H(s)$ (Friston *et al*., 2012). Second, it is suggested that prior beliefs make dark rooms surprising; agents whose model does not consist of priors that make dark rooms surprising stay there indefinitely until death; thus natural selection dictates this will not happen.

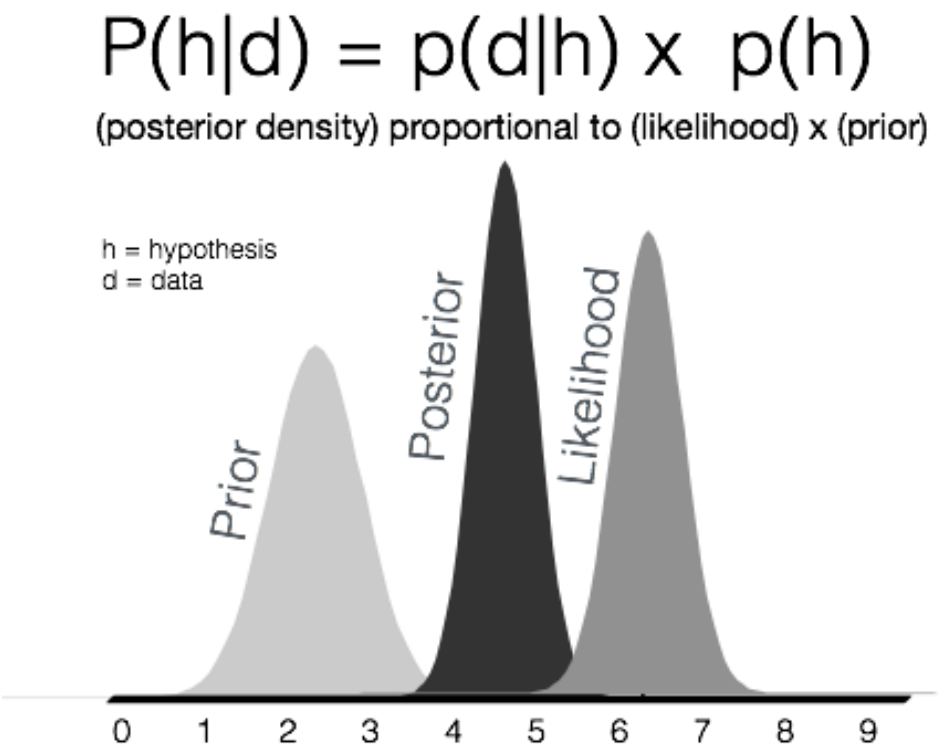

Figure 1.5.2. Bayesian inference method utilised by the brain to evaluate and update predictions. h = hypothesis about the input / the internal model prediction. d = data / sensation input. The posterior density updates the internal model (prior) thereby minimising subsequent prediction error.

1.5.1. Biological evidence and plausibility of predictive coding under the free energy principal: canonical microcircuits.

Predictive coding under the free energy principal requires message passing throughout the brain. This section will focus on how the hierarchical nature of cortical architecture and neurobiology supports predictive coding. While the aim of this section is not to fully reiterate the review in section 1.3, some elements are reframed.

As described in section 1.3, the neuronal populations and their laminar distribution and connectivity in the visual cortex are well documented. Furthermore, this microcircuit architecture is predominantly the same across the cortical sheet, with only subtle differences, which are presumably required specifically for local computation specialities (e.g. the primary visual cortex may have slightly different

local computational needs to the primary motor cortex). Despite this, the concept of a canonical (general) microcircuit has garnered support. Douglas & Martin's work on the cat visual system first documented the concept of a distinct microcircuit. Their model entailed 3 neuronal populations; superficial and deep pyramidal cells and inhibitory interneurons. They proposed all assemblies were fully interconnected and functioned to amplify thalamic inputs to (in this case) V1 (Douglas & Martin, 1991). While the architectural and functional anatomy of the cortical sheet is now understood to be slightly more complex than initially suggested, the concept of a relatively generic cortical microcircuit is still accepted. Figure 1.5.3 illustrates both the Douglas & Martin, and the more recently described Bastos microcircuits (Bastos *et al*., 2012; Douglas & Martin, 1991).

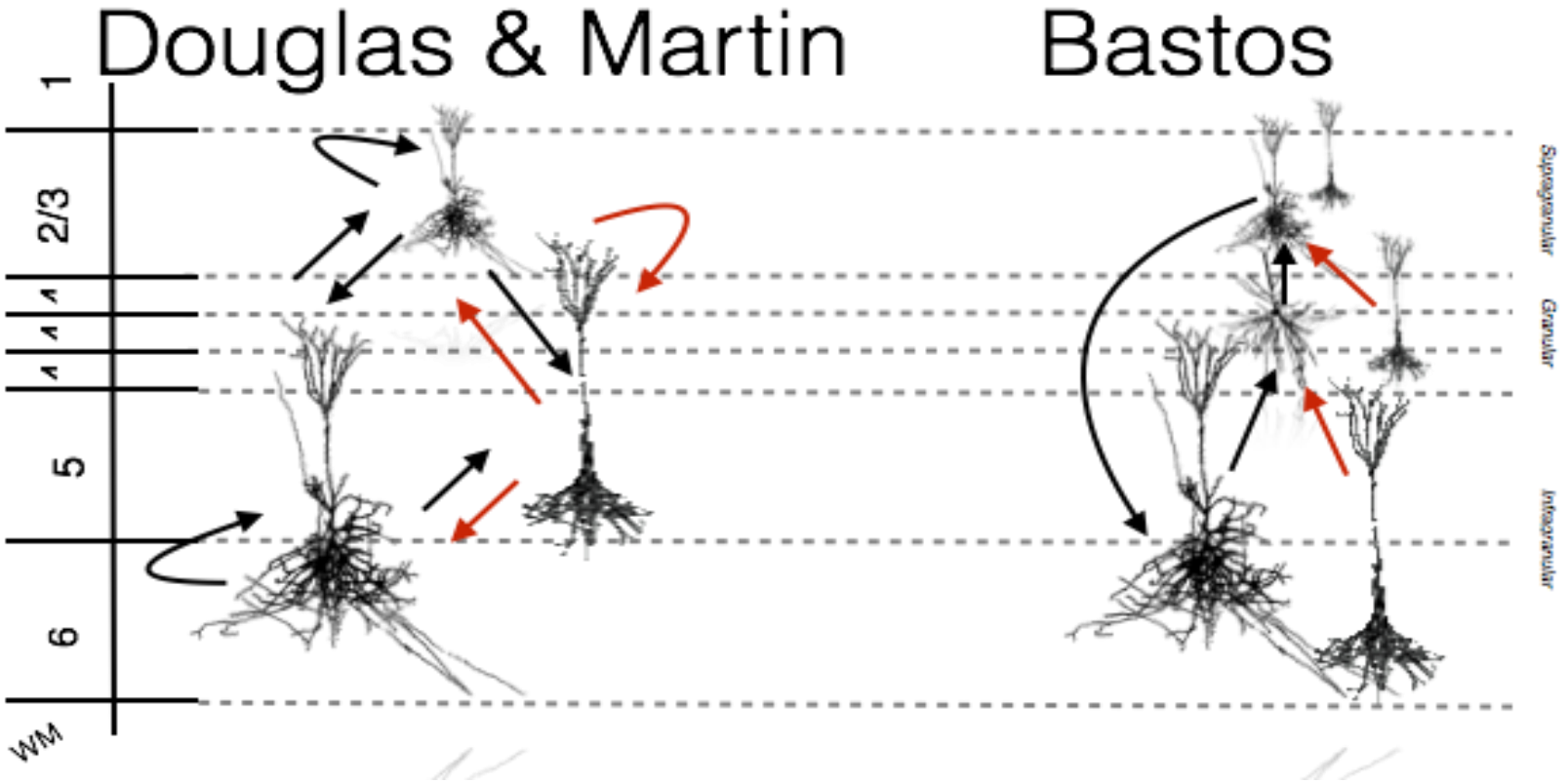

Figure 1.5.3. Left: Douglas & Martin microcircuit of V1 in the cat. Three neuronal populations: superficial and deep pyramidal cells and bipolar inhibitory interneurons. Red connections are inhibitory and black excitatory. Right: Human canonical microcircuit arising from Bastos literature review, features additional layer 4 'granular' layer of spiny stellates and interneurons coupled to principal neurons in each layer (based on the density of pyramidal cells to inhibitory interneurons, it is more likely that the inhibitory cells are not coupled to principals, but rather fewer are better connected across the layers).

Feedforward, feedback and lateral connections, which predominantly originate and terminate in supragranular to granular, infragranular to supra- or infra-granular, and any-layer to the-same-layer, respectively (Purves, 2008), has been interpreted in terms of a predictive coding infrastructure (Friston, 2005). Feedforward and feedback connections are typically excitatory pyramidal projections, which use glutamate and GABA to signal via ionotropic AMPA and $GABA_A$ receptors. Lateral connections are modulatory and slower, hence utilising glutamate via voltage-gated NMDA and metabotropic receptors (Friston, 2005).

Within the functional architecture a distinction is made between intrinsic and extrinsic connectivity. Intrinsic connectivity refers to within the microcircuit, whereas extrinsic refers to between-microcircuit connectivity. The Bastos microcircuit is re-illustrated with these connections labelled in figure 1.5.4 where forward connections enter the microcircuit at layer 4, are excitatory projections and contain sensory data or convey prediction error. For example, in V1, the forward connection might be the LGN afferent to layer 4 of V1. Within the microcircuit, (intrinsic) feedforward connections are unequivocally excitatory and convey prediction errors (figure 6.5). Feedback connections convey predictions (based on priors) and are less well understood since evidence suggests that these feature both excitatory and inhibitory connectivity, with an overall effect of being inhibitory (Bastos *et al*., 2012). Backward connections carry priors (predictions) from other circuits, which enter via both superficial and deep layers and can therefore modulate both predictions and prediction errors (figures 1.5.5, 1.5.6)

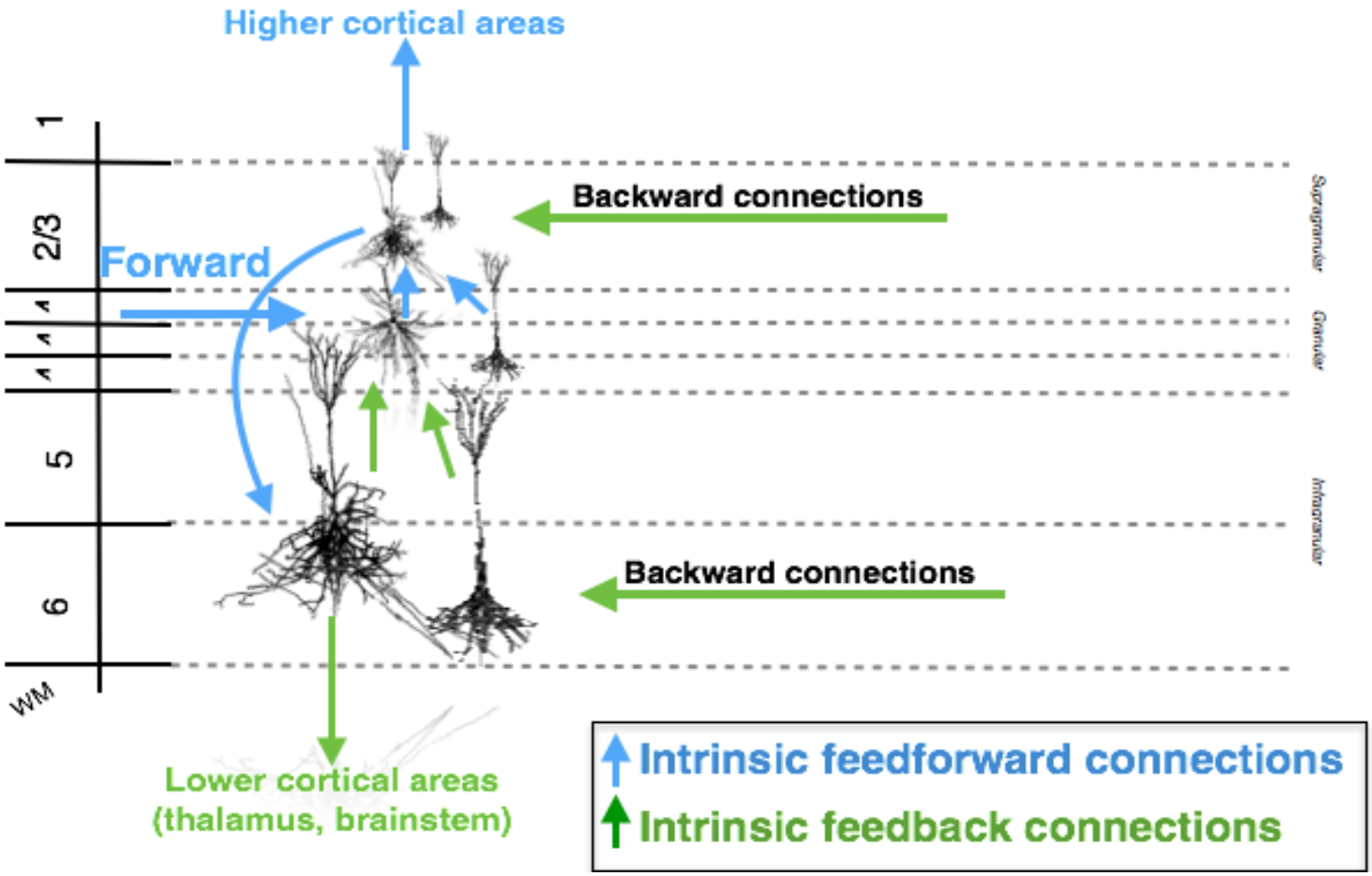

Figure 1.5.4. Bastos' microcircuit with labelled connectivity. Adapted from (Bastos *et al.*, 2012)

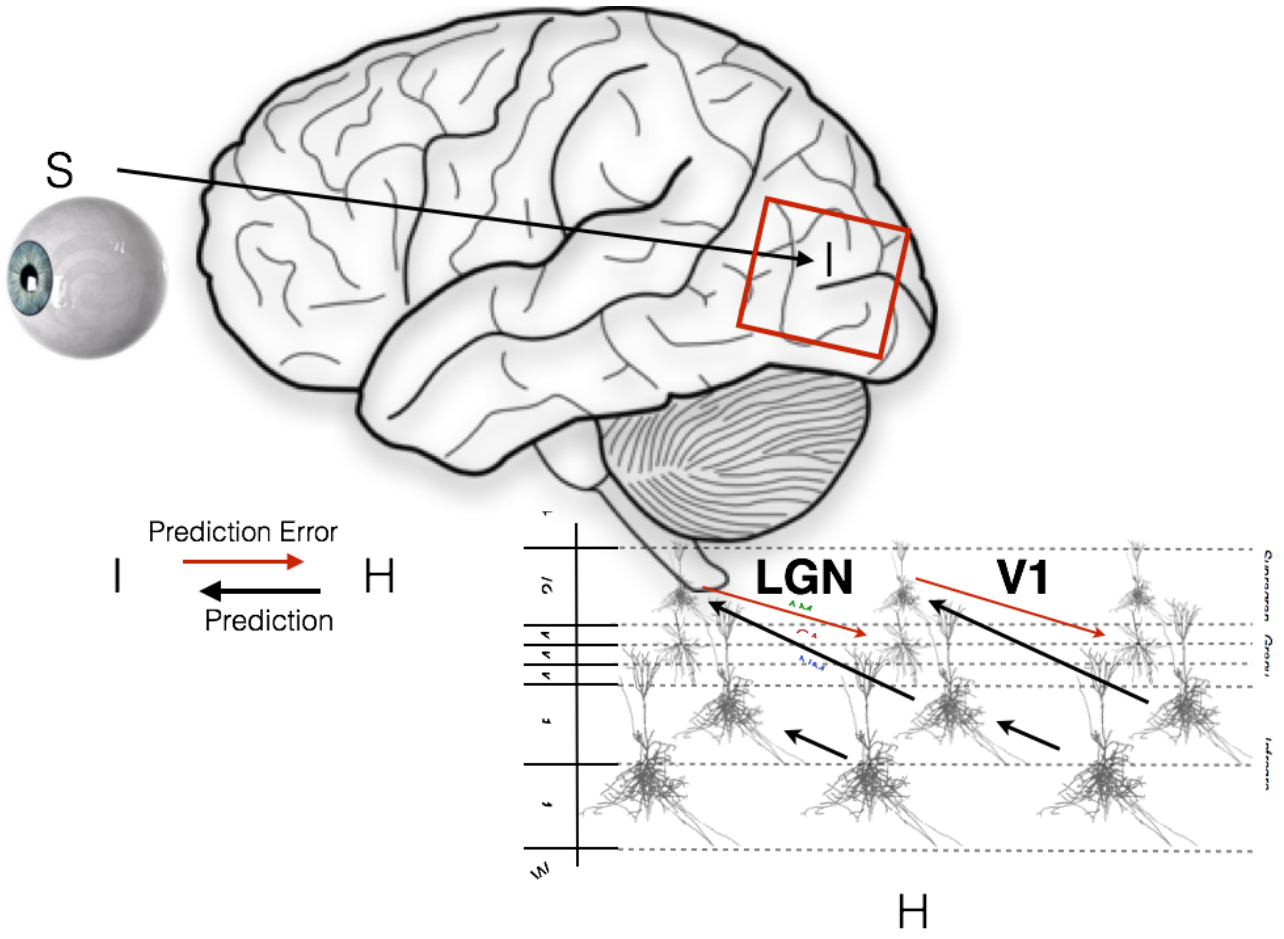

Figure 1.5.5. Illustrating the direction of predictions and prediction error across the cortical microcircuit. Hypotheses (predictions based on priors) are conveyed by the black arrows (feedback connections), illustrating a supra-granular origin while prediction errors (red) are passed by feedforward connections.

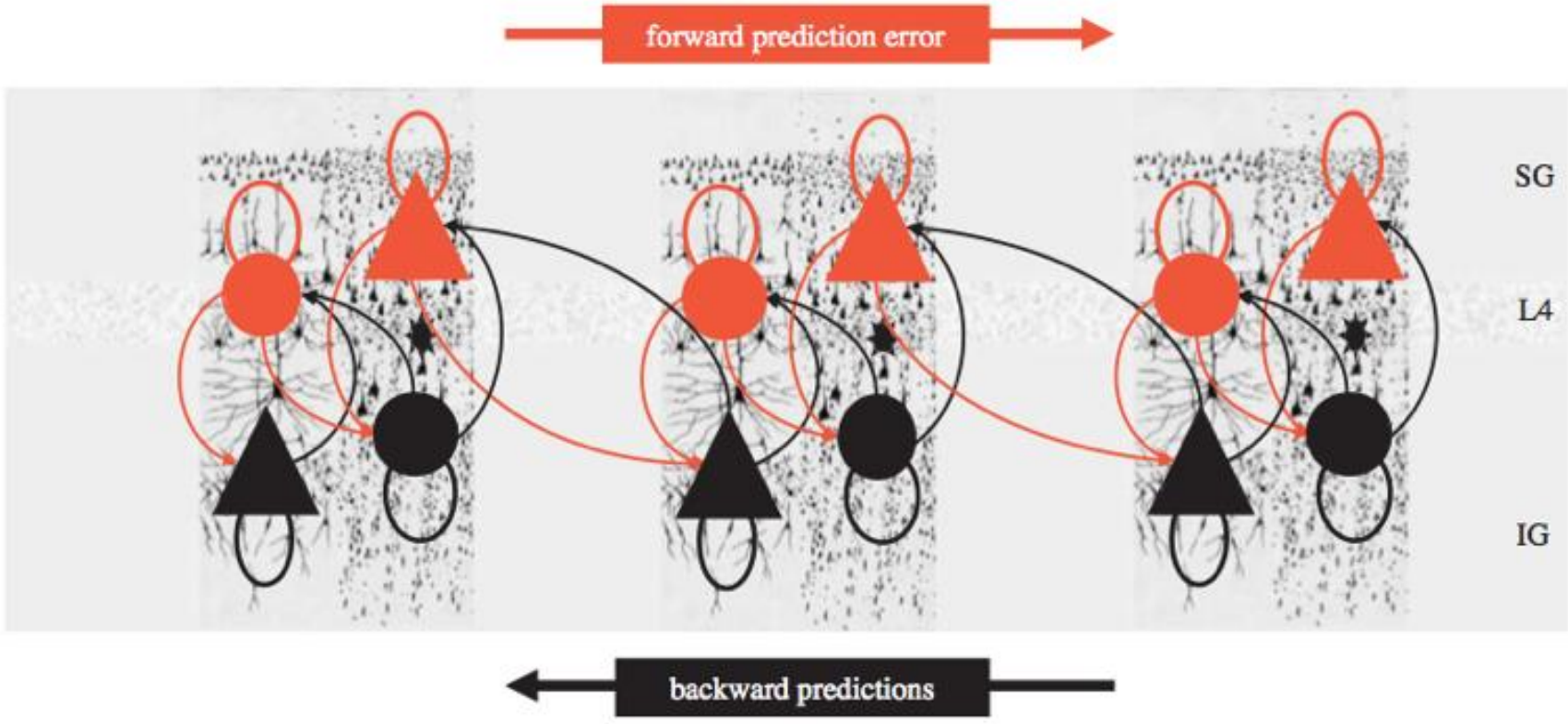

Figure 1.5.6. Illustrating extrinsic, between-circuit message passing. Amended from (Friston & Kiebel, 2009b)

While predictive coding remains a largely theoretical entity due to the difficultly in empirically investigating the underlying neuronal mechanisms hosting such as phenomenon, some authors have suggested that predictive coding explains (or is implemented via) measurable cortical dynamics.

Since the crux of predictive coding is that top-down predictions are compared with bottom-up signals, which result in a prediction error signal, message passing may utilise different frequencies (Arnal & Giraud, 2012). Recent work has provided support for microcircuits as a means of local computation, by demonstrating that superficial layers of visual cortex oscillate at higher (γ, >30Hz) frequencies than deep layers, which oscillate at predominantly β frequencies (figure 1.5.7) (Xing *et al*., 2012). Pinotsis *et al* suggest that this indicates forward connections use γ-frequencies whereas backward connections use β-frequencies (Bosman *et al*., 2012), which results in a '*spectral asymmetry'*. Given the common afferent, this '*synthesis and segregation*' of forward and backward connections is best explained by local, non-linear neuronal computations (canonical microcircuits). Furthermore, it suggests that γ-frequency oscillations are a marker of superficial pyramidal cell (population) encoded prediction error, whereas β-oscillations reference deep pyramidal cell encoded predictions (priors).

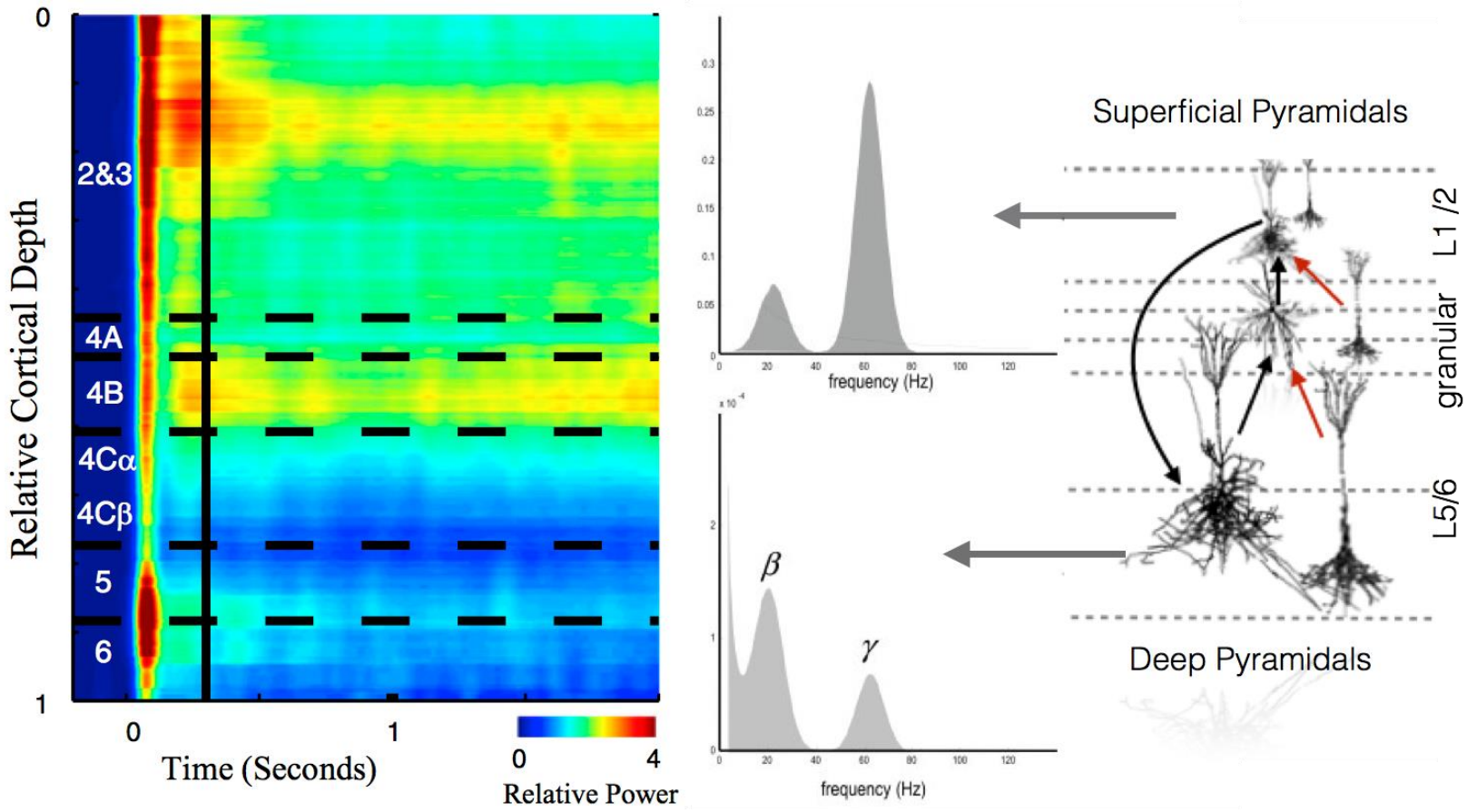

Figure 1.5.7. Spectral asymmetry of pyramidal cells within the same cortical column but in superficial vs. deep layers. Left image depicts laminar distribution of gamma-frequency band power obtained via LFP recording in V1 of Macaque viewing a grating pattern; adapted from Xing (2012). Right image illustrates main laminar architectural contribution to scalp recorded LFP.

1.5.2. Dynamic Causal Modelling.

The previous section provided an overview of how connectivity between neuronal populations, arranged into microcircuits, could host a phenomenon such as predictive coding. Dynamic causal modelling is a framework, which utilises these concepts to enable a computational estimation of population connectivity parameters (cf. effective connectivity, reviewed in Friston, 2011) in said microcircuits based on MEG spectra.

Dynamic causal modelling (DCM) permits *in-vivo* assays of microcircuitry by harnessing the concept of the brain as a generative, Bayes-optimal Helmholtz machine. Computational techniques such as neural mass modelling and mean field models allow synthesis and measurement of the dynamics of large neuronal populations. DCM utilises this computational approach as a surrogate generative model. If the neuronal population dynamics of the DCM generative model match those of the brain, the resulting spectra from the two should match (empirical spectra obtained from the brain using a neurophysiological technique such as MEG). This procedure is depicted in figure 1.5.8.

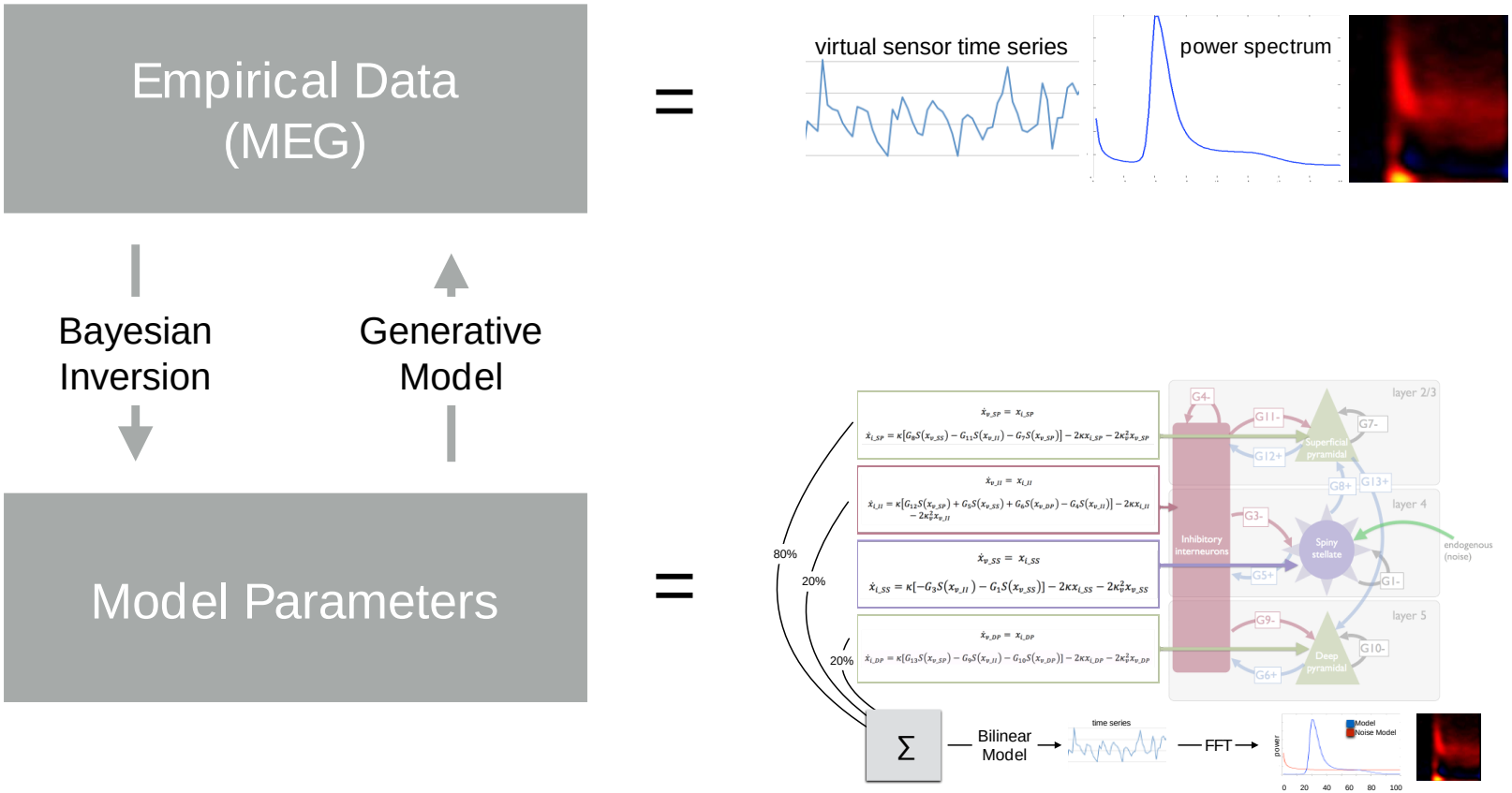

Figure 1.5.8 Model overview. The MEG power spectrum is compared to the model (NMM) using a Bayesian inversion methodology, which updates the (generative) model parameters.

The populations modelled feature between-population, intrinsic microcircuit connections based on known anatomy, the strengths of which are estimated by the modelling procedure (inversion). The populations are modelled using sets of first-order differential equations. DCM implements a variational Bayesian scheme (variational Laplace) to approximate the posterior density (see figures 1.5.2, 1.5.8) of the model parameters by maximising the negative free energy (Friston & Stephan, 2007). Further model specifics and modelling methodologies are provided in chapter 6.

1.6 Aims & Hypotheses

This thesis aims to explore the neurochemical hypotheses of depression presented in section 1.3, using multimodal neuroimaging, including the theories described in section 1.4.

Alterations of the GABAergic and glutamatergic neurotransmitter systems have been reported in major depressive disorder (MDD), both post-mortem *in-vitro* and ante-mortem *in-vivo*. Evidence from magnetic resonance spectroscopy (MRS) studies reported lower bulk concentrations of GABA in currently depressed participants as compared with healthy controls, which may reflect a neurobiological pathology, serve as a biomarker, and guide development of new pharmacological therapies.

If this area of research is to see translation to a clinical setting, the roles of GABA (and glutamate) in depression need to be more fully elucidated. This thesis addresses the following questions: do alterations in GABA concentration reflect state or trait markers of depression? Does the GABA deficit observed in depression reflect '*functional*' GABA? Can computational modelling of cortical neurobiology add disease-relevant sensitivity to primary imaging measures? Does an existing pharmacological compound with antidepressant efficacy act on the GABA system? These questions are approached using multimodal neuroimaging techniques, computational neuronal modelling and pharmacological manipulation.

Chapter 2. Methods

Study of the previously described event-related responses and neurochemistry *in-vivo* requires a multimodal approach utilising neuroimaging, spectroscopy and neurophysiological techniques. These include magnetic resonance imaging (MRI), magnetic resonance spectroscopy (MRS) and magnetoencephalography (MEG). The general approach of the experiments in this thesis, in brief, is to use MRI to construct a high-resolution 3D image of the brain. This allows accurate placing of the MRS voxel, which contains data on the chemicals present, as well as forming a template upon which to project the purely functional MEG data. These techniques, along with methodological issues pertinent to this thesis, are introduced. Experiment-specific methodological particulars are detailed in the corresponding experimental chapters.

2.1 Magnetoencephalography (MEG)

MEG records magnetic fields arising from the brain. MEG has excellent temporal resolution (greater than 1 sample per millisecond) making it ideal for measuring brain function, while also having good spatial resolution compared with similar non-invasive electrophysiological techniques (Hari, Hamalainen, Ilmoniemi, & Lounasmaa, 1991).

2.1.1 MEG Signal & Hardware

Neuronal function requires communication between huge numbers of neurons, termed neuronal populations. Both within and between population communication occurs via neurotransmitters, whose ultimate purpose is to depolarise (or repolarise) surrounding cells. A by-product of this is an electric current, which is either excitatory or inhibitory depending on the cells present (and synapse type and neurotransmitters present). These currents are referred to as either excitatory- or inhibitory- postsynaptic currents (EPSC, IPSC). When a number of these currents occur in parallel (spatially, for example within a population), a weighted portions' summation can be measured by EEG electrodes outside the scalp. The

neurons whose summed currents are actually detected is not equal and depends on the size, orientation and cortical layer in which they reside, which affects the field shape and is termed the lead field (Cuffin & Cohen, 1979). Furthermore, because electrical currents exhibit a magnetic field perpendicular to the direction of the current, given a large enough current (or sensitive enough measure) the magnetic field can also be measured outside the scalp (Baillet, Mosher, & Leahy, 2001; Hari & Salmelin, 2012; Hillebrand & Barnes, 2005; K. Singh, 2006), illustrated in figure 2.1.

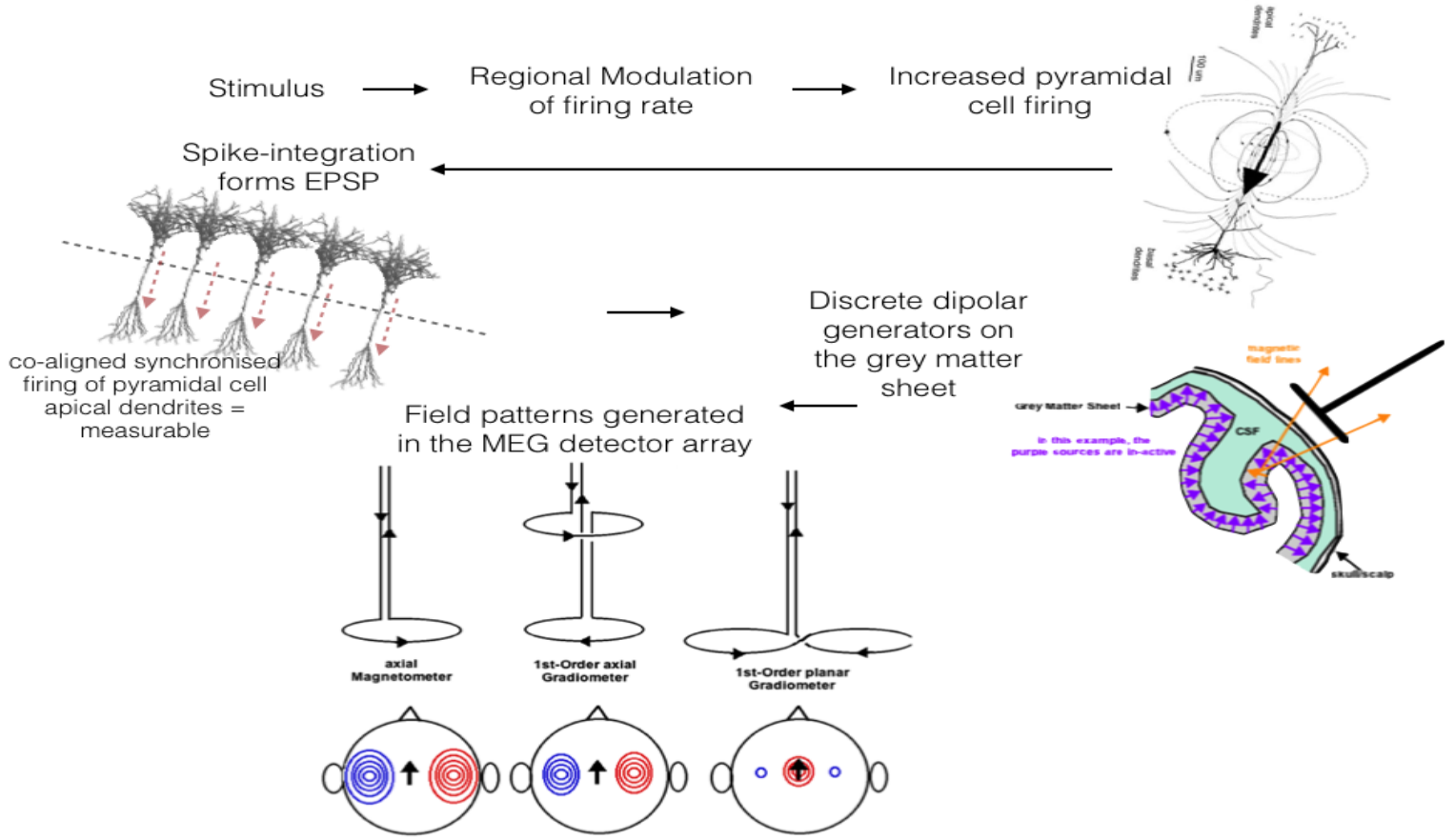

Figure 2.1. Overview of MEG signal generation. Adapted from Singh (2006) and Muthukumaraswamy (2014).

The MEG array comprises several super-conducting quantum interference devices (SQUIDS). Modern MEG systems have ~200-300 SQUIDS, which are made from superconducting material and resemble a ring with a section missing (a junction). These are kept at 4.2°K by immersing the array in liquid helium (inside the plastic head shape, the MEG *dewar*). At this temperature the SQUIDS are superconducting and allow current to flow across the junctions – this current is modulated by the external magnetic field threading the loop (i.e. a portion of the scalp recorded magnetic field). Modern MEG systems further utilise inductive coupling and pickup-coils (also superconducting) to amplify and direct the magnetic field to the SQUIDS (Robinson & Vrba, 1999; Vrba, 2001). Gradiometers (oppositely wound coils) are used as pick-up coils as this makes the SQUIDS more sensitive to specific gradients, and can thereby 'tune' them more towards known neuronal locations (the head), thus increasing sensitivity and decreasing environmental noise. Housing the MEG in a magnetically shielded room provides further noise isolation. While a full review of MEG hardware and physics is outside there remit of this thesis, the reader is directed to the works of Hari and Hamalainen, in particular, one of the first comprehensive reviews of MEG physics and methodologies, see Hamalainen *et al*., (1993).

2.1.2 MEG Signal Analysis

Once data collected by the SQUID array is converted to raw digital amplitudes, a number of steps are taken to make the data useful. For studies which aim to source-localise, that is, to estimate where signals came from in 3D space rather than the 2D distribution of the array, the predominant issues are the forward and inverse problems. If the position, orientation and magnitude of a neuronal current 'source' is known, then calculating what would be recorded at each SQUID site is possible, and referred to as the *forward problem*. Solving this problem requires a conductivity model of the head. However, source-localisation also requires 'solving' the *inverse problem*. The inverse problem refers to localising a current-source (in 3D space) given an externally measured magnetic field (outside the head) without knowing the whereabouts of the source. As such, possible solutions (source

current distributions) have to be constrained based on apriori knowledge (Hari & Salmelin, 2012; Hillebrand & Barnes, 2005; Vrba, 2001).

There are numerous approaches to solving the inverse problem, which rest on different assumptions about the brain sources (different apriori assumptions). These include dipole fitting procedures such as equivalent current dipole (ECD), multiple equivalent current dipole and dipolar scanning approaches. The analysis approach utilised throughout this thesis is that of beamforming (de Graaf, 2008; Vrba, 2001). Beamforming is a mathematical procedure, which, using data from the real sensors, allows synthetic placement of a *virtual sensor* over an exact region of interest and the production of synthetic data. The beamformer used throughout this thesis is the synthetic-aperture magnetometry (SAM) beamformer (Vrba, 2001), which is done by weighting the contribution each physical sensor can make to a virtual sensor using a covariance matric of sensor covariances, resulting in a set of *weights* – this procedure is illustrated in figure 2.3. Weights are calculated based on the covariance among sensors. As with all inverse problem solutions, beamforming makes some assumptions about the data – in the case of SAM, these assumptions are that the observed data are generated by discrete dipolar sources and that the time-series of these sources are not correlated. As such, beamformer analysis is not appropriate for analysis of paradigms that are known to evoke responses from temporally correlated discrete sources.

The SAM beamforming approach is not spatially constrained further than an approximation to the shape and conductance of the head, which is done by co-registering a 3D volume, obtained from a T1 anatomical MRI, to specific locations in the sensor array. The result of limited special constraints is the generation of weights for every possible set of dipoles (source) in the source-space (brain space) at a set resolution (in this thesis, 4mm) (Hari *et al*., 1991; Robinson & Vrba, 1999; Vrba, 2001). Despite solving the forward problem for the entire brain space, typically only very few discrete virtual sensors are of interest in analysing the data. From a given virtual sensor, data is typically subjected to a spectral estimation such as the Fourier transform, or a parametric equivalent. An alternate method for

reconstructing time-frequency is to use the Hilbert transform, an amplitude envelope fitting procedure (figure 2.4). The resulting time – frequency – amplitude data can be used to test experimental hypotheses. The specific parameters used in time-frequency estimation and subsequent analyses differ between experiments and are therefore described in experimental chapters.

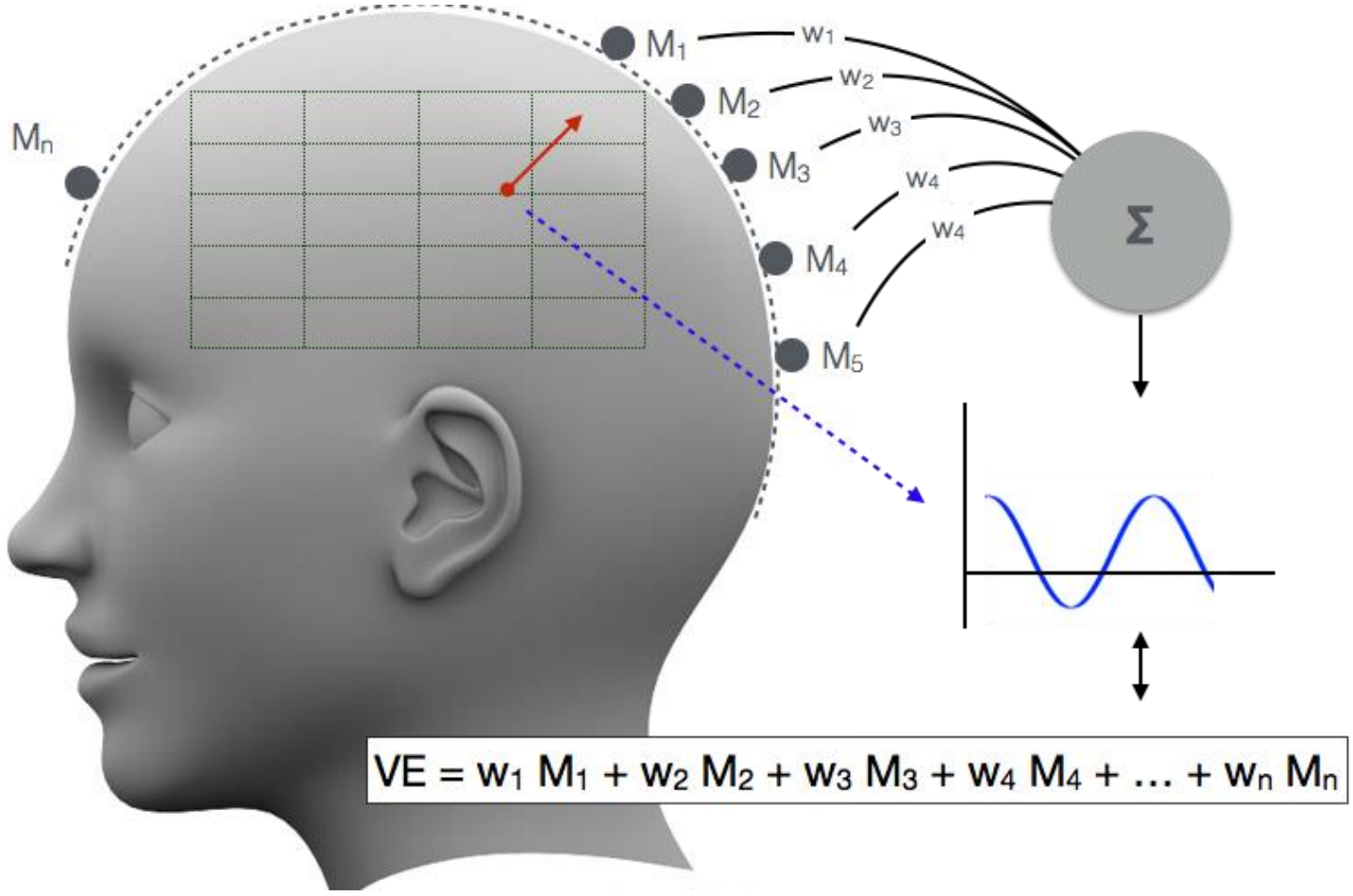

Figure 2.3. Based on that in Baillet *et al* (2001; 2012). Possible sensor contributions to the virtual electrode are weighted to optimise spatial sensitivity.

Another important consideration of MEG data analysis is whether the experimental paradigm produces evoked or induced responses. Both experimental designs tend to be trials based, that is, they involve repeating the same stimulus or task numerous times and averaging the signal over all the trials. Evoked responses are phase-locked to the stimulus onset. When all the trials (waves) are analysed, the peaks and troughs line up during averaging (figure 2.2). This type of evoked analysis is referred to as event-related field (ERF) analysis (or event-related potentials, *ERP*, in the case of EEG). Alternatively, some responses are not phase-locked and therefore simply averaging the 'waves' can flatten out the peaks and troughs (figure 2.2). These responses are, however, time-locked to the stimulus. For these responses, frequency or time-frequency estimation is required, permitting analysis of the amount of power within a certain bandwidth prior to averaging. These responses are referred to as *induced* with increases in power termed *event-related synchronisation* (ERS) and decreased power termed *event-related desynchronisation* (ERD) (Baillet *et al*., 2001; Pfurtscheller *et al*., 1999; Singh, 2006).

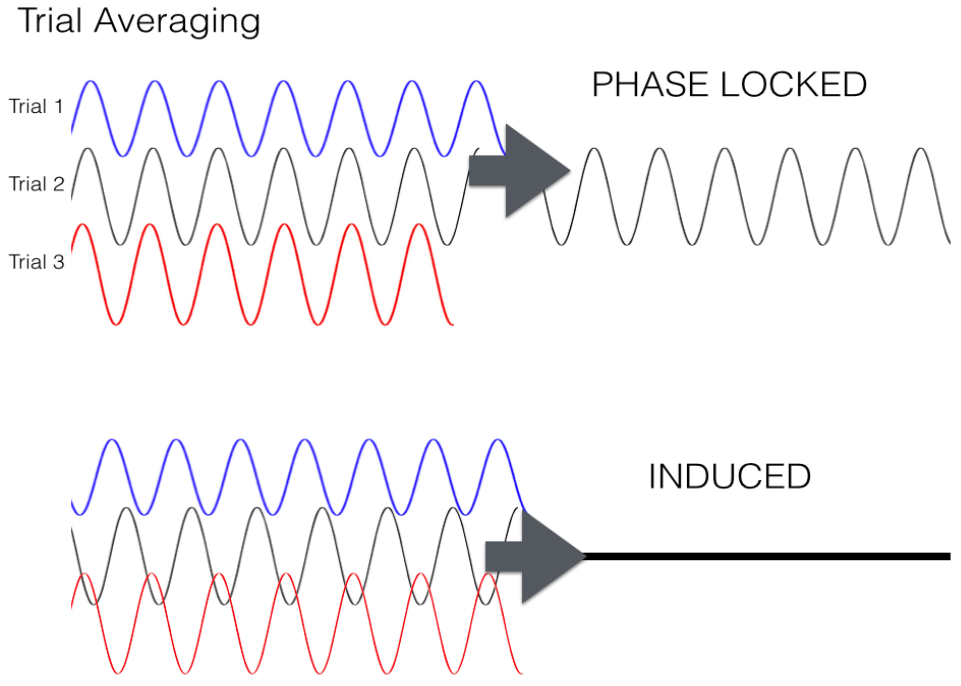

Figure 2.2. Evoked vs. induced responses. Simple trial averaging of induced responses can 'flatten' any stimulus-evoked response.

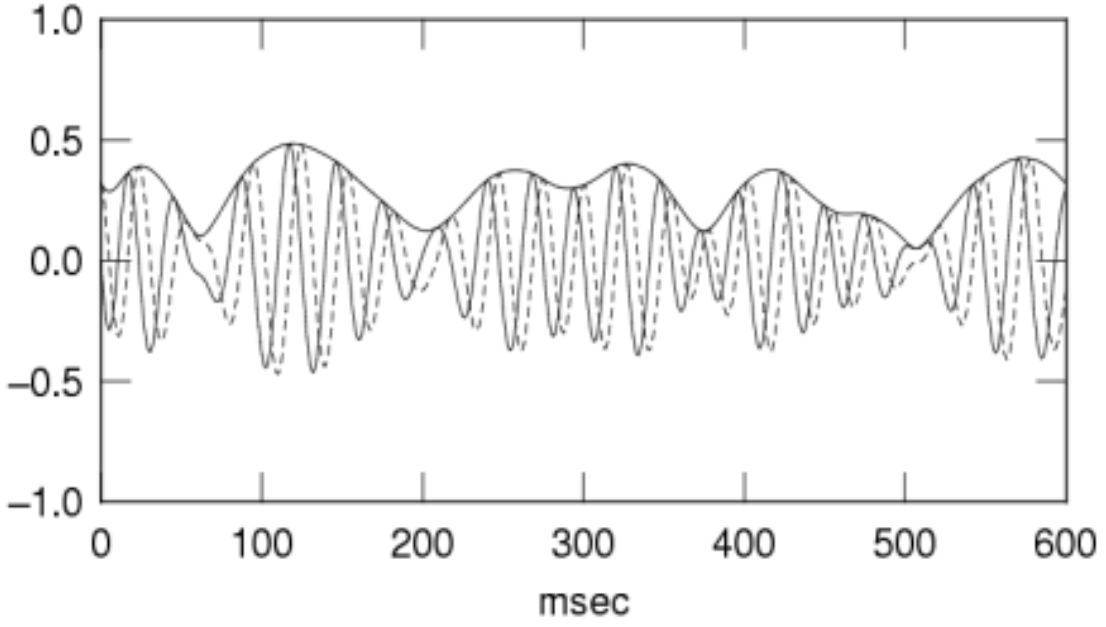

Figure 2.4. Demonstrating the Hilbert transform 'envelope' as the procedure of fitting a line across the positive amplitude peaks.

2.2 Magnetic-resonance Imaging and Spectroscopy

2.2.1 MRI Signal & Hardware

The core principal of Magnetic Resonance Imaging (MRI) is that it utilises a strong, uniform magnetic field along with radio-frequency pulses to manipulate the alignment and spin of hydrogen atoms. As such, the hardware comprising an MRI scanner includes a large magnet (static magnetic field, B_0), gradient coils for producing gradients in field B_0, and radio-frequency transmit- and receive-coils (field B_1) for rotating the magnetisation. The MRI scanner used throughout the experiments in this thesis is a 3 Tesla, GE Signa HDx, located at Cardiff University Brain Research Imaging Centre. While a brief introduction is provided, a full review of MRI physics is outside the scope of this thesis.

Both MRI and magnetic resonance spectroscopy (MRS) are nuclear magnetic resonance (NMR) techniques, relying on the concepts of magnetic resonance and chemical shift. Protons possess a positive charge and spin on an axis, producing a small electrical current and accompanying magnetic field. While the spin

orientations of protons are somewhat arbitrary, when placed in an external magnetic field, many of these spins are aligned in direction (or 180° from) of the applied magnetic field (magnetic moment). Application of a radio-frequency (RF) pulse disrupts this moment, changing the orientation of protons. Post RF pulse, protons re-align to the direction of the external field, emitting energy as they do. The strength of this signal is dependent on the number of nuclei affected by the process.

The most common implementation of MRS is ^{1}H-MRS (proton or hydrogen MRS). MRS utilises the same notion of proton resonance as MRI, but to obtain data on the neurochemicals instead of structure. Hydrogen nuclear spins resonate at different frequencies depending on chemical environment. Since a chemical's resonant frequency (chemical shift) is static, MRS protocols can be developed to target parts of the spectrum that these chemicals occupy (de Graaf, 2008; Mescher, Merkle, Kirsch, Garwood, & Gruetter, 1998). An example MRS spectrum is displayed in figure 2.5a. MRS spectra display the chemical resonance spectrum (x axis) in parts-per-million of the proton frequency (ppm) against chemical shift, so that resonances are stable across field strengths. The y-axis as signal intensity (corresponding to proportional metabolite concentration) (Puts & Edden, 2012). Due to individual differences, MRS neurochemical data are usually reported with reference to a reference chemical; most often water or creatine, since these are stable over time and easy to distinguish in the spectrum.

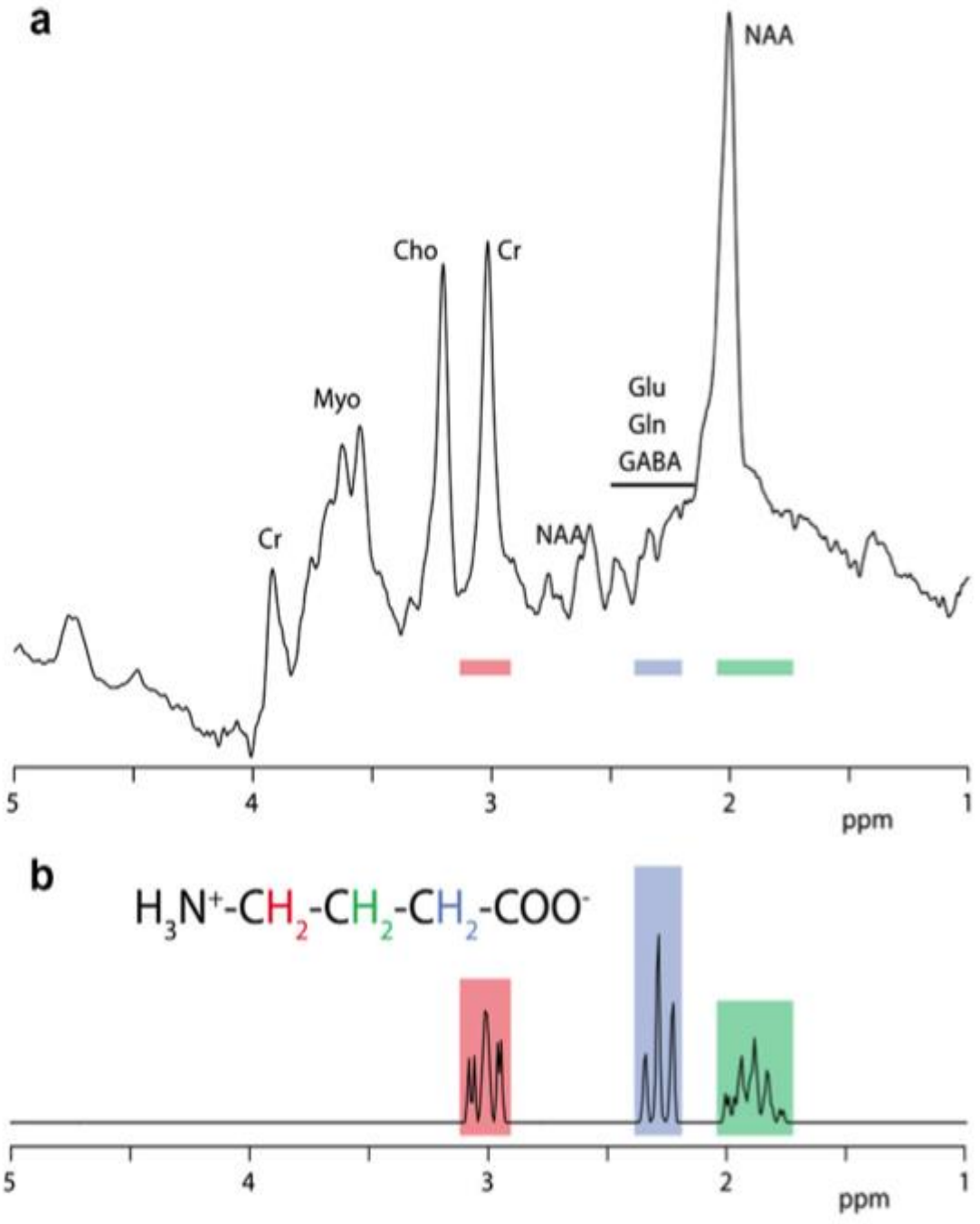

Figure 2.5. (a) a representative MRS spectrum. (b) Illustration of the problem of separation of chemicals, which have overlapping resonance at normal scanner magnet strengths. Taken from Puts (Edden, Puts, Harris, Barker, & Evans, 2013; N. Puts & Edden, 2012).

2.2.2 MRS Signal & Analysis

One of the main issues with MRS for neuroscience is that of multiplets. Multiplets occur because the neurochemicals of interest (e.g. GABA, glutamate, glutamine)

have overlapping spectra because of their similar structure. Furthermore, each chemical may contribute to multiple peaks. For example, GABA contains three methylene groups (figure 2.6), which correspond to three peaks in the MRS spectra (figure 2.5a/b). These peaks also happen to be overlapped by different, more abundant molecules (Cr at 3ppm, glutamine and glutamate at 2.3ppm and N-acetyl aspartate at 1.9/2ppm).

To overcome this overlap in the resonant frequencies, a spectral editing technique referred to as 'difference editing' is employed. The most widely used method, and that used in the experiments of this thesis, is a J-difference sequence, MEGA-PRESS (Fava & Team, 2006; Mescher *et al*., 1998).

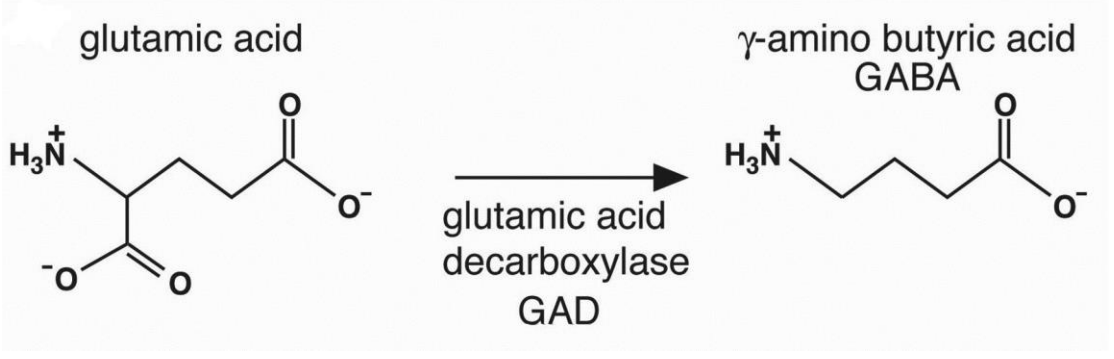

Figure 2.6. Illustrating the chemical similarities of GABA and glutamate, which are both structurally and metabolically, linked.

The GABA peak observed at 3ppm is coupled to that at 1.9ppm. The chemicals that overlap the 3ppm GABA signal, however, are not coupled to the 1.9ppm peak. Thus, a frequency-selective pulse targeting 1.9ppm will also affect the (GABA) coupled 3ppm signal. Difference editing involves obtaining spectra both with and without this frequency selective pulse. Subtracting one from the other results in difference-spectra, which contains only signals at 1.9ppm and signals that appear due to coupling (N. Puts & Edden, 2012). The resulting 3ppm GABA peak is still contaminated by homocarnisine and macro-molecular content, and as such is referred to as 'GABA+' (Edden *et al*., 2013), but is the closest to GABA currently possible.

Chapter 3. Visually evoked and induced oscillatory dynamics and neurochemistry in Remitted Depression

3.1. Abstract

Magnetic resonance spectroscopy studies have consistently demonstrated reduced cortical γ-aminobutyric acid (GABA) concentrations in individuals with major depression. However, evidence for a persistent deficit during remission, which would suggest that GABA dysfunction is a possible trait marker of depression, is equivocal. Although MRS measures total concentration of GABA, magnetoencephalography provides direct measures of neural activity, with cortical γ oscillations shaped by the activity of GABAergic inhibitory interneurons. In this study we investigated whether γ oscillations and GABA concentrations would differ in individuals with remitted depression (RD) compared with never depressed control subjects (ND)

Thirty-seven healthy, unmedicated female volunteers (n = 19 RD, and n = 18 ND) were recruited. The γ oscillation frequencies and amplitudes in the visual cortex, induced by simple grating stimuli, were quantified with time-frequency analyses. Distinct GABA/glutamate + glutamine MRS peaks were resolved from MEGA-PRESS difference spectra in prefrontal, occipital, and subcortical volumes. The RD and ND individuals did not differ in the frequency of subclinical depressive symptoms. The ND were slightly older (mean 23 years vs. 21 years), but age did not correlate with dependent measures.

There were no group differences in GABA levels or induced cortical γ measures. RD individuals had markedly reduced M80 (C1) components of the pattern-onset evoked response (46% reduction, Cohen's d = 1.01, p = .006). Furthermore, limbic GABA concentrations correlate negatively with hedonic tone in RD but not HC.

3.2 Background

Major depressive disorder is a chronic, relapsing condition with a kindling of depression vulnerability and severity over time. Antidepressant treatments acting primarily on the monoamine systems are not universally effective: and incomplete recovery increases the likelihood of recurrence. Our understanding of the neurochemical basis of MDD is still limited (Fava & Team, 2006; Hasler *et al*., 2007). Recent work reinforces the need for alternative or adjunctive pharmacological intervention that targets other neurochemical pathways.

In particular, gamma-amino-butyric acid (GABA), an inhibitory neurotransmitter, is increasingly implicated in the pathophysiology of major depressive disorder (MDD) (Alcaro, Panksepp, Witczak, Hayes, & Northoff, 2010; Kalueff & Nutt, 2007; Krishnan & Nestler, 2008; Luscher *et al*., 2010; Sanacora *et al*., 2003) . Several magnetic resonance spectroscopy (MRS) studies have measured cortical GABA levels during acute depressive illness: decreases of up to 40% have been reported in the occipital cortex (Croarkin *et al*., 2011; Hasler & Northoff, 2011; Sanacora *et al*., 1999), with greater reductions in more melancholic forms (Bhagwagar *et al*., 2007; Hasler *et al*., 2007). Antidepressant treatments, including selective serotonin re-uptake inhibitors (Bhagwagar *et al*., 2008; Sanacora *et al*., 2003) and electroconvulsive therapy (Hasler *et al*., 2005; 2011), but not cognitive behavioural therapy (Bhagwagar *et al*., 2007), have been shown to increase cortical GABA levels in depressed subjects.

While there is some support for altered GABA function in acute MDD, the issue of whether reduced cortical or subcortical GABA levels represent state or trait markers of MDD remains unresolved. MRS evidence is limited and conflicting on the presence of GABA dysfunction in remitted MDD. While Bhagwagar *et al* (2008) found that GABA levels in occipital cortex were approximately 10% lower than in healthy controls, Hasler *et al* (2005) found normal GABA levels in the prefrontal cortex compared to never-depressed individuals.

Neither study estimated GABA concentration in subcortical regions. This is in spite of a wealth of evidence demonstrating abnormal subcortical GABA function in animal models of depression (Kalueff & Nutt, 2007), the functional imaging literature in MDD (Drevets, 2003; Phillips *et al*., 2003) and a small study of [(11)C]flumazenil binding in MDD (Klumpers *et al*., 2009). Investigations of GABA levels in the subcortical regions of MDD individuals and their relatives are therefore warranted.

While MRS-GABA concentration is presumed to have an impact on brain function it does not distinguish between physiologically active and inactive GABA compartments. Furthermore, GABA function could be disturbed at the postsynaptic level in the absence of presynaptic changes in production or release. Additionally, MRS GABA is a combination of GABA and macromolecules. As such MRS GABA should be designated '*GABA+*' (N. Puts & Edden, 2012).

As described in section 1.4, cortical gamma oscillations, as measured by EEG or MEG, are thought to reflect patterns of change in the local field potential arising from an interaction of fast-spiking GABA-mediated interneurons with pyramidal neurons (Brunel, 2003; Spencer, 2009). These rapid oscillations increase during the efficient performance of a task. This reflects the role of the interneurons in coordinating the firing of relevant pyramidal cells in task-specific cortical regions, through the inhibition of non-task-related local activity and inhibition of inputs from extraneous networks. Their putative involvement in high-order cognitive function and perception (Adjamian *et al*., 2004; L. M. Ward, 2003) has led to a keen interest in their role in psychiatric disorders, where such functions are impaired. Using EEG and MEG, previous studies have identified abnormal in gamma band responses in the visual and auditory system of both schizophrenia and bipolar patients (Ethridge *et al*., 2012; Özerdem, Güntekin, Saatçi, Tunca, & Başar, 2010; Spencer, 2011), and abnormal gamma power in response to emotional stimuli in bipolar and unipolar disorders (Liu *et al*., 2012).

Previous work has demonstrated that gamma oscillations are reliably induced in the primary visual cortex by repeated to exposure to a simple visual grating image (Muthukumaraswamy *et al*., 2009). The frequency of these oscillations (the induced gamma frequency, IGF) is highly stable within individuals (Muthukumaraswamy *et al*., 2010), tends to correlate negatively with age across individuals, and demonstrates high heritability in twins (van Pelt *et al*., 2012). Furthermore, correlations have been demonstrated between IGF, occipital MRS GABA+ measures and BOLD responses to the same visual stimulus in healthy volunteers (Muthukumaraswamy *et al*., 2009). Hence, in healthy volunteers, MRS measures of GABA+ concentration translate to functional changes in the post-synaptic actions of interneurons in the cortex. The same might not be true of individuals predisposed to depression if independent pathologies exist at the synapse level, as opposed to synthesis level, of GABA function.

3.3 Experiment: Peak γ-frequency and GABA measures in remitted depressed subjects compared with healthy controls

3.3.1 Rationale

The aim of this study was to test the hypothesis that individuals with remitted depression (RD) differ from never depressed controls (ND) in IGF in the occipital cortex, and in MRS-GABA+ in cortical (occipital and prefrontal) and subcortical regions.

3.3.2 Methods

Recruitment and sample

Thirty seven healthy female volunteers were recruited through the Cardiff University School of Psychology Experiment Management System, a web-based recruitment facility accessed by undergraduates and staff of Cardiff University, an approved advert in the local Press and an through the University's electronic noticeboard. The School of Psychology ethics committee, at Cardiff University, approved the study. All individuals gave their informed consent to participate. Inclusion criteria included female gender, age 18-35, normal or corrected-to-normal vision and current good health. For the RD cohort (n=19) a previous history

of depression was determined using an adapted version of the MINI structured interview (Sheehan *et al*., 1998; Watson *et al*., 1995).

Exclusion criteria for all participants included current or previous psychiatric disorder, determined using the MINI, (depression excepted in the RD group), current use of psychotropic medication, dyslexia, contra-indications to MRI, organic brain disease and drug or alcohol dependence (determined by the MINI). For RD individuals additional information about number of previous episodes, treatments, admissions, symptom severity and self-harm was recorded in order to determine a lifetime severity score based on the Bipolar Affective Disorder Dimensional Scale, version 3.0 (BADDS 3.0; Buckby, Yung, Cosgrave, & Killackey, 2007; Craddock, Jones, Kirov, & Jones, 2004). Those individuals reporting a history of depression secondary to some other axis 1 disorder (anorexia, psychosis, bipolar, drug or alcohol misuse), organic condition or medication were identified by systematic interview and excluded.

Healthy controls were excluded if they had a first degree family history of MDD of bipolar depression, as determined using the Research Diagnostic Criteria, Family History Method (Andreasen, Endicott, Spitzer, & Winokur, 1977; Bredemeier *et al*., 2010). Using the RDC Method the first degree relatives must have experienced, in addition to at least 2 weeks of core depression symptoms, (a) suicidal behaviour, (b) gross impairment of work, housework, school attainment or social withdrawal, (c) ECT (electro-convulsive therapy) or antidepressant medication, or (d) admission to a psychiatric ward. All participants completed a measure of subclinical depressive symptoms in the form of the Mood and Anxiety Symptoms Questionnaire (MASQ) (Watson *et al*., 1995), which has clinical utility in young help-seekers (Buckby *et al*., 2007) and has been employed to screen for depressive disorders.

MEG recording and analysis

During the MEG sessions participants completed a slightly modified version of an established paradigm (Muthukumaraswamy *et al*., 2009), lasting approximately 8

minutes. One hundred and fifty identical visual stimuli were presented on a on a Mitsubishi Diamond Pro 2070 monitor (1,024 × 768 pixels and 100Hz frame rate). Optimised to induce gamma responses in the right primary visual cortex, they consisted of circular, vertical, stationary, maximum-contrast, 3 cycles per degree gratings, presented in the lower left visual field on a mean luminance background, subtended 4° both horizontally and vertically, with the upper right corner of the stimulus located 0.5" horizontally and vertically from a small red fixation point (figure 3.1). Participants were instructed to maintain fixation for the entire experiment and, to maintain attention, were instructed to press a response key as fast as possible at the termination of each stimulation period. The duration of each stimulus was 0.8–2.3s (mean duration 1.55s) followed by 1.5s of the fixation point only.

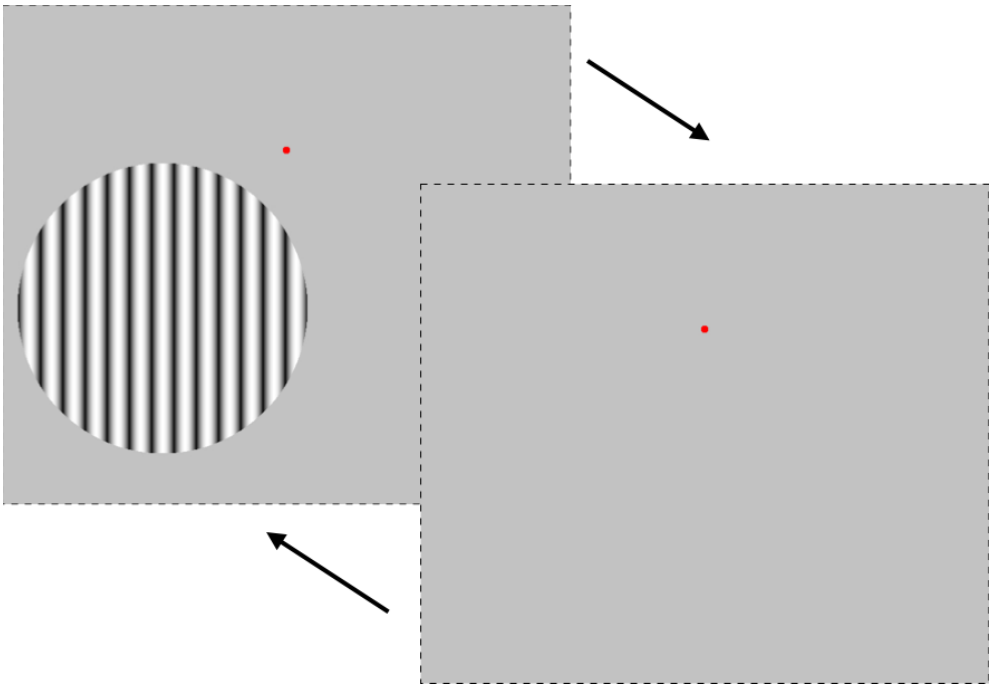

Figure 3.1. 100% contrast, 4 degrees, annular grating paradigm. Button pressed at grating offset.

MEG recordings were made using a 275-channel whole head MEG system in a magnetically shielded room. 29 reference channels were also recorded for noise-cancellation purposes and the primary sensors were analysed as synthetic third-

order gradiometers (Vrba, 2001). Three of the 275 channels were turned off due to excessive sensor noise. Before MEG recording, participants were fitted with three electromagnetic head coils at the two pre-auricular points and nasion. These fiduciary markers were located at specific points to the participant's anatomical MRI scan to enable MEG and MRI co-registration.

Offline, each dataset was band-pass-filtered using a fourth-order bidirectional IIR Butterworth filter into the following four frequency bands: 0 to 20 Hz, 20-40Hz, 40 to 60 Hz and 60-80Hz (Muthukumaraswamy & Singh, 2008). Beamformer analysis using Synthetic Aperture Magnetometry (SAM) was used to localise gamma power changes in the occipital cortex between baseline (-0.8 to 0s) and visual stimulation (0 to 0.8s) for the 4 frequency bands and a broader frequency band of 0-100Hz (Robinson & Vrba, 1999).

Each participant had their peak activity in the primary visual cortex located and virtual electrodes were generated for these locations by SAM beamformer reconstructions obtained using covariance matrices band-pass filtered between 0 and 100 Hz. Time-frequency analyses of these virtual electrodes were conducted using the Hilbert transform between 1 to 100 Hz in 0.5 Hz frequency steps and represented as a percentage change from the average baseline value (-0.8 to 0s) for each frequency band.

Mean responses across all trials were then represented against time and frequency in three-dimensional spectrograms, with the colour of responses representing the power of the response in % change from baseline. A typical spectrogram is shown in figure 3.2. Most spectrograms revealed distinct transient (0 to 0.3s) and sustained (0.3 to 0.8s) gamma band responses in the primary visual cortex, the peak amplitude of the transient response being of higher frequency than the sustained response, consistent with previous work (Gaetz, Roberts, Singh, & Muthukumaraswamy, 2012). Spectrograms with poor signal to noise ratio (indistinct gamma responses in contrast to the background noise) were excluded from the analysis. Mean transient and sustained gamma band

frequencies and amplitudes were then identified for the remaining n=18 RD and n=15 ND individuals using time resolved power x frequency plots (mean responses over 0-0.3 seconds and 0.3-0.8 seconds) across the gamma spectrum (40-100 Hz).

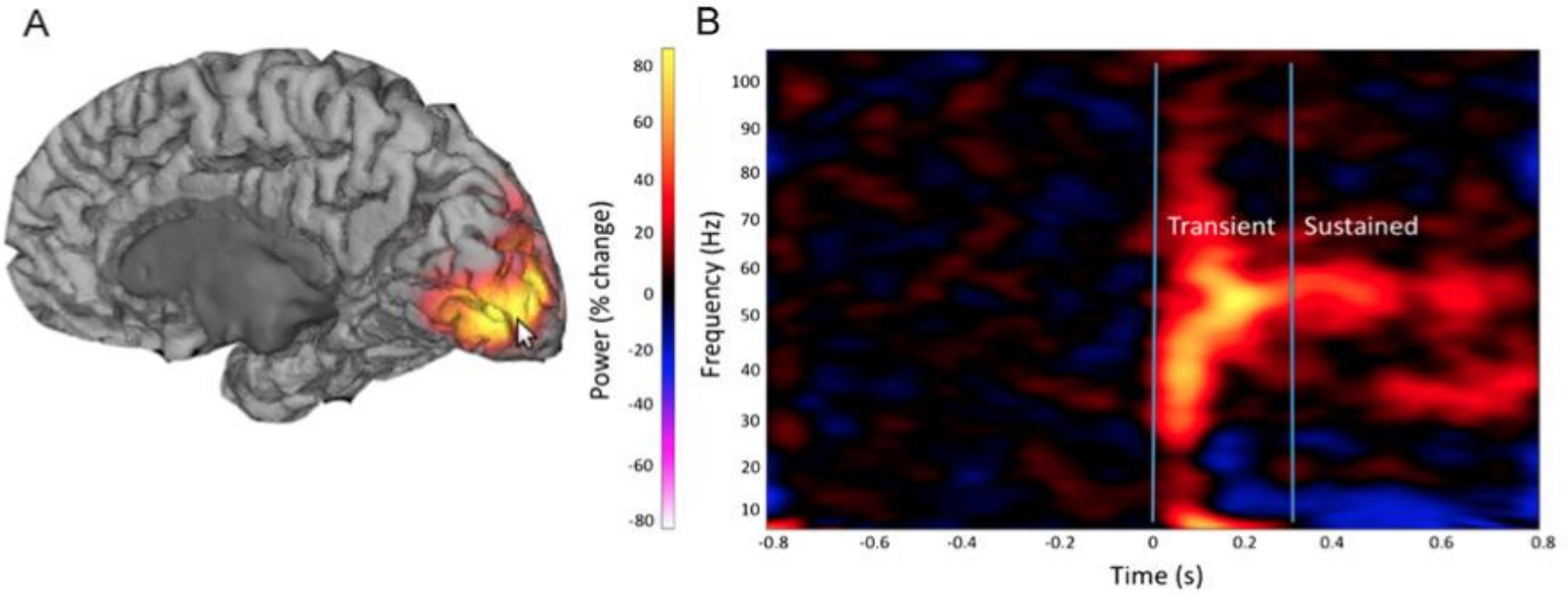

Figure 3.2. Typical MEG data from this experiment. A demonstrates virtual sensor placement (cursor point) over best-performing V1 region (yellow). B shows spectrogram of virtual sensor time-frequency reconstruction where colour heat-map is a function of power (% change from the baseline).

Magnetic resonance spectroscopy procedure

MR spectra were acquired on a GE Signa HDx 3T MRI scanner using the body coil for RF transmission and an eight-channel head coil for signal reception. MEGA-PRESS (Mescher *et al*., 1998) was used to acquire MR spectra in a left limbic volume of 3.0 x 3.5 x 3.5 cm^3 and two cortical volumes, each of 3.0 x 3.0 x 3.0 cm^3, in the left inferior frontal gyrus and bilateral visual cortex, for each subject. The limbic voxel included the striatum, subgenual cingulate, hippocampus, amygdala and thalamus.

These acquisition times provided the best trade off between participant comfort and signal-to-noise ratio, resulting in distinct GABA+ and GLX peaks of approximately Gaussian shape with stable baseline with TE = 68 ms, TR =1.8s, 256 transients of 2k data points, and 16 ms editing pulses applied at 1.9 ppm (ON) and 7.5 ppm (OFF). Data were processed using in-house software written in MATLAB; 4 Hz exponential windowing was applied prior to Fourier transformation. A Gaussian model was used to fit the GABA and GLX peaks in the difference spectrum, and concentrations were quantified in institutional units relative to the unsuppressed water peak from the same volume. Although the GABA+ peak is essentially a couplet it approximates well to a single Gaussian and alternative model fits (e.g. bimodal Gaussian fitting) provided no advantage over fitting to a single Gaussian.

To correct for variable amounts of CSF within the MRS voxels across participants (particularly for the subcortical voxel), high resolution anatomical images were acquired with a T1-weighted 3D FSPGR sequence (TR/TE/TI = 7.8/3.0/450ms, flip angle=20° FOV = 256*192*172mm, 1mm isotropic resolution, 8min acquisition time) during the same session as the MRS. The images were segmented in to white matter, grey matter and CSF using an established segmentation method for MR images (www.fmrib.ox.ac.uk/analysis/research/fast/). The reported GABA and GLX concentrations were scaled linearly to account for differences in CSF volume and variations in spectroscopy profiles for tissue and water (Geramita *et al*., 2011).

Higher-level analysis

Student's t test for independent samples was used to determine any differences in dependent measures between groups. We also examined correlations between IGF and occipital GABA+ measures across the whole sample.

3.3.3 Results

The ND individuals were slightly older than the RD individuals (23 years (SD=2.6) versus 21 years (SD=1.5), t(35)=2.9, p=0.006) but the small variance in age did not correlate with any of the dependent MEG and MRS measures. Most individuals in the RD group met criteria for a history of melancholic depression. Thirteen of the eighteen RD individuals had a BADDS score of 60 or above, indicating a history of at least one severe depression (defined as eight or more depressive symptoms, or major depression accompanied by a serious suicide attempt, ECT treatment or hospitalisation (Craddock *et al*., 2004). Despite this, groups did not differ on current levels of general depression symptoms or anhedonia as measured by sub scores of the MASQ: mean General Distress, Depression (GDD) scores = 20.4 (RD) versus 18.5 (ND), (t(33)=1.0 p=0.30), and mean Anhedonic Depression (AD) scores = 60.0 versus 57.4, (t(33)=0.9, p=0.37).

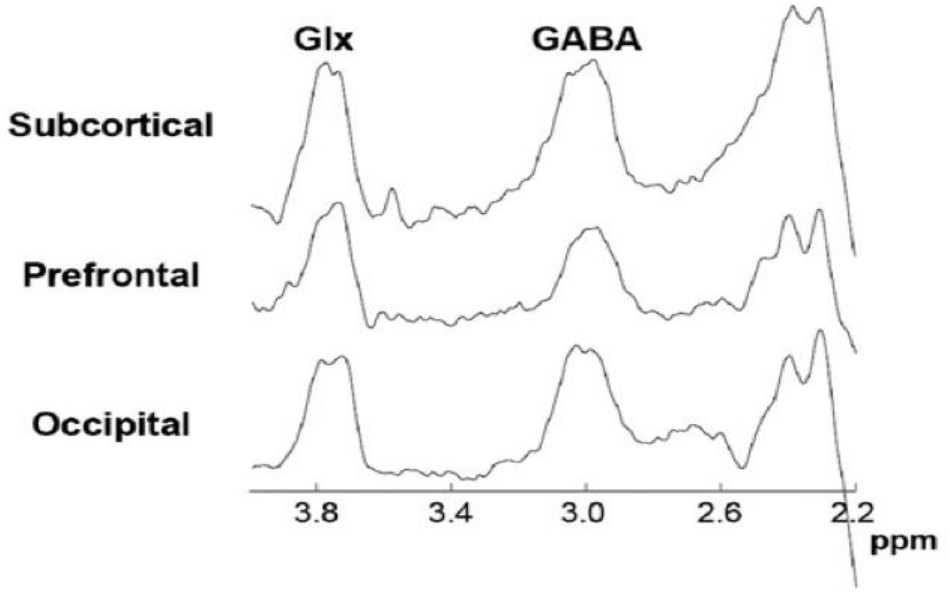

Figure 3.3 Representative MRS spectra from one participant with GABA and Glx labelled.

Representative (edited) spectra acquired from the three MRS voxels are shown in Figure 3.3. There were no group differences in occipital MRS-GABA+ ($t(32)=0.507$, $p=0.616$), IGF (transient, $t(31)=0.667$, $p=0.509$, or sustained, $t(30)=0.486$, $p=0.630$) or gamma power (transient, $t(30)=0.183$, $p=0.943$, or sustained, $t(31)=0.008$, $p=0.994$). In addition, there were no group differences in prefrontal or subcortical MRS-GABA+ measures ($t(34)=0.288$, $p=0.775$; $t(34)=1.346$, $p=0.187$). Figure 3.4 demonstrates pair-wise between-group differences in occipital GABA+ and IGF.

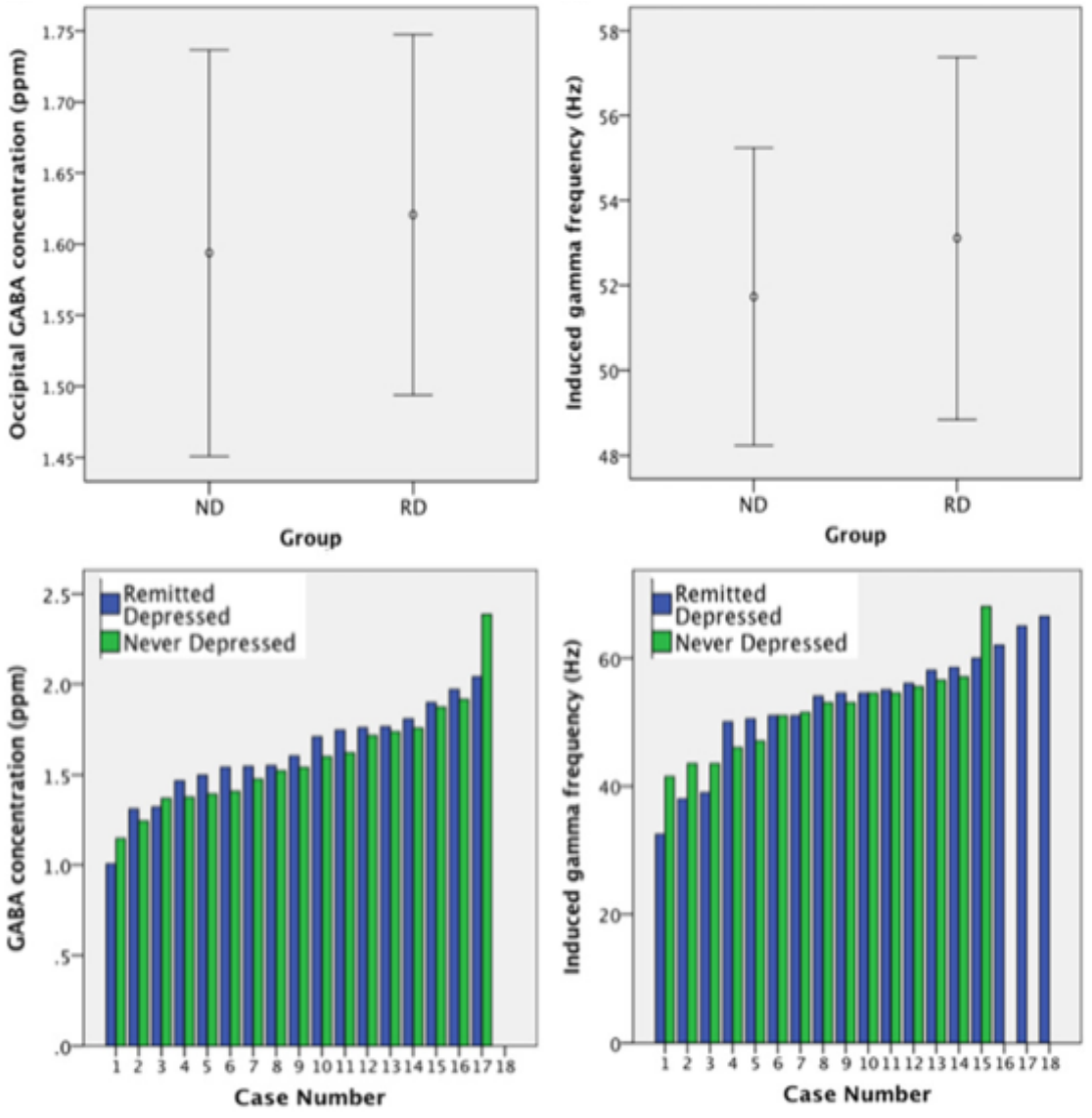

Figure 3.4. Pair-wise differences between groups for occipital MRS GABA and V1 IGF.

Time-resolved (transient and sustained) changes in power of MEG responses across the entire frequency range were calculated. Observation revealed a marked group difference in the power of the transient responses (0-0.3s) at approximately 10Hz, suggestive of a difference in evoked response (figure 3.5).

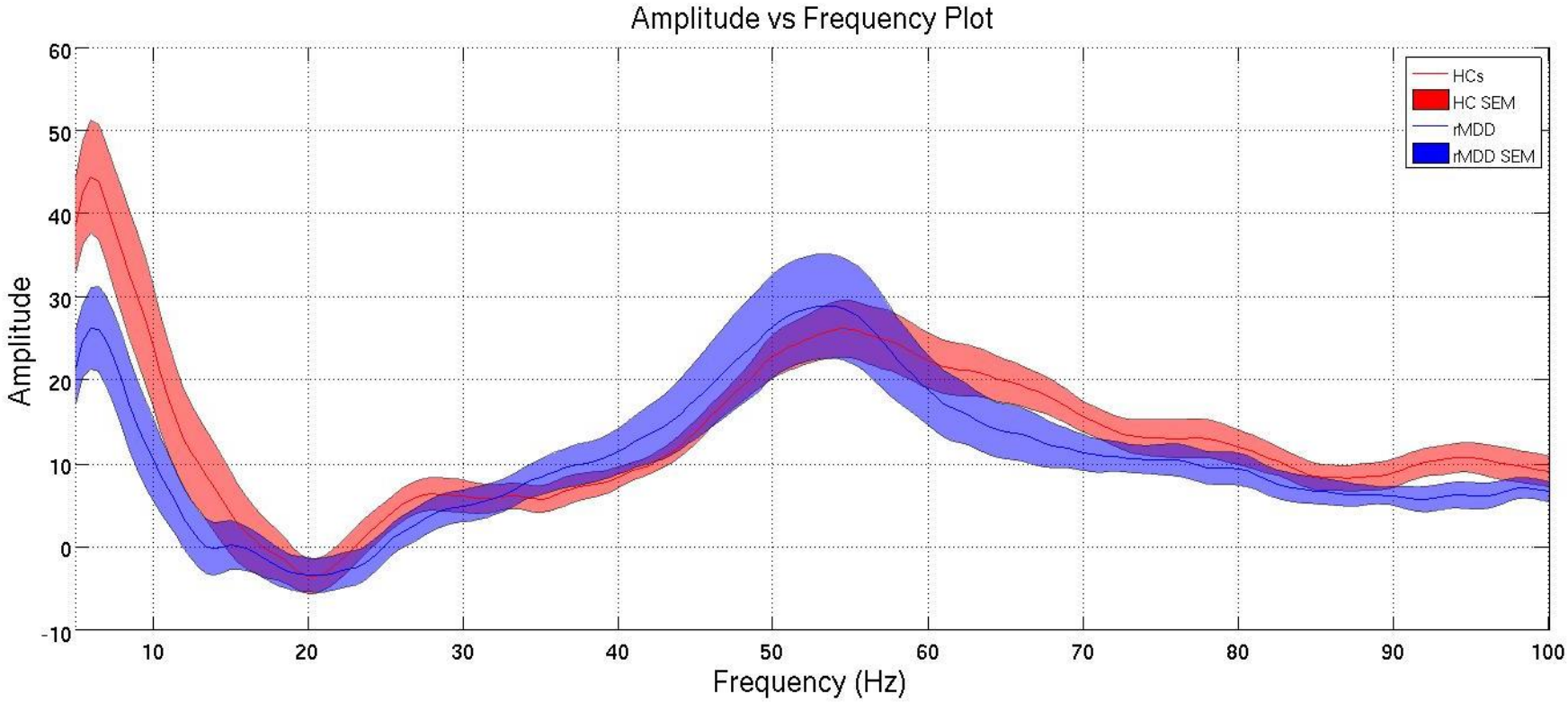

Figure 3.5. Mean power vs. frequency for each group (red, ND; blue RD). Evident difference in power between groups at ~5Hz.

3.3.4 Discussion

This is the first study to use IGF as a surrogate *in vivo* estimate of the action of GABAergic interneurons on cortical pyramidal cells in unmedicated RD, in combination with MRS measures of GABA+ concentration. It is also the first study to investigate GABA+ concentrations in RD in both cortical and subcortical regions.

The key finding is that remitted depressed subjects have normal IGF and MRS-GABA+ concentrations in the occipital cortex. Hence, two independent imaging measures support the conclusion that occipital GABA interneuron function is normal in young women with remitted, formerly severe MDD. Further observation revealed normal GABA+ levels in prefrontal and subcortical regions, suggesting that the lack of a GABA deficit in remitted MDD is not regionally specific.

These findings contrast with those of Bhagwagar *et al*. (2008), who found a reduction in GABA levels in the occipital region in RD. This contrasting finding could be due to several methodological differences. Firstly, this study used water as a concentration reference, whereas the former study used creatine. If creatine were affected by MDD, this could account for the discrepancy. Second, this study used a larger voxel size and longer acquisition, affording higher signal/noise ratio. Third, the former attempted to correct for the effect of macromolecules. Fourth, the former excluded non-recurrent depression, and participants were older.

These findings are broadly consistent with those of Hasler *et al*. (2005), who demonstrated normal prefrontal GABA levels in remitted MDD. As well as replicating their findings for prefrontal GABA levels (albeit with a more infero-lateral voxel), this study provides additional evidence of normal subcortical and occipital GABA+ levels and normal gamma oscillations, the latter providing a complementary surrogate marker of inhibition- excitation balance in the cortex. The sample recruited by Hasler *et al* (2005) was similar to this study in that it included younger individuals with single episodes of illness.

It is possible that the GABA deficits previously reported in RD (Bhagwagar & Cowen, 2007) represent a biomarker of more recurrent illness. Although this study found no significant differences in GABA+ levels between individuals with single episode or recurrent illness, the study was not sufficiently powered to examine this question. Alternatively, the GABA deficits might represent markers of longer illness duration per se.

A recent study employed MRS to measure GABA levels in the parieto-occipital cortex of a similarly aged cohort of never- depressed young adults with a parental history of MDD (Taylor *et al*., 2011a). Family history is the most established risk factor for MDD. However, no difference in GABA levels was reported between this group and an age-matched group without a family history of MDD. Considering these findings, together with those presented here, and those of Hasler *et al* (2005), it might be concluded that any GABA deficits observed in acute MDD reflect state as opposed to trait biomarkers of illness.

3.4 Experiment: Marked reductions in early visual evoked response in remitted depressed subjects compared with healthy, never depressed controls.

3.4.1 Rationale

The previous section detailed an experiment focussing on differences in GABA and IGF, in remitted depression. Another common approach to analysing cortical responses derived from this type of visual data is that of VEP/Fs. VEFs typically reference early ERPs in the visual cortex and are linked with basic level stimulus encoding and attention. Despite this, alterations of their latency and amplitude have been demonstrated in current-episode major depression as well as other psychiatric illness.

3.4.2 Methods

The sample consisted those remitted depressed subjects and never-depressed controls described in experiment 3.3. Virtual sensor data from the aforementioned visual grating paradigm were used to assess pattern-onset VEFs. Virtual sensor data were averaged across trials and evoked fields flipped so that the large ~100ms response, M100, was positive going.

3.4.3 Results

Large group differences were evident in the time locked (evoked) responses 80 milliseconds after the visual stimulus (the M80 or C1 response). Baseline-corrected evoked amplitudes revealed a 46% decrease in the mean M80 visual evoked response in the RD group compared to the ND group (Cohen's D = 1.01, $t(31) = 2.92$, $p = 0.006$; 95% confidence intervals of the difference = 14%-78%). Mean evoked amplitudes for both groups are shown in Figure 3.5. The size of the group difference is further illustrated in figures 3.6 and 3.7, where ranked amplitudes for n=14 RD and n=14 ND individuals are contrasted. Samples of equal size were selected on the basis of age, by excluding the oldest ND individual (whose age, at 31 years, was more than 2 standard deviations from the mean) and the three youngest RD individuals (aged 19, 20 and 20 years). The resulting mean ages of RD and ND groups were 21 years (SD=1.6) versus 22 years (SD=1.7), respectively). Bootstrapping with 1000 iterations confirmed a significant group difference at p=0.016. M100 amplitudes were not correlated with lifetime severity of illness (BADDS scores) in the RD individuals (r=0.087, p=0.733).

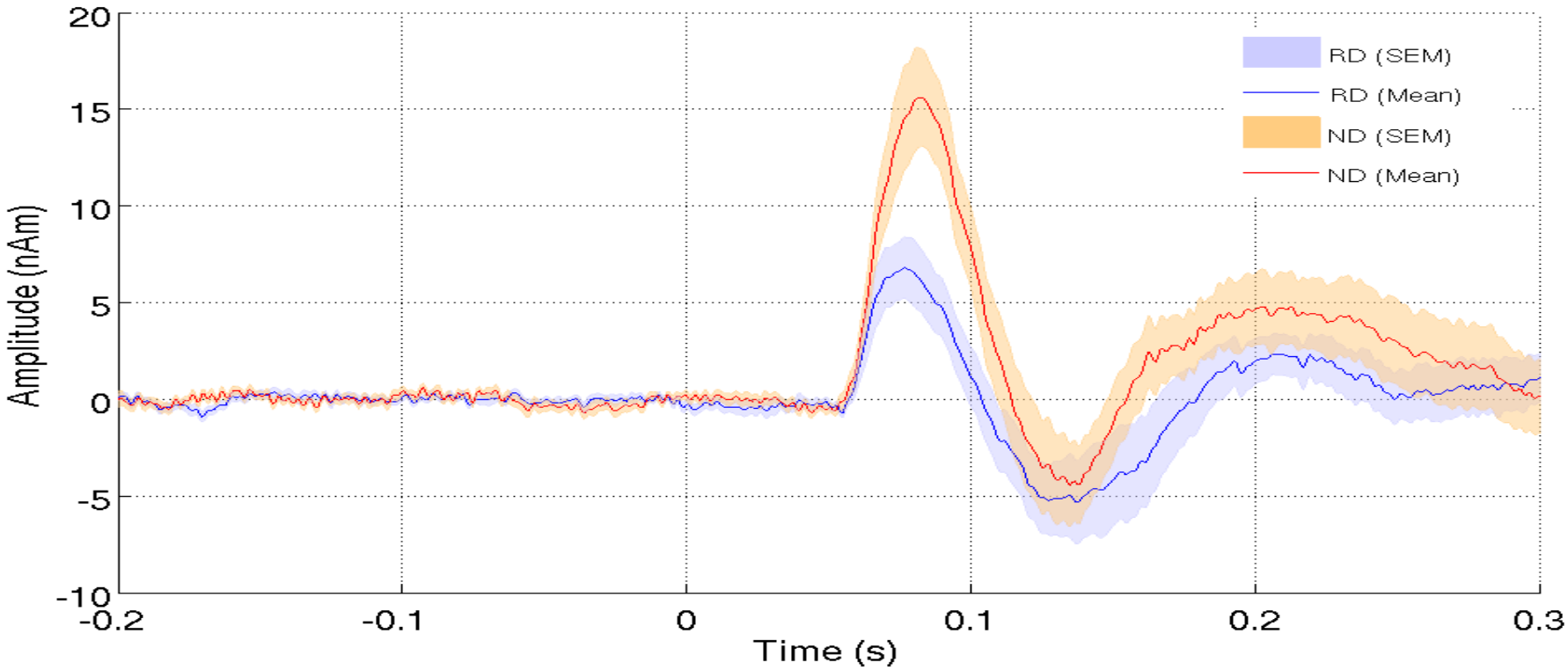

Figure 3.6. Evoked spectra for the visual evoked response. At 80ms the amplitude of RD subjects (blue) is 46% less than ND (red).

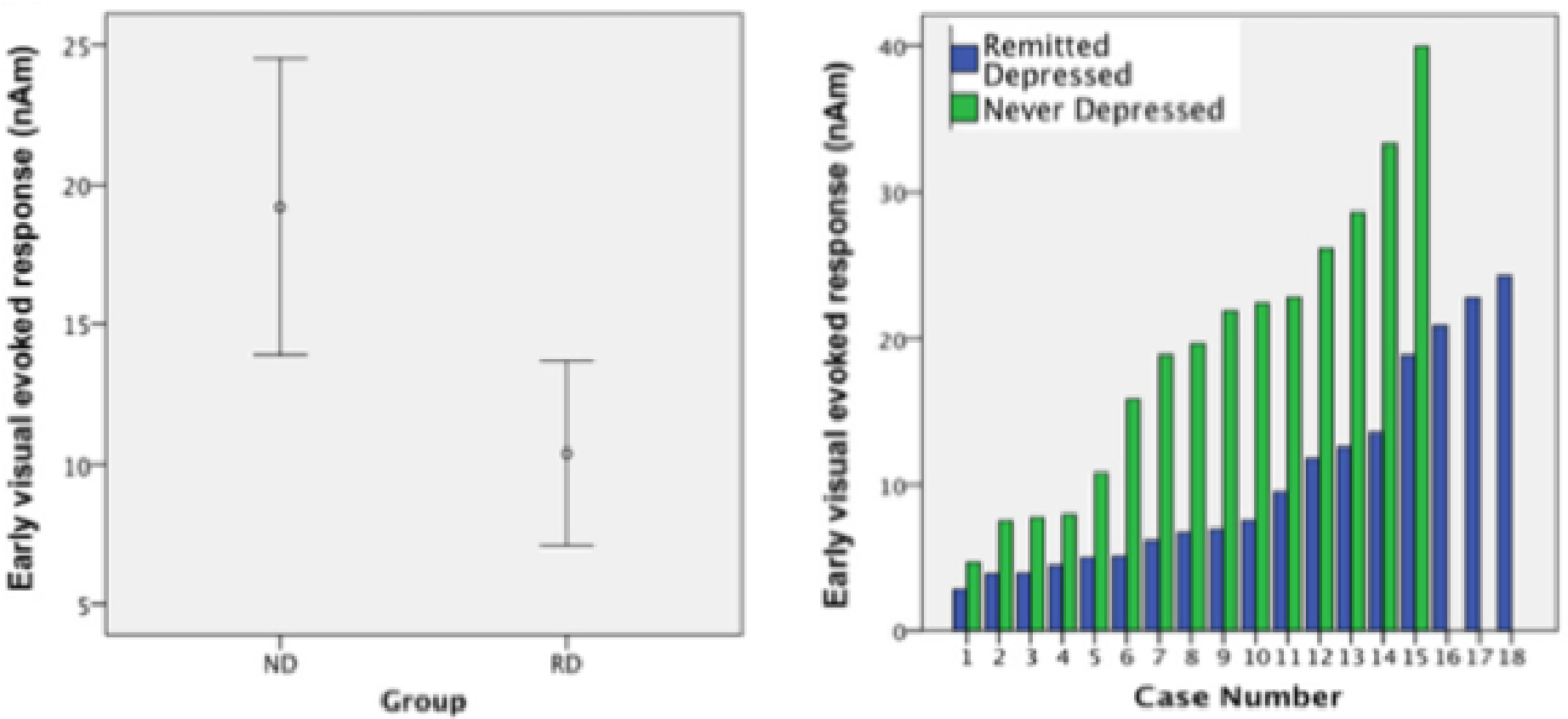

Figure 3.7. 14 age matches RD and ND subjects' amplitude at 80ms, obtained from the virtual sensor over V1.

3.4.4 Discussion

The key finding presented here is that remitted depressed subjects demonstrated a 46% decrease in the C1 (M80) component of the pattern-onset visual evoked response, compared with the never depressed controls. This is particularly striking, given that subclinical depression symptom scores in the RD individuals did not differ from the normal, never-depressed population.

The pattern-onset VEF is generated predominantly by dorsal stream projections to V1. In the RD individuals, M80 VEFs were not correlated with indices of illness recurrence or severity. This supports the proposition that early VEF suppression is not state-dependent and could be a trait marker of MDD.

Similarly, reduced amplitudes of early (pattern-reversal) VEFs have been reported in acute depression, which are putatively explained in terms of reduced glutamate-mediated plasticity (58). With the 3T MRI utilised in this study, separation of glutamate from similar compounds (glutamine, GABA) is not possible, however higher-field MR technologies enable this.

It is now imperative to determine whether the early VEFs deficit observed in acute and remitted MDD is also present in individuals with a first-degree family history of depression; follow-up studies would determine its value in predicting future depression.

3.6 General Discussion

This study had some limitations. Personal history of depression was determined retrospectively and not from clinical records. However, this study utilised a valid structured interview to determine the diagnosis, and it was observed that the individuals had good recollection of their symptoms. Poor quality or incomplete case records are less reliable than a structured interview. It could be argued that in selecting unmedicated RD individuals this study was biasing the sample toward a

less severely ill population. However, the great majority had experienced severe episodes. The main advantage of selecting unmedicated individuals is that confounding influences of medication on imaging and behavioural measures can be excluded. For example, there is preclinical evidence to suggest that antidepressants alter GABA function, independent of illness (Gotlib & Hamilton, 2008; Sands, Reisman, & Enna, 2004). Only a small number of the sample (n=6) presented here had experienced recurrent depression, consistent with their young age.

There is some evidence to suggest that GABA measures are affected by the follicular phase of the menstrual cycle in women (Epperson *et al*., 2002), which would have added noise to the data and diminished the ability to determine group differences. However, GABA values did not differ between individuals taking the oral contraceptive pill, where the follicular phase is suppressed (n=15), and those not taking the pill ($p<0.5$), and variances were comparable. This argues against a significant effect of the menstrual cycle on the data. The GABA measure included contributions from coedited macromolecules, a limitation of MEGA-PRESS at 3T. Methods for correction entail a penalty in signal/noise, acquisition time, and/or make modelling assumptions, affecting reproducibility (O'Gorman, Edden, Michels, & Murdoch, 2007). However, macromolecules are unlikely to mask any effect of remitted MDD on neurotransmitters. Shimming was difficult in the subcortical region, reflected in higher linewidth and reduced signal/noise ratio.

In summary, evidence from two independent imaging measures supports the conclusion that any GABA deficits observed in acute depression do not represent trait markers of illness. However, this study presents evidence to suggest that early visual evoked potentials are markedly reduced in remitted depression and might prove to be useful trait markers.

Chapter 4. Oscillatory dynamics of face processing in Remitted Depression

4.1 Abstract

Healthy and remitted-depressed participants performed explicit and implicit emotional face discrimination tasks while in a MEG scanner. ERF and induced gamma measures were analysed for between group differences. Whole-brain independent group tests on beamformer images revealed gamma frequency band (>30Hz) power increases in left insula in remitted depressed (RD) compared with never depressed (ND) subjects in response to fearful faces but not to sad, happy or neutral faces. Magnitude of gamma response to fearful faces in left insula correlated negatively with local grey matter volume in ND but not RD. Greater gamma oscillatory power in the left insula while explicitly discriminating fearful faces demonstrated in remitted depressed subjects compared to controls demonstrates a new role for the insula in face processing.

ERF analysis demonstrated decreased M300 (P300) amplitude in right middle-occipital gyrus during implicit emotional face tasks in RD participants compared with ND controls, across all face conditions (i.e. irrespective of emotion) and in two separate paradigm recordings. A reduction in M300 amplitude during implicit but not explicit emotion processing in remitted depression may reflect the negative-emotion bias associated with depressive disorders and suggests that this may be a trait marker of depression.

4.2 Background

Functional neuroimaging studies have demonstrated that the anterior cingulate cortex (ACC) is associated with both processing and experience of emotion, whilst the dorsolateral prefrontal cortex (DLPFC) is associated with regulating emotion (Gotlib & Hamilton, 2008; Phillips *et al*., 1997). The ACC, DLPFC, orbitofrontal cortex (OFC), ventral medial prefrontal cortex and limbic structures (amygdala, insula, putamen, nucleus accumbens, parahippocampal gyrus) have been

repeatedly reported to demonstrate different activity in depressed participants compared with healthy participants across a wide range of paradigms designed to probe specific aspects of behaviour.

Behavioural studies have demonstrated that the '*mood congruent emotion processing*' commonly observed in depression is reflected by responses to emotional face discrimination tasks. Depressed subjects show a robust bias in facial emotion recognition whereby neutral expressions are interpreted as sad, and happy faces interpreted as neutral. (Bourke, Douglas, & Porter, 2010; Chen *et al*., 2009)

Face processing models, informed by behavioural and imaging data suggest a 2-part system. The first component is primarily concerned with visual analysis of variable and fixed facial features and comprising the inferior occipital gyrus, fusiform gyri (including FFA) and superior temporal sulci. The second, higher-level component processes information about the face, such as emotion, and comprises the aforementioned emotion-related structures of the limbic system and OFC (Stein *et al*., 2007; Stuhrmann, Suslow, & Dannlowski, 2011). Abnormalities have been demonstrated in both parts of this processing system in depression. Current models suggest that emotion identification associated regions (amygdala and OFC) exhibit increased activity in depression while emotion regulation associated regions (DLPFC and ACC) exhibit decreased activity.

A further structure implicated in face processing is the (bilateral) insula. Imaging studies have demonstrated activation of the insula to faces exhibiting disgust (Phillips *et al*., 1997; Sprengelmeyer *et al*., 2011), and disgust and happy expressions (Chen *et al*., 2009; Takahashi *et al*., 2010). However, abnormalities of the insula cortices during face perception have largely been reported in anxiety disorders rather than depression (Stein *et al*., 2007). While evidence of a functional difference in insula cortex during emotion processing in depression is lacking, structural abnormalities have been reported (Sprengelmeyer *et al*., 2011). Reduced grey matter volume of the insula correlated with the magnitude of

disgust-recognition deficit (Sprengelmeyer *et al*., 2011). Furthermore, volumetric MRI has demonstrated reduced insular cortex volume in both MDD and RD subjects compared with healthy, never depressed controls (Takahashi *et al*., 2010).

The brain regions described thus far have been implicated in depression utilising functional MRI, however neurophysiological measures have also contributed to the face processing literature. One component of the ERP, the negative-going 170ms response (N170) is considered face-specific and localised to the fusiform gyrus (or fusiform face area), occipital face area and/or middle occipital gyrus. The face-specificity of this response suggests it represents some aspect of face processing, and its localisation to a predominantly visual region might suggest it reflects some aspect of facial feature processing (Wong, Fung, McAlonan, & Chua, 2009). Despite this, there is some contention over the role of the N170 as some have demonstrated manipulation of the response using emotional face stimuli (Monroe *et al*., 2011) and others have demonstrated manipulation by spatial attention (Mohamed, Neumann, & Schweinberger, 2009) while others have argued that by controlling for inter-stimulus perceptual variability, the N170 is actually not face specific (Thierry, Martin, Downing, & Pegna, 2007).

Besides the N170, alterations of the P300 have also been reported in depression. The P300 is regularly elicited by auditory odd-ball paradigms (Squires *et al*., 1975), with alteration of this component reported in depression, anxiety (Boudarene, 1997), schizophrenia (Morstyn *et al*., 1983) and other psychiatric disorders. More recently the P300 has been studied as a component of face processing, with reduced P300 amplitude reported in depression for processing of happy and fearful faces compared to neutral faces (Cavanagh, & Geisler, 2006). This suggests that the P300 component plays one of two roles: it may contribute to higher-order processing, rather than early-component feature encoding, and therefore reflect emotion processing; or, it may suggest that the processing dysfunction observed in depression starts early-on in the processing stream, and may therefore be independent of facial expression.

Besides stimulus-evoked activity measures (i.e. phase locked to stimulus), stimulus-induced measures have also been investigated in response to faces. Lee *et al* (2010) investigated differences in γ-oscillatory activity in healthy, major depression (MDD / unipolar) and bipolar disorder participants during an implicit emotional face discrimination task. The task consisted of 4 facial expressions (sad, angry, happy and neutral) and participants were instructed to pick the gender of each face. MDD participants demonstrated significantly decreased γ-oscillations in left parahippocampal gyrus and right middle temporal gyrus, along with an increase in γ-oscillations in left superior temporal gyrus, left cuneus and right precentral gyrus. The authors suggest this represents an over-activation of bottom-up appraisal mechanisms, which might be associated with the generation of emotions in depressed subjects. However, a methodological concern of this study is the ability to spatially localise and discriminate between these structures of close proximity using MEG (as compared with fMRI) due to the inverse problem.

While dysfunctions of (emotional) face-processing regions have been associated with subjects currently suffering a depressive episode, whether these phenomena occur in remittance of depressive symptoms is an important question. The enhanced sensitivity to negative stimuli in depression has been suggested to persist in remittance in the form of enhanced sensitivity to negative feedback (Santesso *et al*., 2008). However, altered BOLD responses to emotional face tasks between current and remitted disease states have been demonstrated (Keedwell *et al*., 2009).

4.3 Experiment: Explicit and implicit emotional face processing tasks.

4.3.1 Rationale

Based on the above literature, it was hypothesised that differences exist in the ERF N170, later ERF components and induced gamma, during emotional face tasks, in RD participants compared with ND.

4.3.2 Methods

Thirty-seven healthy female volunteers were recruited from the staff and student body of Cardiff University. Nineteen had no history of depression while eighteen had suffered from depression but were currently remitted and unmedicated. All participants gave informed consent. Details of participants in this study have been reported in the previous chapter, thus a shorter description is included here. All individuals were aged 18-35, and had normal or normal-corrected vision. History of depressive symptoms and illness was determined using an adaptation of the Mini International Neuropsychiatric Interview (MINI) and Bipolar Affective Disorder Dimensional Scale (BADDS),

With the exception of depression in the remitted depressed group, participants were excluded if they had any history of psychiatric disorder, were taking psychotropic medication or had contra-indications to MRI/MEG scanning. Participants reporting depression as a secondary to some other axis 1 disorder were identified via interview and excluded.

MEG Paradigm, Recording and Analysis

During MEG recordings, participants completed three emotional faces tasks. These consisted of an explicit emotional face discrimination task and two implicit emotional face tasks. The explicit task entailed pseudorandom presentation of four facial expressions: fear, happy, sad and neutral. The face images were from the Ekman faces set (Young, Perrett, Calder, & Sprengelmeyer, 2002). Participants were instructed to respond with the displayed expression via a four-choice button box (left to right: fear, sad, happy, neutral).

The first implicit task entailed viewing 100%-intensity fearful, 50%-intensity fearful and neutral faces (as defined in the Ekman set). Participants were instructed to respond with the gender of the face. The second implicit task replicated the first, substituting the 100% and 50% fearful faces for 100% and 50% sad faces. The order of implicit tasks was counter-balanced.

Tasks ran for 150 trials where a face stimulus was displayed for 1500ms followed by 2500ms during which a question mark appeared on screen to prompt participants to respond. Participants were instructed to respond promptly and received an error message if no response was detected during the response time. Stimuli were displayed on a Mitsubishi Diamond Pro 2070 CRT monitor (1024 x 768 at 100Hz, physical screen size 450x300mm) at a distance of 2030mm. Faces were presented centrally at a visual angle of 6.556° horizontally and 7.486° vertically.

MEG was recorded with a CTF 275-channel whole-head MEG system and sensors were analysed as synthetic 3rd-order gradiometers (Vrba, 2001). Three sensors were switched off due to excessive noise. Fiducial points were marked using electromagnetic head-coils attached 1cm above the nasion and anterior to each tragus. These were used to co-register the data to an anatomical T1-weighed MRI (^{F}SPGR).

In order to analyse both event-related fields (evoked) and gamma oscillations (induced), a broad-frequency (10-100Hz) synthetic-aperture magnetometry (SAM) analysis was run on a 90-300ms time window (post-stimulus onset), after bi-directional Butterworth band-pass filtering into 20Hz windows between 0-100Hz. Merging all participants three dimensional functional maps into one four-dimensional file (i.e. X x Y x Z x participant) allows searching through all participants datasets to find common peaks suitable for a 'best-performing' virtual sensor placement in an objective manner. In house software was used to search across participant files in template space and find common peaks within a specific trap radius. Co-ordinates were translated back to individual MRI space for virtual sensor placement. Applying this pipeline to the explicit task data successfully identified common peaks in the right middle-occipital gyrus for fear, happy and sad face onset and left middle-occipital gyrus for neutral.

SAM analysis was run for gamma and event related analyses separately in order to maximise sensitivity (although used the same algorithm). SAM was on the 110-

400ms window post-stimulus onset on data band-pass filtered to the gamma range (55-150 Hz) with a baseline of -290-0ms. These images depicted gamma responses in several areas of cortex across participants and conditions. As such, a group-level approach was taken to gamma analysis. Using FSL Randomise, (Winkler, Ridgway, Webster, Smith, & Nichols, 2014) permutation testing (unpaired t-tests) were performed on 15 controls vs. 11 RD individuals for each face condition with 5000 permutations and 5 mm variance smoothing. This resulted in t-statistic and corrected p-value voxel maps demonstrating significant between-group differences across the brain.

For the ERF analysis, the same SAM algorithm was run on data band-pass filtered to low frequencies (1-30 Hz) with an active time 0-400 ms and baseline -290-0 ms. An averaged-statistical image revealed clear peaks in the occipital gyrus. Subsequent analysis found common peaks in left middle-occipital gyrus for fear, happy and neutral face onset, and right-middle occipital gyrus for sad face onset. Time frequency analysis of virtual sensors was performed and, in order to ensure ERF waveforms were not inverted, whole-wave flips were performed on the basis of the strong ~50-60ms deflection being positive. To extract peak amplitudes in a non-biased way, and to simultaneously correct for multiple comparisons, a permutation-based unpaired-t test analysis was performed in a sliding time window across each data point of the evoked spectra, (with 2000 permutations). This procedure was repeated for the implicit tasks analysis.

Whole-brain gamma analysis was performed using FSL Randomise and ERF analysis using a virtual sensor approach. For both sad and fearful implicit tasks, the virtual sensors were localised over source peaks in right middle occipital gyrus.

MRI Procedure

High-resolution anatomical T1-weighted 3D MRIs were collected on each participant using a GE Signa HDx 3T MRI scanner for co-registration of MEG data. The sequence consisted of repetition time 7.8s, echo time 3s and inversion time 450ms with a flip angle of 20° and field view 256 x 192 x 172mm, 1mm isotropic

resolution. Grey matter was quantified using the FAST (Zhang, Brady, & Smith, 2001) automated pipeline built into FSL (Smith *et al*., 2004).

4.3.3 Results

Sample Characteristics and Symptoms

Never depressed participants (ND) were slightly older than remitted depressed participants (RD), (ND 23, RD 20 [t(35)=2.2, p=0.032]) however age did not correlate with MEG measures. Further descriptive statistics in table 4.1.

	RD Group	ND Group	t	p
Age	20	23	2.2	0.0320*
BDI Score	5.07	3.39	-1.15	0.261
TAI Score	14.75	12.67	-1.2	0.242
No Episodes	2			
Melancholia	0.77			
BADDS Score	64.2			
Left Insula Y Power	1.5	0.2	5.12	0.0022*
Left Insula Grey Volume	6679	6898	1.158	0.255

Table 4.1. *Significant at alpha = 0.05.

Not all participant data was available for all tasks due to incomplete recordings, or the lack of a peak around which to place a sensor. Thus, for the ERF analysis, the explicit task sample consisted 15 ND and 11 RD. For the sad implicit task 16 ND and 14 RD and for the fear implicit task 15 ND and 15 RD. For the gamma analyses the explicit task consisted of 15 ND and 11 RD while the sad implicit sample consisted 17 ND and 14 RD and the fear implicit sample consisted 16 ND and 15 RD.

Button box responses were available for the implicit tasks, during which there was no difference in performance between the groups for the implicit tasks. Button box data for the explicit task was not available due to en error in experimental design.

4.4 Results: Increased left insula gamma power in response to fearful faces in formerly depressed subjects during an explicit face-processing task

The whole-brain group-level SAM analysis of the explicit task data revealed significantly increased γ- power in patients compared to controls in subcortical areas, with a peak in left insula cortex, in response to fearful face onset but not neutral, happy or sad faces ($t(25)=5.12$, $p=0.0022$, figure 4.1).

Gamma power at this location correlated negatively with left insula cortex grey matter volume collapsed across the groups ($r=-0.389$, $n=26$, $p<0.05$ after bootstrapping) however this was stronger in controls than patients ($R^2=33.9\%$ vs. 1.1% respectively, see figure 4.2) despite a lack of difference in insula grey between groups.

Difference (t-statistic) peaks in other regions were found for sad, happy and neutral face conditions, however these were not significant after correction for multiple comparisons. Whole-brain group-SAM for the implicit face tasks revealed significant clusters for each condition, however, none of these were significant after multiple comparison correction.

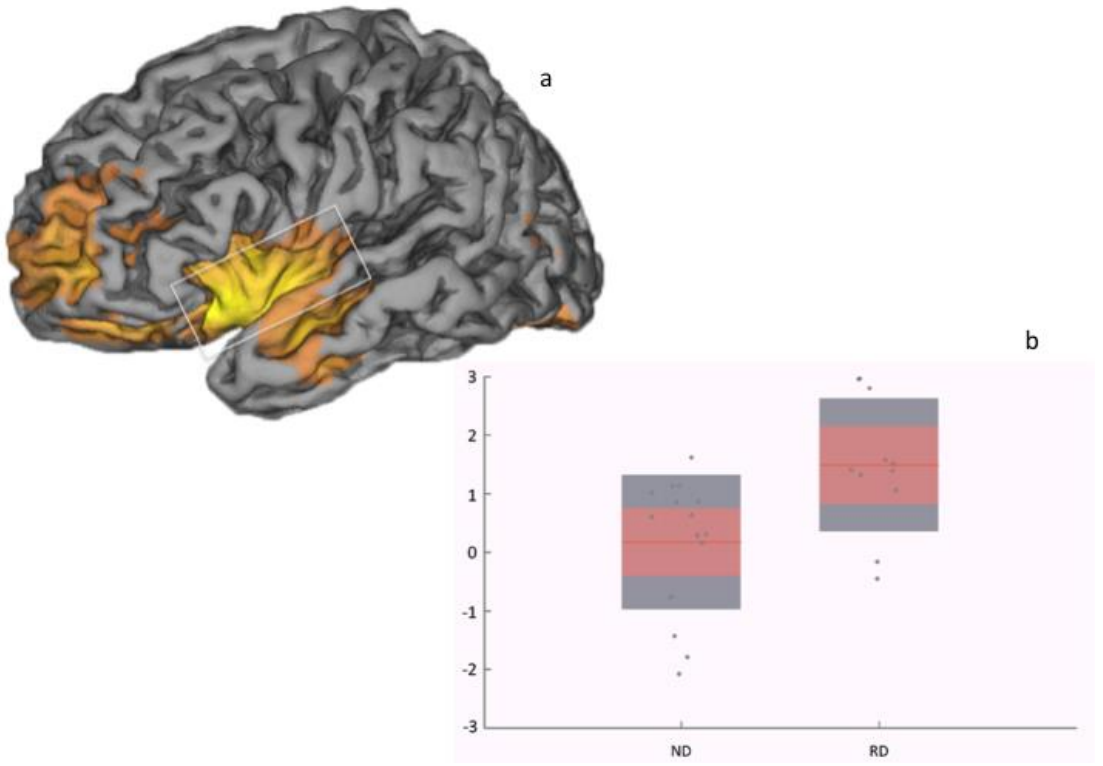

Figure 4.1. (a) Significant gamma power increases in left insula in patients compared to controls during the explicit task in response to fearful face onset (t-value cut off = 3).(**b**) Scatter diagram for never and remitted depressed groups. Pink bars represent 95% CI, grey bars demonstrate 1 standard deviation.

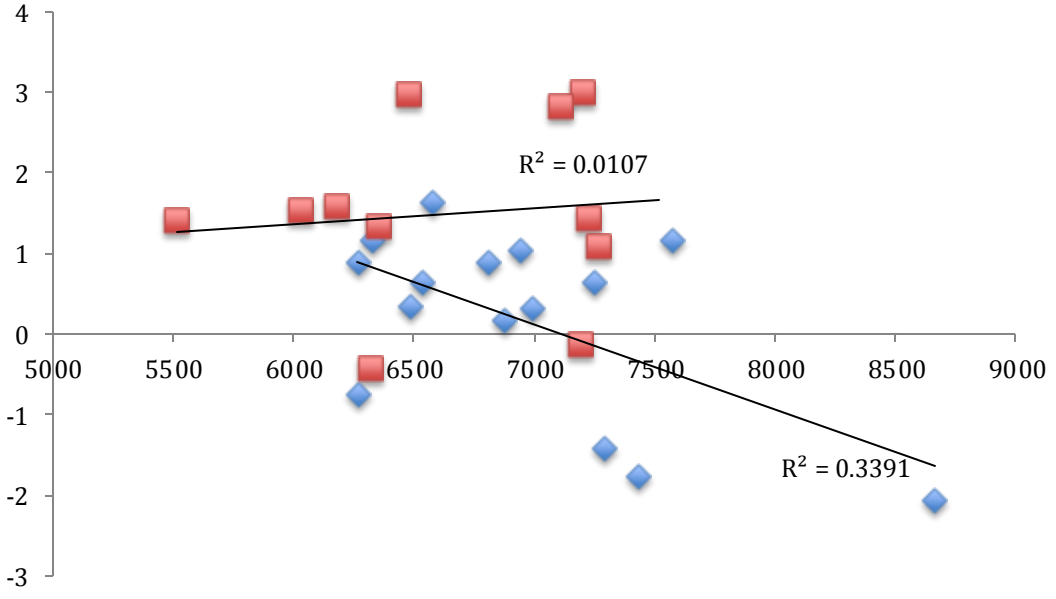

Figure 4.2. Scatter plot demonstrating correlations between left insula grey matter volume (x axis) and gamma power (scaled) in the same region in response to fearful face presentation. ND = blue, RD = red. Significant across the sample after bootstrapping.

Condition	Co-ordinate (TC)	Structure	t	P*
Fear	-31.1 15.1 -11	Insula	5.124981	0.0022**
Fear	27.1 -53.2 -9	Parahippocampal Gyrus	4.987974	0.998
Fear	-43.2 -69.3 -29	Left Fusiform Gyrus	4.213851	0.995
Happy	-13.1 -21.1 -7	Midbrain	4.134197	0.0976
Happy	-19.1 -79.3 55	Parietal cortex	3.204208	0.2366
Happy	35.1 -55.2 -15	Right fusiform gyrus	3.179447	0.1736
Neutral	19.1 -57.2 73	Right post-central gyrus	3.773767	0.071
Neutral	-23.1 -29.1 51	Left post-central gyrus	3.735057	0.0636
Sad	-23.1 -69.3 63	Superior parietal lobule	3.345065	0.405

Table 4.2. Explicit Task gamma frequency cluster peaks

*Showing multiple comparison corrected p-values.

** Significant at given p-value.

4.5 Results: Reduced M300 ERF amplitude in formerly depressed subjects during implicit face processing as compared with healthy, never depressed controls

One of the experimental aims was to localise the face-specific M170 response, as well as later components of the ERF thought to reflect higher-level (i.e. emotional processing) aspects of stimulus processing. Thus time points through the duration of the visual evoked response were statistically compared between groups where peaks were evident.

For the explicit task, the M170 was not clearly distinguished in all participants, or all conditions (figure 4.3) and hence was not tested statistically. The 170ms response emerged during the implicit face tasks (figure 4.3, lower panels). This was tested between groups, however, it was not statistically different in amplitude or latency for either implicit face task.

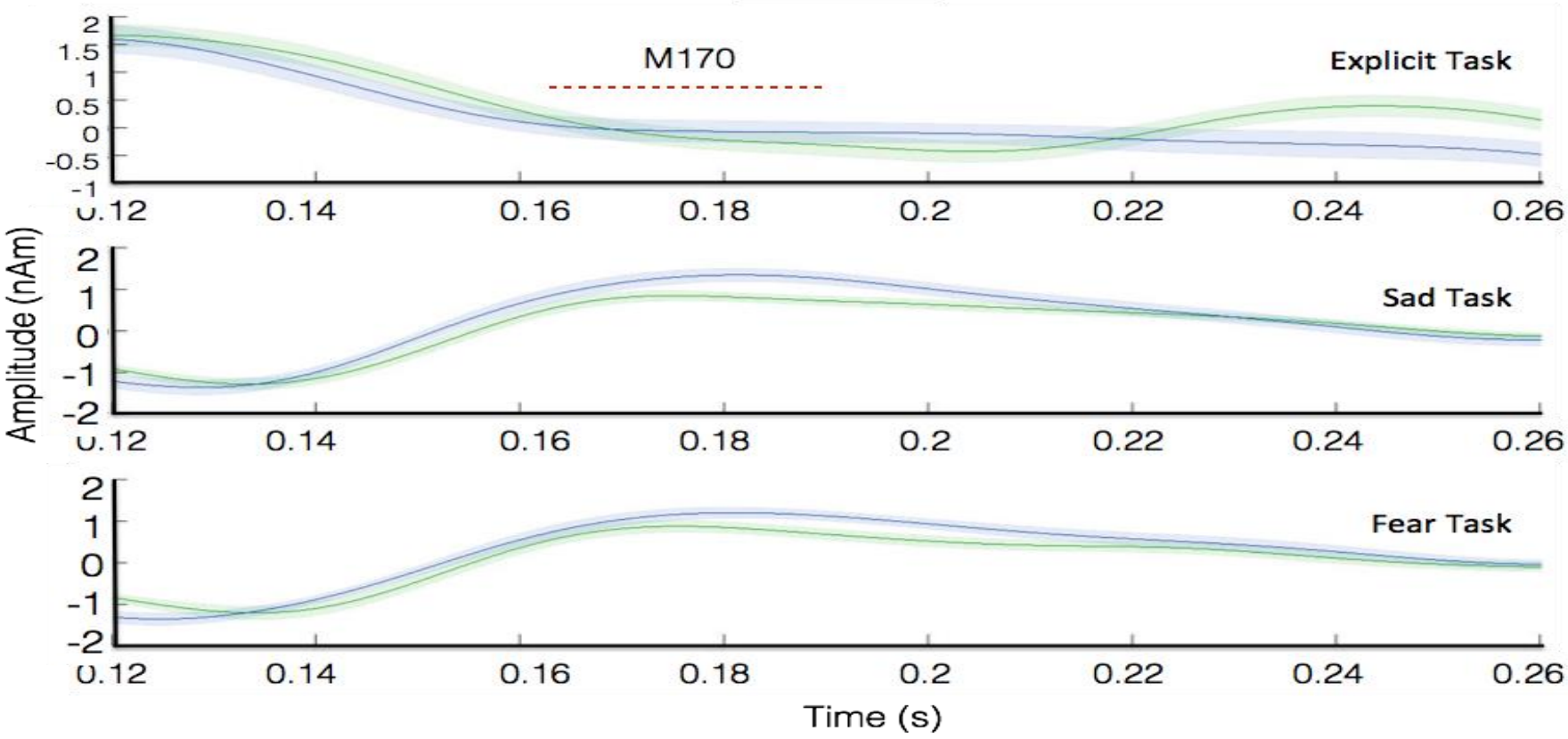

Figure 4.3. Event-related field time course around 170ms for each task. Blue = RD, green = ND. Face-specific M170 deflection evident for implicit tasks (sad and fear) but not explicit time course. NB. Waveforms collapsed across conditions.

Implicit tasks raw-spectra demonstrated a notable difference between groups for each condition at approximately 300ms. Subsequent analysis revealed decreased M300 (P300) amplitude in the RD group compared to ND in both sad and fear tasks. This was significant within-task when collapsed across conditions (i.e. full, mild and neutral intensities, figure 4.4) and also across task (i.e. concatenating fear and sad faces but excluding neutral, figure 4.5).

Task	Conditions	Group	M300 Amplitude				
			Mean	SD	t	p	Cohen's d
Fear	100% Fear 50% Fear Neutral	ND = RD =	-0.1570 -0.9369	0.3856 0.6818	4.24	0.00005	1.4
Sad	100% Sad 50% Sad Neutral	ND = RD =	-0.4159 -1.1077	0.4794 0.7120	-4.3231	0.000039	1.14
Fear + Sad	100% Fear 100% Sad 50% Fear 50% Sad	ND = RD =	-0.1513 -0.5452	0.4025 0.4232	8.1144	0.0005	0.95

Table 4.3. Implicit Task: M300 Amplitudes

Implicit task M300 results per task and condition.

Analyses using a two dimensional randomisation test with 2000 permutations revealed strong differences between the groups (fear-face task [t(91)=4.2358,p=0.00005], sad-face task [t(91)=-4.3231, p=0.000039], sad and fear excluding neutral: [t(91]=8.1144, p=0.0005], table 4.3).To determine whether the stronger t-statistic difference in the across-tasks comparison was due to an effect of emotional faces or just increased statistical power (due to increased sample size), an ANOVA was performed to assess whether face emotion affected M300 amplitude (using full and mild intensities of fear and sad vs. neutral faces). This revealed no significant effect of emotion ($p>0.05$), but a significant effect of group ($p<0.001$).

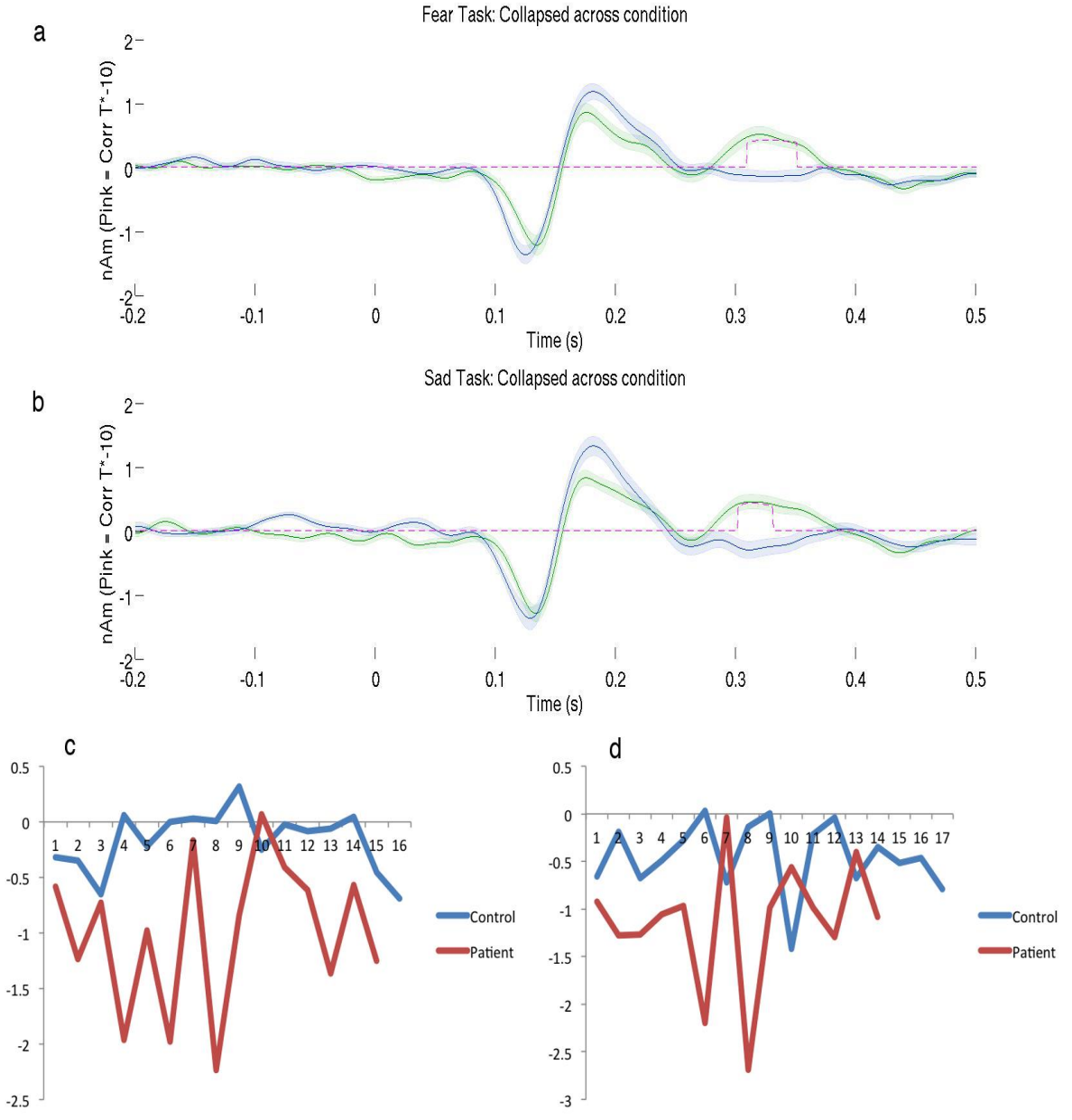

Figure 4.4. RD (blue) had significantly reduced M300 amplitude across all faces compared with ND for both the fearful**(a)** and sad **(b)** implicit paradigms. [x: time (s), y: Amplitude (nAm), Pink dashed line represents multiple comparison corrected t-value/10].(**c)**Fear task per-participant M300 amplitudes (mean of conditions full, mild and neutral). (**d)**Sad task per-participant M300 amplitudes (mean of conditions full, mild and neutral).

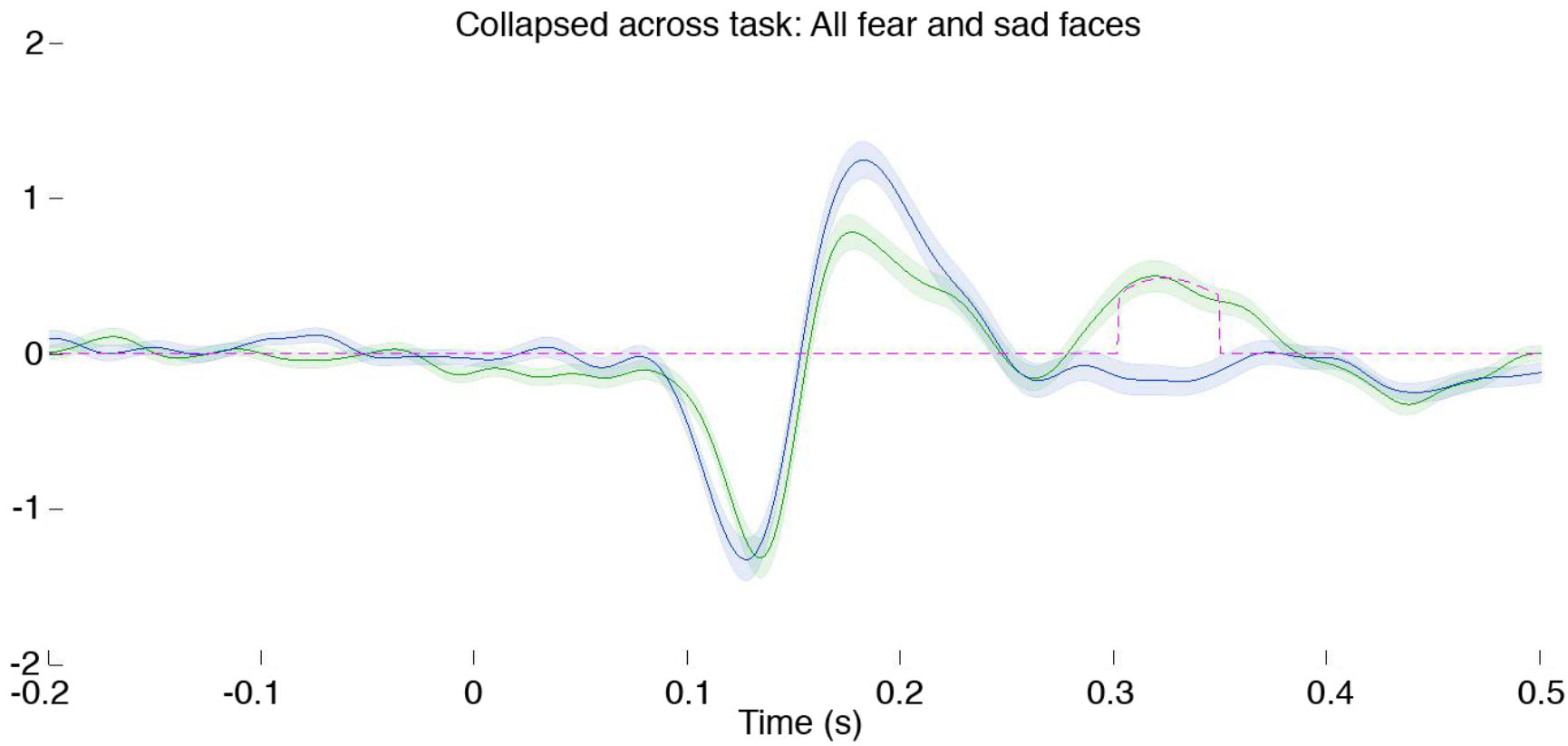

Figure 4.5. RD significantly reduced M300 in across-task analysis of emotional faces, compared with ND (excluding neutral faces). Pink dashed line represents t-value (-log10 for scaling).

4.6 Discussion

Analysis of both ERF and gamma measures revealed two main results. First, during the explicit emotional identification task, RD individuals demonstrate increased gamma power in the left insula compared to ND individuals in response to fearful faces, but not happy, sad or neutral faces, and this gamma-power correlated negatively with left-insula grey matter volume strongly in controls but not patients. Second, during two separate recordings of implicit emotion tasks (one utilising sad faces, the other fearful), RD individuals demonstrate reduced M300 amplitude for three intensities of facial expression, including neutral, compared with ND individuals.

Previous studies have demonstrated an important role for the insula cortex in processing faces expressing disgust. Studies have reported increased BOLD activation to faces expressing disgust (Phillips *et al*., 1997). This study suggests that the insula also responds to fearful faces, and that gamma oscillatory power in this structure is greater in remitted-depressed subjects than controls. Increased gamma oscillatory power is assumed to reflect greater population entrainment and synchrony, thereby assuming greater 'activation', a similar assumption to the BOLD response. This is in concordance with an fMRI study which previously demonstrated that the insula is involved in fear-face processing in healthy participants (Schienle *et al*., 2002) however, this is the first study to show a functional difference in RD.

During a similar paradigm, Lange *et al* (2003) demonstrated a greater BOLD response to neutral compared to fearful faces in the insula cortex in healthy participants during passive viewing, gender discrimination (implicit) and explicit expression distinction tasks. A number of clusters were reported for both fear>negative and negative>fear contrasts with the insula cortex as the only structure significant for neutral>fear for all three conditions (passive, implicit and explicit). These study results are inconsistent with this finding because only fearful faces during the explicit task elicited a gamma peak in the left insula.

The difference in gamma power in remitted depressed subjects in the left insula to only fearful faces and during only the explicit face task suggests that this finding is both specific to fearful facial expressions and requires the subject to be explicitly attending to, and identifying, the facial expression. Future studies should examine whether the left insula also exhibits increased gamma power to faces of disgust in RD.

The finding of reduced M300 amplitude in RD individuals to differing intensities of both fearful and sad faces might reflect the negative stimuli bias observed in current depression. However, the M300 difference was also observed in the neutral face condition, and amplitude differences were only significant when full and mild intensities and neutral faces were collapsed together and compared between groups. Furthermore, response data (gender discrimination) indicated no difference in accuracy between groups. An ANOVA demonstrated no main effect of emotion on M300, only group. It is likely that, per-condition, the M300 amplitude is truly different between our groups (as evident in figure 4b/c), however due to lack of statistical power this is only significant when conditions are combined.

A previous study reported reduced P300 amplitude in current episode depression in response to fearful and happy faces in a visual oddball task. Here the authors suggested this reflected diminished cognitive processing ability during emotional processing (Cavanagh *et al*., 2006). Although the tasks are slightly different, the data presented here could suggest that this reduction in cognitive processing ability during emotion processing is present in remitted depressed subjects. These data suggest that the P300 amplitude is modulated in remitted depression independent of facial expression, since neutral faces also demonstrate a difference between groups. A prominent different between these experiments is that Cavanagh (2006) selected a cluster of midline electrodes and performed a sensor level analysis whereas the approach in this experiment utilised beamforming source-localisation and a virtual occipital sensor approach with subsequent permutation testing.

Given the effect of group upon M300 amplitude during the implicit tasks, it is surprising that the M300 amplitude difference was not observed during the explicit face task. The key difference between the paradigms is that during the implicit task participants were instructed to identify only the gender of the faces presented, whereas the explicit task required identification of the emotion being expressed. Participants did not differ in accuracy during the implicit task however accuracy on the explicit task is unknown. These results suggest that some processing that occurs during the implicit task, but not explicit, accounts for the M300 amplitude difference between the groups. One explanation is that groups differed in their accuracy during the explicit task, and this is why the M300 difference is not present in the explicit task. This is unlikely due to the simplicity of the task. An alternative explanation is that the M300 amplitude reflects the negative-emotion-bias during only implicit emotion processing, and that this bias is diminished when attention is focussed upon explicitly identifying the facial expression.

Using EEG, one group demonstrated reduced visual oddball evoked P300 amplitude in depressed and bipolar patients compared with controls. This study was repeated once 18 participants reached remission (8 MDD, 10 BD) and demonstrated that amplitudes did not change significantly for either recovered bipolar disorder or major depression subjects (Bange & Bathien, 1998). A commonality between the paradigm in this study and that of Bange (1998), is the implicit discriminative nature: implicit facial expression discrimination and implicit visual oddball discrimination. In light of this, the result described here could represent a trait marker of implicit processing dysfunction (of the visual system) in depression. This could also account for the lack of 300ms response in our explicit face task data.

Few studies have focussed on ERF and gamma responses during face processing in remitted depression. In this respect, this study is novel. Furthermore, results demonstrate that remitted depressed subjects exhibit higher gamma in the left insula to fearful faces and reduced M3 amplitude to faces, compared to controls,

during implicit facial emotion processing tasks. Together, these findings demonstrate that neuronal functioning during emotional face processing is altered in remitted depression compared with healthy controls. Moreover, these results indicate differences in both basic sensory (middle occipital / visual area) and higher-order (insula) regions activity in face processing in remitted depression. Finally, emotional face processing differences observed in remitted depression differ depending on task instruction (explicit vs. implicit identification).

An important consideration of this work should be the molecular implications given the theorised biogenesis of gamma-frequency oscillations. Evidence suggests that gamma-frequency oscillations are generated by the interaction of inhibitory interneurons and excitatory pyramidal cells in the cortex. Neural network models of cortical microcircuits, informed by in-vitro slice work on common receptor types, demonstrates that the frequency of gamma oscillations is determined by the decay time constant of $GABA^A$ receptors on interneurons synapsing onto pyramidal neurons. This suggests that gamma oscillations are predominantly shaped by GABAergic inhibition, and specifically by the synaptic properties of $GABA^A$ receptors at inhibitory-excitatory synapses. However, the specific molecular underpinning of oscillatory power is less well elucidated. Spencer (2009) found that decreasing NMDA input to a pyramidal-interneuron network increased gamma power. A plausible explanation for this is that a consequence of reduced-NMDA input is mutual disinhibition, permitting increased excitation-mediated entrainment of pyramidal cells (Homayoun & Moghaddam, 2007), and thus RD subjects exhibit higher gamma power during processing of fearful faces as a function of greater resource load, or activation, by altered glutamatergic function. Computational modelling of MEG data may help to resolve exactly what increased oscillatory power represents, as well as further determining the roles of GABA and glutamate function in the pathophysiology of depression.

Chapter 5. Visual oscillatory dynamics and neurochemistry in current episode MDD and those with a family history of MDD

5.1 Abstract

Alterations of the GABAergic neurotransmitter system have been reported in numerous mood disorders, including current episode MDD, at both the post-mortem *in-vitro* and ante-mortem *in-vivo* molecular level. Evidence from *in-vivo* spectroscopy studies report lower bulk concentrations of GABA in currently depressed participants as compared with ND controls, however this reduction in concentration does not appear present in remittance. It is now important to fully elucidate the occurrence of GABA reductions across current episode, remittance and vulnerability to depression.

The experiment detailed in this chapter concerns subjects with a current episode of depression and those with no personal history of depression, but a first-degree family history. These data are merged with those previously detailed, forming four groups: 18 never depressed (ND), and 18 never depressed but with a family history of depression (FH), 15 remitted-depressed (RD), and 13 currently-depressed (CD) participants. The ND and RD groups are those data described in chapter 3. Resting occipital MR spectroscopy (MEGA-PRESS) were acquired, along with high-frequency magnetoencephalographic oscillatory data induced utilizing a 4° circular, vertical grating. Analysis of variance tests revealed no difference between GABA+ or IGF between groups.

5.2. Background

Section 1.3.2 reviewed the evidence for a deficit in GABAergic function in major depressive disorder. Subsequently, the experiment detailed in chapter 3 did not demonstrate a GABA+ concentration or GABAergic functional deficit in the visual cortex of remitted-depressed subjects using either ^{1H}MR spectroscopy or induced γ-frequency oscillations as a marker of GABAergic function as compared with healthy, never depressed controls. The experiment did however reveal a marked

reduction (46%) in the amplitude of the early visually evoked C1 (M80) component in remitted depressed subjects. These results suggest both that the GABAergic deficit documented in current-episode depression is a *state* component or marker of depression and also that the reduced C1 amplitude in remitted depression could be a trait marker of depression. In order to evaluate these hypotheses this chapter describes data from two further samples: a group of currently depressed subjects (who meet MINI criteria for current episode MDD) and a further group with no personal history of depression but with a parent who suffers depression.

While reports of reduced MRS GABA+ in remitted depression have, until now, been equivocal, multiple studies have reported reduced GABA+ in acute (current-episode) depression in visual cortex (Sanacora *et al*., 1999), in adolescents with highly anhedonic depression in anterior cingulate cortex (Gabbay *et al*., 2012) and in treatment resistant depression in both OCC and ACC (Price *et al*., 2009). Reduced plasma GABA levels have also been reported in acutely depressed subjects (Petty *et al*., 1992), suggesting a brain-wide deficit in GABA concentration and/or function in depression.

The biggest predictor of depression is a family history of depression (commonly a parent). Depression is estimated to be 40-50% heritable, although this is driven mainly by women, with heritability rates significantly higher in women than men (Bierut *et al*., 1999). Studying subjects with a family history of depression allows for identification of heritable behavioural and imaging characteristics associated with depression. Lisiecka and colleagues (2012) demonstrated that although healthy subjects with a family history of MDD did not perform differently from non-family history comparators during an inhibition of emotion task, they did display a '*negative neural drift*' in that they demonstrated increased BOLD activation during inhibiting of negative stimuli in the right cingulate cortex and left caudate nucleus. This study was the first to demonstrate that, while the negative stimuli bias observed in acute MDD is not observed behaviourally in family history groups, altered activation patterns of the cingulate cortex and caudate nucleus are observed when compared with non-family history control subjects.

The peak frequency of gamma-frequency oscillations (30+ Hz) has recently been estimated to be 91% heritable (van Pelt *et al*., 2012). Thus, altered $GABA_A$ receptor function may explain our hypothesised change in peak gamma-frequency. If observed in family history subjects as well as acutely depressed subjects, this would suggest that altered GABA function is a trait marker of depression.

No studies to date have demonstrated altered MRS GABA+ levels in healthy subjects with a family history of depression, but one study has reported elevated glutamate (Taylor *et al*., 2011a). Given the coupled roles of GABA and glutamate in the cortex, this finding may reflect a prodromal vulnerability to altered GABA function.

This experiment addressed the following hypotheses: in acutely depressed subjects, MRS GABA+ in the occipital cortex will be reduced compared with healthy control subjects (Sanacora *et al*., 1999). Furthermore, the peak frequency of induced gamma-frequency oscillations will be reduced, suggestive not only of a reduction in GABA levels, but in $GABA_A$ receptor function and altered excitatory-inhibitory balance. Finally, the amplitude of the C1 / M80 component of the visual evoked field will be reduced in accordance with the finding reported in remitted depressed subjects in chapter 3.

It is further hypothesised that healthy subjects with a family history of depression will demonstrate reduced MRS GABA+ and peak gamma frequency in the occipital cortex, demonstrating that altered GABA function is a trait marker of depression.

5.3 Experiment: Measures of visual cortex γ oscillations and GABA across current episode, remittance and a family history of major depression.

5.3.1 Rationale

The conclusion of the experiment detailed in chapter 3 formed two distinct hypotheses. Namely that the GABAergic deficit reported in the brains of subjects with current-episode depression is a state marker, and is thus not present in remittance, or vulnerability to depression. Secondly, the reduced C1 amplitude observed in remitted depressed subjects represents a trait marker of depression (or possibly of vulnerability to depression). This chapter describes two further samples recruited to test these hypotheses.

5.4 Methods

Recruitment and sample

Thirty-one female volunteers were recruited through the Cardiff University School of Psychology's online Experimental Management System and through the University Online Noticeboard. Besides depression or a family history of depression, subject inclusion criteria further included: female, aged 18-35 and normal or corrected-normal visual acuity.

Data from the healthy subjects and remitted depressed subjects, detailed in chapter 3, were combined with those detailed in this chapter to form four comparable groups. The 31 newly recruited subjects consisted of N=18 healthy, never depressed subjects with a first-degree family history of depression (a parent). The sample further consisted of N=13 currently depressed but un-medicated subjects who, at screening, scored >13 on the BDI and on scanning day met MINI criteria for a current major depressive episode. All subjects underwent screening using the MINI and BDI and took part in MEG and MRS scans. Subjects were reimbursed £15 to compensate for their time.

With the exception of depression and comorbid anxiety in the depression group, subjects were excluded based on meeting MINI criteria for any psychiatric disorder (including manic or hypo-manic episode and psychotic disorders, panic disorder,

agoraphobia, and social phobia, OCD, PTSD, alcohol abuse or dependence, anorexia or bulimia nervosa). Further exclusion criteria included suitability and willingness to participate in MRI and MEG scans (i.e. no common contra-indications to MRI).

MEG, MRS & Paradigm

MEG data were collected while subjects performed 2 basic visual stimulation tasks. The tasks were displayed on a Mitsubishi Diamond Pro 2070 monitor (1024 × 768 pixels and 100Hz frame rate) positioned 186cm from the eye. Task 1, as detailed in chapter 3, consisted of a 4° static, circular grating patch with vertical, (3-cycles-per-degree, maximum contrast) black/white square-wave blocks on a mean luminance background. The stimulus was displayed in the lower-left quadrant of the screen subtended 4° horizontally and vertically, with the upper right corner of the stimulus located 0.5" horizontally and vertically from a small red fixation point. The stimulus was on for between 0.8 and 2.3s (mean duration 1.55s) followed by 1.5s of the fixation point only.

Task two also utilised a maximum contrast, circular grating patch with square-wave 3 c.p.d. vertical bars. This grating was larger than the first, at 8° and presented centrally, with the red fixation square in the centre of the annular grating. The data from this second paradigm are not presented here. MEG was recorded using a CTF MedTech 275-channel system in a magnetically shielded room. Data were recorded at 1200Hz and channels were analysed as synthetic third-order gradiometers (Vrba, 2001).

MEG data were epoched into 2s trials and artefacts rejected based upon visual inspection of sensor-trace for every trial. Datasets were band-pass filtered using a Butterworth bi-directional filter in 0.5 Hz steps between 0 and 100Hz. Resulting data were passed through the synthetic aperture magnetometry (SAM) (Robinson & Vrba, 1999) beamformer, applied to estimate source-space amplitudes from sensor space. Subsequent source-space, spatially-filtered paired-t-statistic (stimulus vs. baseline) maps were used to identify peak V1 amplitudes, which

invariably fall around the midline of V1. A virtual sensor was created at this best-performing site for time-frequency analysis using the Hilbert transform (with amplitude represented as percentage-change from baseline). Peak frequency and amplitude measures are extracted by averaging across a time window of interest. For this study, the frequency and amplitude of the non-phase locked (induced) gamma response were utilised (0.3 to 0.8s). This pipeline is graphically represented in figure 5.1.

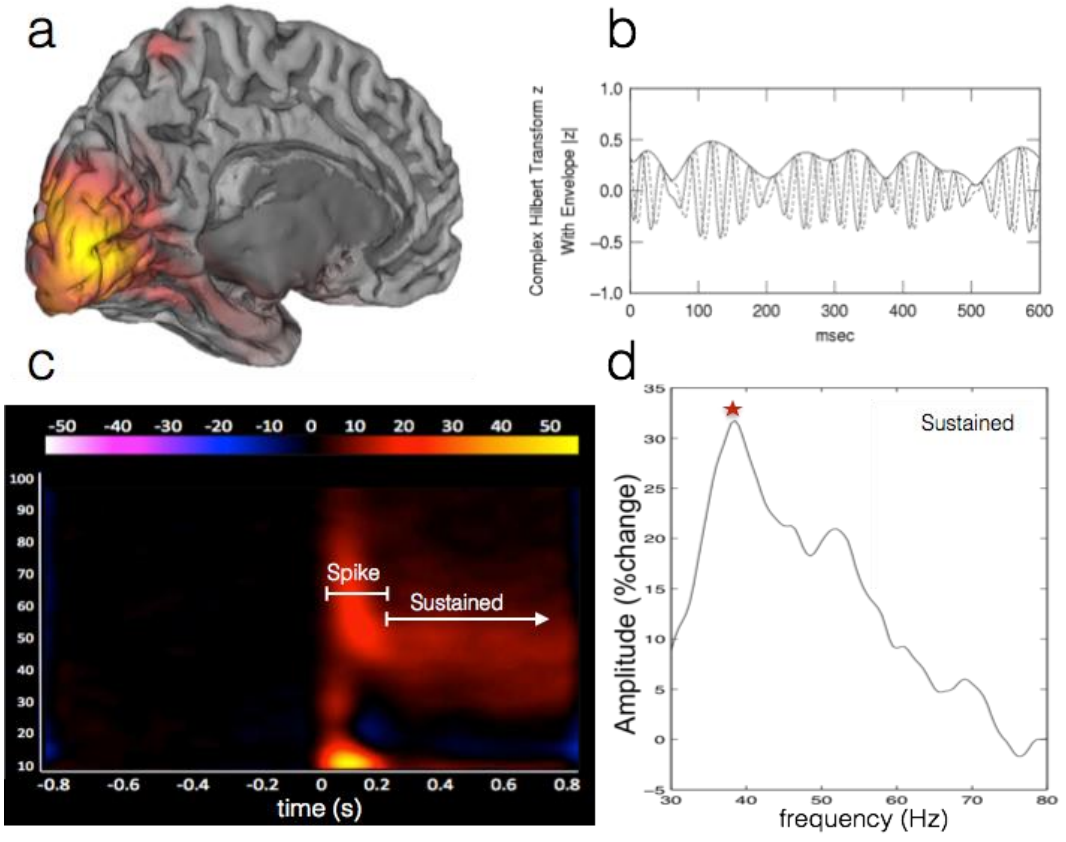

Figure 5.1. Graphic representation of MEG visual paradigm analysis pipeline. Best-performing location in t-statistic SAM image (a), is passed through Hilbert transform to estimate frequency contributions (b). (c) demonstrates the time-frequency-amplitude data for the virtual sensor location. Mean power in the sustained component of the response is plotted in (d), from which peak frequency and amplitude for this component are extracted.

The MRI scan protocol consisted of one 10-minute F-SPGR scan and one 8 minute MEGA-PRESS spectroscopy acquisition (Mescher *et al*., 1998; O'Gorman, Michels, Edden, Murdoch, & Martin, 2011). MR data were acquired on a GE Signa

HDx 3T MRI scanner using the body coil for RF transmission and an eight-channel head coil for signal reception. The T1-weighted scan sequence (3D structural FSPGR: TR= 7.8, TE= 3.0, TI= 450ms, flip angle= 20° FOV = 256*192*172mm, 1mm isotropic resolution) was used both for MEG co-registration and for tissue-correction of spectroscopy data.

The 3 x 3 x 3cm^3 MR spectroscopy voxel was placed bilaterally in visual cortex and aligned with the calcarine fissure (figure 5.2). The spectroscopy protocol (TE = 68 ms, TR =1.8s, 256 transients of 2000 data points) utilised 16ms editing pulses applied at 1.9 ppm (ON) and 7.5 ppm (OFF) (Gannet Toolbox). Fourier transform revealed distinct, approximately Gaussian peaks corresponding to GABA+ and Glx (fig 5.2). GABA+ concentration was quantified in institutional units, referenced to the unsuppressed water peak. Voxel tissue composition was accounted for by segmenting a mask of the MRS voxel on a T1 image and approximating the contribution of CSF, white- and grey-matter in the voxel space.

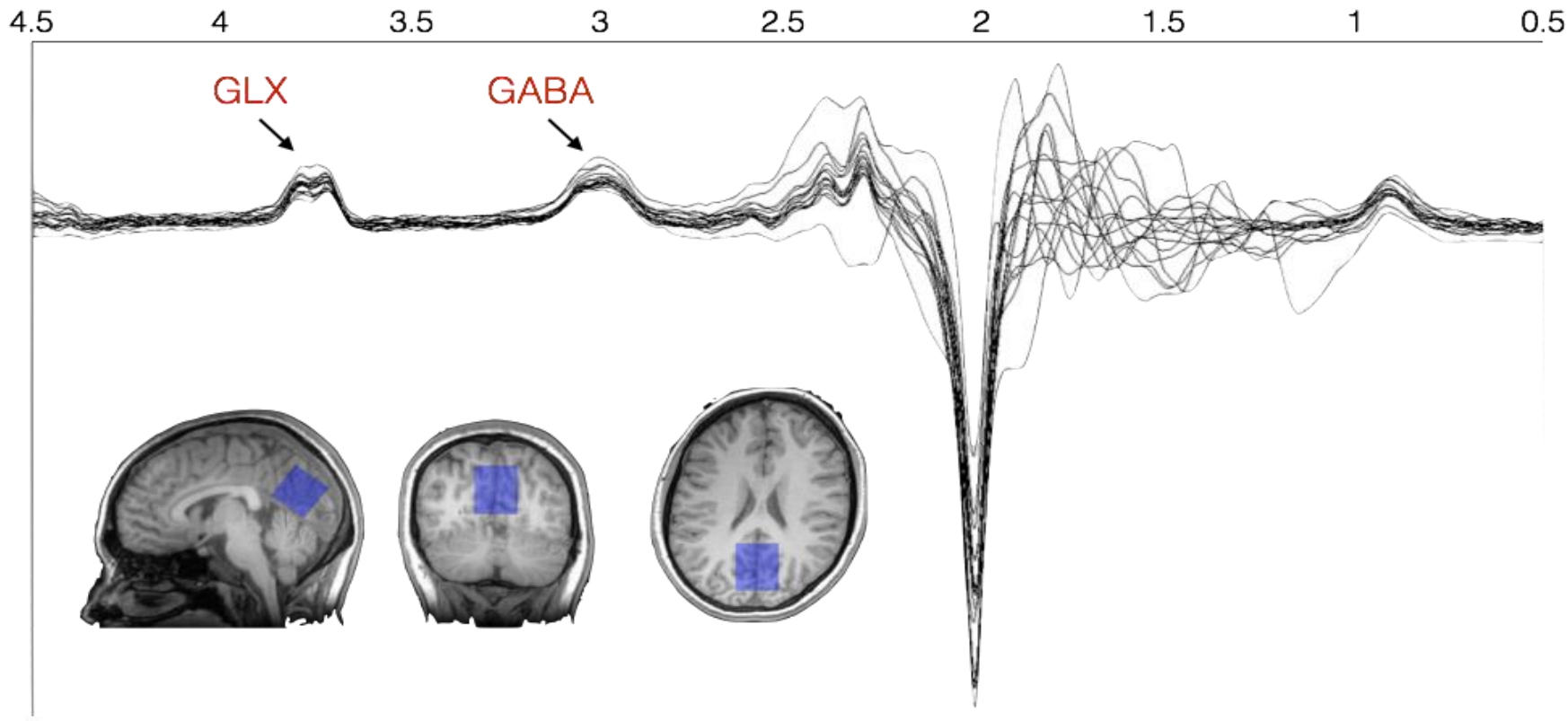

Figure 5.2. Occipital voxel position (mask) overlaid on a T1 structural image. All subjects' edited spectra showing clear GABA and GLX peaks.

5.5 Results

Three subjects were excluded based on their spectroscopy data quality, with a quality criterion of GABA+ $\leq$ 3ppm. The resulting N=12 subjects meeting criteria for a current major depressive episode (current depression group, '*CD*') and N=16 subjects with a family history of depression ('*FH*') were matched (by age as closely as possible) with N=12 healthy, never depressed ('*ND*') subjects and N=14 remitted depressed ('*RD*') subjects from the experiments in chapter 3, summarised in table 5.1.

Group		Age	BDI
ND	Mean	22.8	2.6
(N=12)	SD	3.1	2.6
FH	Mean	20	5.8
(N=16)	SD	2.1	5.6
RD	Mean	20.4	5
(N=14)	SD	1.3	4.4
CD	Mean	22.58	34.6
(N=12)	SD	3.9	9

*Note: exclude GABA ppm>3

Table 5.1. Age and BDI score for each group. ND

Previous research has demonstrated that the peak frequency of induced gamma-frequency oscillations is negatively correlated with age (Gaetz *et al*., 2012). This could be explained by a reduction in the number of parvalbumin containing GABAergic interneurons, which has been shown to decline with age in rats (Krzywkowski, De Bilbao, Senut, & Lamour, 1995). Coupling this finding with evidence that cortical GABA levels correlate with MRS obtained GABA strongly suggests that cortical GABA+ levels could also be largely influenced by age. As such, both dependent measures (MRS GABA+ and peak gamma frequency) were orthogonalised with respect to age by subtracting the regression weights from the original measures. Raw versus adjusted values for each measure are plotted in figure 5.3 showing a strong correlation (suggesting that raw values were not strongly under the influence of age). Group mean values both pre- and post-

adjusting for age are listed in table 5.2. Only age-adjusted values were used in statistical analyses.

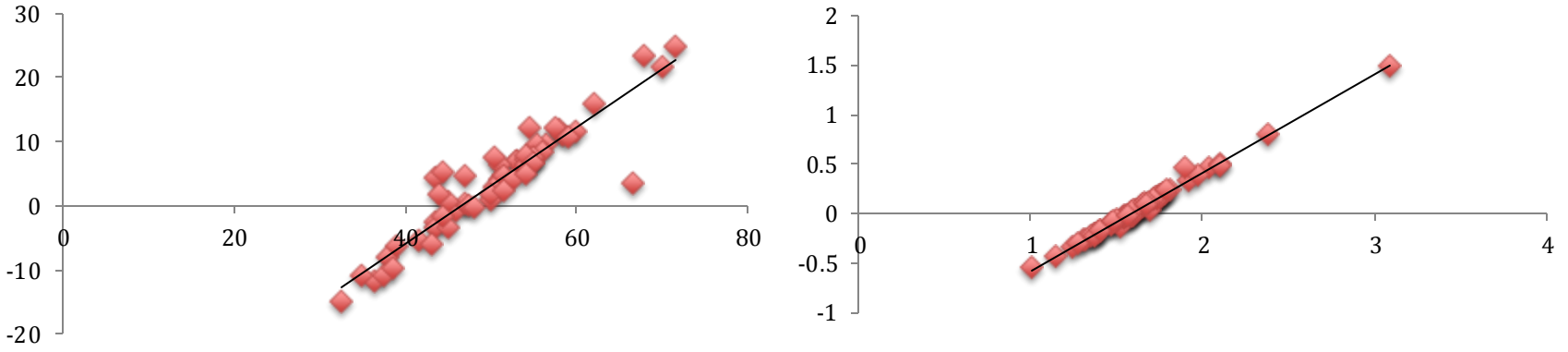

Figure 5.3. Left: Raw peak gamma frequency (x) vs. age-adjusted peak gamma frequency (y). Right: Raw GABA+ in ppm (x) vs. age-adjusted GABA+ (y).

Group		Age	ϒ Freq (Hz)	ϒ Amp	ϒ Freq AGE ADJUST	GABA+ (ppm<3)	GABA+ AGE ADJUST
ND	Mean	22.8	49.83	25.45	4.34	1.58	-0.02
(N=12)	SD	3.1	5.28	11.28	5.43	0.33	0.33
FH	Mean	20	49.78	24.71	2.12	1.62	0.03
(N=16)	SD	2.1	8.45	14.23	8.31	0.09	0.09
RD	Mean	20.4	51.6	26.83	4.28	1.63	0.04
(N=14)	SD	1.3	8.91	15.64	8.72	0.26	0.26
CD	Mean	22.58	49.08	25.47	3.40	1.63	0.03
(N=12)	SD	3.9	9.42	14.41	9.56	0.26	0.25

Table 5.2. Group means for pre- and post- adjustment of dependent measures.

A multivariate ANOVA was employed to address the hypotheses that GABA and peak gamma-frequency measures are reduced in currently depressed subjects. MANOVA revealed no difference between groups in age-adjusted V1 peak gamma frequency ($F(3)=0.235$, $p=0.8$) or occipital MRS GABA+ ($F(3)=0.186$, $p=0.9$), nor in the amplitude of the peak gamma frequency measures ($F(3)=0.058$, $p=0.9$). Figure 5.4 illustrates group means with 95% confidence interval for peak-frequency and GABA+ measures.

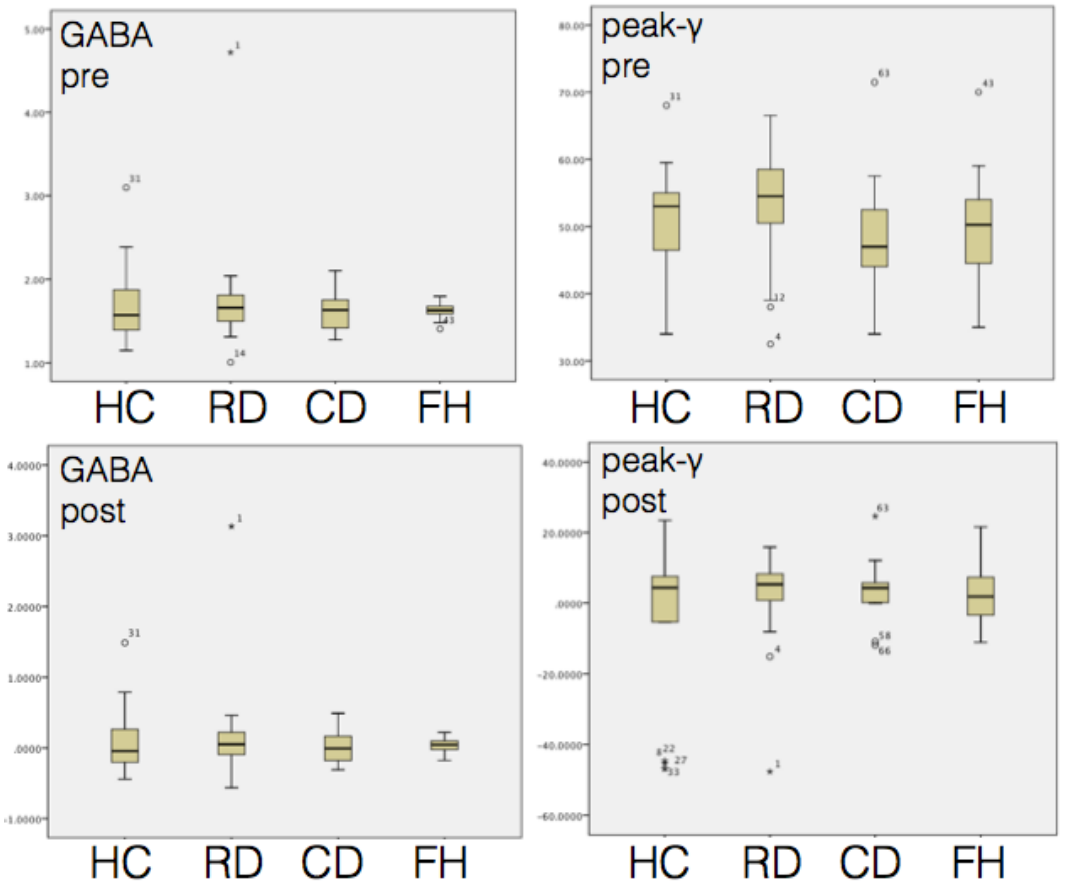

Figure 5.4. Group means for induced gamma frequency and GABA+ levels.

To address the hypothesis that the amplitude of the C1 / M80 component of the visually evoked response will be reduced in current episode depressed subjects (and possibly family history subjects. In concordance with remitted subjects), evoked, filtered (0-20Hz) spectra form the time-frequency analysis were plotted for each subject to identify subject-specific components from the pattern-onset

waveform ('W' shape based on strong C1/M80 component). Amplitude spectra were polarity-flipped (multiplied by -1) for subjects exhibiting strong positive C1 amplitude with subsequent negative deflection, as this was assumed to reflect an issue whereby the SAM beamformer inaccurately detects the polarity of evoked waveforms. Peak amplitude of the M80 was determined and entered into higher-level statistical analysis. The spectra for each group are displayed in figure 5.5. MANOVA (amplitude and latency vs. group) revealed a significant effect of group on M80 amplitude ($F(3)=6.7$, $p=0.001$). *Post-hoc* Bonferroni t-tests revealed that CD and FH groups showed no difference to HC in M80 amplitude or latency; however, RD had significantly reduced M80 amplitude compared with FH and CD as well as the previously mentioned comparison with HC (Bonferroni corrected p-values for RD vs. CD $p=0.003$ and FH $p=0.001$).

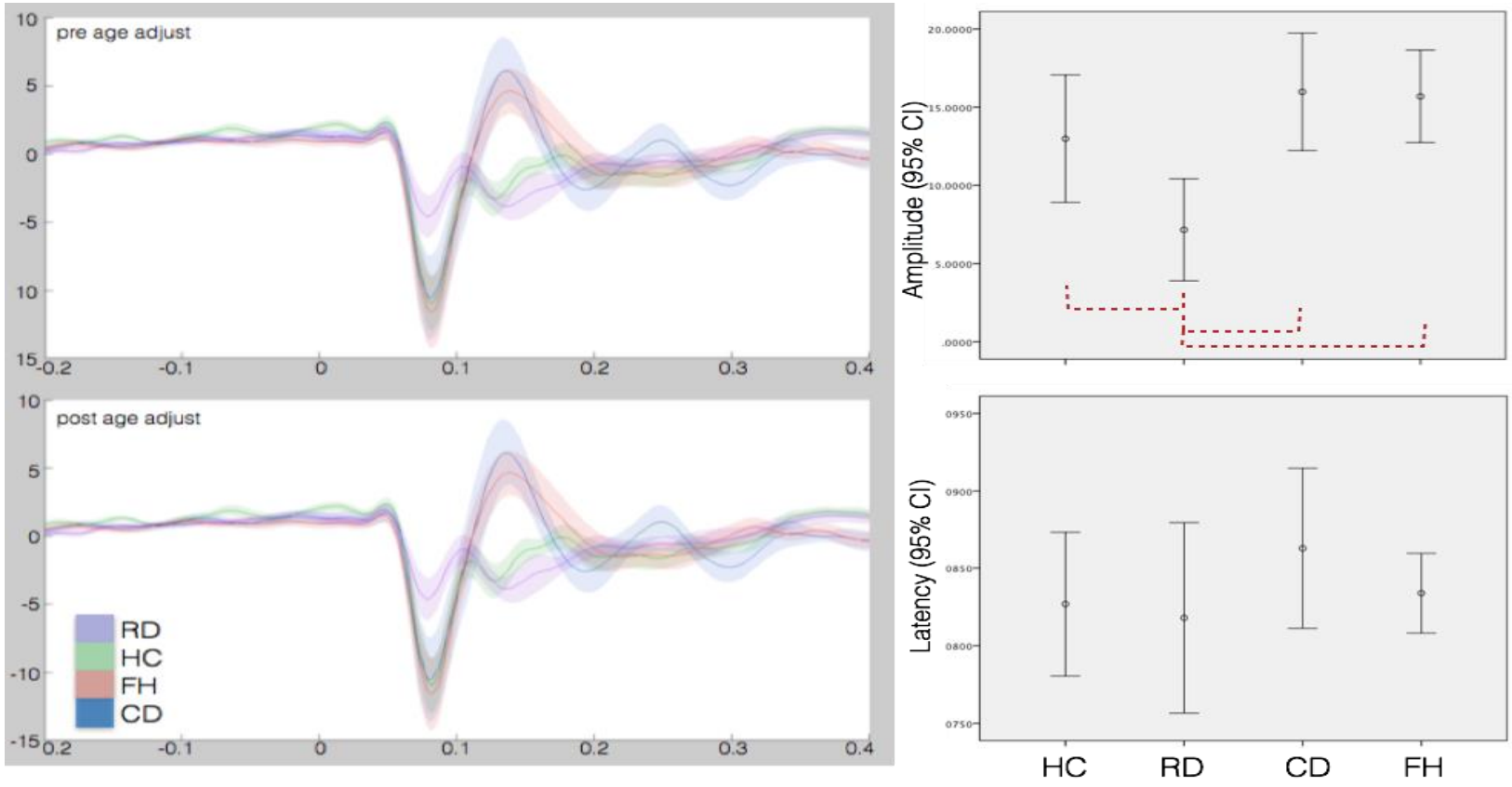

Figure 5.5. Visually evoked spectra for each group for the first 400 ms after stimulus onset. Left: the spectra for each group. Right: Error bar diagrams for the latency and amplitude of the M80 component for each group.

5.6 Discussion

Statistical tests revealed that occipital GABA concentrations and peak-gamma frequency were not altered in subjects meeting criteria for a current major depressive episode, or in healthy subjects with a family history of depression (the null-hypothesis). Furthermore, the reduction in amplitude of the visual evoked response M80 component, observed in remitted depression, was not observed in currently depressed of family history groups using the same healthy, never depressed control group.

The finding that occipital GABA+ measures are not altered in the current depression group is a failure to replicate previous findings which reported a 52% reduction in occipital GABA levels in a similarly sized (n=14) and unmedicated sample (Sanacora *et al*., 1999). A key difference between the studies, however, is that the patients described by Sanacora and colleagues (1999) were a mixed population of male and female, and were an average age of 42.9 +/- 9.2 years, suggesting more variation in their ages and therefore illness-history than the sample recruited here (mean age 22.5). Furthermore, 12 of the 14 subjects reported had known comorbidities (including psychosis, OCD, alcohol abuse, bipolar disorder and anorexia nervosa) and 11 of the 14 were considered treatment-resistant. The discrepancy between study findings may be due to the comorbidities, since GABAergic deficits have been shown in other psychiatric disorders such as psychosis and bipolar disorder (Benes *et al*., 2007) and alcohol abuse (Behar *et al*., 1999). In this respect, the subjects described in this study represent a less complex pathology and are therefore better suited to answering the question of whether a GABA deficit exist solely in depressed subjects.

Besides the differences in population characteristics, there were some methodological differences between this study and that reported by Sanacora *et al* (1999). While the MR spectroscopy voxel was positioned similarly (centred on the midline of the occipital cortex), they used a 2.1T Oxford scanner where this study utilised a 3T GE scanner. Additionally, while both studies employed difference-

editing techniques, they utilised the DANTE pipeline, whereas this study used MEGA-PRESS, and subtle differences may exist between these acquisition protocols.

The hypothesis that PIGF would be lower in currently depressed subjects was informed by literature suggesting that gamma (30+ Hz) frequency oscillations are driven by an interaction of cortical GABAergic interneurons acting (reciprocally) upon superficial layer pyramidal neurons (Sohal, 2012), a theory supported by modelling studies which demonstrate that peak gamma frequency is dependent on GABA:AMPA ratio (Brunel, 2003) and a reported correlation between peak induced gamma frequency and MRS GABA+ concentration in V1 (Muthukumaraswamy *et al*., 2009). Together these reports suggest that PIGF references GABAergic function, particularly via fast $GABA_A$ receptors. Since the previously reported reduction in GABA+ levels in depressed subjects was suggested to reflect an alteration in the functional physiology of GABA in depression, rather than just a global volume reduction, PIGF was employed as a measure of GABAergic function. No difference was found in PIGF of the CD group compared with HC. However, since no difference was found in MRS GABA measures either, these null findings support one another.

No difference in GABA or PIGF was found in the family history group. The hypothesis for GABA and PIGF in the family history group relied upon the assumption that both measures would be reduced in the CD group. Since PIGF is highly heritable, at approximately ~90%, (van Pelt *et al*., 2012), and so is depression, we hypothesised that PIGF would be reduced in the FH group. If MRS GABA+ was also reduced compared to the control group, this would suggest that the altered GABAergic function giving rise to gamma oscillations is a trait marker of depression and would have potential as a biological marker. Finding that neither measure was reduced in the FH group supports the notion that GABA and PIGF may not be reduced in the CD group.

While the GABA and PIGF results presented here do not couple with hypotheses from the imaging literature, this is the first study to investigate PIGF in currently depressed subjects as a marker of GABAergic function, and the first to combine this sample with samples of remitted depressed subjects and family history subjects in order to identify the type of biomarker any positive finding might represent.

In contrast with the hypothesis, the visually evoked M80 component was not reduced in CD or FH groups. A reduction in M80 amplitude was hypothesised because in an earlier study (chapter 3), RD subjects exhibited a 46% reduction in pattern-onset M80 amplitude.

Few other studies have reported changes in early VEPs in psychiatric disorders, and only one reported altered C1 (M80 equivalent) amplitude in major depression. Normann *et al* (2007) utilised a small (0.5°) checkerboard-reversal while recording EEG. Forty depressed subjects and seventy-four control subjects participated in the study. They demonstrated that the whole group (CD + HC) demonstrated markedly decreased M80 amplitude after 10 minutes of visual presentation compared with baseline, and increased P1 and N1 after 30 minutes of visual presentation. Between groups analysis of a subset of matched depressed and control subjects revealed that in the CD group, C1 and N1 were actually increased in amplitude while P1 was decreased. The authors suggest that this represents impaired-response plasticity in the depressed group. While this study is difficult to compare directly with the results described in this chapter because of differences in methodology, the findings of Normann *et al* (2007) suggest that depressed subjects' visually evoked C1 (M80) amplitude is less-plastic and thereby less affected by visual stimulation.

Finding a reduction in visually evoked M80 amplitude in remitted depressed subjects but not currently depressed or family history subjects rules out the M80 as a state- or vulnerability marker of depression. One explanation is that reduced M80

is a marker of recovery from depression and future studies should investigate whether there is a clinical-improvement-dependent decrease in M80 amplitude.

Chapter 6. Dynamic causal modelling of canonical micro circuitry under the free energy principal: predictors of imaging measures and inference on the depressed brain.

6.1 Rationale

Dynamic causal modelling (DCM) is a statistical inference technique for neuroimaging, which relies on predictive coding under the free energy principal. The concepts of predictive coding and free energy form a unified theory of the hierarchical brain, explaining how the brain is optimised in its anatomy to generate a model of '*the world'* in order to explain its senses (Clark, 2012). A particular implementation of DCM utilises a neuronal mass model, based upon neuronal assemblies in a biologically plausible canonical microcircuit. Using a Bayesian approach to match the spectra of this generative model to MEG obtained *in-vivo* spectra permits inference about laminar specific cortical circuit connectivity from MEG spectra.

In this experiment DCM was applied to MEG spectra obtained from the four cohorts described in the previous chapter. DCM may be more sensitive to alterations in the disease state than conventional neurophysiology or neuroimaging measures, which could be advantageous in studying psychiatric disorders, such as depression, where specific neurobiological anomalies are hypothesised. As such, DCM may reveal alterations of components of the GABAergic system at the microcircuit level, but which are not always of great enough effect size to influence the MRS GABA and MEG γ-oscillation measures utilised in previous chapters.

Two statistical analyses were performed: first, parameters from the model were compared between groups. Second, the ability of the model parameters to predict primary imaging measures (GABA & γ-frequency / amplitude) was evaluated between groups using the Fisher r-to-z transform. Differences in these correlations

may explain why purportedly global GABAergic dysfunction in depressed subjects may not result in altered γ-measures.

6.2 Background

For an introduction to, and overview of predictive coding and dynamic causal modelling, the reader is directed to section 1.5 of the introductory literature.

6.3 Methods

6.3.1 Subject characteristics

The data described in chapter 5 was used in this experiment. This consisted of four subject groups: healthy controls, healthy subjects with a family history of major depressive disorder, currently depressed subjects and remitted depressed subjects. Population size, mean age and BDI score are summarised in table 5.1.

6.3.2 DCM & canonical microcircuit model

A broad range of attributes including membrane potentials, conductance and time constants, among others, define neuronal populations. Mean field approximations summarise the behaviour of a neuronal population in terms of an ensemble density (Moran *et al*., 2009). Neural mass models describe the interaction of the means in this ensemble.

Under the assumption that the data represents a stochastic, stationary process (i.e. the probability distribution is not affected by time), neurophysiological data can be summarised as a cross-spectral density matrix; $g(w)_c$ at frequency w (for each frequency of interest). These cross-spectral densities summarise long time-series data compactly and additionally permit analysis of modelling using conventional spectral analysis. In this experiment, the power spectral density of the virtual sensor time series was modelled.

DCM implements a neural mass model where each population within a defined microcircuit is modelled with pairs of first-order differential equations;

$$\dot{x}_v \doteq x_i$$
$$\dot{x}_i \doteq \kappa H\big(E(x) + C(u)\big) - 2\kappa x_1 - \kappa^2 x_v$$

(3)

where k = rate constant, vectors x_v and x_i correspond to the mean voltages and currents (microcircuit population output), of which each element corresponds to the hidden state of the population at each source. $E(x)$ and $C(u)$ represent endogenous and exogenous components respectively. These equations serve to convolve presynaptic inputs into postsynaptic responses. This model has been described and implemented previously (Moran *et al*., 2009, Muthukumaraswamy *et al*., 2013). The endogenous component, $E(x)$, is a mixture of the mean firing rates of other populations. These are a sigmoid activation function dependent on membrane depolarisation approximated with a linear gain function. Endogenous inputs can be intrinsic or extrinsic. Intrinsic connections can arise form any population, while extrinsic connections arise only from excitatory pyramidal populations (i.e. projection neurons). The resulting model output is converted to time series data by a bilinear modelling procedure, to which the noise model described below is added post-hoc.

Exogenous inputs, $C(u) = Cu$, are scaled by the exogenous input matrix $C \in \Re^{sxs}$ (where $\Re^{sxs}$ is a connection matrix) so that each source-specific innovation $u(t) \in \Re^{sx1}$ excites the spiny stellate populations. The spectral density of exogenous input, $g(w)_w$, comprises white / Gaussian (α) and pink (f^{-1}) (β) noise;

$$g_k(w)_u = \alpha_u + \beta_u / w$$

(4)

The cortical microcircuit in figure 6.9.1 was constructed based on the description by Bastos *et al* (2012). Unlike the model described by Moran (2009), this model consists of four populations, superficial and deep pyramidal populations, granular-

layer spiny stellates and cross-laminar inhibitory interneurons. This model differs from that of Bastos *et al* (2012) in the addition of an excitatory connection between superficial pyramidal and deep pyramidal populations (G13+) and having removed an inhibitory connection between superficial pyramidal and spiny stellate populations (G2). The differential equations describing these populations, along with an overview of the signal generation, are presented in figure 6.9.2.

The previously prescribed generative model is inverted to obtain the posterior densities of the parameters using variational Bayes, as detailed in equation (1) by maximising the negative free energy (equation 2) (Friston & Penny, 2011). Since the shape and orientation of neuronal populations, relative to the cortical surface are known to affect the contribution strength of each population to scalp recordings (see chapter 1.3), the output of each source, $g(x)$, is a weighted mixture of x_v (mean voltage) with greater weighting on superficial pyramidal populations (80%) than deep pyramidal or interneuron populations (20% each).

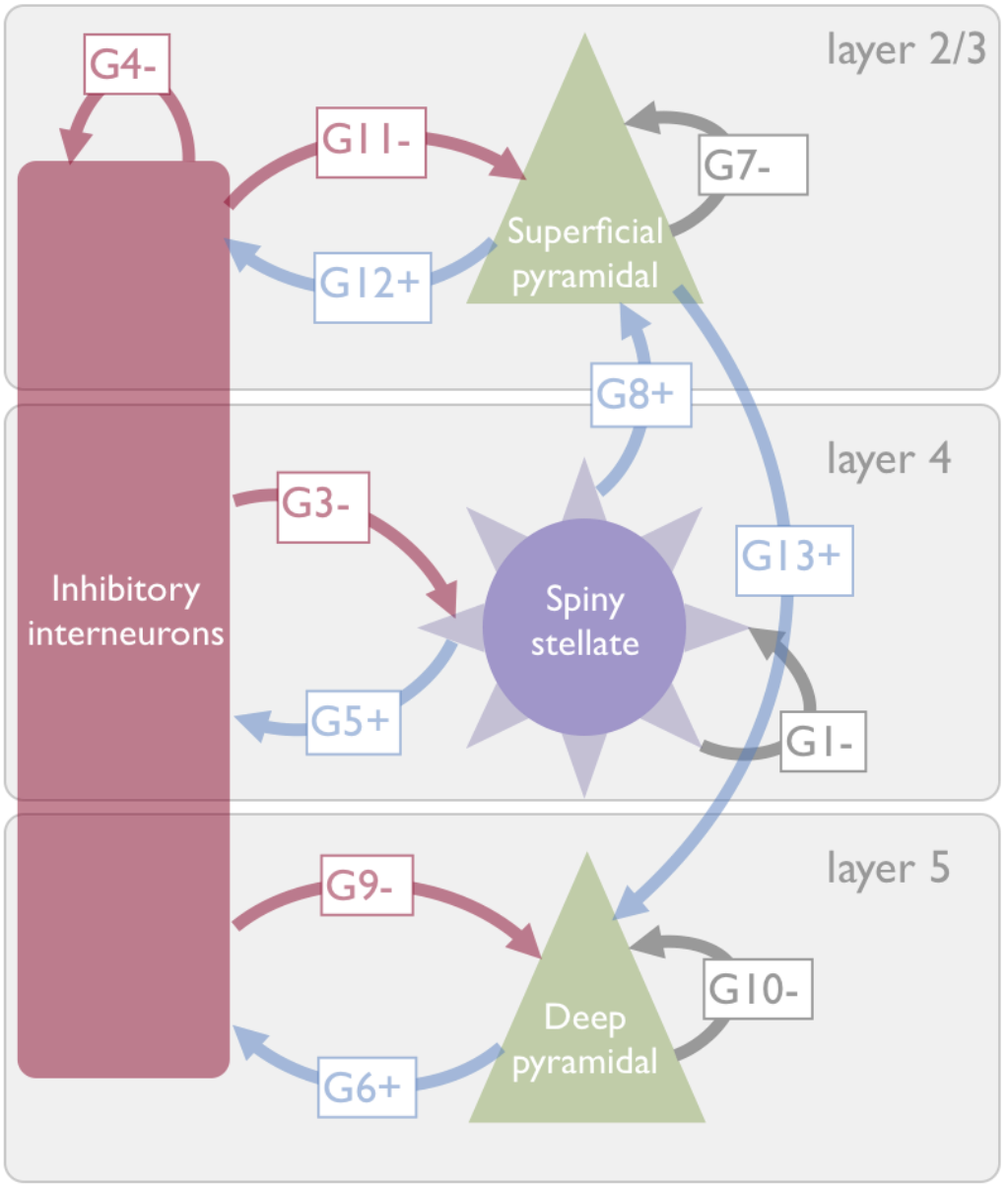

Figure 6.9.1. The canonical microcircuit. Each G number represents an anatomical connection between 2 populations. The sign (+/-) refers to excitatory or inhibitory connection.

6.3.3 Model Parameter Selection Procedure

The model fitting procedure used in this experiment involved three components. Initially, a minimally prescribed (maximum variables) model was fit, whereby 16 parameters are able to vary (by 1/8 around a prior). These parameters, and their priors, are found in table 6.2. The initial fitting of this 16-parameter combination results in a 'best estimate' for the posterior density, but does not consider permutations of the parameters (i.e. including 16 parameters rather than a subset). As such, a post-hoc Bayesian model selection technique, described by Friston (2011), was employed. This technique uses the Laplace approximation (Gaussian) to estimate the posterior density on every possible combination of variable parameters without refitting the model. This method is equivalent to fitting the model several times over, on each iteration fixing one of the variable parameters then comparing the log-evidence (free energy) for each model.

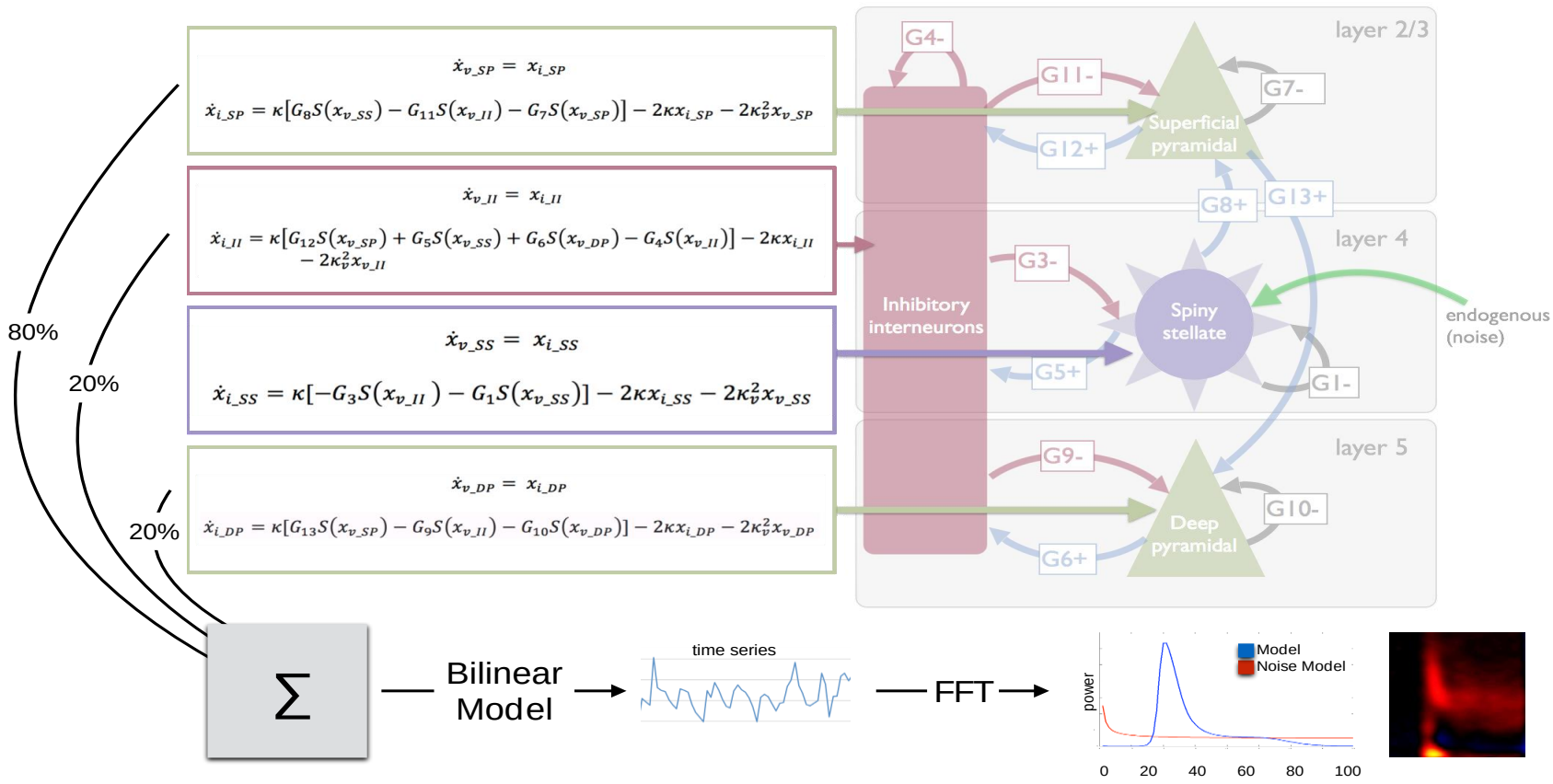

Figure 6.9.2 Coloured boxes: Summary of state equations for the neuronal mass model describing the voltages of each population accor ding to their excitatory and inhibitory inputs. Population outputs are weighted (left) to produce a single model output. This is converted to a time series, Fourier transformed (as per empirical data) and a noise model added post-hoc so as to match brain data.

Parameter	Description	Prior π (σ)
G1 (intrinsic)	SS self-gain, inhibitory	0.0962 (1/8)
G3 (intrinsic)	II → SS, inhibitory	0.5163 (1/8)
G4 (intrinsic)	II self-gain, inhibitory	0.0405 (1/8)
G5 (intrinsic)	SS → II, excitatory	0.2708 (1/8)
G6 (intrinsic)	DP → II, excitatory	0.6978 (1/8)
G7 (intrinsic)	SP self-gain, inhibitory	0.3997 (1/8)
G8 (intrinsic)	SS → SP, excitatory	1.2351 (1/8)
G9 (intrinsic)	II → DP, inhibitory	0.4567 (1/8)
G10 (intrinsic)	DP self-gain, inhibitory	0.4379 (1/8)
G11 (intrinsic)	II → SP, inhibitory	0.5173 (1/8)
G12 (intrinsic)	SP → II, excitatory	0.3120 (1/8)
G13 (intrinsic)	SP → DP, excitatory	0.7613 (1/8)
D **	Firing rate gain function	0.0312 (1/8)
b1* (α)	White (Gaussian) noise	(1/8)
b2* (β)	Pink noise (1/f)	(1/8)
L	Weighting on J	1.93 (1/8)
T1	Time constant: II	0.2460 (0)
T2	Time constant: SP	0.3922 (0)
T3	Time constant: SS	0.1313 (0)
T4	Time constant: DP	0.1178 (0)

*b1+b2 = $C(u)$,

**D = $E(x)$

Table 6.2. Showing only parameters whose prior may vary in fitting the model.

6.4 Results

The post-hoc parameter selection procedure resulted identified a best-fit model required 9 variable parameters, including 4 inhibitory and 1 excitatory parameter as well as firing rate and model noise parameters (G1, 7, 8, 9, 11; L, D and b1 & b2). Group averages for these parameters are depicted in figure 6.9.3.

Multivariate ANOVA was used to compare means for each group (HC, RD, CD, FH) for each parameter with post-hoc Bonferroni tests. There was no main effect of group on model parameters (table 6.3.) however; custom hypothesis tests (simple contrasts) revealed that both CD and FH groups differed significantly from HC in the strength of G9 (interneuron mediated inhibition of infragranular pyramidal cells: CD: F=0.118, p=0.026, FH: F=0.102, p=0.038). This was not significant in post-hoc Bonferroni tests (p=0.157 and p=0.227 respectively).

Model Parameter	F	p	df
G1	.375	.772	3
G7	1.319	.277	3
G8	1.484	.228	3
G9	2.168	.101	3
G11	.582	.629	3
D	1.903	.139	3
b1	1.588	.202	3
b2	.937	.428	3
L	1.024	.389	3

Table 6.3. MANOVA interaction term for between-group effects on the model parameters.

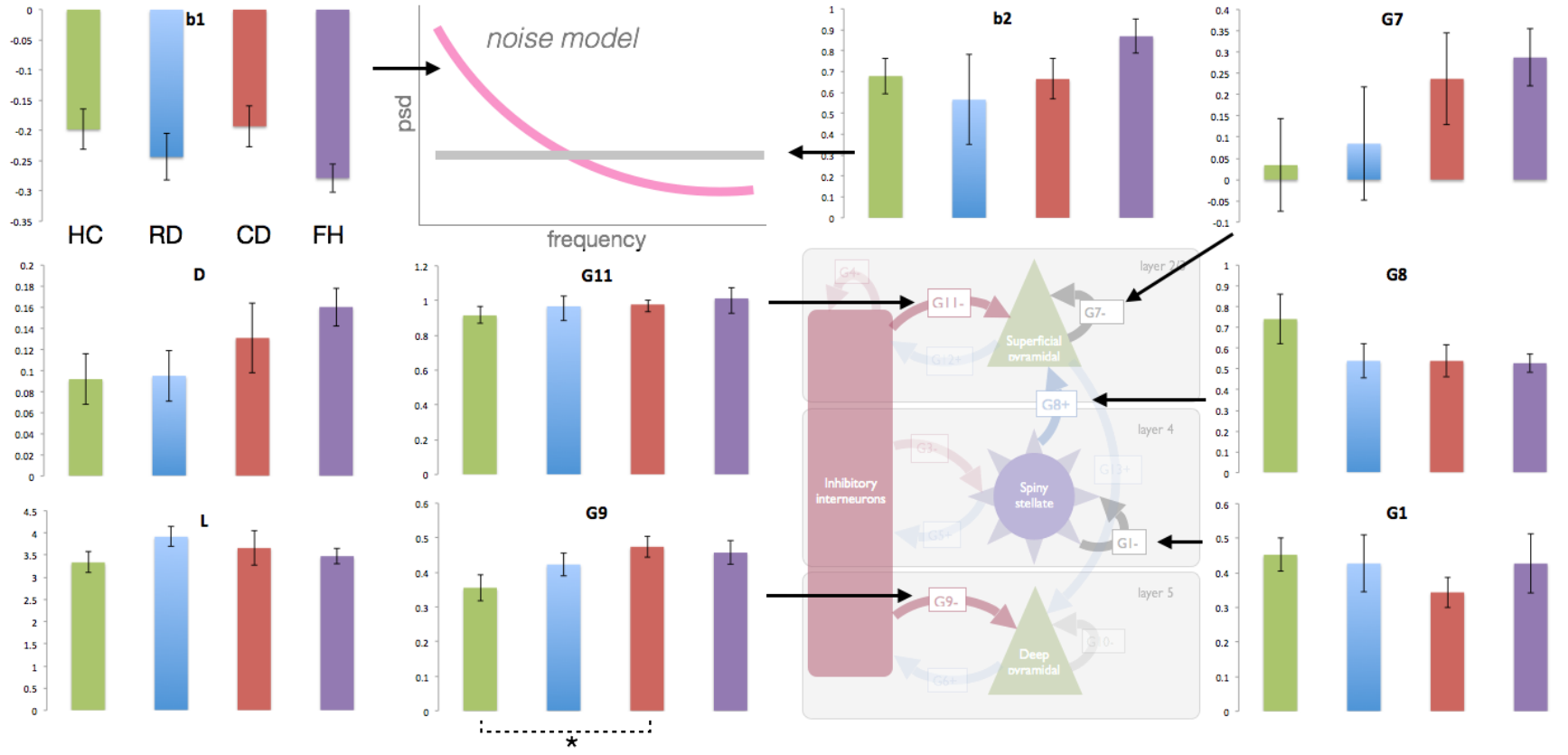

Figure 6.9.3. Demonstrating the parameters needed to vary in order to fit the data. Green = healthy controls, Blue = remitted depression group, red = current depressive episode group, purple = family history of depression group.

6.5 Discussion

The results of this study demonstrated a trend towards increased interneuron-mediated inhibition of layer 5/6 pyramidal cells in subjects meeting MINI criteria for a major depressive episode, as well as healthy subjects reporting a family history of major depression (who are therefore assumed to have a vulnerability to depression) compared with the healthy control group.

The finding of altered interneuron-mediated inhibition (inhibitory interneuron function) is in support of the main hypothesis of chapter 5; that is, GABAergic function is altered in depressed subjects. While these differences were not significant after multiple comparison correction, the study does suggest that DCM could be a sensitive tool for studying clinical groups or differences induced by pharmacological manipulation, and may be more sensitive to altered neurophysiology than standard imaging measures (or may form a useful adjunct). A trend towards (but failure to reach significance in) altered G9, and therefore altered GABAergic inhibition, is also fitting with the MRS and peak-induced gamma frequency results described in chapter 5. Combined, these multimodal imaging and modelling results report no difference in GABAergic measures in depressed subjects, compared with controls.

The visual stimulation (grating) paradigm utilised in this MEG experiment was chosen because it reliably induces a gamma-band response. As such, the intrinsic 'G' parameters selected by the *post-hoc* Bayesian model selection procedure supports theoretical evidence that gamma responses are a locally generated phenomenon, mediated by an interplay of superficial pyramidal cells and inhibitory interneurons (PING) (Brunel, 2003). Parameters G1, 7, 8, and 11 act directly on these populations, altering the amount of excitation or inhibition within the populations.

The inhibitory parameter G9 affects deep layer (L5/6) pyramidal cells, which contribute less to the gamma-band response, but are associated with beta-

frequency responses (figure 6.7, as in Xing, 2012). As such, follow-up analyses should investigate whether similar paradigms induce a beta-frequency response. Moreover, subsequent spectral-DCM studies in healthy subjects should focus on the relationship between intrinsic microcircuit parameters and frequency-specific oscillatory responses. This approach could both validate the microcircuit model, and provide evidence from humans to support theories from computational neuroscience about the neuronal aetiology of frequency-specific oscillations.

This experiment is the first to apply a DCM canonical microcircuit model to probe the neurobiology of major depressive disorder. From this perspective, this study suggests that the DCM approach to studying clinical neurobiology is, when paired with a strong hypothesis, statistically sensitive and may be particularly useful in studying disorders where altered spectral responses are observed, such as in schizophrenia and epilepsy.

Chapter 7. Effect of a NMDA receptor antagonist ketamine on oscillations in primary visual and motor cortices and dynamic causal modelling

7.1. Abstract.

The NMDA receptor antagonist ketamine has demonstrated remarkable and rapid antidepressant efficacy in treatment resistant depressed subjects. The mechanism of action of ketamine is complex and not fully understood, with altered glutamatergic function, alterations of high-frequency oscillatory power (Wood *et al*., 2012) and global effects on γ-amino butyric acid (GABA) levels (Wood & Hertz, 1980) all noted pre-clinically in animal studies. Here we used magnetoencephalography (MEG) in a single blind, crossover study to assess the neuronal effects of 0.5 mg/kg intravenous ketamine on task-related high-frequency oscillatory activity in visual and motor cortices. Consistent with preclinical findings, ketamine reduced peak gamma frequency in visual cortex and significantly increased gamma-band amplitudes in motor and visual cortices – an effect previously linked to cortical pyramidal cell disinhibition, providing directly translatable evidence of this hypothesis to humans.

7.2 Background

In the first clinical trial of ketamine as an antidepressant treatment for treatment-refractory MDD (treatment resistant depression), Zarate and colleagues (2006) demonstrated that a 0.5mg/kg infusion over 40 minutes significantly reduced depressive symptoms within 110 minutes compared with subjects receiving placebo. Moreover, 71% of the n=17 subjects who received ketamine met criteria for 'responding' and 29% met criteria for remission within 24 hours. Understanding the mechanism of this effect, through studying its neurophysiological correlates, will aid in the refinement of biomarkers of anti-depressant responses, and may provide novel mechanistic targets for future pharmacotherapeutic development. For an introduction to the proposed mechanism of action of ketamine, as well as an

overview of the current imaging and preclinical literature on the use of ketamine, the reader is directed to section 1.2.5.

7.3 Experiment: Effects of sub-anaesthetic, intravenous ketamine on visual and motor cortex responses

7.3.1 Rationale

The aforementioned studies support the disinhibition hypothesis of NMDAR antagonism because increased superficial pyramidal cell excitement permits increased synchrony and thereby increased gamma power. While evidence of this mechanism accumulates in preclinical models, translation into humans is lacking, despite the proposed functional link with its antidepressant effect. Magnetoencephalography (MEG) is a powerful tool for measuring pharmacologically induced changes in oscillatory dynamics in humans because of the increased sensitivity to altered neuronal function afforded by this approach compared with common imaging techniques such as functional MRI or near-infrared spectroscopy (reviewed in Muthukumaraswamy, 2014). Using MEG, this experiment aimed to determine whether ketamine-induced NMDAR antagonism indeed results in altered cortical excitation-inhibition balance in humans. To date, there has been no MEG study in humans comparing the effect of ketamine on gamma band oscillations in a placebo-controlled, single blind crossover design.

7.3.2 Methods

The study took the form of a placebo-controlled, single blind crossover design. Subjects made 2 or 3 visits to CUBRIC. Day 1 (optional, completed by some on day 2) consisted of a screening questionnaire using the MINI to screen for any psychiatric illness and discussion about the tasks involved in the study and collection of informed consent signature. Days 2 and 3 were identical apart from the infusion (which alternated so that whichever drug was not administered on day 2 (placebo or ketamine) was administered on day 3). Days 2 and 3 were scheduled a minimum of 2 weeks apart to allow for washout. Drug order was pseudo-random and sessions counterbalanced.

Experiment days consisted of a 90-minute MEG scan where a number of paradigms were completed, including a simple visual grating and motor abduction paradigm detailed below. The scan protocol is depicted in figure 7.1. On either day 2 or 3, subjects who had not previously had an MRI scan in CUBRIC participated in a 12-minute structural MRI before commencement of the study day. All subjects fasted for 8 hours (or overnight) before taking part in each study day.

After scanning, subjects were given lunch (a choice of sandwich), completed the 5-ADSC and BDI questionnaires and remained under the supervision of an anaesthetist for a minimum of 1 hour (>90 minutes after infusion terminated), or until the clinician discharged them.

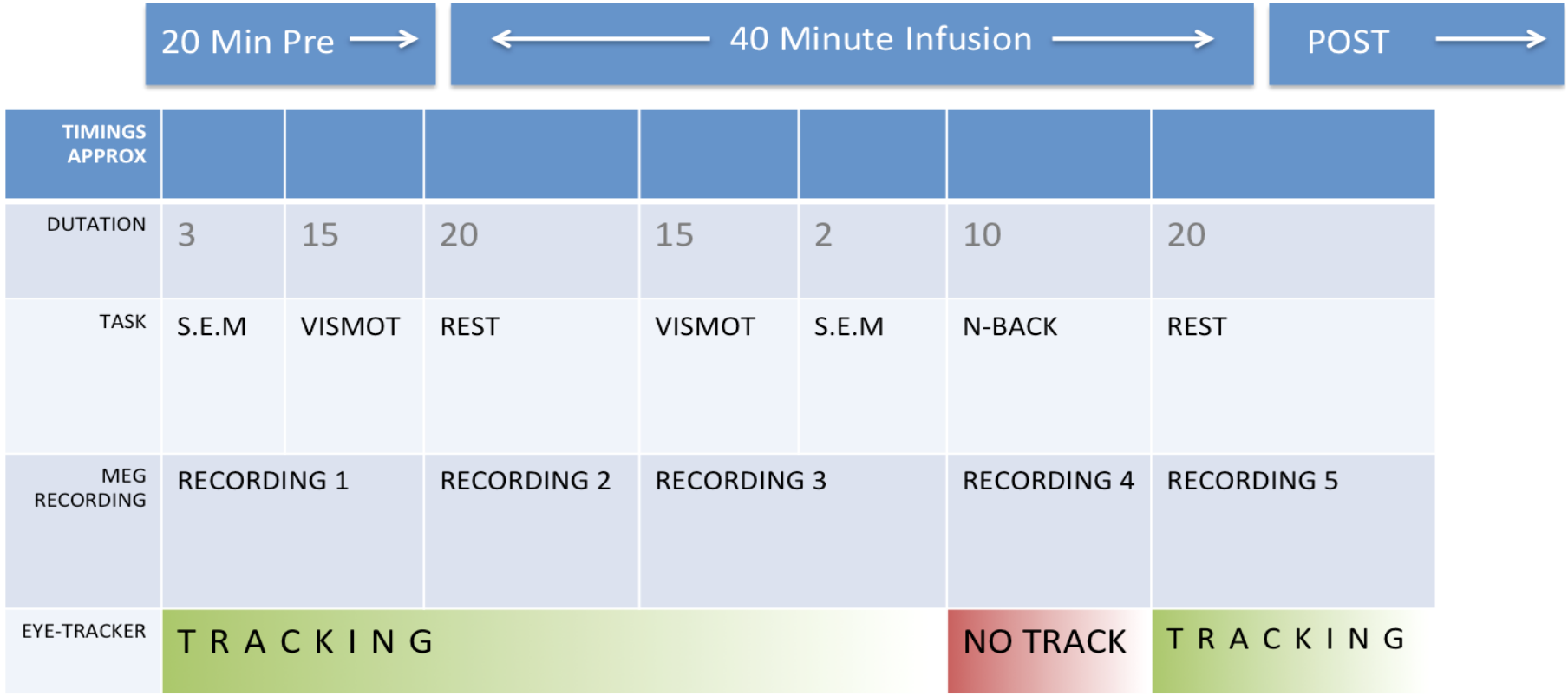

Figure 7.1. MEG scan and infusion timetable. S.E.M, saccadic eye movement; VISMOT, visuomotor paradigm described here; N-BACK, working memory task; REST, resting recording with no task.

7.3.2.1 Sample characteristics

Twenty healthy, male subjects between the ages of 18-45 were recruited to the study. None had any history of psychiatric disorder as screened by the MINI. Those who use recreational drugs or who smoked more than 5 cigarettes a day were excluded. All subjects had a BMI between 18 - 30 kg/m^2.

7.3.2.2 Experimental Procedure, Recordings & Analysis

MEG & Peripheral Recordings

The 275-channel CTF MEG suite at CUBRIC was operated in supine position to keep subjects confortable. A further 29 channels were recorded for noise cancellation. Fiducial (reference) coils were attached 1cm superior to the nasion and, bilaterally, 1cm anterior to the tragus for assessment of head position within the MEG dewar. MEG data were sampled at 1200Hz using axial gradiometers analysed as synthetic third-order gradiometers (Vrba, 2001). Peripheral CNS and physiological monitoring equipment included heart rate (HR), non-invasive blood-pressure cuff (BP), oxygen saturation (SpO_2) and expired carbon-dioxide concentrations ($EtCO_2$) using a Veris MR Vital Signs monitoring system (*Pulse Oximetry*, MedRad). Further peripheral measures included bipolar electro-ocular (EOG) and electrocardiogram (ECG) recordings and electro-myographic (EMG) recordings of (facial) frontalis and temporalis musculature. Finally, pupilometry and corneal-reflection eye tracking was recorded (see figure 7.1 for paradigms recorded) using an IVIEW X MEG ('MEG250' by SensoMotoric Instruments) for monocular tracking of the right eye.

Racemic ketamine hydrochloride was obtained from the Pharmacy Department, University Hospital of Wales. Infusions were administered at a rate of 0.25mg/kg ketamine in 50mL saline, over 40 minutes (or in the case of placebo condition, saline only, over the same time) via intravenous cannula in the dorsum of the left hand. An initial bolus of 0.25mg was administered immediately prior to commencement of the 40-minute infusion (resulting in 0.5mg/kg total), which was controlled by an Asena-PK infusion pump (Alaris Medical, UK).

Visual Grating & Motor Abduction Paradigm

The visuomotor paradigm has been utilised and described in previous pharmaco-MEG studies (Muthukumaraswamy *et al*., 2013) and is based on two separate (one visual, one motor) paradigms (Muthukumaraswamy *et al*., 2013) but which has been packaged into one task. Both the task(s) have been shown to elicit a strong response in their respective primary cortices (V1, M1), including a gamma frequency response widely assumed to be PING generated (see discussion).

Subjects were presented with a vertical, stationary, square-wave grating patch (3 cycles per degree) on a mean luminance background. Of a total 150 trials, 75 were displayed at maximum contrast, while the remaining 75 were displayed at 70%. The patch was subtended 8° both horizontally and vertically around the centre, with a continually displayed, small, central, red fixation square. The grating patch was displayed for between 1.5 and 2s with 3s ISI (fixation square only). Stimuli were displayed by a Sanyo XP41 LCD back-projection system displaying at 1024 x 768 at 60Hz. Subjects were instructed to fixate on the red square throughout the trial and perform a finger abduction at grating-offset. Finger abduction was of the right first dorsal interosseus so that the index finger made a short, sharp abduction in the direction of the thumb. This finger abduction was recorded by both a bipolar EMG electrode placed either end of the muscle, and by an optical displacement meter (Muthukumaraswamy, 2010).

All subjects had a structural MRI scan (either as part of the study, or as volunteers in previous studies in CUBRIC). This was conducted on a GE HDx 3T MR scanner with 8 channel head coil. The sequence was a fast spoiled gradient echo (FSPGR) anatomical scan obtained with 1mm isotropic voxel resolution. Co-registration with MEG data was achieved by matching the fiducial coil positions recorded in MEG to the same location on MR images (by eye, using photographs).

MEG Pre-processing

Markers were placed at the initiation of finger abduction, based on a shift in the amplitude of the optical displacement meter (change by 3 standard deviations above mean noise, as per (Cheyne *et al*., 2008)). Where noise masked a shift corresponding to a displacement, the EMG trace from the first dorsal interosseus was used instead. Placement of all markers was visually inspected. Data were epoched into 4s trials (from 2s before to 2s after the visual stimulus onset - a marker automatically sent to an auxiliary channel on the MEG acquisition computer by the stimulus host computer) to create a dataset containing only visual grating trials. The original dataset was further epoched into 4.5s trials consisting of 1.5 pre- and 3s post- finger abduction onset to create a dataset of only motor responses.

Trials from both datasets were visually inspected for gross artefacts (head movements affecting a large number of sensors). Data were further quality controlled by rejecting trials based on blinks, for which a blink threshold of 70muV was used for the EOG trace during stimulation. Trials were further quality controlled using response time; either the optical displacement meter or finger EMG (whichever was used to epoch the dataset) was used to define a response. Response time was calculated as the difference between response (peak at 3 SD above mean noise, indicative of response) and the stimulus offset time.

Motor response source localisation

For source localisation datasets were beamformed using SAM (Vrba, 2001) (4mm isotropic resolution) with a set of beamformer weights calculated from a global covariance matrix in the gamma frequency band. The motor paradigm elicits a narrowband response between 60-90 Hz (Muthukumaraswamy *et al*., 2013). SAM was used to generate a virtual sensor for each beamformer voxel and statistical (paired *t*-test) images of pre-stimulus vs. post-stimulus power were generated.

The virtual sensor location used for analysis was defined based on best-performing location (highest t-statistic). Time windows for the reconstruction were guided by

previous reports (Cheyne *et al*., 2008; Hamandi *et al*., 2011; Muthukumaraswamy, 2010) where a baseline of -1.3 to -1s was contrasted with 0-0.3s active.

The motor paradigm gamma-response is termed *movement-related gamma synchrony* (MRGS). The motor paradigm also elicits a robust bilateral beta de-synchronisation (*motor related beta de-synchronisation*) followed by a contralateral beta-rebound (*post-movement beta rebound / synchronisation*, PMBR). The beamforming and virtual sensor reconstruction procedure was repeated for each of these components with the beta range defined as 15 – 30 Hz. Guided by previous reports (Muthukumaraswamy *et al*., 2012), the beta desynchronisation component was identified between -0.3-3s while the beta-rebound component was identified between 1-2.5s post finger-abduction. Virtual sensors were created separately for each subject and each condition (pre- and post- placebo and ketamine).

The time-frequency content of the virtual sensors was estimated by applying the Hilbert transform to estimate the amplitude content in 0.5 Hz windows between 1 – 100 Hz. In the first instance, for both experimental paradigms, the time-frequency spectra were estimated on the whole trial (including baseline period), with no baseline correction applied, to check for drug-induced differences in the pre-stimulus period which might confound any stimulus induced changes in frequency or amplitude. Those sensors that did not show a difference in baseline time-frequency content were included in a second spectral estimation analysis using the same approach (Hilbert transform on 0.5 Hz windows between 1-100 Hz) with amplitude calculated as percentage change from baseline (baseline defined as the trial duration up to stimulus onset or finger abduction). Alternatively, sensors that did show a difference in baseline spectra in the initial analysis were re-analysed using a subtracted baseline approach. This approach permits analysis of stimulus-induced changes in time-frequency content while accounting for pre-stimulus changes and has been used previously (Campbell, Sumner, Singh, & Muthukumaraswamy, 2014; Muthukumaraswamy *et al*., 2013). For gamma-range analysis, peak amplitude measures were utilised. For beta-band analysis, mean amplitude was used in place of peak amplitude.

Visual response source localisation

Analysis of visual responses was procedurally the same as motor responses, however, based on previously reported optimisation, the visual paradigm gamma range was defined as 30-80 Hz (broad), beta as 13 – 30 Hz (Muthukumaraswamy & Singh, 2012) and for SAM, a -1.5s to 0s baseline was contrasted with 0-1.5s active period. As per the motor analysis, time frequency content was reconstructed at a best-performing virtual sensor location (this time in V1), this time using the Fourier transform, which, given that frequency is stable across time, provides better estimation of frequency content, but as a consequence is less sensitive to time resolved changes than the Hilbert transform.

For statistical analyses, a 2 x 2 repeated-measures ANOVA was used, with condition and time as factors (condition = ketamine or placebo, time = pre- or post/during- infusion), with the interaction term of primary interest.

7.3.3 Results

Mean subject age was 25.7 (SD 6.2, range 19-39). Of the twenty recruited subjects, 1 withdrew prior to ketamine infusion and an error was made in MEG acquisition for a second, so that at analysis n=18 subjects.

Sub No.	Age	Post-QC. Data Available For:		
		Visual Analysis (all)	Motor Gamma	Motor Beta
1	34	Yes	Yes	Yes
2	23	*Recording error*		
3	36	Yes	Yes	Yes
4	24	Yes		Yes
5	25	Yes		
6	--	*Withdrawn*		
7	28		Yes	Yes
8	29	Yes	Yes	Yes
9	30	Yes	Yes	Yes
10	21	Yes	Yes	Yes
11	23	Yes	Yes	Yes
12	21	Yes	Yes	Yes
13	20	Yes	Yes	Yes
14	20	Yes		
15	22	Yes		
16	19	Yes	Yes	Yes
17	21	Yes	Yes	Yes
18	20	Yes		
19	39			
20	35	Yes	Yes	Yes

Table 7.1. List of subjects and ages. Those included in each step of analysis indicated by 'yes'.

Measures such as response time during the motor abduction, number of visibly noisy trials and extent of head-movement could bias any effects observed in dependent measures if these are significantly increased or reduced by either drug. As such, these were compared between conditions (see table 7.2). Response time, head movement and trials rejected did not change between conditions. As expected, EOG velocity during a saccadic eye-movement task decreased significantly in velocity after ketamine (drug by time interaction, $F(1,16)=6.833$, $p=0.019$), demonstrating significantly more sedation in the post-ketamine condition than other conditions.

Eye tracking data with corneal reflexion was available for only 2 subjects both pre- and post- ketamine. For these subjects, maximum eye movement (in visual degrees) was calculated for each trial for both vertical and horizontal movements. These were entered to a paired-t of post vs. pre infusion for each subject and condition, revealing no differences in eye movements post ketamine infusion (table 7.3, figure 7.3).

		Pre Placebo	Post Placebo	Pre Ketamine	Post Ketamine
Response Time (emg)	Mean	0.31	0.26	0.33	0.35
	SD	0.07	0.11	0.10	0.08
Response Time (LM)	Mean	0.47	0.49	0.60	0.57
	SD	0.24	0.17	0.16	0.21
	Amp	0.23	0.11	0.26	0.29
	SD	0.51	0.36	0.62	0.75
Head Movement	Mean	0.48	0.37	0.33	0.30
	SD	0.40	0.30	0.56	0.38
Visual Trials Rejected	Mean	24	18	18.11	29.44
	SD	24.27	18.27	15.41	17.66
Motor Trials Rejected	Mean	11.16	8.91	9.66	14.16
	SD	14.34	15.58	13.65	11.73

Table 7.2. Mean response time and head-movements by condition. No significant difference in the number of rejections between conditions.

Subject	Direction	Mean	SD	t	DF	p
1	Horizontal	0.049	0.39	0.535	17	0.6
	Vertical	-0.35	1.36	-1.098	17	0.287
2	Horizontal	-0.018	0.13	-0.702	26	0.489
	Vertical	-0.34	0.30	-0.589	26	0.561

Table 7.3. Pre and Post ketamine infusion corneal reflexion eye movements compared for 2 subjects.

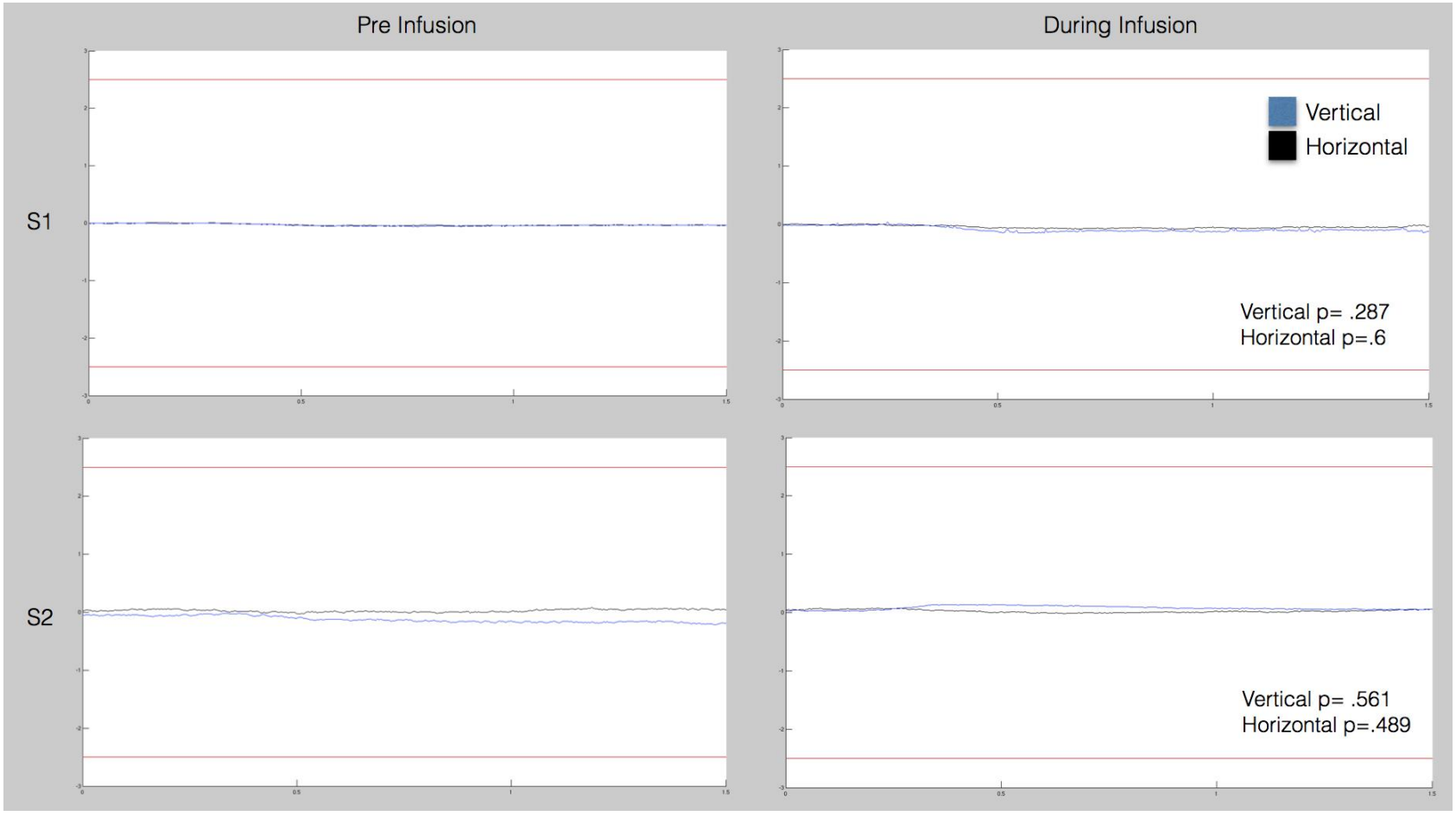

Figure 7.3. Eye tracker eye movements in visual degrees for 2 subjects showing horizontal and vertical movements, pre and post ketamine infusion.

Visual grating stimulus

The visual grating stimulus utilised here robustly elicits both phase-locked and induced gamma responses in V1. The virtual sensor reconstruction demonstrated no difference in pre-stimulus gamma-frequency content, so a percentage-change from baseline approach was utilised for analysis. Peak analysis was conducted by collapsing data over time into transient (0-300ms, evoked / phase-locked) and sustained (300-1500ms, induced / non-phase-locked) responses and plotting the frequency vs. power plots so as to visually inspect peak amplitudes.

Two-way, repeated measures ANOVA was utilised to assess both frequency and amplitude measures. For high contrast, ANOVA interaction (drug x time) revealed no difference in amplitude ($F(1,15)=1.361$, $p=0.261$) but, as hypothesised, an effect whereby ketamine infusion reduced peak frequency ($F(1,15)=4.461$, $p=.052$).

The same analyses were performed for the lower contrast grating. This revealed a significant elevation of induced gamma amplitude after ketamine ($F(1,15)=4.79$, $p=.045$) but no effect on frequency ($F(1,15)=.319$, $p=.58$). These measures are summarised in figure 7.4 with condition mean measures in table 7.5.

For both maximum and 70% contrast visual stimuli, beta frequency (13 - 30 Hz) event related desynchronisation was reduced post ketamine (see figure 7.4, top). For both contrasts the ANOVA was highly significant ($F(1,15)>120$, $p<10^{-8}$).

HIGH CONTRAST	**Pre Placebo**		**Post Placebo**	
	Frequency	Amplitude	Frequency	Amplitude
Mean	50.66	184.08	51.40	184.99
St Error	1.42	30.50	1.20	34.64
	Pre Ketamine		**Post Ketamine**	
	Frequency	Amplitude	Frequency	Amplitude
Mean	51.22	170.80	49.10	205.98
St Error	0.84	23.81	1.19	37.65
LOW CONTRAST	**Pre Placebo**		**Post Placebo**	
	Frequency	Amplitude	Frequency	Amplitude
Mean	42.96	86.47	45.40	85.48
St Error	1.93	14.29	1.52	15.55
	Pre Ketamine		**Post Ketamine**	
	Frequency	Amplitude	Frequency	Amplitude
Mean	45.35	86.57	46.58	113.82
St Error	1.29	10.83	1.56	16.07

Table 7.5. Average frequency, amplitude and fit error for each condition for the induced response.

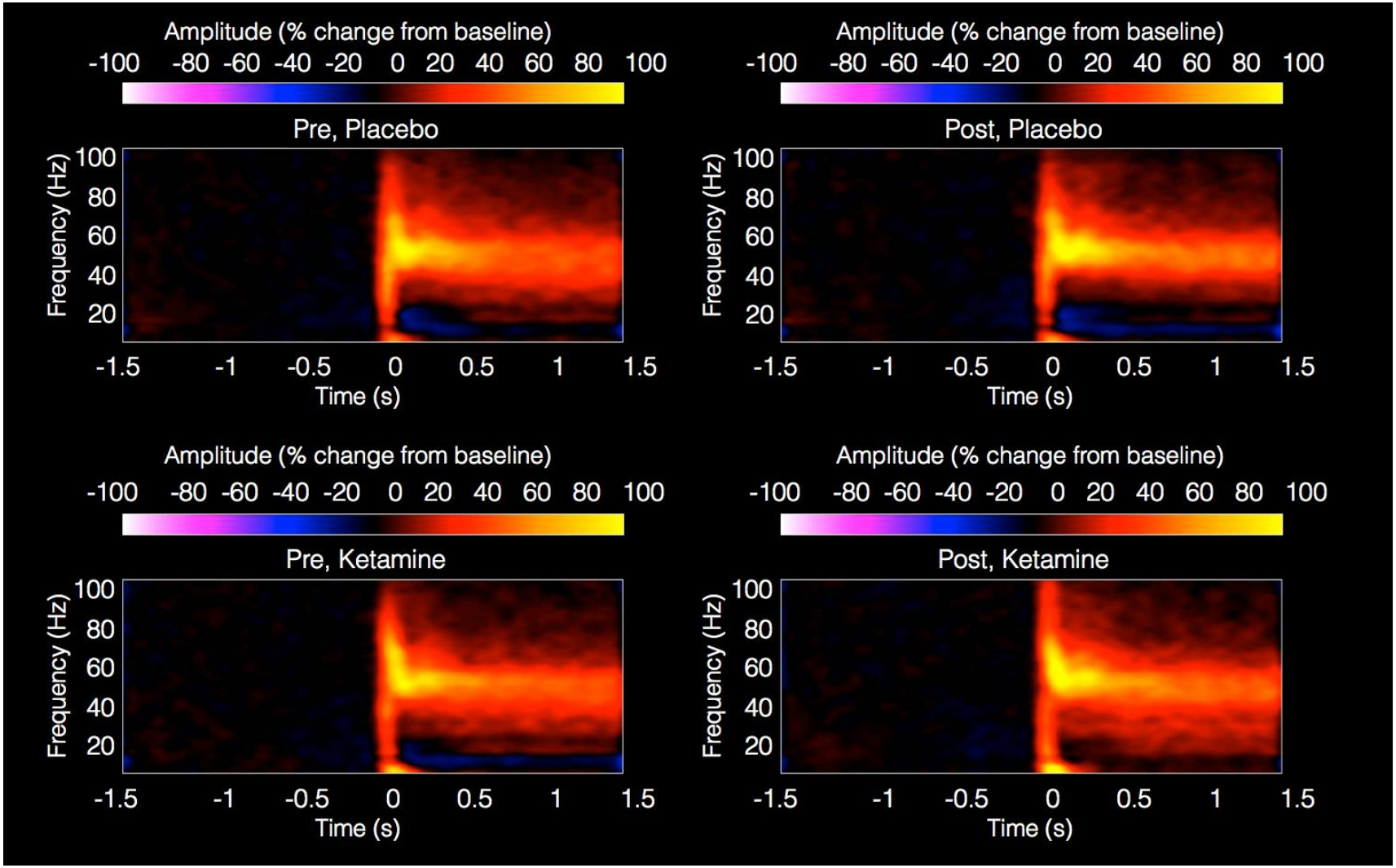
Amplitude (% change from baseline)
-100 -80 -60 -40 -20 0 20 40 60 80 100
Pre, Placebo
Post, Placebo
Pre, Ketamine
Post, Ketamine
Frequency (Hz)
100
80
60
40
20
-1.5 -1 -0.5 0 0.5 1 1.5
Time (s)

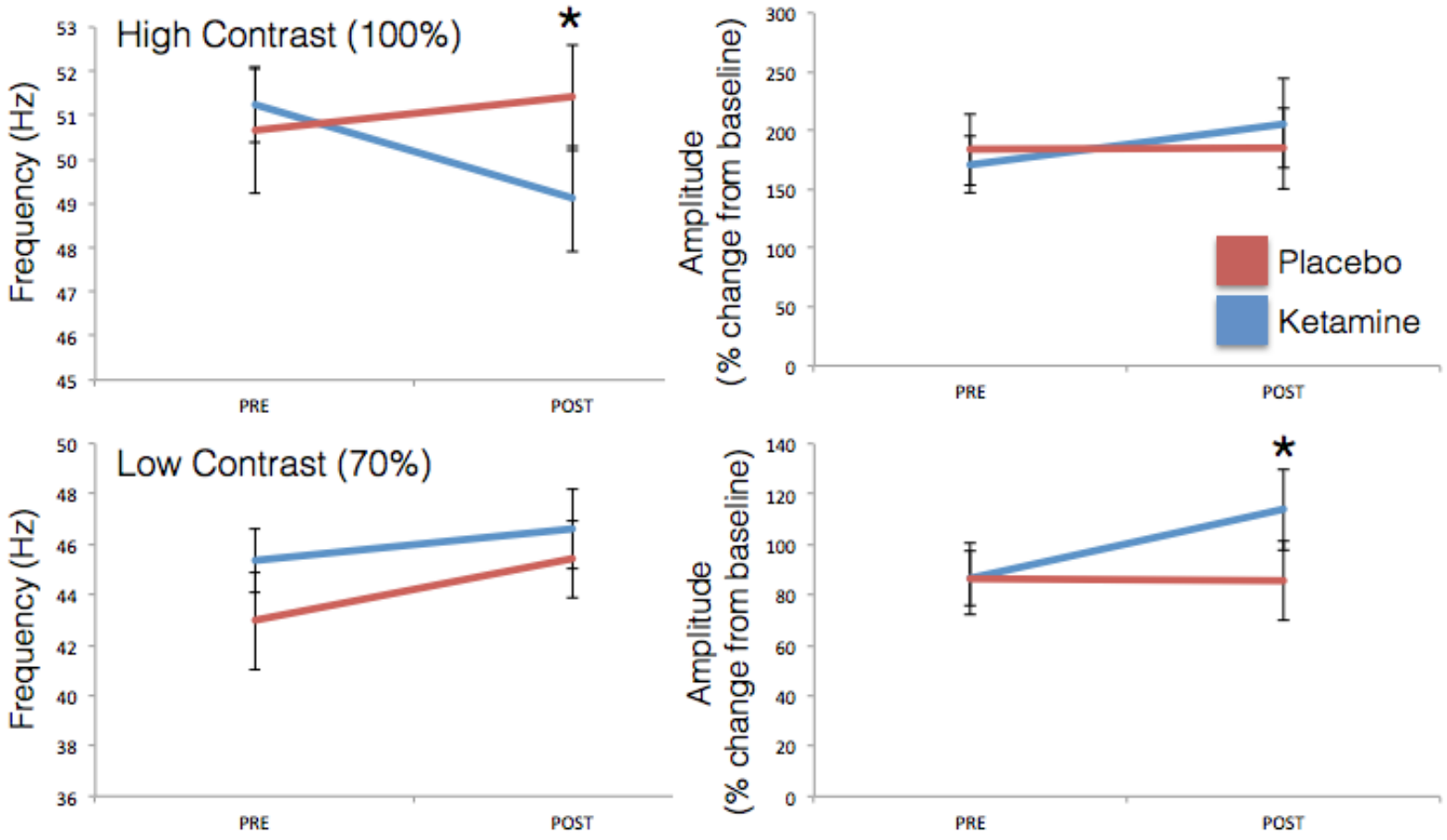

Figure 7.4. Top: spectrogram showing time, frequency and amplitude for the high contrast grating for each condition. Bottom: induced gamma response in V1 for frequency (left) and amplitude (right) for high (top) and low (bottom) contrasts.

In addition to high frequency oscillatory activity, VEFs were also analysed. Using source-localised data from V1, data were band-pass filtered (Butterworth) 1 – 30Hz and baseline adjusted using a relative change method (-0.2 – 0s relative to stimulus onset). Since SAM data is sometimes missing the polarity data present in VEP data, waveforms were manually orientated (where necessary) based on a positive M1 (P1) component. Repeated measures ANOVA was run at every sample point for 0 – 3s and corrected using a post-hoc false-discovery rate (FDR). No significant drug, time or drug*time interaction was observed at any data point after FDR correction. Figure 7.5 shows waveforms for each condition, with both pre- and post-FDR correction overlaid.

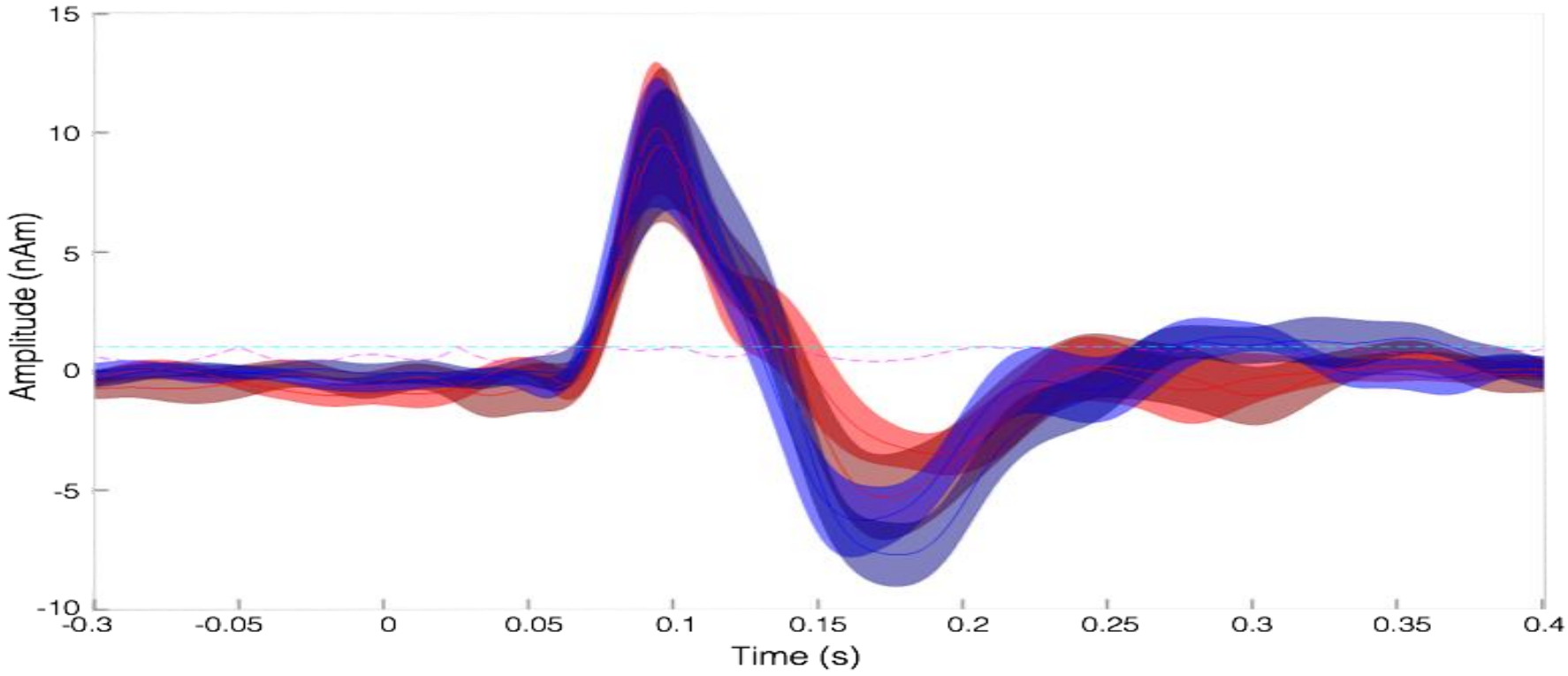

Figure 7.5. Visual evoked spectra from V1 virtual electrode. Red = placebo (saline), blue = ketamine. Light colour = pre-drug administration; dark colour = during drug administration. Pink dashed line = uncorrected p-value from repeated measure ANOVA interaction effect, cyan dashed line = FDR corrected.

Motor paradigm

The finger abduction task robustly elicits 4 components: a contralateral movement-related gamma synchrony, bilateral beta desynchrony followed by a contra-lateral beta-rebound (described previously, see Muthukumaraswamy (2010)). A virtual sensor was created corresponding to each component. Time-frequency analysis revealed an effect of drug on the baseline amplitude of the beta-rebound sensor (PMBR) ($F(1,12)=4.18$, $p=0.0463$), hence subsequent time-frequency analysis of this sensor utilised a subtracted-baseline approach. The MRGS and bilateral MRBD sensors did not differ in pre-stimulus amplitude, thus a relative change approach was used in subsequent time-frequency analyses (in percentage-change from baseline).

Movement related gamma synchrony

Repeated measures ANOVA with drug and time (pre vs. post) as factors was used. Gamma amplitude was significantly increased in a drug*time interaction ($F(1,11)=8.95$, $p=0.014$) as evident in figure 7.6. There was no effect on frequency.

Movement-related beta-desynchrony & Post-movement beta synchrony

Time-frequency analysis of the left and right movement-related beta desynchrony virtual sensors revealed increased power of ipsilateral (right) beta desynchrony (drug*time interaction, $F(1,12)=7.178$, $p=0.02$) but no effect on contralateral beta desynchrony (see figure 7.6) or frequency measures. There was no effect of drug or time on beta frequency or amplitude in the PMBS sensor. Mean measures for each component are listed in table 7.7.

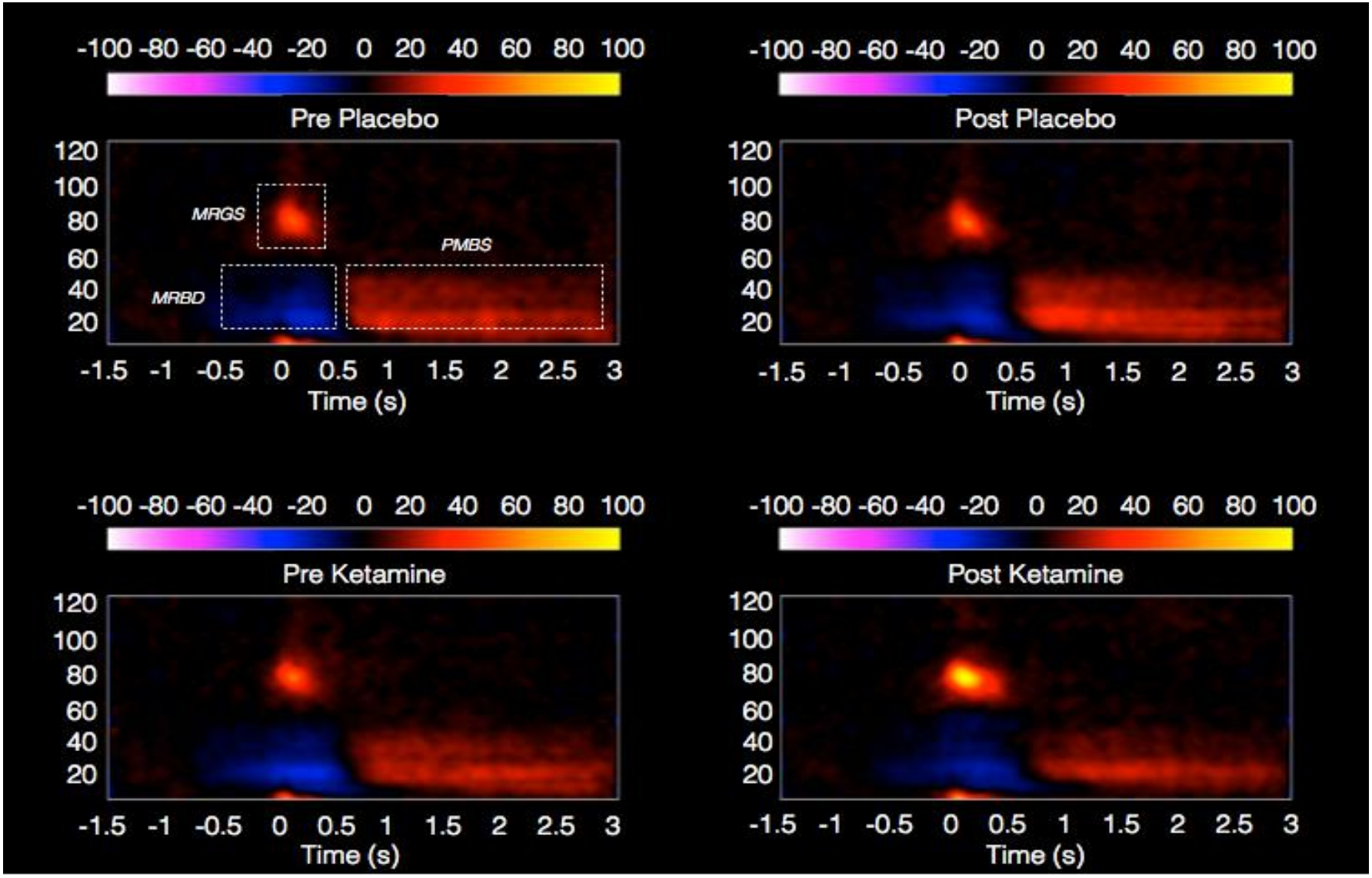
-100 -80 -60 -40 -20 0 20 40 60 80 100
Pre Placebo
120
100
80
60
40
20
MRGS
PMBS
MRBD
-1.5 -1 -0.5 0 0.5 1 1.5 2 2.5 3
Time (s)
-100 -80 -60 -40 -20 0 20 40 60 80 100
Post Placebo
120
100
80
60
40
20
-1.5 -1 -0.5 0 0.5 1 1.5 2 2.5 3
Time (s)
-100 -80 -60 -40 -20 0 20 40 60 80 100
Pre Ketamine
120
100
80
60
40
20
-1.5 -1 -0.5 0 0.5 1 1.5 2 2.5 3
Time (s)
-100 -80 -60 -40 -20 0 20 40 60 80 100
Post Ketamine
120
100
80
60
40
20
-1.5 -1 -0.5 0 0.5 1 1.5 2 2.5 3
Time (s)

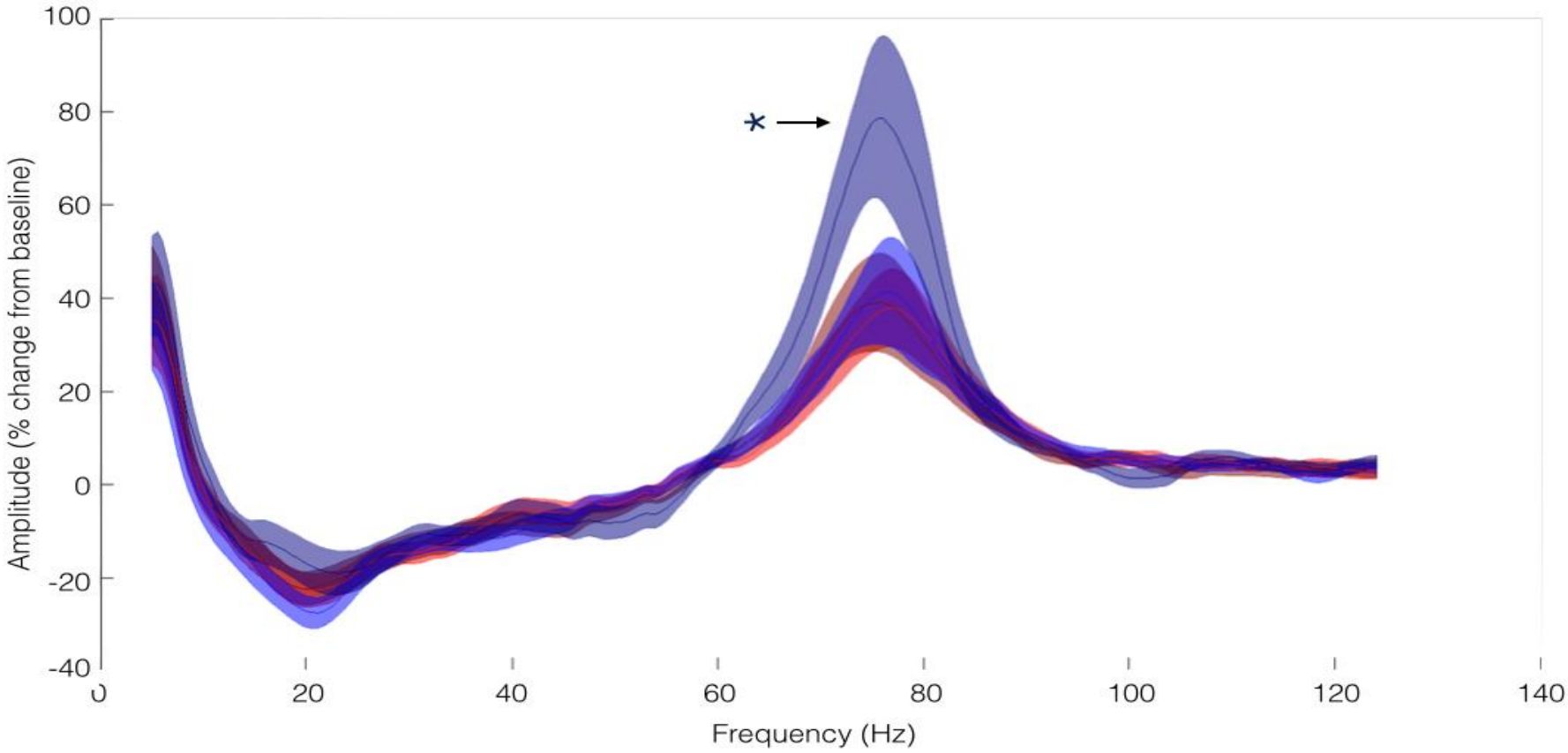

Figure 7.6. Top: time-frequency reconstructions for each condition (averaged over subjects) from M1 contralateral gamma-located virtual sensor, with amplitude depicted by heat-map colours. Note increased colour-intensity (power) of MRGS in post-ketamine. Bottom: power-frequency for each condition (shading = SEM). Red = placebo, blue = ketamine. Light = pre- drug and dark colour = post / during drug.

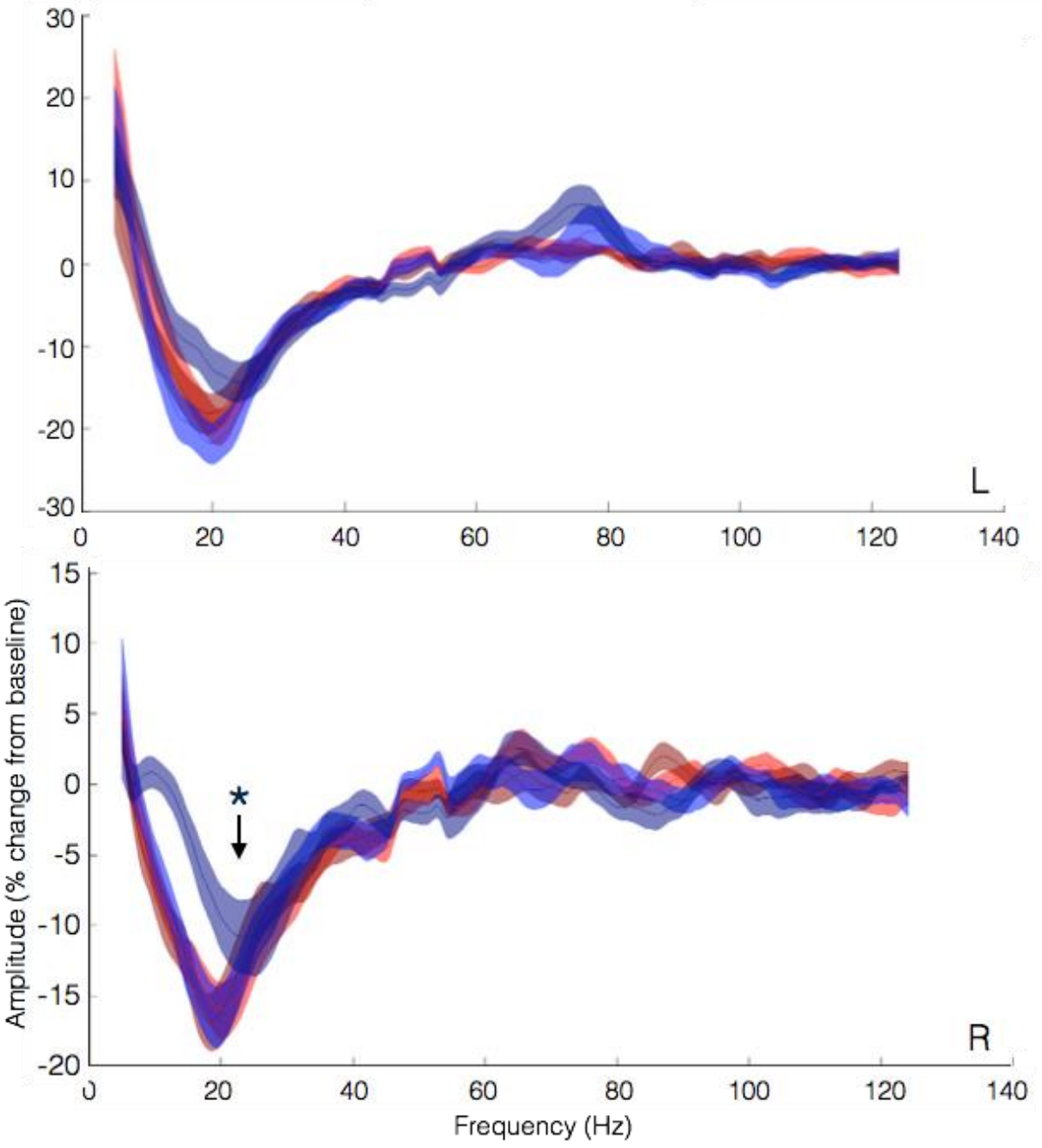

Figure 7.7. Top: Left beta-desynchronisation virtual sensor, amplitude-frequency plot. Bottom: Right beta-desynchronisation virtual sensor. Red = placebo, blue = ketamine. Light = pre- drug and dark colour = post / during drug.

			Peak Frequency	Peak Amplitude	Mean Amp (Where used)
MRGS	Pre Placebo	Mean	76.54166667	41.422475	
		SD	3.414263752	29.14563436	
	Post Placebo	Mean	75.75	45.24466667	
		SD	5.211438468	36.7904114	
	Pre Ketamine	Mean	78.20833333	45.577275	
		SD	4.387266354	41.02053198	
	Post Ketamine	Mean	74.16666667	85.3874	
		SD	3.277563766	66.12037713	
MRBD Left	Pre Placebo	Mean	21.84615385	-21.76375385	-15.31340735
		SD	3.19103311	6.588722662	6.056783654
	Post Placebo	Mean	21.19230769	-20.26270769	-14.76864615
		SD	3.544587785	8.11810032	6.412487294
	Pre Ketamine	Mean	19.61538462	-24.102	-17.06655101
		SD	3.001068186	8.948937082	8.116998527
	Post Ketamine	Mean	23.65384615	-17.3404	-12.15338103
		SD	4.718688975	8.666206369	7.656192715
MRBD Right	Pre Placebo	Mean	20.92307692	-17.68454615	-13.00123507
		SD	3.296754426	6.901485208	5.459895518
	Post Placebo	Mean	20.26923077	-18.04042308	-12.4140248
		SD	3.677722261	7.814619336	6.610371443
	Pre Ketamine	Mean	20.46153846	-17.54250769	-12.57946412
		SD	2.410580311	7.426666701	6.064520655
	Post Ketamine	Mean	23.11538462	-13.5219	-8.656081052
		SD	3.465026732	11.13654697	7.743854137
PMBR	Pre Placebo	Mean	18.92307692	0.5367846154	0.3349063845
		SD	2.243937702	0.2697239788	0.1629812574
	Post Placebo	Mean	17.76923077	0.5943307692	0.3858602254
		SD	1.985524538	0.2093755413	0.1148808263
	Pre Ketamine	Mean	19.15384615	0.6368	0.4263542046
		SD	1.985524538	0.2093755413	0.1148808263
	Post Ketamine	Mean	21.80769231	0.5915076923	0.4140593392
		SD	1.588217837	0.2445059524	0.1617528074

Table 7.6. Summary table. Mean frequency and amplitude for each component of the motor response.

7.3.2 Discussion

This study reported findings from a combined visuomotor MEG paradigm recorded during a placebo-controlled, crossover, and single blind study of the effects of 0.5mg/kg/40 minutes intravenous ketamine on cortical oscillations.

In motor cortex, repeated measures ANOVA revealed significant amplitude increase of MRGS and right MRBD after ketamine administration. In visual cortex, induced gamma amplitude was significantly increased following ketamine to low-contrast (70%) grating patches, but not maximum contrast patches. During high contrast visual stimulation, peak gamma frequency was reduced. Furthermore, for both contrasts, alterations in gamma co-occur with a highly significant decrease in beta frequency event related desynchronisation (i.e. increased beta amplitude). These findings are in accordance with hypotheses from preclinical studies, however in human V1, the two hypothesised findings (increase amplitude and reduced frequency of gamma) occur in different tasks and appear to be contrast dependent.

According to the PING model, gamma-band oscillations are generated locally by an interplay of superficial-layer pyramidal cell and inhibitory interneuron populations (Brunel, 2003; Sohal, 2012); a hypothesis supported by preclinical and primate studies (Bastos, Briggs, Alitto, Mangun, & Usrey, 2014; Xing *et al*., 2012). Both PING and preclinical studies, such as that described by Wood, Kim and Moghaddam (2012), demonstrate that NMDA receptor antagonism increases gamma oscillation amplitude, presumably via disinhibition (Homayoun & Moghaddam, 2007) of pyramidal cell populations. Our results in motor and visual cortex are in support of this mechanism.

The lack of increased gamma amplitude to maximum contrast gratings in visual cortex is surprising, given that the visual stimulation paradigm used in this study has

been widely utilised for the primary purpose of eliciting a robust gamma response. This raises the possibility of a ceiling effect, whereby the visual paradigm response is so strong that affected receptors are at full saturation, meaning pharmacological up-regulation, or subtle modulations, are ineffective. Indeed, several studies have shown strong contrast dependence of MEG visual gamma responses (Perry, Brindley, Muthukumaraswamy, Singh, & Hamandi, 2014). While previous human pharmacological studies have shown increases in gamma oscillatory responses (Campbell *et al*., 2014; Saxena *et al*., 2013) here we used a different stimulus configuration which induces a higher amplitude response than those studies used. Similarly, the lack of effect in visual cortex is unlikely due to a dose-dependence issue, since the primary receptor target of ketamine, the NMDA receptor, has a similar density and laminar distribution in visual cortex as motor cortex (Zilles, Palomero-Gallagher, & Schleicher, 2004).

It is known in both animal (Ray & Maunsell, 2010) and human (Perry *et al*., 2014) data that contrast strongly predicts frequency in V1 and the frequency and amplitude of LFP measures in V1 are not independent (Gieselmann & Thiele, 2008), and our data are consistent with this showing lower peak frequencies to the lower contrast stimuli. The finding of reduced peak frequency to high contrast grating, but not the low contrast grating may reflect limitations in the estimation of peak frequency. It may be that high contrast stimuli, which elicit high amplitude responses close the amplitude ceiling, result in drug manipulation altering the frequency of the response. In this case high signal-to-noise levels permit excellent estimation of frequency.

Conversely low contrast stimuli elicit lower amplitude responses (not at ceiling), and hence estimation of peak frequencies to low contrast stimuli is less accurate than of high contrast stimuli due to decreased signal-to-noise ratio. This might result in an amplitude shift but no reduction in frequency to the lower contrast stimulus. Alternatively, it may be that for the lower contrast stimuli, parameters determining peak frequency may be closer to floor levels making them more difficult to modulate. Nevertheless, when taken together, the visual data from this study can

be interpreted as directional modulation toward both reduced frequency (visual) and increased amplitude (visual and motor).

This is not the first study to demonstrate localised effects of ketamine; Wood *et al* (2012) showed that NMDAR antagonism using MK801 in rats increased gamma amplitude in ACC but not OFC. Given that ketamine is used to model schizophrenia (Frohlich & Van Horn, 2014), and also shows efficacy as an antidepressant (Zarate *et al*., 2006), mapping the brain regions which show increased gamma amplitude to NMDAR antagonism is an important step in understanding how resulting behavioural effects are related to locally observed phenomena.

Individuals with treatment refractory major depressive disorder and schizophrenia have both demonstrated altered excitability in the motor cortex in TMS studies (Maeda, Keenan, & Pascual-Leone, 2000; Pascual-Leone, Manoach, Birnbaum, & Goff, 2002), suggesting that this region may be particularly well suited to studying effects related to these disorders.

Previous work has revealed a role for NMDA receptors in long term potentiation (Collingridge, Isaac, & Wang, 2004). LTP provides a molecular mechanism accounting for learning via synaptic potentiation and associativity. LTP is considered a driver of neuronal plasticity, which is defined as the ability to acquire information and make appropriate responses to subsequent stimuli. The ability to modulate plasticity, through pharmacological manipulation of NMDA receptors, could therefore be beneficial in depression, where sensory, cognitive, emotional and social remodelling may be therapeutic (Duman, 2002).

A recent preclinical study demonstrated *in vivo* that NMDA receptors in the sensorimotor and motor cortices are critical for task-related learning. Furthermore, in visual cortex, the expression of NMDA receptors is experience-dependent on a short timescale, whereby visual experience can result in rapid insertion of NMDARs at the postsynaptic membrane. As such, the NMDAR antagonist induced increase in gamma amplitude in the visual and motor cortices presented in this paper may

reference a modulation of synaptic plasticity in response to a simple visuomotor paradigm.

To summarise, this study demonstrated that ketamine mediated NMDAR antagonism increases the amplitude of both beta and gamma oscillations in the motor and visual cortices and reduced the peak gamma frequency of visual cortex in response to 100% contrast visual stimulation. This supports a preclinical model of NMDAR antagonism increasing cortical excitability via disinhibition of pyramidal cells, and may be important for NMDAR mediated LTP. Given existing hypotheses about altered cortical excitation to inhibition balance in major depressive disorder, the finding presented here may reflect both the mechanism by which ketamine exerts its antidepressant effect, and a potential biomarker.

7.4 Experiment: Ketamine affects microcircuit effective connectivity in V1: a DCM pilot study.

7.4.1 Rationale

Preclinical evidence suggests that the NMDA receptor antagonist ketamine increases the amplitude (power) of high-frequency (gamma band) oscillations via dis-inhibition of cortical pyramidal cells. The aforementioned study failed to find increased gamma-band amplitude in a maximum contrast visual stimulation task, but did find increased V1 gamma to 70% contrast stimulation and M1 gamma-band amplitude in a motor (finger-abduction) paradigm. Dynamic causal modelling of canonical microcircuits for spectral responses provides a novel; non-invasive, *in-vivo* method for addressing the disinhibition hypothesis is humans.

The neuronal mass model utilised in this experiment has been described previously (see chapter 6). This canonical-microcircuit, guided by the known architecture of human V1, contains four distinct neuronal populations: superficial pyramidal cells, granular layer spiny-stellate cells, infragranular (layer 5/6) pyramidal cells and across-layer inhibitory interneurons. Each of these populations has known anatomical projections (either excitatory of inhibitory) to other populations within the same microcircuit (intrinsic connections), thus if the mechanism of ketamine is to

increase gamma-power by disinhibition of pyramidal cells, particular connections within the model will be increased or decreased accordingly.

This pilot study aimed to address 2 questions: first, does ketamine significantly alter the strength of any model parameters, as compared with placebo? Second, in addressing the aforementioned disinhibition hypothesis, after ketamine, which parameters predict the amplitude of gamma-band oscillations?

7.4.2 Methods

Data from the subjects described in section 7.3.2.1, who were included in the visual grating paradigm analysis, were used in this experiment. The participant sample consisted of 19 male subjects aged between 19-39 with a BMI between 18 - 30 kg/m^2 and no history of psychiatric disorder.

The DCM canonical microcircuit described in chapter 6 was implemented. See 6.3.2 for a full description of the model and implementation. The V1 virtual electrode time-frequency data served as input for the model to match. Briefly, the procedure entailed fitting a full model, whereby the parameters in table 7.7 were able to vary by 0.125 around a prior value in order to fit the data. *Post-hoc* Bayesian model selection using the Laplace approximation (as described by Friston, 2011) was implemented to select the minimally-required selection of variable parameters (a subset) to fit the data and estimate their strength without having to rerun the model.

Parameter	Description	Prior π (σ)
G1 (intrinsic)	SS self-gain, inhibitory	0.0962 (1/8)
G3 (intrinsic)	II → SS, inhibitory	0.5163 (1/8)
G4 (intrinsic)	II self-gain, inhibitory	0.0405 (1/8)
G5 (intrinsic)	SS → II, excitatory	0.2708 (1/8)
G6 (intrinsic)	DP → II, excitatory	0.6978 (1/8)
G7 (intrinsic)	SP self-gain, inhibitory	0.3997 (1/8)
G8 (intrinsic)	SS → SP, excitatory	1.2351 (1/8)
G9 (intrinsic)	II → DP, inhibitory	0.4567 (1/8)
G10 (intrinsic)	DP self-gain, inhibitory	0.4379 (1/8)
G11 (intrinsic)	II → SP, inhibitory	0.5173 (1/8)
G12 (intrinsic)	SP → II, excitatory	0.3120 (1/8)
G13 (intrinsic)	SP → DP, excitatory	0.7613 (1/8)
D	Firing rate gain /	0.0312 (1/8)
b1 (α)	White (Gaussian) noise	(1/8)
b2 (β)	Pink noise (1/f)	(1/8)
L	Weighting on J	1.93 (1/8)
T1	Time constant: II	0.2460 (0)
T2	Time constant: SP	0.3922 (0)
T3	Time constant: SS	0.1313 (0)
T4	Time constant: DP	0.1178 (0)

Table 7.7. Parameters in the DCM CMC NMM. SS = Spiny stellate cell, II = inhibitory interneuron, SP = superficial pyramidal cell, DP = deep pyramidal cell.

7.4.3 Results

Post-hoc Bayesian model selection found that variation in 6 parameters was needed to fit the data (G1, 3, 5, 7, 8, & 11). These correspond to spiny-stellate population self-inhibition (G1-), Interneuron-mediated inhibition of spiny-stellates (G3-), Spiny-stellate mediated excitation of inhibitory interneurons (G5+), superficial pyramidal cells self-inhibition (G7-), spiny-stellate mediated excitation of superficial pyramidal cells (G8+) and interneuron-mediated inhibition of superficial pyramidal cells (G11-). These are depicted in figure 7.9.

To address the question of whether ketamine significantly altered the strength of any of these parameters, they were entered into a repeated-measures ANOVA with

drug (saline vs. ketamine) and time (pre vs. post administration) as factors. Parameter G1 demonstrated a significant increase in a drug by time interaction, demonstrating that ketamine significantly increased the strength of G1 ($F(1, 15)=5.408$, $p=0.029$), see table 7.8 for ANOVA results for the interaction term, for each parameter tested.

Drug*Time Interaction	F	p	df
G1	5.805	*.029*	1,15
G3	2.091	.169	1,15
G5	0.160	.695	1,15
G7	0.137	.717	1,15
G8	0.13	.723	1,15
G11	0.132	.721	1,15

Table 7.8. Repeated measures ANOVA, drug*time interaction univariate results.

To address the pyramidal cell disinhibition hypothesis of ketamine's mechanism of action, a correlative analysis was performed. Note that this preliminary analysis aimed to demonstrate a relationship between gamma-band peak amplitude and model parameters in the absence of ketamine-elevated gamma amplitude (i.e. as per section 7.3.3, ketamine did not significantly increase gamma amplitude in the 100% contrast visual data analysis, although a trend was evident).

Correlational analyses were performed by investigating correlations between post-ketamine infusion model parameters (6 G-parameters) and peak gamma-band amplitude. Where model parameters were significant, the same comparison was made in the pre-ketamine administration data. Analyses demonstrated that post ketamine infusion, G5+ ($r=.572$, $n=16$, $p=.021$ $r^2=32.7\%$), G7- ($r=.518$, $n=16$, $p=.04$ $r2=26.9\%$) and G8+ ($r=.704$, $n=16$, $p=.002$, $r2=49.6\%$) significantly predicted peak gamma-band amplitude. G7- and G8+ also predicted peak gamma-band amplitude in the pre-infusion data (G7: $r=.518$, $n=16$, $p=.04$, $r^2=26.8\%$ and G8: $r=.688$, $n=16$, $p=.003$, $r^2=47.3\%$), however G5+ did not ($r=.-.177$, $n=16$, $p=.513$). Critically, false discovery rate calculation (based on the number of comparisons and p-values obtained) revealed that only the G8 correlations (both pre and post) met FDR-

adjusted significance thresholds (adjusted p-values (*q-value*) = 0.0135 and 0.0135, respectively). The post-infusion G5+ correlation did not reach significance after FDR correction (FDR-derived threshold 0.016, FDR-adjusted p=0.063) however a Fisher r-to-z transform demonstrated a significant difference between the pre- and post-infusion G5+ and peak gamma band amplitude correlation coefficients (p=0.0349 two-way).

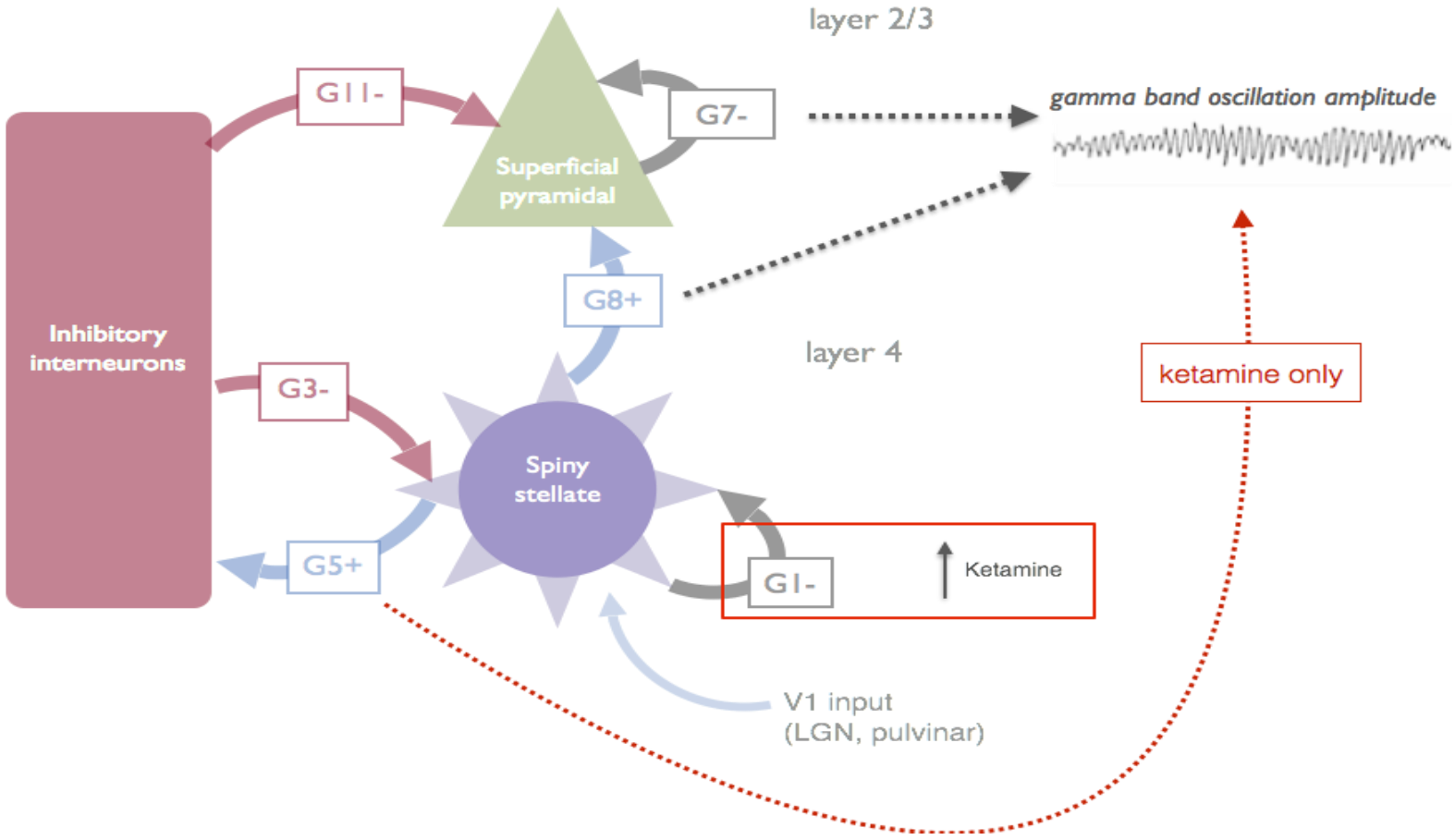

Figure 7.9. Showing the variable intrinsic 'G' parameters required to fit the model. Repeated-measures ANOVA revealed that ketamine significantly increased the strength of G1- (red box). Correlative analysis further revealed that during ketamine administration the strength of G5+ predicts gamma-band (30-80Hz) peak amplitude, but not pre-ketamine.

7.4.4 Discussion

The results of this study, illustrated in figure 7.9, demonstrate that ketamine significantly increased the effective strength of spiny-stellate self-inhibition (*gain*). Furthermore, correlational analysis demonstrated that model parameters G8+ and G7- predict peak gamma-band amplitude. However, with administration of ketamine, G5+ also predicts peak gamma-band amplitude (and that the relationship is significantly different to pre-ketamine infusion).

The excitatory drive to the canonical microcircuit enters the column in layer 4, the spiny stellate population. Since it is the self-gain of this population (G1) which ketamine increased, this suggests that ketamine must act locally to increase G1 via a presynaptic modulation or autoregulatory mechanism whereby NMDAR antagonism increases self-inhibition (self-gain). Little literature has examined NMDA receptors located on spiny stellate cells, however (in rats) layer-4 spiny-stellate populations have been shown to possess co-localised AMPA and NMDA receptors (Feldmeyer, Egger, Lubke, & Sakmann, 1999) and (in mouse) contain functionally-distinct subunit compositions in barrel cortex (Fleidervish, Binshtok, & Gutnick, 1998). Thus, while spiny-stellates contribute a minimal 'direct signal' to non-invasive neurophysiology measures such as MEG, ketamine binding to spiny-stellates with multiple configurations of NMDAR may have a number of local microcircuit effects.

Of particular interest is the effect that layer 4 stellate cells might have on the gamma band response, since this was also shown to be altered by ketamine in experiment 7.3. The predictive coding model of cortical message passing suggests that modulatory connections between columns (inter-microcircuit) use NMDA receptors, and as such an extended model of the visual cortex, which links V1 with up- and down-stream visual processing area microcircuits (e.g. V2 and LGN) would help to further explain the effects of NMDAR antagonism on local gamma. This is particularly relevant since the superficial 'gamma generating' cells are a major postsynaptic target for modulatory NMDAR projections between columns (Friston, 2005). Figure 7.9.1 demonstrates how deeper layer NMDAR mediated modulatory

connections from V2 synapse onto the superficial pyramidal cells of V1 responsible for the gamma oscillation studied in experiment 7.3. This model explains how NMDAR antagonism could directly modulate the dynamics of gamma oscillations, but does not provide a mechanistic explanation for the pyramidal cell disinhibition noted in rodent studies (Wood *et al*., 2012).

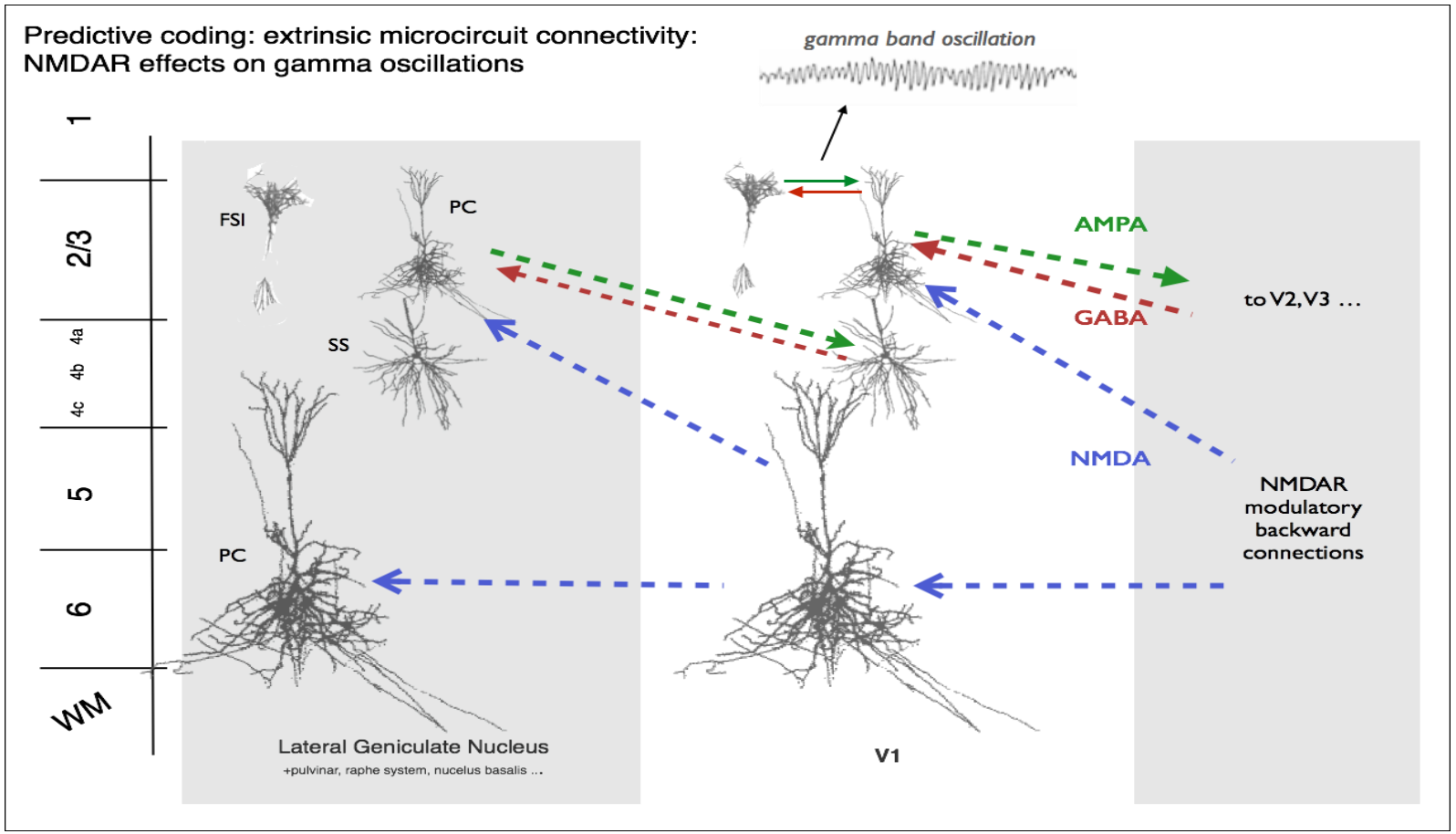

Figure 7.9.1 Depicting extrinsic feedforward/ feedback and modulatory connections, which are thought to be mediated by AMPA / GABAA and NMDARs, respectively (Friston, 2005).

The second finding, that spiny stellate excitation of inhibitory interneuron populations (G5) predicts gamma-band amplitude after ketamine but not before suggests that ketamine has an effect across the microcircuit, and does not just affect the superficial-layer 'gamma generator' populations. This finding, coupled with the finding that both G7 and G8 predict gamma-band amplitude regardless of ketamine administration, suggests a level of cross-layer coupling. That is, after ketamine administration, deeper-layer (L4, G5) interactions could also be contributing to oscillations in the gamma-band.

A known issue with this study is that the microcircuit architecture is modelled on V1, however the amplitude response from V1 to 100% contrast stimuli (experiment in 7.3) was not significantly altered by ketamine administration. While the lower, 70% contrast stimulus, and motor (M1) spectral response were both altered (gamma-band amplitude increased), there is no available microcircuit based upon the known laminar-architecture of M1. Therefore, modelling of the lower contrast visual stimuli is indicated. Future work should also develop detailed microcircuits for other cortical areas of interest. This microcircuit models only one type of excitatory parameter, which is fast and therefore best reflects AMPA receptor mediated excitation. Ketamine, however, shows affinity for NMDA receptors, therefore a model that also includes a slower excitatory parameter (NMDAR) would be beneficial. Such a model has been described by Moran and colleagues (2011).

Despite these limitations, this study demonstrates a methodological proof-of-principal that a spectral-DCM approach to pharmacological-neurophysiology studies in humans can add additional insight into the underlying functional changes induced by a pharmacological manipulation.

7.5 General Discussion

The experiments described in this section aimed to investigate possible mechanisms of the NMDA receptor antagonist drug, ketamine. While preclinical rodent reports allowed generation of a strong directional hypothesis for the effect of

ketamine on high-frequency oscillatory activity, little or no previous reports have investigated the action of ketamine on pattern-onset, visual-evoked responses or using a spectral-DCM canonical microcircuit.

The analysis of oscillatory activity revealed that human primary motor cortex (M1) displays the same gamma-band amplitude increase previously reported in preclinical local-field potential recordings using similar drugs (Homayoun & Moghaddam, 2007; Oke *et al*., 2010), however analysis of primary visual cortex (V1) activity demonstrated this only for 70% contrast stimuli, and not for 100% contrast grating stimuli. Failure to demonstrate a significant amplitude increase in visual cortex to 100% contrast gratings may be due to the small dose administered (0.5mg/kg) compared with preclinical studies. Alternatively, it may reflect a difference in the local neuronal architecture between M1 and V1 since the size and density of cell populations and receptor distributions change subtly across the cortex (for example, the motor cortex does not have a granular layer). Nevertheless, the finding of increased gamma-band amplitude in M1 after ketamine administration strongly supports the disinhibition hypothesis put forth by Homayoun and Moghaddam (2007).

The DCM results provide proof-of-principal that spectral-DCM analysis using an informed and suitable cortical model will add useful information about laminar-specific population dynamics in future MEG studies. Development of a motor-cortex microcircuit, which contains both AMPA and NMDA excitatory receptors, would be of great use in addressing the link between preclinical hypotheses (such as the aforementioned hypothesis of disinhibition) and human spectral responses.

This experiment was motivated by the fact that ketamine has recently demonstrated rapid antidepressant efficacy. Evidence of altered inhibitory-excitatory balance in depression suggests that ketamine's antidepressant action might be to address this imbalance (since it is an NMDAR antagonist). Previously described literature demonstrated that in computation models, excitation to inhibition ratio directly affected the peak frequency of gamma-band oscillations. However, the results of

this experiment indicate that ketamine affects the amplitude of gamma-band responses. Future experiments should evaluate whether ketamine-induced changes in gamma-band amplitude correlate with depressive symptoms or severity, as this would suggest a common pathway between its mechanism as an antidepressant and mechanism in boosting gamma-band amplitude.

Chapter 8. General Discussion

8.1 Summary of findings

This thesis utilised MRS GABA+ and MEG obtained visually evoked and oscillatory responses to investigate the GABAergic hypothesis of major depressive disorder. High frequency oscillatory activity is interpreted under the pyramidal-interneuron gamma (PING) model, whereby peak oscillation frequency reflects a local interaction of GABA and glutamate via pyramidal cells and inhibitory interneurons and is highly dependent on GABA concentration.

The experiment detailed in chapter 3 found no alteration in GABA+ levels or gamma-frequency oscillations in V1 in remitted depressed subjects (previous reports were equivocal), and a subsequent experiment (chapter 5) demonstrated no alteration of these measures in currently-depressed subjects or healthy subjects with a family history of depression compared with a never-depressed control group.

Chapters 3 & 5 further demonstrated that formerly depressed subjects demonstrated significantly reduced (46%) amplitude of the pattern-onset visually evoked field M80 component. This was not evident in subsequent analysis of current depression of family history groups, suggesting the visually evoked M80 may be a trait marker of recovery from depression.

Chapter 2 investigated MEG responses of remitted depressed and healthy subjects while completing explicit and implicit emotion discrimination face tasks. Compared with healthy controls, the remitted depressed group exhibited increased gamma amplitude in the left insula during explicit processing of fearful faces, supporting previous functional MRI studies. During the implicit face task, the remitted group demonstrated significantly decreased M300 amplitude in the middle occipital gyrus irrespective of facial emotion.

Dynamic causal modelling for spectral responses was employed to investigate microcircuit effective connectivity between the four populations, using the MEG data form a visual grating stimulus paradigm. DCM has been suggested to be more sensitive to disease state differences that primary imaging measures such as oscillatory frequency. DCM did not reveal a significant difference between groups for model parameters after multiple comparison correction, however the depressed group demonstrated a trend towards increased inhibitory interneuron mediated inhibition of deep-layer pyramidal cells. This may support preclinical hypotheses implicating altered GABAergic interneuron function in psychiatric disorders.

The final experiment explores the effects of ketamine, an NMDAR antagonist anaesthetic drug, on oscillatory MEG measures. This was motivated by the remarkably rapid antidepressant effect of ketamine reported by Zarate and colleagues (2006). In accordance with preclinical pharmaco-neurophysiology studies, ketamine significantly increased gamma band amplitude in primary motor cortex (M1) and in primary visual cortex (V1) to 70% contrast stimuli, but not 100% contrast stimuli. Furthermore, ketamine reduced the peak frequency of gamma oscillations in V1 to 100% contrast stimuli. Ketamine additionally increased the amplitude of beta oscillations in both M1 and V1 regardless of stimulation paradigm of contrast.

An implementation of dynamic causal modelling of the visual MEG response to ketamine, utilising the aforementioned V1 canonical model, revealed preliminary evidence that ketamine significantly increases self-gain in layer 4 spiny stellate populations in V1. Furthermore, the strength of an excitatory parameter from deep-layer pyramidal cells to inhibitory interneurons was found to predict gamma amplitude after ketamine.

8.2 Interpretation and future research

8.2.1 No difference in V1 GABA+ or gamma band responses in remitted depression but markedly reduced pattern-onset M80 amplitude

Addressing an apparent conflict in the GABAergic deficit hypothesis literature (Bhagwagar & Cowen, 2007, Hasler *et al*., 2005) this experiment examined GABA in remitted depressed subjects using both MRS GABA+ and high-frequency visual cortex oscillations. Neither measure differed between formerly depressed subjects and matched controls, suggesting that the previously reported GABAergic deficit present in acute MDD is not a trait marker of depression and may therefore normalise with remission. MRS GABA+ was also obtained for a prefrontal and a subcortical limbic voxel, neither of which showed differences between the groups, suggesting that the lack of a GABA deficit in remitted MDD is not regionally specific.

These findings are broadly consistent with those of Hasler *et al*. (2005), who demonstrated normal prefrontal GABA levels in remitted MDD. As well as replicating their findings for prefrontal GABA levels, this study provides additional evidence of normal subcortical and occipital GABA+ levels and normal gamma oscillations. It is possible that the GABA deficits previously reported in formerly depressed subjects (Bhagwagar *et al*., 2008; Bhagwagar & Cowen, 2007) represent a biomarker of more recurrent illness.

The experiment reported that remitted depressed subjects demonstrated a 46% decrease in the M80 (C1) amplitude component of the pattern-onset VEF, compared with never depressed controls. This is particularly striking because subclinical depression symptom scores in the formerly depressed individuals did not differ from the normal, never-depressed population. In the remitted depression individuals, M80 VEFs were not correlated with indices of illness recurrence or severity, supporting the proposition that early visually evoked response suppression is not state-dependent and could be a trait marker of MDD.

8.2.2 No difference in V1 GABA+, gamma band responses or spectral DCM microcircuit connectivity between currently depressed subjects, formerly depressed subjects, family-history positive healthy subjects and healthy controls

A follow up to the previous experiment recruited subjects experiencing a current episode of depression ('*CD*': unmedicated, female, meeting MINI current major depressive episode criteria) and healthy subjects with a first-degree family history of depression (FH group) in order to explore both the lack of GABAergic deficit observed in the previous chapter, as well as to characterise the M80 amplitude reduction observed in remitted depression.

The finding that occipital GABA+ measures were not altered in the current depression group was a failure to replicate previous findings which reported a 52% reduction in occipital GABA levels in a similarly sized (n=14) and also unmedicated sample (Sanacora *et al*., 1999). The experiment sample characteristics may account for this difference, since the subjects described by Sanacora and colleagues (1999) were male and female, and were an average age of 42.9 +/- 9.2 years, suggesting more variation in their ages and illness history than the sample recruited in this experiment (mean age 22.5). Furthermore, 12 of the 14 subjects reported by Sanacora *et al* had diagnosed psychiatric comorbidities and 11 of the 14 were considered treatment-refractory. Thus the discrepancy between experimental results may be due to the subject comorbidities (because GABAergic deficits have been shown in other psychiatric disorders including bipolar (Benes *et al*., 2007) and alcohol disorder (Behar *et al*., 1999)). In this respect, the subjects described in this study represent a less complex pathology and are therefore better suited to answering the question of whether a GABA deficit exist solely in depressed subjects.

No difference in GABA or peak gamma frequency was found in the family history group. The hypothesis for GABA and peak gamma frequency in the family history group relied upon the assumption that both measures would be reduced in the CD

group. Both peak gamma frequency and depression are highly heritable (peak gamma: ~90%, see Van Pelt, 2012), suggesting that peak gamma frequency would be reduced in the FH group (since their affected family would be assumed to be also). If MRS GABA+ were also reduced compared to the control group, this would suggest that the altered GABAergic function, giving rise to gamma oscillations, is a trait marker of depression and would have potential as a biological marker. Finding that neither measure was reduced in the FH group supports the notion that both GABA and peak gamma frequency may not be reduced in the CD group.

While the GABA and peak gamma frequency results presented here do not couple with hypotheses from the imaging literature, this is the first study to investigate peak gamma frequency in currently depressed subjects as a marker of GABAergic function, and the first to combine this sample with samples of remitted depressed subjects and family history subjects in order to identify the type of biomarker any positive finding might represent.

In the DCM analysis, finding altered interneuron-mediated inhibition (inhibitory interneuron function) is actually in support of the main hypothesis of chapter 5; that is, GABAergic function may be altered in depressed subjects – despite a null findings reported in the experiment. Combined, these multimodal imaging and modelling results report no difference in GABAergic measures in depressed subjects, compared with controls.

The inhibitory parameter G9 affects deep layer (L5/6) pyramidal cells, which contribute less to the gamma-band response, but are associated with beta-frequency responses. As such, follow-up analyses should investigate whether similar paradigms induce a beta-frequency response. Moreover, subsequent spectral-DCM studies in healthy subjects should focus on the relationship between intrinsic microcircuit parameters and frequency-specific oscillatory responses in order to validate the microcircuit model.

This experiment is the first to apply a spectral-DCM of a V1 canonical microcircuit model to probe the neurobiology of major depressive disorder. The results suggest that the DCM approach to studying clinical neurobiology is, when paired with a strong hypothesis, statistically sensitive and may be particularly useful in studying disorders where altered spectral responses are observed, such as in schizophrenia and epilepsy.

8.2.3 Increased gamma band amplitude in the left insula of formerly depressed subjects in response to fearful faces during an explicit emotion recognition face paradigm, and reduced M300 amplitude irrespective of face emotion during implicit emotion recognition task

During the explicit emotional identification task, RD individuals demonstrated increased gamma amplitude in the left insula compared to ND individuals in response to fearful faces. This measure of gamma-amplitude correlates negatively with left-insula grey matter volume in ND, but not RD. During two separate MEG recordings of implicit emotion processing face tasks (one utilising sad faces, the other fearful), RD individuals demonstrate reduced M300 amplitude regardless of face expression and intensity.

Previous studies have demonstrated an important role for the insula cortex in processing faces expressing disgust, where authors have reported increased BOLD activation to faces expressing disgust (Phillips *et al*., 1997). This experiment reports that the insula also responds to fearful faces, and that gamma oscillatory amplitude in this region is greater in remitted-depressed subjects than controls. Increased gamma oscillatory power is assumed to reflect greater population entrainment and synchrony, and thus increased neuronal resources are being used, a similar assumption to increased BOLD response. This is in concordance with an fMRI study which previously demonstrated that the insula is involved in fear-face processing in healthy participants (Schienle *et al*., 2002), however this is the first study to show a functional difference in remitted depression.

Reduced M300 amplitude in remitted depression individuals to differing intensities of both fearful and sad faces could reflect the negative stimuli bias observed in current episode depression. However, the M300 difference was also observed in the neutral face condition, and amplitude differences only reached statistical thresholds when full and mild intensities and neutral faces were collapsed together. Response data (cued gender discrimination) indicated no difference in accuracy between groups and an ANOVA demonstrated no main effect of emotion on M300, only group. It is likely that, per-condition, the M300 amplitude is truly different between groups, however due to lack of statistical power this is only significant when conditions are combined.

It is surprising that the difference in M300 amplitude was not observed during the explicit face task. The key difference between the paradigms is that, during the implicit task, participants were instructed to identify only the gender of the faces presented, whereas the explicit task required identification of the emotion being expressed. These results suggest that an experimentally induced difference in neuronal function occurs between the implicit and explicit tasks, which accounts for the M300 amplitude difference between the groups. Thus, the M300 amplitude could reflect the depression-related negative-emotion-bias during only implicit emotion processing, with the bias being diminished when attention is focussed upon explicitly identifying the facial expression.

This study is novel in that few studies have focussed on ERF and gamma responses during face processing in remitted depression. Together, these findings demonstrate that neuronal function, during emotional face processing, is altered in remitted depression compared with healthy controls. Moreover, these results indicate differences in the activity of both basic sensory (middle occipital / visual area) and higher-order (insula) regions in face processing in remitted depression. Finally, emotional face processing differences observed in remitted depression differ depending on task instruction (explicit vs. implicit identification).

8.2.4 Ketamine significantly increases beta and gamma oscillation amplitudes in primary motor and visual cortices and reduced peak gamma frequency to 100% contrast stimuli.

Under the PING model (*pyramidal – interneuron gamma*) Homayoun and Moghaddam (2007) demonstrated that NMDA receptor antagonism resulted in disinhibition of pyramidal cell populations, which resulted in increased gamma amplitude. Results reported in chapter 7 are in accordance with the preclinical findings of both Homayoun and Moghaddam (2007) and Oke and colleagues (2010), whereby NMDAR antagonism increased gamma-band amplitude in motor cortex, suggesting that ketamine exerts the same mechanism in humans, and this may ultimately involve disinhibition of superficial pyramidal cell populations.

Increased gamma-band amplitude observed after ketamine administration could be a 'cortex-wide' phenomenon (Lazarewicz *et al*., 2010) and the results of this study are in accordance with this hypothesis.

This study is the first to explore changes in oscillatory dynamics in humans brought about by ketamine administration. It provides an important translation of a preclinical theory of ketamine's effect on high-frequency oscillatory amplitude to humans.

The pilot DCM analysis of the effect of ketamine on V1 microcircuit effective connectivity demonstrated that ketamine significantly increased the effective strength of spiny-stellate self-inhibition (*gain*). Excitatory drive to the canonical microcircuit enters the column in layer 4, the spiny stellate population. Since it is the self-gain of this population (G1) which ketamine increased, this suggests that ketamine must act locally to increase G1 via a presynaptic modulation or autoregulatory mechanism whereby NMDAR antagonism increases self-inhibition (gain).

Additionally, correlational analysis demonstrated that while model parameters G8+ and G7- (reciprocal superficial pyramidal cell and interneuron connections) predict peak gamma-band amplitude regardless of drug manipulation, after ketamine G5+ (excitatory connection from deep layer pyramidal cells to interneurons) also predicts peak gamma-band amplitude. This suggests that ketamine has an effect across the microcircuit – not just targeting the layer 4 population (as described above). Coupled with the finding that both G7 and G8 predict gamma-band amplitude regardless of ketamine administration, this suggests a level of cross-layer coupling, that is, ketamine administration results in deeper-layer (L4, G5) interactions also contributing to oscillations in the gamma-band. Such cross-layer coupling has been reported after NMDAR antagonism preclinically, where it resulted in frequency matching of layers in laminar specific recordings (Anver *et al*., 2010).

A known issue with this study is that the microcircuit architecture is modelled on V1, however the spectral response from V1 (experiment in 7.3) was not altered by ketamine administration. While the motor (M1) spectral response was altered (gamma-band amplitude increased), there is no available microcircuit based upon the known laminar-architecture of the region. As such, future work should include developing detailed microcircuits for other cortical areas of interest. Additionally, this microcircuit models only one fast excitatory connection, reflecting AMPA receptor mediated excitation. As such, a model possessing an NMDAR mediated connection would be better model effects of an NMDAR targeting drug such as ketamine (such as model has been described by Moran and colleagues, 2011).

8.3 Research impact

The experiments detailed in the earlier chapters of this thesis are primarily concerned with investigating reports of altered GABAergic function in depressive disorders. The most important outcome of these experiments is the finding of normal MRS GABA+ levels in the visual cortex of both depressed and formerly depressed individuals. This disparity with the literature may be reflected by the differences in clinical characteristics – where the subjects described in the

experiments of this thesis represent a relatively simpler pathology and clinical history than in other reports such as in Sanacora *et al* (1999). This finding should be taken into consideration by other experimenters working on refining the GABAergic hypothesis of depression and mood disorder more broadly.

Findings in formerly depressed individuals that the 1) M80 VER amplitude is reduced, and 2) that altered function during emotional face processing is observed in the insula cortex and middle occipital gyrus, are both suggestive that the study of remitted depressed subjects may provide a tool to better understand neurobiological mechanisms in depression. These experiment findings should inform follow up studies attempting to characterise responses as biological markers of disease.

The later experiments of this thesis are concerned with neuronal modelling of spectral responses (DCM of MEG data) and pharmacological-MEG. The DCM analyses, although preliminary in nature, suggest that spectral-DCM could add an extra level of sensitivity to both clinical and pharmacological MEG and EEG studies. As such, these methodologies mean that neurophysiology studies can address more neurobiologically specific hypotheses about abnormal or drug-induced alterations of neuronal function without having to move to the preclinical domain.

Finally, the pharmacological MEG experiment in chapter 7 demonstrates that the pharmaco-MEG approach to studying neuropharmacology is a sensitive enough measure to compare with preclinical invasive methodologies, and is therefore useful in translating preclinical research into humans. The methodology also has the potential to better characterise and validate hypotheses about the neuronal generators of the MEG signal. Combining the data-rich MEG signal with pharmaco-therapy has great potential in the relatively novel domain of 'personalised medicine,' where a scan at diagnosis may help predict which patients are most likely to respond to a given drug.

References

Acosta, G. B., & Rubio, M. C. (1994). GABAA receptors mediate the changes produced by stress on GABA function and locomotor activity. *Neuroscience Letters*, *176*(1), 29–31.

Adams, M. M., Hof, P. R., Gattass, R., Webster, M. J., & Ungerleider, L. G. (2000). Visual cortical projections and chemoarchitecture of macaque monkey pulvinar. *Journal of Comparative Neurology*, *419*(3), 377–393.

Adjamian, P., Holliday, I. E., Barnes, G. R., Hillebrand, A., Hadjipapas, A., & Singh, K. D. (2004). Induced visual illusions and gamma oscillations in human primary visual cortex. *The European Journal of Neuroscience*, *20*(2), 587–592. doi:10.1111/j.1460-9568.2004.03495.x

Akbarian, S., & Huang, H.-S. (2006). Molecular and cellular mechanisms of altered GAD1/GAD67 expression in schizophrenia and related disorders. *Brain Research Reviews*, *52*(2), 293–304. doi:10.1016/j.brainresrev.2006.04.001

Alcaro, A., Panksepp, J., Witczak, J., Hayes, D. J., & Northoff, G. (2010). Is subcortical–cortical midline activity in depression mediated by glutamate and GABA? A cross-species translational approach. *Neuroscience and Biobehavioral Reviews*, *34*(4), 592–605.

Altamura, C., Maes, M., Dai, J., & Meltzer, H. Y. (1995). Plasma concentrations of excitatory amino acids, serine, glycine, taurine and histidine in major depression. *European Neuropsychopharmacology : the Journal of the European College of Neuropsychopharmacology*, *5 Suppl*, 71–75.

Anand, A., Li, Y., Wang, Y., Wu, J., Gao, S., Bukhari, L., *et al*. (2005). Activity and connectivity of brain mood regulating circuit in depression: a functional magnetic resonance study. *Biological Psychiatry*, *57*(10), 1079–1088. doi:10.1016/j.biopsych.2005.02.021

Andreasen, N. C., Endicott, J., Spitzer, R. L., & Winokur, G. (1977). The family history method using diagnostic criteria. Reliability and validity. *Archives of General Psychiatry*, *34*(10), 1229–1235.

Anver, H., Ward, P. D., Magony, A., & Vreugdenhil, M. (2010). NMDA Receptor

Hypofunction Phase Couples Independent γ-Oscillations in the Rat Visual Cortex. *Neuropsychopharmacology*, *36*(2), 519–528. doi:10.1038/npp.2010.183

Arnal, L. H., & Giraud, A.-L. (2012). Cortical oscillations and sensory predictions. *Trends in Cognitive Sciences*, *16*(7), 390–398. doi:10.1016/j.tics.2012.05.003

Ashburner, J., & Friston, K. J. (2000). Voxel-based morphometry--the methods. *NeuroImage*, *11*(6 Pt 1), 805–821. doi:10.1006/nimg.2000.0582

Auer, D. P., Pütz, B., Kraft, E., Lipinski, B., Schill, J., & Holsboer, F. (2000). Reduced glutamate in the anterior cingulate cortex in depression: an in vivo proton magnetic resonance spectroscopy study. *Biological Psychiatry*, *47*(4), 305–313. doi:10.1016/S0006-3223(99)00159-6

Baillet, S., Mosher, J. C., & Leahy, R. M. (2001). Electromagnetic brain mapping. *Signal Processing Magazine, IEEE*, *18*(6), 14–30.

Bak, L. K., Schousboe, A., & Waagepetersen, H. S. (2006). The glutamate/GABA-glutamine cycle: aspects of transport, neurotransmitter homeostasis and ammonia transfer. *Journal of Neurochemistry*, *98*(3), 641–653. doi:10.1111/j.1471-4159.2006.03913.x

Bange, F., & Bathien, N. (1998). Visual cognitive dysfunction in depression: an event-related potential study. *Electroencephalography and Clinical Neurophysiology/Evoked Potentials Section*, *108*(5), 472–481. doi:10.1016/S0168-5597(98)00024-0

Barone, P., Batardiere, A., Knoblauch, K., & Kennedy, H. (2000). Laminar distribution of neurons in extrastriate areas projecting to visual areas V1 and V4 correlates with the hierarchical rank and indicates the operation of a distance rule. *Journal of Neuroscience*, *20*(9), 3263–3281.

Bartos, M., Vida, I., & Jonas, P. (2007). Synaptic mechanisms of synchronized gamma oscillations in inhibitory interneuron networks. *Nature Publishing Group*, *8*(1), 45–56. doi:10.1038/nrn2044

Bastos, A. M. A., Usrey, W. M. W., Adams, R. A. R., Mangun, G. R. G., Fries, P. P., & Friston, K. J. K. (2012). Canonical microcircuits for predictive coding. *Neuron*, *76*(4), 695–711. doi:10.1016/j.neuron.2012.10.038

Bastos, A. M., Briggs, F., Alitto, H. J., Mangun, G. R., & Usrey, W. M. (2014).

Simultaneous Recordings from the Primary Visual Cortex and Lateral Geniculate Nucleus Reveal Rhythmic Interactions and a Cortical Source for Gamma-Band Oscillations. *Journal of Neuroscience*, *34*(22), 7639–7644. doi:10.1523/JNEUROSCI.4216-13.2014

Behar, K. L., Rothman, D. L., Petersen, K. F., Hooten, M., Delaney, R., Petroff, O. A., *et al*. (1999). Preliminary evidence of low cortical GABA levels in localized 1H-MR spectra of alcohol-dependent and hepatic encephalopathy patients. *The American Journal of Psychiatry*, *156*(6), 952–954.

Bekkers, J. M., & Stevens, C. F. (1989). NMDA and non-NMDA receptors are co-localized at individual excitatory synapses in cultured rat hippocampus. *Nature*, *341*(6239), 230–233. doi:10.1038/341230a0

Belelli, D., Harrison, N. L., Maguire, J., Macdonald, R. L., Walker, M. C., & Cope, D. W. (2009). Extrasynaptic GABAA Receptors: Form, Pharmacology, and Function. *Journal of Neuroscience*, *29*(41), 12757–12763. doi:10.1523/JNEUROSCI.3340-09.2009

Benes, F. M., Lim, B., Matzilevich, D., Walsh, J. P., Subburaju, S., & Minns, M. (2007). Regulation of the GABA cell phenotype in hippocampus of schizophrenics and bipolars. *Proceedings of the National Academy of Sciences*, *104*(24), 10164.

Bhagwagar, Z., & Cowen, P. J. (2007). "It's not over when it's over": persistent neurobiological abnormalities in recovered depressed patients. *Psychological Medicine*, *38*(03). doi:10.1017/S0033291707001250

Bhagwagar, Z., & Goodwin, G. M. (2005). Lamotrigine in the treatment of bipolar disorder. *Expert Opinion on Pharmacotherapy*, *6*(8), 1401–1408. doi:10.1517/14656566.6.8.1401

Bhagwagar, Z., Wylezinska, M., Jezzard, P., Evans, J., Ashworth, F., Sule, A., *et al*. (2007). Reduction in Occipital Cortex γ-Aminobutyric Acid Concentrations in Medication-Free Recovered Unipolar Depressed and Bipolar Subjects. *Biological Psychiatry*, *61*(6), 806–812. doi:10.1016/j.biopsych.2006.08.048

Bhagwagar, Z., Wylezinska, M., Jezzard, P., Evans, J., Boorman, E., M Matthews, P., & J Cowen, P. (2008). Low GABA concentrations in occipital cortex and anterior cingulate cortex in medication-free, recovered depressed patients. *The*

International Journal of Neuropsychopharmacology / Official Scientific Journal of the Collegium Internationale Neuropsychopharmacologicum (CINP), *11*(2), 255–260. doi:10.1017/S1461145707007924

Bhagwagar, Z., Wylezinska, M., Taylor, M., Jezzard, P., Matthews, P. M., & Cowen, P. J. (2004). Increased brain GABA concentrations following acute administration of a selective serotonin reuptake inhibitor. *The American Journal of Psychiatry*, *161*(2), 368–370.

Bierut, L. J., Heath, A. C., Bucholz, K. K., Dinwiddie, S. H., Madden, P. A., Statham, D. J., *et al*. (1999). Major depressive disorder in a community-based twin sample: are there different genetic and environmental contributions for men and women? *Archives of General Psychiatry*, *56*(6), 557–563.

Binesh, N., Kumar, A., Hwang, S., & Mintz, J. (2004). Neurochemistry of late-life major depression: A pilot two-dimensional MR spectroscopic study - Binesh - 2004 - Journal of Magnetic Resonance Imaging - Wiley Online Library. *Journal of Magnetic ….*

Block, W., Träber, F., Widdern, von, O., Metten, M., Schild, H., Maier, W., *et al*. (2009). Proton MR spectroscopy of the hippocampus at 3 T in patients with unipolar major depressive disorder: correlates and predictors of treatment response. *The International Journal of Neuropsychopharmacology*, *12*(3), 415–422. doi:10.1017/S1461145708009516

Bocchio-Chiavetto, L., Bagnardi, V., Zanardini, R., Molteni, R., Nielsen, M. G., Placentino, A., *et al*. (2010). Serum and plasma BDNF levels in major depression: a replication study and meta-analyses. *The World Journal of Biological Psychiatry : the Official Journal of the World Federation of Societies of Biological Psychiatry*, *11*(6), 763–773. doi:10.3109/15622971003611319

Bosman, C. A., Schoffelen, J.-M., Brunet, N., Oostenveld, R., Bastos, A. M., Womelsdorf, T., *et al*. (2012). Attentional stimulus selection through selective synchronization between monkey visual areas. *Neuron*, *75*(5), 875–888. doi:10.1016/j.neuron.2012.06.037

Boudarene, M. (1997). [Stress, anxiety and and event related pot... [Encephale. 1997 Jul-Aug] - PubMed - NCBI. *L'Encéphale*.

Bourke, C., Douglas, K., & Porter, R. (2010). Processing of facial emotion

expression in major depression: a review. *Australian and New Zealand Journal of Psychiatry*, *44*(8), 681–696. doi:10.3109/00048674.2010.496359

Bowery, N. G., Hill, D. R., Hudson, A. L., Doble, A., Middlemiss, D. N., Shaw, J., & Turnbull, M. (1980). (-)Baclofen decreases neurotransmitter release in the mammalian CNS by an action at a novel GABA receptor. *Nature*, *283*(5742), 92–94.

Brambilla, P., Perez, J., Barale, F., Schettini, G., & Soares, J. C. (2003). GABAergic dysfunction in mood disorders. *Molecular Psychiatry*, *8*(8), 721–737. doi:10.1038/sj.mp.4001362

Bramon, E., Rabe-Hesketh, S., Sham, P., Murray, R. M., & Frangou, S. (2004). Meta-analysis of the P300 and P50 waveforms in schizophrenia. *Schizophrenia Research*, *70*(2-3), 315–329. doi:10.1016/j.schres.2004.01.004

Bredemeier, K., Spielberg, J. M., Silton, R. L., Berenbaum, H., Heller, W., & Miller, G. A. (2010). Screening for depressive disorders using the Mood and Anxiety Symptoms Questionnaire Anhedonic Depression Scale: a receiver-operating characteristic analysis. *Psychological Assessment*, *22*(3), 702–710. doi:10.1037/a0019915

Bremner, J. D., Narayan, M., Anderson, E. R., Staib, L. H., Miller, H. L., & Charney, D. S. (2000). Hippocampal Volume Reduction in Major Depression. *The American Journal of Psychiatry*, *157*(1), 115–118.

Bruder, G., & Kayser, J. (2009). Eventrelated brain potentials in depression: Clinical, cognitive and neurophysiologic implications.

Brunel, N. (2003). What Determines the Frequency of Fast Network Oscillations With Irregular Neural Discharges? I. Synaptic Dynamics and Excitation-Inhibition Balance. *Journal of Neurophysiology*, *90*(1), 415–430. doi:10.1152/jn.01095.2002

Buckby, J. A., Yung, A. R., Cosgrave, E. M., & Killackey, E. J. (2007). Clinical utility of the Mood and Anxiety Symptom Questionnaire (MASQ) in a sample of young help-seekers. *BMC Psychiatry*, *7*, 50. doi:10.1186/1471-244X-7-50

Buzsáki, G., & Wang, X.-J. (2012). Mechanisms of Gamma Oscillations. *Annu Rev Neurosci*, *35*(1), 203–225. doi:10.1146/annurev-neuro-062111-150444

Cabranes, J. A., Ancín, I., Santos, J. L., Sánchez-Morla, E., García-Jiménez, M. A.,

Rodríguez-Moya, L., *et al*. (2012). P50 sensory gating is a trait marker of the bipolar spectrum. *European Neuropsychopharmacology : the Journal of the European College of Neuropsychopharmacology*. doi:10.1016/j.euroneuro.2012.06.008

Caetano, S. C., Hatch, J. P., Brambilla, P., Sassi, R. B., Nicoletti, M., Mallinger, A. G., *et al*. (2004). Anatomical MRI study of hippocampus and amygdala in patients with current and remitted major depression. *Psychiatry Research*, *132*(2), 141–147. doi:10.1016/j.pscychresns.2004.08.002

Campbell, A. E., Sumner, P., Singh, K. D., & Muthukumaraswamy, S. D. (2014). Acute Effects of Alcohol on Stimulus-Induced Gamma Oscillations in Human Primary Visual and Motor Cortices, 1–10. doi:10.1038/npp.2014.58

Cardin, J. A., Carlén, M., Meletis, K., Knoblich, U., Zhang, F., Deisseroth, K., *et al*. (2009). Driving fast-spiking cells induces gamma rhythm and controls sensory responses. *Nature*, *459*(7247), 663–667. doi:10.1038/nature08002

Carlén, M., Meletis, K., Siegle, J. H., Cardin, J. A., Futai, K., Vierling-Claassen, D., *et al*. (2011). A critical role for NMDA receptors in parvalbumin interneurons for gamma induction and behavior. doi:10.1038/mp.2011.31

Cavanagh, J., & Geisler, M. W. (2006). Mood effects on the ERP processing of emotional intensity in faces: a P3 investigation with depressed students. *International Journal of Psychophysiology : Official Journal of the International Organization of Psychophysiology*, *60*(1), 27–33. doi:10.1016/j.ijpsycho.2005.04.005

Chen, Y.-H., Dammers, J., Boers, F., *et al*. (2009). The temporal dynamics of insula activity to disgust and happy facial expressions: a magnetoencephalography study. *NeuroImage*, *47*(4), 1921–1928. doi:10.1016/j.neuroimage.2009.04.093

Cheyne, D., Bells, S., Ferrari, P., *et al*. (2008). Self-paced movements induce high-frequency gamma oscillations in primary motor cortex. *NeuroImage*, *42*(1), 332–342. doi:10.1016/j.neuroimage.2008.04.178

Choudary, P. V. (2005). Altered cortical glutamatergic and GABAergic signal transmission with glial involvement in depression. *Proceedings of the National Academy of Sciences*, *102*(43), 15653–15658. doi:10.1073/pnas.0507901102

Clark, A. (2012). Dreaming the Whole Cat: Generative Models, Predictive

Processing, and the Enactivist Conception of Perceptual Experience. *Mind.Oxfordjournals.org*.

Collingridge, G. L., Isaac, J. T. R., & Wang, Y. T. (2004). Receptor trafficking and synaptic plasticity. *Nature Publishing Group*, *5*(12), 952–962. doi:10.1038/nrn1556

Di Russo. (2002). Cortical sources of the early components of the visual evoked potential., *15*(2), 95–111. Retrieved from http://eutils.ncbi.nlm.nih.gov/entrez/eutils/elink.fcgi?dbfrom=pubmed&id=11835601&retmode=ref&cmd=prlinks

Cousijn, H., Haegens, S., Wallis, G., Near, J., Stokes, M. G., Harrison, P. J., & Nobre, A. C. (2014). Resting GABA and glutamate concentrations do not predict visual gamma frequency or amplitude. *Proceedings of the …*.

Craddock, N., Jones, I., Kirov, G., & Jones, L. (2004). BioMed Central | Sorry. *BMC Psychiatry*.

Craddock, N., O'Donovan, M. C., & Owen, M. J. (2006). Genes for schizophrenia and bipolar disorder? Implications for psychiatric nosology. *Schizophrenia Bulletin*, *32*(1), 9–16. doi:10.1093/schbul/sbj033

Crane, G. (1959). Cyloserine as as antidepressant agent. *The American Journal of Psychiatry*, *115*(11), 1025–1026.

Croarkin, P. E., Levinson, A. J., & Daskalakis, Z. J. (2011). Evidence for GABAergic inhibitory deficits in major depressive disorder. *Neuroscience and Biobehavioral Reviews*, *35*(3), 818–825. doi:10.1016/j.neubiorev.2010.10.002

Cuffin, B. N., & Cohen, D. (1979). Comparison of the magnetoencephalogram and electroencephalogram. *Electroencephalography and Clinical Neurophysiology*, *47*(2), 132–146. doi:10.1016/0013-4694(79)90215-3

de Graaf, R. A. (2008). *In Vivo NMR Spectroscopy*. John Wiley & Sons.

Diner, B. C., Holcomb, P. J., & Dykman, R. A. (1985). P300 in major depressive disorder. *Psychiatry Research*, *15*(3), 175–184.

Douglas, R. J., & Martin, K. A. (1991). A functional microcircuit for cat visual cortex. *The Journal of Physiology*.

Drevets, W. C. (2003). Neuroimaging abnormalities in the amygdala in mood disorders. *Annals of the New York Academy of Sciences*, *985*, 420–444.

Drevets, W. C., Frank, E., Price, J. C., Kupfer, D. J., & Holt, D. (1999). Pet imaging of serotonin 1A receptor binding in depression. *Biological ….*

Duman, R. S. (2002). Pathophysiology of depression: the concept of synaptic plasticity. *European Psychiatry : the Journal of the Association of European Psychiatrists*, *17 Suppl 3*, 306–310.

Duman, R. S., & Li, N. (2012). A neurotrophic hypothesis of depression: role of synaptogenesis in the actions of NMDA receptor antagonists. *Philosophical Transactions of the Royal Society B: Biological Sciences*, *367*(1601), 2475–2484. doi:10.1038/nn1153

Duman, R. S., & Monteggia, L. M. (2006). A neurotrophic model for stress-related mood disorders. *Biological Psychiatry*, *59*(12), 1116–1127. doi:10.1016/j.biopsych.2006.02.013

Edden, R. A. E., Puts, N. A. J., Harris, A. D., Barker, P. B., & Evans, C. J. (2013). Gannet: A batch-processing tool for the quantitative analysis of gamma-aminobutyric acid-edited MR spectroscopy spectra. *Journal of Magnetic Resonance Imaging*, n/a–n/a. doi:10.1002/jmri.24478

Eickhoff, S. B., Rottschy, C., & Zilles, K. (2007). Laminar distribution and co-distribution of neurotransmitter receptors in early human visual cortex. *Brain Structure & Function*, *212*(3-4), 255–267.

Epperson, C. N., Haga, K., Mason, G. F., Sellers, E., Gueorguieva, R., Zhang, W., *et al*. (2002). Cortical γ-Aminobutyric Acid Levels Across the Menstrual Cycle in Healthy Women and Those With Premenstrual Dysphoric Disorder: A Proton Magnetic Resonance Spectroscopy Study. *Archives of General Psychiatry*, *59*(9), 851–858. doi:10.1001/archpsyc.59.9.851

Erlander, M. G., Erlander, M. G., Tobin, A. J., & Tobin, A. J. (1991). The structural and functional heterogeneity of glutamic acid decarboxylase: a review. *Neurochemical Research*, *16*(3), 215–226.

Ethridge, L. E., Hamm, J. P., Shapiro, J. R., Summerfelt, A. T., Keedy, S. K., Stevens, M. C., *et al*. (2012). Neural activations during auditory oddball processing discriminating schizophrenia and psychotic bipolar disorder. *Biological Psychiatry*, *72*(9), 766–774. doi:10.1016/j.biopsych.2012.03.034

Fava, M., & Team, S. D. S. (2006). PsychiatryOnline | American Journal of

Psychiatry | Evaluation of Outcomes With Citalopram for Depression Using Measurement-Based Care in STAR*D: Implications for Clinical Practice. *American Journal of …*.

Feldmeyer, D., Egger, V., Lubke, J., & Sakmann, B. (1999). Reliable synaptic connections between pairs of excitatory layer 4 neurones within a single "barrel" of developing rat somatosensory cortex. *The Journal of Physiology*, *521 Pt 1*, 169–190.

Fiorillo, C. D. (2010). A neurocentric approach to Bayesian inference. *Nature Reviews. Neuroscience*. doi:10.1038/nrn2787-c1

Fischl, B., Sereno, M. I., Tootell, R., & Dale, A. M. (1999). High-resolution intersubject averaging and a coordinate system for the cortical surface. *Human Brain …*.

Fitzpatrick, D., Lund, J. S., Schmechel, D. E., & Towles, A. C. (1987). Distribution of GABAergic neurons and axon terminals in the macaque striate cortex. *The Journal of Comparative Neurology*, *264*(1), 73–91. doi:10.1002/cne.902640107

Fleidervish, I. A., Binshtok, A. M., & Gutnick, M. J. (1998). Functionally Distinct NMDA Receptors Mediate Horizontal Connectivity within Layer 4 of Mouse Barrel Cortex. *Neuron*, *21*(5), 1055–1065. doi:10.1016/S0896-6273(00)80623-6

Foster, B. L., Bojak, I., & Liley, D. T. J. (2008). Population based models of cortical drug response: insights from anaesthesia. *Cognitive Neurodynamics*, *2*(4), 283–296. doi:10.1007/s11571-008-9063-z

Friston, K. (2005). A theory of cortical responses. *… Transactions of the Royal Society B: …*.

Friston, K. J. (2011). Functional and Effective Connectivity: A Review. *Brain Connectivity*, *1*(1), 13–36. doi:10.1089/brain.2011.0008

Friston, K. J., & Kiebel, S. (2009a). Predictive coding under the free-energy principle. *Philosophical Transactions of the Royal Society B: Biological Sciences*, *364*(1521), 1211–1221. doi:10.1098/rstb.2008.0300

Friston, K. J., & Stephan, K. E. (2007). Free-energy and the brain. *Synthese*, *159*(3), 417–458. doi:10.1007/s11229-007-9237-y

Friston, K., & Kiebel, S. (2009b). Cortical circuits for perceptual inference. *Neural Networks*.

Friston, K., & Penny, W. (2011). Post hoc Bayesian model selection. *NeuroImage*, *56*(4), 2089–2099. doi:10.1016/j.neuroimage.2011.03.062

Friston, K., Kilner, J., & Harrison, L. (2006). A free energy principle for the brain. *Journal of Physiology-Paris*.

Friston, K., Thornton, C., & Clark, A. (2012). Free-energy minimization and the dark-room problem. *Frontiers in Psychology*, *3*, 130. doi:10.3389/fpsyg.2012.00130

Frodl, T., Meisenzahl, E., Zetzsche, T., Bottlender, R., Born, C., Groll, C., *et al*. (2002). Enlargement of the amygdala in patients with a first episode of major depression. *Biological Psychiatry*, *51*(9), 708–714.

Frohlich, J., & Van Horn, J. D. (2014). Reviewing the ketamine model for schizophrenia. *Journal of Psychopharmacology*, *28*(4), 287–302. doi:10.1177/0269881113512909

Fu, C. H. Y., Williams, S. C. R., Cleare, A. J., *et al*. (2004). Attenuation of the neural response to sad faces in major depression by antidepressant treatment: a prospective, event-related functional magnetic resonance imaging study. *Archives of General Psychiatry*, *61*(9), 877–889. doi:10.1001/archpsyc.61.9.877

Gabbay, V., Mao, X., Klein, R. G., *et al*. (2012). Anterior Cingulate Cortex - Aminobutyric Acid in Depressed Adolescents: Relationship to Anhedonia. *Archives of General Psychiatry*, *69*(2), 139–149. doi:10.1001/archgenpsychiatry.2011.131

Gaetz, W., Roberts, T. P. L., Singh, K. D., & Muthukumaraswamy, S. D. (2012). Functional and structural correlates of the aging brain: relating visual cortex (V1) gamma band responses to age-related structural change. *Human Brain Mapping*, *33*(9), 2035–2046. doi:10.1002/hbm.21339

Geramita, M., van der Veen, J. W., Barnett, A. S., Savostyanova, A. A., Shen, J., Weinberger, D. R., & Marenco, S. (2011). Reproducibility of prefrontal γ-aminobutyric acid measurements with J-edited spectroscopy. *NMR in Biomedicine*, *24*(9), 1089–1098. doi:10.1002/nbm.1662

Gieselmann, M. A., & Thiele, A. (2008). Comparison of spatial integration and surround suppression characteristics in spiking activity and the local field potential in macaque V1. *European Journal of Neuroscience*, *28*(3), 447–459.

doi:10.1111/j.1460-9568.2008.06358.x

Gotlib, I. H., & Hamilton, J. P. (2008). Neuroimaging and Depression: Current Status and Unresolved Issues. *Current Directions in Psychological Science*, *17*(2), 159–163. doi:10.1111/j.1467-8721.2008.00567.x

Graham, J. (1982). Some topographical connections of the striate cortex with subcortical structures in Macaca fascicularis. *Experimental Brain Research. Experimentelle Hirnforschung. Expérimentation Cérébrale*, *47*(1), 1–14.

Gregory, R. L. (1980). Perceptions as Hypotheses. *Philosophical Transactions of the Royal Society B: Biological Sciences*, *290*(1038), 181–197. doi:10.1098/rstb.1980.0090

Haenschel, C., & Linden, D. (2011). *Handbook of Schizophrenia Spectrum Disorders, Volume II* (pp. 449–480). Dordrecht: Springer Netherlands. doi:10.1007/978-94-007-0831-0_18

Haenschel, C., Bittner, R. A., Haertling, F., Rotarska-Jagiela, A., Maurer, K., Singer, W., & Linden, D. E. J. (2007). Contribution of impaired early-stage visual processing to working memory dysfunction in adolescents with schizophrenia: a study with event-related potentials and functional magnetic resonance imaging. *Archives of General Psychiatry*, *64*(11), 1229–1240. doi:10.1001/archpsyc.64.11.1229

Haeusler, S. S., & Maass, W. W. (2007). A statistical analysis of information-processing properties of lamina-specific cortical microcircuit models. *Cerebral Cortex (New York, N.Y. : 1991)*, *17*(1), 149–162. doi:10.1093/cercor/bhj132

Haile, C. N., Murrough, J. W., Iosifescu, D. V., Chang, L. C., Jurdi, Al, R. K., Foulkes, A., *et al*. (2014). Plasma brain derived neurotrophic factor (BDNF) and response to ketamine in treatment-resistant depression. *The International Journal of Neuropsychopharmacology / Official Scientific Journal of the Collegium Internationale Neuropsychopharmacologicum (CINP)*, *17*(2), 331–336. doi:10.1017/S1461145713001119

Hall, S. D., Holliday, I. E., Hillebrand, A., Singh, K. D., Furlong, P. L., Hadjipapas, A., & Barnes, G. R. (2005). The missing link: analogous human and primate cortical gamma oscillations. *NeuroImage*, *26*(1), 13–17. doi:10.1016/j.neuroimage.2005.01.009

Hamandi, K., Singh, K. D.,& Muthukumaraswamy, S. (2011). Reduced movement-related beta desynchronisation in juvenile myoclonic epilepsy: A MEG study of task specific cortical modulation. *Clinical Neurophysiology*, *122*(11), 2128–2138. doi:10.1016/j.clinph.2011.04.017

Hari, R., & Salmelin, R. (2012). Magnetoencephalography: From SQUIDs to neuroscience. Neuroimage 20th anniversary special edition. *NeuroImage*, *61*(2), 386–396. doi:10.1016/j.neuroimage.2011.11.074

Hari, R., Hamalainen, M., Ilmoniemi, R., & Lounasmaa, O. V. (1991). MEG versus EEG localization test. *Annals of Neurology*, *30*(2), 222–223. doi:10.1002/ana.410300221

Hasler, G., Neumeister, A., van der Veen, J. W., *et al*. (2005). Normal Prefrontal Gamma-Aminobutyric Acid Levels in Remitted Depressed Subjects Determined by Proton Magnetic Resonance Spectroscopy. *Biological Psychiatry*, *58*(12), 969–973. doi:10.1016/j.biopsych.2005.05.017

Hasler, G & Northoff, G. (2011). Discovering imaging endophenotypes for major depression. *Molecular Psychiatry*, *16*(6), 604–619. doi:10.1038/mp.2011.23

Hasler, G., van der Veen, J. W., Tumonis, T., Meyers, N., Shen, J., & Drevets, W. C. (2007). Reduced prefrontal glutamate/glutamine and {gamma}-aminobutyric acid levels in major depression determined using proton magnetic resonance spectroscopy. *Archives of General Psychiatry*, *64*(2), 193.

Hastings, R. S., Parsey, R. V., Oquendo, M. A., Arango, V., & Mann, J. J. (2004). Volumetric analysis of the prefrontal cortex, amygdala, and hippocampus in major depression. *Neuropsychopharmacology*, *29*(5), 952–959. doi:10.1038/sj.npp.1300371

Hämäläinen, M., Hari, R., Ilmoniemi, R. J., Knuutila, J., & Lounasmaa, O. V. (1993). Magnetoencephalography—theory, instrumentation, and applications to noninvasive studies of the working human brain. *Reviews of Modern Physics*, *65*(2), 413–497. doi:10.1103/RevModPhys.65.413

Helmholtz, H. (1909). Handbuch der physiologischen Optik. *Hamburg: Voss*.

Herrero, J. L., Gieselmann, M. A., Sanayei, M., & Thiele, A. (2013). Attention-Induced Variance and Noise Correlation Reduction in Macaque V1 Is Mediated by NMDA Receptors. *Neuron*, *78*(4), 729–739.

doi:10.1016/j.neuron.2013.03.029

Hevers, W., Hevers, W., Hadley, S. H., Hadley, S. H., Luddens, H., Luddens, H., *et al*. (2008). Ketamine, But Not Phencyclidine, Selectively Modulates Cerebellar GABAA Receptors Containing 6 and Subunits. *Journal of Neuroscience*, *28*(20), 5383–5393. doi:10.1523/JNEUROSCI.5443-07.2008

Hillebrand, A., & Barnes, G. R. (2005). Beamformer Analysis of MEG Data. In *International Review of Neurobiology* (Vol. 68, pp. 149–171). Elsevier. doi:10.1016/S0074-7742(05)68006-3

Homayoun, H., & Moghaddam, B. (2007). NMDA Receptor Hypofunction Produces Opposite Effects on Prefrontal Cortex Interneurons and Pyramidal Neurons. *Journal of Neuroscience*, *27*(43), 11496–11500. doi:10.1523/JNEUROSCI.2213-07.2007

Horner, M. J., Ries, L., Krapcho, M., & Neyman, N. (2009). SEER Cancer Statistics Review 1975-2006 - Previous Version - SEER Cancer Statistics.

Işıntaş, M., Ak, M., Erdem, M., Oz, O., & Ozgen, F. (2012). [Event-related potentials in major depressive disorder: the relationship between P300 and treatment response]. *Türk Psikiyatri Dergisi = Turkish Journal of Psychiatry*, *23*(1), 33–39.

Kalueff, A. V., & Nutt, D. J. (2007). Role of GABA in anxiety and depression. *Depression and Anxiety*, *24*(7), 495–517. doi:10.1002/da.20262

Keedwell, P., Drapier, D., Surguladze, S., *et al*. (2009). Neural markers of symptomatic improvement during antidepressant therapy in severe depression: subgenual cingulate and visual cortical responses to sad, but not happy, facial stimuli are correlated with changes in symptom score. *Journal of Psychopharmacology*, *23*(7), 775–788. doi:10.1177/0269881108093589

Kendler, K. S., Thornton, L. M., & Gardner, C. O. (2000). Stressful life events and previous episodes in the etiology of major depression in women: an evaluation of the “kindling” hypothesis. *The American Journal of Psychiatry*, *157*(8), 1243–1251.

Kessler, R. C., Berglund, P., Demler, O., Jin, R., Koretz, D., Merikangas, K. R., *et al*. (2003). The Epidemiology of Major Depressive DisorderResults From the National Comorbidity Survey Replication (NCS-R). *Jama*, *289*(23), 3095–3105. doi:10.1001/jama.289.23.3095

Klumpers, U. M. H., Veltman, D. J., Drent, M. L., Boellaard, R., Comans, E. F. I., Meynen, G., *et al*. (2009). Reduced parahippocampal and lateral temporal GABAA-[11C]flumazenil binding in major depression: preliminary results. *European Journal of Nuclear Medicine and Molecular Imaging*, *37*(3), 565–574. doi:10.1007/s00259-009-1292-9

Kollmar, R., Kollmar, R., Markovic, K., Markovic, K., Thürauf, N., Thürauf, N., *et al*. (2008). Ketamine followed by memantine for the treatment of major depression. *The Australian and New Zealand Journal of Psychiatry*, *42*(2), 170. doi:10.1080/00048670701787628

Koychev, I., El-Deredy, W., Mukherjee, T., Haenschel, C., & Deakin, J. F. W. (2012). Core dysfunction in schizophrenia: electrophysiology trait biomarkers. *Acta Psychiatrica Scandinavica*, *126*(1), 59–71. doi:10.1111/j.1600-0447.2012.01849.x

Krishnan, V., & Nestler, E. J. (2008). The molecular neurobiology of depression. *Nature*, *455*(7215), 894–902. doi:10.1038/nature07455

Krzywkowski, P., De Bilbao, F., Senut, M. C., & Lamour, Y. (1995). Age-related changes in parvalbumin- and GABA-immunoreactive cells in the rat septum. *Neurobiology of Aging*, *16*(1), 29–40. doi:10.1016/0197-4580(95)80005-C

Kumar, P., Harmer, C. J., & Dourish, C. T. (2013). Neuroimaging Approaches to theUnderstanding of Depression andthe Identification of NovelAntidepressants.

Lakatos, P., Karmos, G., Mehta, A. D., Ulbert, I., & Schroeder, C. E. (2008). Entrainment of Neuronal Oscillations as a Mechanism of Attentional Selection. *Science*, *320*(5872), 110–113. doi:10.1126/science.1154735

Lang, U. E., & Borgwardt, S. (2013). Molecular mechanisms of depression: perspectives on new treatment strategies. *Cellular Physiology and Biochemistry : International Journal of Experimental Cellular Physiology, Biochemistry, and Pharmacology*, *31*(6), 761–777. doi:10.1159/000350094

Lange, C., & Irle, E. (2004). Enlarged amygdala volume and reduced hippocampal volume in young women with major depression. *Psychological Medicine*, *34*(6), 1059–1064.

Lange, K., Williams, L. M., Young, A. W., Bullmore, E. T., Brammer, M. J., Williams, S. C. R., *et al*. (2003). Task instructions modulate neural responses to fearful

facial expressions. *Biological Psychiatry*, *53*(3), 226–232. doi:10.1016/S0006-3223(02)01455-5

Lazarewicz, M. T., Ehrlichman, R. S., Maxwell, C. R., Gandal, M. J., Finkel, L. H., & Siegel, S. J. (2010). Ketamine modulates theta and gamma oscillations. *Journal of Cognitive Neuroscience*, *22*(7), 1452–1464.

Lee, P.-S., Chen, Y.-S., Hsieh, J.-C., *et al*. (2010). Distinct neuronal oscillatory responses between patients with bipolar and unipolar disorders: A magnetoencephalographic study. *Journal of Affective Disorders*, *123*(1-3), 270–275. doi:10.1016/j.jad.2009.08.020

Lee, S., Kwan, A. C., Zhang, S., *et al*. (2012). Activation of specific interneurons improves V1 feature selectivity and visual perception. *Nature*, *488*(7411), 379–383. doi:10.1038/nature11312

Letinic, K., Zoncu, R., & Rakic, P. (2002). Origin of GABAergic neurons in the human neocortex. *Nature*, *417*(6889), 645–649. doi:10.1038/nature00779

Lewis, S. (2012). Synaptic physiology: It takes two for NMDA receptors. *Nature Reviews. Neuroscience*. doi:10.1038/nrn3337

Li, N., Lee, B., Liu, R.-J., Banasr, M., Dwyer, J. M., Iwata, M., *et al*. (2010). mTOR-dependent synapse formation underlies the rapid antidepressant effects of NMDA antagonists. *Science*, *329*(5994), 959–964. doi:10.1126/science.1190287

Lisiecka, D. M., Carballedo, A., Fagan, A. J., Connolly, G., Meaney, J., & Frodl, T. (2012). Altered inhibition of negative emotions in subjects at family risk of major depressive disorder. *Journal of Psychiatric Research*, *46*(2), 181–188. doi:10.1016/j.jpsychires.2011.10.010

Liu, T.Y., Hsieh, J.C., Chen, Y.S., *et al*. (2012). Different patterns of abnormal gamma oscillatory activity in unipolar and bipolar disorder patients during an implicit emotion task. *Neuropsychologia*, 1–7. doi:10.1016/j.neuropsychologia.2012.03.004

Lorenzetti, V., Allen, N. B., Fornito, A., & Yücel, M. (2009). Structural brain abnormalities in major depressive disorder: a selective review of recent MRI studies. *Journal of Affective Disorders*, *117*(1-2), 1–17. doi:10.1016/j.jad.2008.11.021

Luck, S. J. (2005). An introduction to the event-related potential technique (cognitive neuroscience).

Luscher, B., Shen, Q., Sahir, N. (2010). The GABAergic deficit hypothesis of major depressive disorder. *Molecular Psychiatry*, *16*(4), 383–406. doi:10.1038/mp.2010.120

Luykx, J. J.,Laban, K. G., van den Heuvel, M. P., *et al*. (2011). Region and state specific glutamate downregulation in major depressive disorder: A meta-analysis of 1H-MRS findings. *Neuroscience and Biobehavioral Reviews*, *36*(1), 198–205. doi:10.1016/j.neubiorev.2011.05.014

Maeda, F., Keenan, J. P., & Pascual-Leone, A. (2000). Interhemispheric asymmetry of motor cortical excitability in major depression as measured by transcranial magnetic stimulation. *The British Journal of Psychiatry*, *177*(2), 169–173. doi:10.1192/bjp.177.2.169

Malkesman, O., Austin, D. R., Tragon, T., Wang, G., Rompala, G., Hamidi, A. B., *et al*. (2012). Acute D-serine treatment produces antidepressant-like effects in rodents. *The International Journal of Neuropsychopharmacology / Official Scientific Journal of the Collegium Internationale Neuropsychopharmacologicum (CINP)*, *15*(8), 1135–1148. doi:10.1017/S1461145711001386

Markov, N. T., Misery, P., Falchier, A., Lamy, C., Vezoli, J., Quilodran, R., *et al*. (2011). Weight Consistency Specifies Regularities of Macaque Cortical Networks. *Cerebral …*.

Markram, H., Toledo-Rodriguez, M., Wang, Y., Gupta, A., Silberberg, G., & Wu, C. (2004). Interneurons of the neocortical inhibitory system. *Nature Reviews. Neuroscience*, *5*(10), 793–807. doi:10.1038/nrn1519

Mazaheri, A., & Van Diepen, R. (2014). Gamma Oscillations in a Bind? *Cerebral Cortex*. doi:10.1093/cercor/bhu136

Mescher, M., Merkle, H., Kirsch, J., Garwood, M., & Gruetter, R. (1998). Simultaneous in vivo spectral editing and water suppression. *NMR in Biomedicine*, *11*(6), 266–272.

Michael, N., Erfurth, A., Ohrmann, P., Arolt, V., Heindel, W., & Pfleiderer, B. (2003). Neurotrophic effects of electroconvulsive therapy: a proton magnetic resonance study of the left amygdalar region in patients with treatment-resistant

depression. *Neuropsychopharmacology*, *28*(4), 720–725. doi:10.1038/sj.npp.1300085

Michel, N., Erfurth, A., Ohrmann, P., Arolt, V., Heindel, W., & Pfleiderer, B. (2003). Metabolic changes within the left dorsolateral prefrontal cortex occurring with electroconvulsive therapy in patients with treatment resistant unipolar depression. *Psychological Medicine*, *33*(7), 1277–1284.

Milne, A., MacQueen, G. M., Yucel, K., Soreni, N., & Hall, G. B. C. (2009). Hippocampal metabolic abnormalities at first onset and with recurrent episodes of a major depressive disorder: a proton magnetic resonance spectroscopy study. *NeuroImage*, *47*(1), 36–41. doi:10.1016/j.neuroimage.2009.03.031

Moghaddam, B., Adams, B., Verma, A., & Daly, D. (1997). Activation of glutamatergic neurotransmission by ketamine: a novel step in the pathway from NMDA receptor blockade to dopaminergic and cognitive disruptions associated with the prefrontal cortex. *The Journal of Neuroscience : the Official Journal of the Society for Neuroscience*, *17*(8), 2921–2927.

Mohamed, T. N., Neumann, M. F., & Schweinberger, S. R. (2009). Perceptual load manipulation reveals sensitivity of the face... : NeuroReport. *Neuroreport*.

Moller, H. J. (2003). Bipolar disorder and schizophrenia: Distinct illnesses or a continuum? *Journal of Clinical Psychiatry*, *64*, 23–27.

Monkul, E. S., Hatch, J. P., Nicoletti, M. A., Spence, S., Brambilla, P., Lacerda, A. L. T., *et al*. (2007). Fronto-limbic brain structures in suicidal and non-suicidal female patients with major depressive disorder. *Molecular Psychiatry*, *12*(4), 360–366. doi:10.1038/sj.mp.4001919

Monroe, J. F., Griffin, M., Pinkham, A., *et al*. (2011). The fusiform response to faces: Explicit versus implicit processing of emotion. *Human Brain Mapping*, n/a–n/a. doi:10.1002/hbm.21406

Moran, R. J., Stephan, K. E., Dolan, R. J., & Friston, K. J. (2011). Consistent spectral predictors for dynamic causal models of steady-state responses. *NeuroImage*, *55*(4), 1694–1708. doi:10.1016/j.neuroimage.2011.01.012

Moran, R. J., Stephan, K. E., Seidenbecher, T., Pape, H.-C., Dolan, R. J., & Friston, K. J. (2009). Dynamic causal models of steady-state responses. *NeuroImage*, *44*(3), 796–811. doi:10.1016/j.neuroimage.2008.09.048

Morstyn, R., Duffy, F. H & McCarley, R. W. (1983). Altered P300 Topography in Schizophrenia. *Archives of General Psychiatry*, *40*(7), 729–734. doi:10.1001/archpsyc.1983.01790060027003

Möhler, H. (2012). The GABA system in anxiety and depression and its therapeutic potential. *Biological Psychiatry*, *62*(1), 42–53. doi:10.1016/j.neuropharm.2011.08.040

Muhammad, R. (2009). The Mouse Visually Evoked Potential: Neural Correlates and Functional Applications. *PhD Thesis*, 1–123.

Muthukumaraswamy, S. D. (2010). Functional Properties of Human Primary Motor Cortex Gamma Oscillations. *Journal of Neurophysiology*, *104*(5), 2873–2885. doi:10.1152/jn.00607.2010

Muthukumaraswamy, S. D. (2014). The use of magnetoencephalography in the study of psychopharmacology (pharmaco-MEG). *Journal of Psychopharmacology (Oxford, England)*. doi:10.1177/0269881114536790

Muthukumaraswamy, S. D., & Singh, K. D. (2008). Spatiotemporal frequency tuning of BOLD and gamma band MEG responses compared in primary visual cortex. *NeuroImage*, *40*(4), 1552–1560. doi:10.1016/j.neuroimage.2008.01.052

Muthukumaraswamy, S. D., & Singh, K. D. (2012). Visual gamma oscillations: The effects of stimulus type, visual field coverage and stimulus motion on MEG and EEG recordings. *NeuroImage*. doi:10.1016/j.neuroimage.2012.12.038

Muthukumaraswamy, S. D., Carhart-Harris, R. L., Moran, R. J., Brookes, M. J., Williams, T. M., Errtizoe, D., *et al*. (2013). Broadband Cortical Desynchronization Underlies the Human Psychedelic State. *Journal of Neuroscience*, *33*(38), 15171–15183. doi:10.1523/JNEUROSCI.2063-13.2013

Muthukumaraswamy, S. D., Edden, R. A. E., Jones, D. K., Swettenham, J. B., & Singh, K. D. (2009). Resting GABA concentration predicts peak gamma frequency and fMRI amplitude in response to visual stimulation in humans. *Proceedings of the National Academy of Sciences*, *106*(20), 8356–8361. doi:10.1073/pnas.0900728106

Muthukumaraswamy, S. D., Singh, K. D., Swettenham, J. B., *et al*. (2010). Visual gamma oscillations and evoked responses: Variability, repeatability and structural MRI correlates. *NeuroImage*, *49*(4), 3349–3357.

doi:10.1016/j.neuroimage.2009.11.045

Muthukumaraswamy, S. D., Myers, J. F. M., Wilson, S. J., NUTT, D. J., Lingford-Hughes, A., Singh, K. D., & Hamandi, K. (2012). The effects of elevated endogenous GABA levels on movement-related network oscillations. *NeuroImage*, *66C*, 36–41. doi:10.1016/j.neuroimage.2012.10.054

Niedermeyer, E., & da Silva, F. (2005). Electroencephalography: Basic Principles, Clinical Applications, and Related ... - Google Books.

Normann, C., Schmitz, D., Fürmaier, A., *et al*. (2007). Long-Term Plasticity of Visually Evoked Potentials in Humans is Altered in Major Depression. *Biological Psychiatry*, *62*(5), 373–380. doi:10.1016/j.biopsych.2006.10.006

Nutt, D. J., & Malizia, A. L. (2001). New insights into the role of the GABAA—benzodiazepine receptor in psychiatric disorder. *The British Journal of Psychiatry*, *179*(5), 390–396. doi:10.1192/bjp.179.5.390

O'Gorman, R. L., Edden, R., Michels, L., & Murdoch, J. B. (2007). Precision and repeatability of in vivo GABA and glutamate quantification. *Proc ISMRM*.

O'Gorman, R. L., Michels, L., Edden, R. A., Murdoch, J. B., & Martin, E. (2011). In vivo detection of GABA and glutamate with MEGA-PRESS: Reproducibility and gender effects. *Journal of Magnetic Resonance Imaging*, *33*(5), 1262–1267. doi:10.1002/jmri.22520

O'Kusky, J., & Colonnier, M. (1982). A laminar analysis of the number of neurons, glia, and synapses in the adult cortex (area 17) of adult macaque monkeys. *The Journal of Comparative Neurology*, *210*(3), 278–290. doi:10.1002/cne.902100307

Oke, O. O., Magony, A., Anver, H., *et al*. (2010). High-frequency gamma oscillations coexist with low-frequency gamma oscillations in the rat visual cortex in vitro. *European Journal of Neuroscience*, *31*(8), 1435–1445. doi:10.1111/j.1460-9568.2010.07171.x

Özerdem, A., Güntekin, B., Saatçi, E., Tunca, Z., & Başar, E. (2010). Disturbance in long distance gamma coherence in bipolar disorder. *Progress in Neuro-Psychopharmacology and Biological Psychiatry*, *34*(6), 861–865. doi:10.1016/j.pnpbp.2010.04.001

Pascual-Leone, A., Manoach, D. S., Birnbaum, R., & Goff, D. C. (2002). Motor

cortical excitability in schizophrenia. *Biological Psychiatry*, *52*(1), 24–31. doi:10.1016/S0006-3223(02)01317-3

Perrine, S. A., Ghoddoussi, F., Michaels, M. S., Sheikh, I. S., McKelvey, G., & Galloway, M. P. (2014). Ketamine reverses stress-induced depression-like behavior and increased GABA levels in the anterior cingulate: An 11.7T (1)H-MRS study in rats. *Progress in Neuro-Psychopharmacology and Biological Psychiatry*, *51*, 9–15. doi:10.1016/j.pnpbp.2013.11.003

Perry, G., Brindley, L. M., Muthukumaraswamy, S. D., Singh, K. D., & Hamandi, K. (2014). Evidence for increased visual gamma responses in photosensitive epilepsy. *Epilepsy Research*, *108*(6), 1076–1086. doi:10.1016/j.eplepsyres.2014.04.012

Petty, F. (1995). GABA and mood disorders: a brief review and hypothesis. *Journal of Affective Disorders*, *34*(4), 275–281. doi:10.1016/0165-0327(95)00025-I

Petty, F., Kramer, G. L., Gullion, C. M., & Rush, A. J. (1992). Low plasma gamma-aminobutyric acid levels in male patients with depression. *Bps*, *32*(4), 354–363.

Pfleiderer, B., Michael, N., Erfurth, A., Ohrmann, P., Hohmann, U., Wolgast, M., *et al*. (2003). Effective electroconvulsive therapy reverses glutamate/glutamine deficit in the left anterior cingulum of unipolar depressed patients. *Psychiatry Research*, *122*(3), 185–192.

Pfurtscheller, G.,& Lopes da Silva, F. H. (1999). Event-related EEG/MEG synchronization and desynchronization: basic principles. *Clinical Neurophysiology : Official Journal of the International Federation of Clinical Neurophysiology*, *110*(11), 1842–1857.

Phillips, M. L., Drevets, W. C., Rauch, S. L., & Lane, R. (2003). Neurobiology of emotion perception I: the neural basis of normal emotion perception. *Biological Psychiatry*, *54*(5), 504–514. doi:10.1016/S0006-3223(03)00168-9

Phillips, M. L., Young, A. W., Senior, C., Brammer, M., Andrew, C., Calder, A. J., *et al*. (1997). A specific neural substrate for perceiving facial expressions of disgust. *Nature*, *389*(6650), 495–498. doi:10.1038/39051

Price, R. B., Shungu, D. C., Mao, X., Nestadt, P., Kelly, C., Collins, K. A., *et al*. (2009). Amino Acid Neurotransmitters Assessed by Proton Magnetic Resonance Spectroscopy: Relationship to Treatment Resistance in Major

Depressive Disorder. *Biological Psychiatry*, *65*(9), 792–800. doi:10.1016/j.biopsych.2008.10.025

Purves, D. (2008). Purves: Principles of cognitive neuroscience - Google Scholar.

Puts, N., & Edden, R. (2012). In vivo magnetic resonance spectroscopy of GABA: A methodological review. *Progress in Nuclear Magnetic Resonance …*.

R Singh, (2000). P 300 EVENT RELATED POTENTIAL IN DEPRESSION. *Indian Journal of Psychiatry*, *42*(4), 402.

Rajkowska, G., O'Dwyer, G., Teleki, Z., *et al*. (2006). GABAergic Neurons Immunoreactive for Calcium Binding Proteins are Reduced in the Prefrontal Cortex in Major Depression. *Neuropsychopharmacology*, *32*(2), 471–482. doi:10.1038/sj.npp.1301234

Rang, H. P., Dale, M. M., Ritter, J. M., & Flower, R. J. (2003). [CITATION][C]. *Rang and Dale's Pharmacology*.

Rao, R. P., & Ballard, D. H. (1999). Predictive coding in the visual cortex: a functional interpretation of some extra-classical receptive-field effects. *Nature Neuroscience*, *2*(1), 79–87. doi:10.1038/4580

Ray, S., & Maunsell, J. H. R. (2010). Differences in gamma frequencies across visual cortex restrict their possible use in computation. *Neuron*, *67*(5), 885–896. doi:10.1016/j.neuron.2010.08.004

Robinson, S. E., & Vrba, J. (1999). 401 Authorization Required. *Recent Advances in …*.

Salisbury, D & Shenton, M. (1999). ScienceDirect.com - Biological Psychiatry - P300 topography differs in schizophrenia and manic psychosis. *Biological Psychiatry*.

Sanacora, G., Gueorguieva, R., Epperson, C. N., Wu, Y.-T., Appel, M., Rothman, D. L., *et al*. (2004). Subtype-specific alterations of gamma-aminobutyric acid and glutamate in patients with major depression. *Archives of General Psychiatry*, *61*(7), 705–713. doi:10.1001/archpsyc.61.7.705

Sanacora, G., Mason, G. F., Rothman, D. L., & Krystal, J. H. (2002). Increased occipital cortex GABA concentrations in depressed patients after therapy with selective serotonin reuptake inhibitors. *The American Journal of Psychiatry*, *159*(4), 663–665.

Sanacora, G., Fenton, L. R., Fasula, M. K., *et al*. (2006). Cortical γ-Aminobutyric Acid Concentrations in Depressed Patients Receiving Cognitive Behavioral Therapy. *Biological Psychiatry*, *59*(3), 284–286. doi:10.1016/j.biopsych.2005.07.015

Sanacora, G., Mason, G. F., Rothman, D. L., *et al*. (1999). Reduced cortical {gamma}-aminobutyric acid levels in depressed patients determined by proton magnetic resonance spectroscopy. *Archives of General Psychiatry*, *56*(11), 1043.

Sanacora, G., Mason, G. F., Rothman, D. L., *et al*. (2003). Increased cortical GABA concentrations in depressed patients receiving ECT. *The American Journal of Psychiatry*, *160*(3), 577–579.

Sanacora, G., Zarate, C. A., Krystal, J. H., *et al*. (2008). Targeting the glutamatergic system to develop novel, improved therapeutics for mood disorders. *Nature Reviews Drug Discovery*, *7*(5), 426–437. doi:10.1038/nrd2462

Sands, S. A., Reisman, S. A., & Enna, S. J. (2004). Effect of antidepressants on GABAB receptor function and subunit expression in rat hippocampus. *Biochemical Pharmacology*, *68*(8), 1489–1495. doi:10.1016/j.bcp.2004.07.027

Santesso, D. L., Steele, K. T., Bogdan, R., Holmes, A. J., Deveney, C. M., Meites, T. M., & Pizzagalli, D. A. (2008). Enhanced negative feedback responses in remitted depression. *Neuroreport*, *19*(10), 1045–1048. doi:10.1097/WNR.0b013e3283036e73

Sargent, P. A., Kjaer, K. H., Bench, C. J., Rabiner, E. A., Messa, C., Meyer, J., *et al*. (2000). Brain serotonin1A receptor binding measured by positron emission tomography with [11C]WAY-100635: effects of depression and antidepressant treatment. *Archives of General Psychiatry*, *57*(2), 174–180.

Saxena, N., Muthukumaraswamy, S. D., Diukova, A., Singh, K., Hall, J., & Wise, R. (2013). Enhanced Stimulus-Induced Gamma Activity in Humans during Propofol-Induced Sedation. *PLoS ONE*, *8*(3), e57685. doi:10.1371/journal.pone.0057685

Schienle, A., Stark, R., Walter, B., Blecker, C., Ott, U., Kirsch, P., *et al*. (2002). The insula is not specifically involved in disgust processing: an fMRI study. *Neuroreport*, *13*(16), 2023–2026.

Sen, S., Duman, R., & Sanacora, G. (2008). Serum brain-derived neurotrophic factor, depression, and antidepressant medications: meta-analyses and implications. *Biological Psychiatry*, *64*(6), 527–532. doi:10.1016/j.biopsych.2008.05.005

Sheehan, D. V., Lecrubier, Y., Sheehan, K. H., Amorim, P., Janavs, J., Weiller, E., *et al*. (1998). The Mini-International Neuropsychiatric Interview (M.I.N.I.): the development and validation of a structured diagnostic psychiatric interview for DSM-IV and ICD-10. *The Journal of Clinical Psychiatry*, *59 Suppl 20*, 22–33– quiz 34–57.

Sheline, Y. I., Barch, D. M., Donnelly, J. M., Ollinger, J. M., Snyder, A. Z., & Mintun, M. A. (2001). Increased amygdala response to masked emotional faces in depressed subjects resolves with antidepressant treatment: an fMRI study. *Biological Psychiatry*, *50*(9), 651–658.

Singer, W. (1999). Neuronal synchrony: a versatile code for the definition of relations? *Neuron*, *24*(1), 49–65– 111–25.

Singh, K. (2006). Magnetoencephalography. *Methods in Mind, the MIT Press, Cambridge, MA*, 190–225.

Skolnick, P. (1999). Antidepressants for the new millennium. *European Journal of Pharmacology*, *375*(1-3), 31–40.

Smith, S. M., Jenkinson, M., Woolrich, M. W., Beckmann, C. F., Behrens, T. E. J., Johansen-Berg, H., *et al*. (2004). Advances in functional and structural MR image analysis and implementation as FSL. *NeuroImage*, *23 Suppl 1*, S208–19. doi:10.1016/j.neuroimage.2004.07.051

Sohal, V. S. (2012). Insights into Cortical Oscillations Arising from Optogenetic Studies. *Biological Psychiatry*, *71*(12), 1039–1045. doi:10.1016/j.biopsych.2012.01.024

Souza, V. B., Muir, W. J., Walker, M. T., Glabus, M. F., Roxborough, H. M., Sharp, C. W., *et al*. (1995). Auditory P300 event-related potentials and neuropsychological performance in schizophrenia and bipolar affective disorder. *Biological Psychiatry*, *37*(5), 300–310. doi:10.1016/0006-3223(94)00131-L

Spencer, K. (2009). The functional consequences of cortical circuit abnormalities on gamma oscillations in schizophrenia: insights from computational modeling.

Frontiers in Human Neuroscience, *3*. doi:10.3389/neuro.09.033.2009

Spencer, K. M. (2011). Baseline gamma power during auditory steady-state stimulation in schizophrenia. *Frontiers in Human Neuroscience*, *5*, 190. doi:10.3389/fnhum.2011.00190

Spencer, K. M., Nestor, P. G., Niznikiewicz, M. A., Salisbury, D. F., Shenton, M. E., & McCarley, R. W. (2003). Abnormal neural synchrony in schizophrenia. *Journal of Neuroscience*, *23*(19), 7407–7411.

Sprengelmeyer, R.,Steele, J. D., Mwangi, B., *et al*. (2011). The insular cortex and the neuroanatomy of major depression. *Journal of Affective Disorders*, *133*(1-2), 120–127. doi:10.1016/j.jad.2011.04.004

Squires, N. K., Squires, K. C., & Hillyard, S. A. (1975). Two varieties of long-latency positive waves evoked by unpredictable auditory stimuli in man. *Electroencephalography and Clinical Neurophysiology*, *38*(4), 387–401.

Stein, M. B., Simmons, A. N., Feinstein, J. S., *et al*. (2007). Increased amygdala and insula activation during emotion processing in anxiety-prone subjects. *The American Journal of Psychiatry*, *164*(2), 318–327. doi:10.1176/appi.ajp.164.2.318

Stone, J. M., Dietrich, C., Edden, R., *et al*. (2012). Ketamine effects on brain GABA and glutamate levels with 1H-MRS: relationship to ketamine-induced psychopathology, 1–2. doi:10.1038/mp.2011.171

Stuhrmann, A., Suslow, T., & Dannlowski, U. (2011). Facial emotion processing in major depression: a systematic review of neuroimaging findings. *Biology of Mood & Anxiety Disorders*, *1*(1), 10. doi:10.1186/2045-5380-1-10

Takahashi, T., Yücel, M., Lorenzetti, V., Tanino, R., Whittle, S., Suzuki, M., *et al*. (2010). Volumetric MRI study of the insular cortex in individuals with current and past major depression. *Journal of Affective Disorders*, *121*(3), 231–238. doi:10.1016/j.jad.2009.06.003

Tao, R., & Auerbach, S. B. (2000). Regulation of serotonin release by GABA and excitatory amino acids. *Journal of Psychopharmacology*, *14*(2), 100–113.

Taylor, M. J., Mannie, Z. N., Norbury, R., Near, J., & Cowen, P. J. (2011a). Elevated cortical glutamate in young people at increased familial risk of depression. *The International Journal of Neuropsychopharmacology / Official Scientific Journal of*

the Collegium Internationale Neuropsychopharmacologicum (CINP), *14*(2), 255–259. doi:10.1017/S1461145710001094

Taylor, M. J., Tiangga, E. R., Ni Mhuircheartaigh, R., & Cowen, P. (2011b). Lack of effect of ketamine on cortical glutamate and glutamine in healthy volunteers: a proton magnetic resonance spectroscopy study. *Journal of Psychopharmacology*. doi:10.1177/0269881111405359

Thierry, G., Martin, C. D., Downing, P., & Pegna, A. J. (2007). Controlling for interstimulus perceptual variance abolishes N170 face selectivity : Abstract : Nature Neuroscience. *Nature Neuroscience*.

Traub, R. D., Spruston, N., Soltesz, I., Konnerth, A., Whittington, M. A., & Jefferys, G. R. (1998). Gamma-frequency oscillations: a neuronal population phenomenon, regulated by synaptic and intrinsic cellular processes, and inducing synaptic plasticity. *Progress in Neurobiology*, *55*(6), 563–575.

Uhlhaas, P. J. (2013). Dysconnectivity, large-scale networks and neuronal dynamics in schizophrenia. *Current Opinion in Neurobiology*, *23*(2), 283–290. doi:10.1016/j.conb.2012.11.004

Uhlhaas, P. J., & Singer, W. (2010). Abnormal neural oscillations and synchrony in schizophrenia. *Nature Reviews. Neuroscience*, *11*(2), 100–113. doi:10.1038/nrn2774

Van Essen, D. C., Anderson, C. H., & Felleman, D. J. (1992). Information processing in the primate visual system: an integrated systems perspective. *Science*, *255*(5043), 419–423.

Van Essen, D. C., Newsome, W. T., Maunsell, J. H., & Bixby, J. L. (1986). The projections from striate cortex (V1) to areas V2 and V3 in the macaque monkey: asymmetries, areal boundaries, and patchy connections. *The Journal of Comparative Neurology*, *244*(4), 451–480. doi:10.1002/cne.902440405

van Pelt, S., Boomsma, D. I., & Fries, P. (2012). Magnetoencephalography in Twins Reveals a Strong Genetic Determination of the Peak Frequency of Visually Induced Gamma-Band Synchronization. *Journal of Neuroscience*, *32*(10), 3388–3392. doi:10.1523/JNEUROSCI.5592-11.2012

Vrba, J. (2001). Signal Processing in Magnetoencephalography. *Methods*, *25*(2), 249–271. doi:10.1006/meth.2001.1238

Vythilingam, M., Vermetten, E., Anderson, G. M., Luckenbaugh, D., Anderson, E. R., Snow, J., *et al*. (2004). Hippocampal volume, memory, and cortisol status in major depressive disorder: effects of treatment. *Biological Psychiatry*, *56*(2), 101–112. doi:10.1016/j.biopsych.2004.04.002

Walter, M., Henning, A., Grimm, S., Schulte, R. F., Beck, J., Dydak, U., *et al*. (2009). The Relationship Between Aberrant Neuronal Activation in the Pregenual Anterior Cingulate, Altered Glutamatergic Metabolism, and Anhedonia in Major Depression. *Archives of General Psychiatry*, *66*(5), 478–486. doi:10.1001/archgenpsychiatry.2009.39

Wang, X. J & Buzsáki, G. (1996). Gamma oscillation by synaptic inhibition in a hippocampal interneuronal network model. *The Journal of Neuroscience : the Official Journal of the Society for Neuroscience*, *16*(20), 6402–6413.

Wang, X.J. (2010). Neurophysiological and Computational Principles of Cortical Rhythms in Cognition. *Physiological Reviews*, *90*(3), 1195–1268. doi:10.1152/physrev.00035.2008

Ward, L. M. (2003). Synchronous neural oscillations and cognitive processes. *Trends in Cognitive Sciences*, *7*(12), 553–559.

Warnking, J. (2002). fMRI Retinotopic Mapping—Step by Step. *NeuroImage*, *17*(4), 1665–1683. doi:10.1006/nimg.2002.1304

Watson, D., Weber, K., Assenheimer, J. S., Clark, L. A., Strauss, M. E., & McCormick, R. A. (1995). Testing a tripartite model: I. Evaluating the convergent and discriminant validity of anxiety and depression symptom scales. *Journal of Abnormal Psychology*, *104*(1), 3–14.

Whiting, P. J.,(2003). GABA-A receptor subtypes in the brain: a paradigm for CNS drug discovery? *Drug Discovery Today*, *8*(10), 445–450.

Whittington, M. A., Traub, R. D., & Jefferys, J. G. R. (1995). Synchronized oscillations in interneuron networks driven by metabotropic glutamate receptor activation. *Nature*, *373*(6515), 612–615.

Whittington, M. A., Traub, R. D., Kopell, N., Ermentrout, B., & Buhl, E. H. (2000). Inhibition-based rhythms: experimental and mathematical observations on network dynamics. *International Journal of Psychophysiology : Official Journal of the International Organization of Psychophysiology*, *38*(3), 315–336.

Wierońska, J. M., Pałucha-Poniewiera, A., Nowak, G., & Pilic, A. (2012). Depression Viewed as a GABA/Glutamate Imbalance in the Central Nervous System. *Clinical, Research and Treatment Approaches to Affective Disorders,*, *ISBN: 978-953-51-0177-2*.

Winkler, A. M., Ridgway, G. R., Webster, M. A., Smith, S. M., & Nichols, T. E. (2014). Permutation inference for the general linear model. *NeuroImage*, *92*, 381–397. doi:10.1016/j.neuroimage.2014.01.060

Wolosker, H., Dumin, E., Balan, L., & Foltyn, V. N. (2008). d-Amino acids in the brain: d-serine in neurotransmission and neurodegeneration. *FEBS Journal*, *275*(14), 3514–3526. doi:10.1111/j.1742-4658.2008.06515.x

Wong, T., Fung, P., McAlonan, G., & Chua, S. (2009). Spatiotemporal dipole source localization of face processing ERPs in adolescents: a preliminary study. *Behavioral and Brain Functions : BBF*, *5*(1), 16. doi:10.1186/1744-9081-5-16

Wood, J. D., & Hertz, L. (1980). Ketamine-induced changes in the GABA system of mouse brain. *Biological Psychiatry*, *19*(8), 805–808.

Wood, J., Kim, Y., & Moghaddam, B. (2012). Disruption of prefrontal cortex large scale neuronal activity by different classes of psychotomimetic drugs. *Journal of Neuroscience*, *32*(9), 3022–3031. doi:10.1523/JNEUROSCI.6377-11.2012

Xing, D., Yeh, C.I., Burns, S., & Shapley, R. M. (2012). Laminar analysis of visually evoked activity in the primary visual cortex. *Proceedings of the National Academy of Sciences*, *109*(34), 13871–13876. doi:10.1073/pnas.1201478109

Yeap, S., Kelly, S. P., Reilly, R. B., Thakore, J. H., & Foxe, J. J. (2009). Visual sensory processing deficits in patients with bipolar disorder revealed through high-density electrical mapping. *Journal of Psychiatry & Neuroscience : JPN*, *34*(6), 459–464.

Yeap, S., Kelly, S. P., Sehatpour, P., Magno, E., Javitt, D. C., Garavan, H., *et al*. (2006). Early visual sensory deficits as endophenotypes for schizophrenia: high-density electrical mapping in clinically unaffected first-degree relatives. *Archives of General Psychiatry*, *63*(11), 1180–1188. doi:10.1001/archpsyc.63.11.1180

Yildiz-Yesiloglu, A., & Ankerst, D. P. (2006). Review of 1H magnetic resonance spectroscopy findings in major depressive disorder: A meta-analysis. *Psychiatry Research: Neuroimaging*, *147*(1), 1–25. doi:10.1016/j.pscychresns.2005.12.004

Young, A. W., Perrett, D. I., Calder, A. J., & Sprengelmeyer, R. (2002). Young: Facial Expressions of Emotion: Stimuli and... - Google Scholar. *Edmunds*.

Yuille, A., & Kersten, D. (2006). Vision as Bayesian inference: analysis by synthesis? *Trends in Cognitive Sciences*, *10*(7), 301–308. doi:10.1016/j.tics.2006.05.002

Yüksel, C., & Öngür, D. (2010). Magnetic Resonance Spectroscopy Studies of Glutamate-Related Abnormalities in Mood Disorders. *Biological Psychiatry*, *68*(9), 785–794. doi:10.1016/j.biopsych.2010.06.016

Zarate, C. A., Singh, J. B., Carlson, P. J., Brutsche, N. E., Ameli, R., Luckenbaugh, D. A., *et al*. (2006). A randomized trial of an N-methyl-D-aspartate antagonist in treatment-resistant major depression. *Archives of General Psychiatry*, *63*(8), 856–864. doi:10.1001/archpsyc.63.8.856

Zhang, Y., Brady, M., & Smith, S. (2001). Segmentation of brain MR images through a hidden Markov random field model and the expectation-maximization algorithm. *IEEE Transactions on Medical Imaging*, *20*(1), 45–57. doi:10.1109/42.906424

Zilles, K., Palomero-Gallagher, N., & Schleicher, A. (2004). Transmitter receptors and functional anatomy of the cerebral cortex. *Journal of Anatomy*, *205*(6), 417–432. doi:10.1111/j.0021-8782.2004.00357.x

Appendix 1

Spectrogram data of participants in the experiment detailed in chapter 3.

Controls listed first (1:n) followed by patients (1:n).

N	Spectrogram	Induced Response (0 – 0.3 s)	Evoked Response (0.3 – 0.8 s)
1	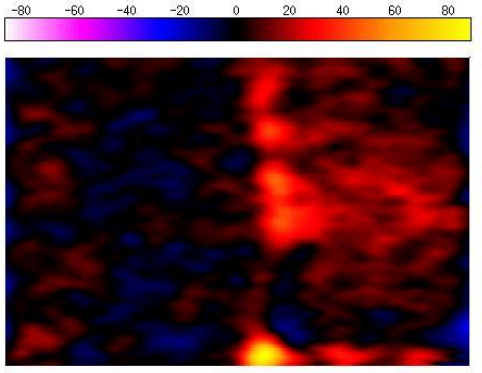	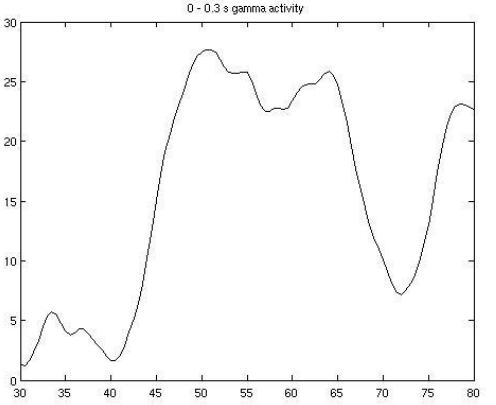	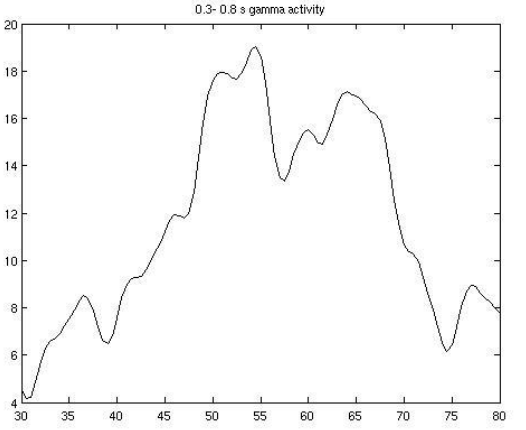

2	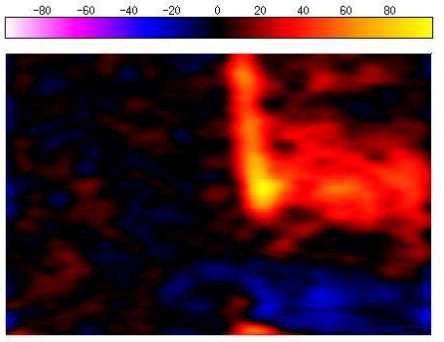 -80 -60 -40 -20 0 20 40 60 80	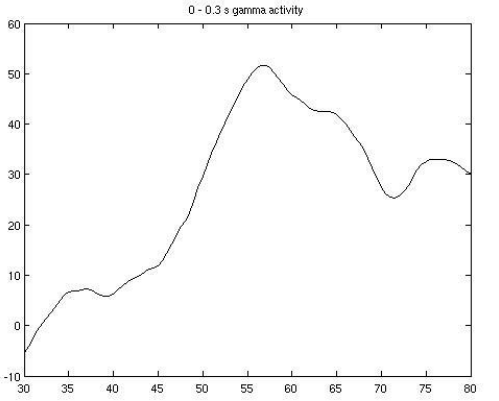 0 - 0.3 s gamma activity	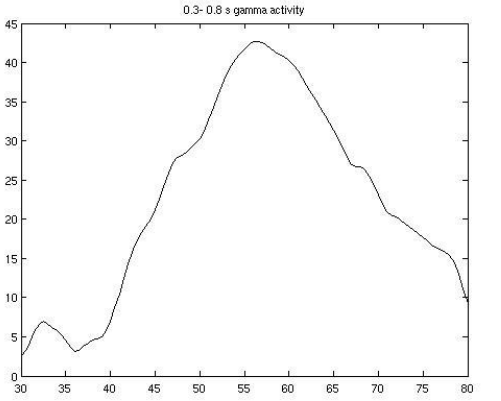 0.3- 0.8 s gamma activity
3	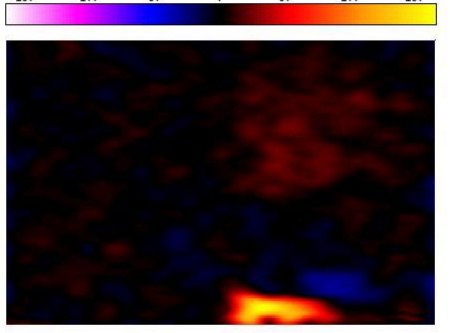 -150 -100 -50 0 50 100 150	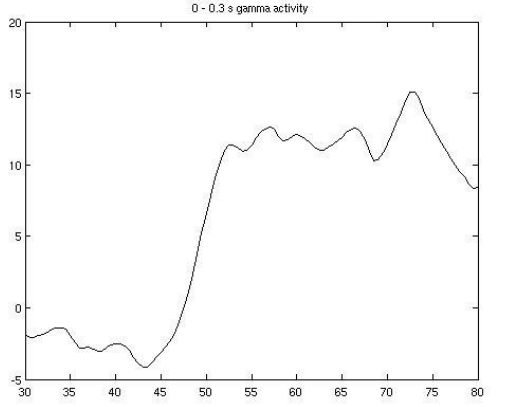 0 - 0.3 s gamma activity	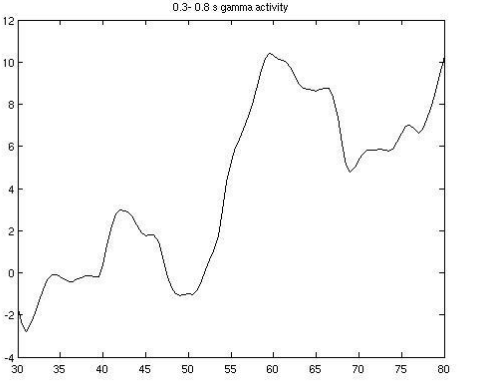 0.3- 0.8 s gamma activity

4	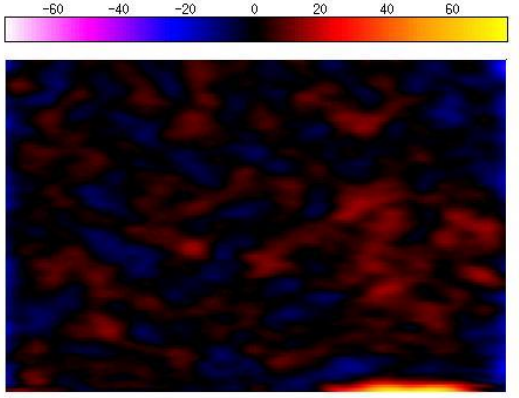 -60 -40 -20 0 20 40 60	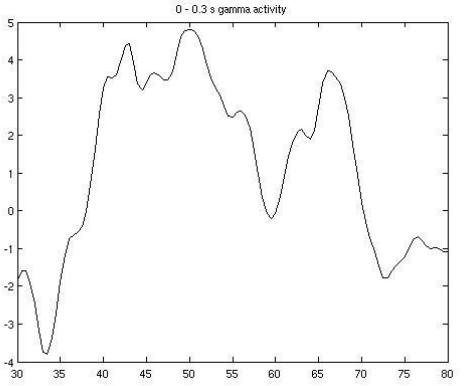 0 - 0.3 s gamma activity	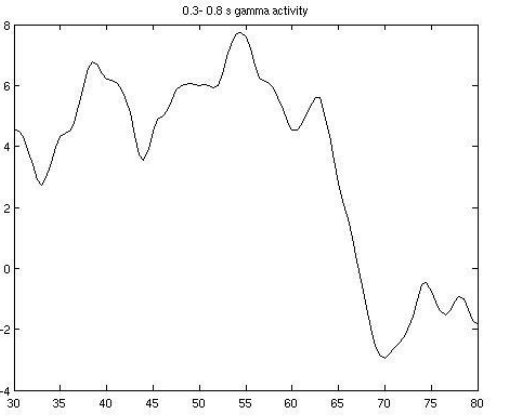 0.3- 0.8 s gamma activity
5	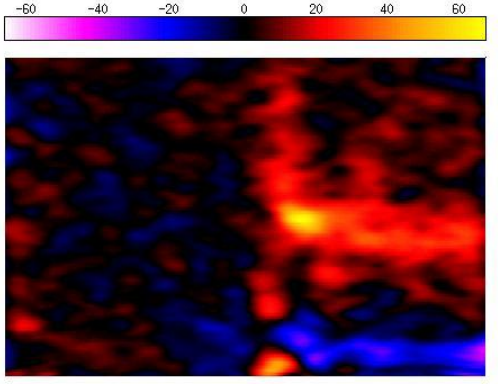 -60 -40 -20 0 20 40 60	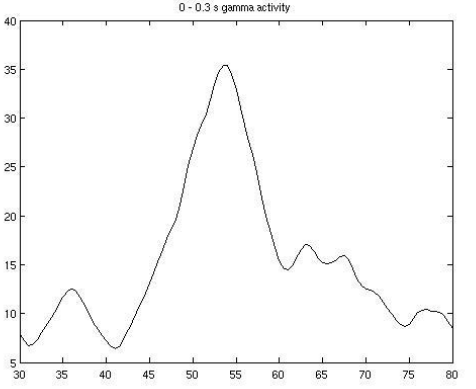 0 - 0.3 s gamma activity	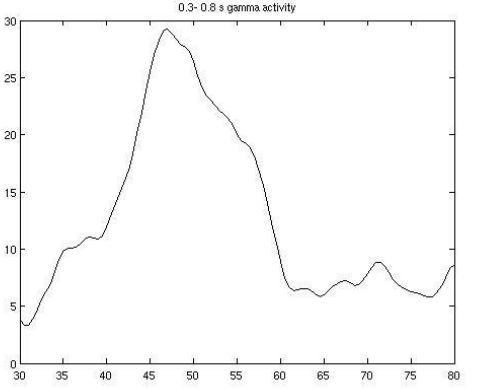 0.3- 0.8 s gamma activity

6	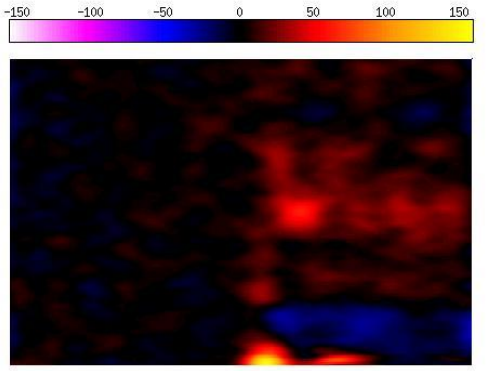 −150 −100 −50 0 50 100 150	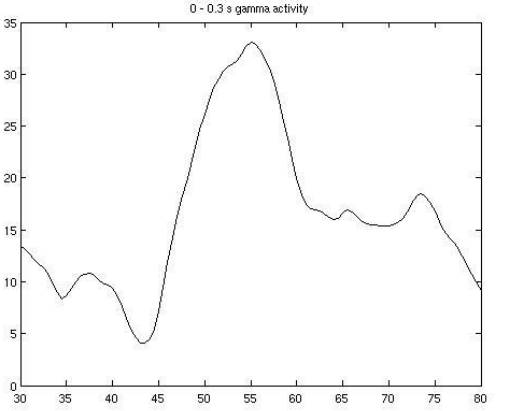 0 - 0.3 s gamma activity	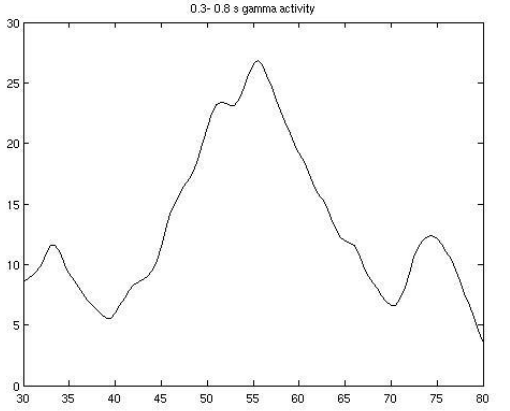 0.3- 0.8 s gamma activity
7	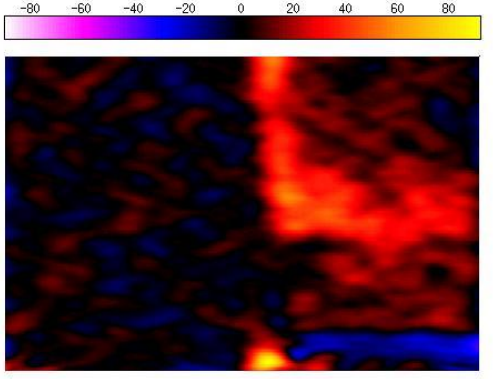 −80 −60 −40 −20 0 20 40 60 80	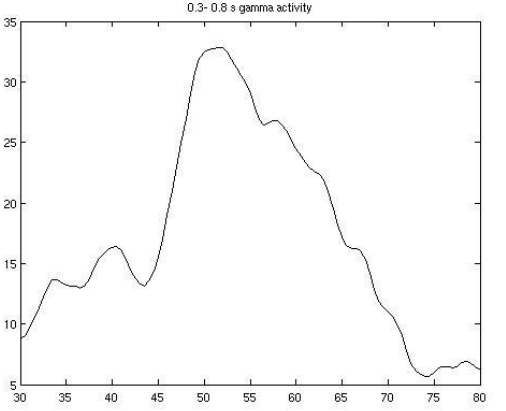 0.3- 0.8 s gamma activity	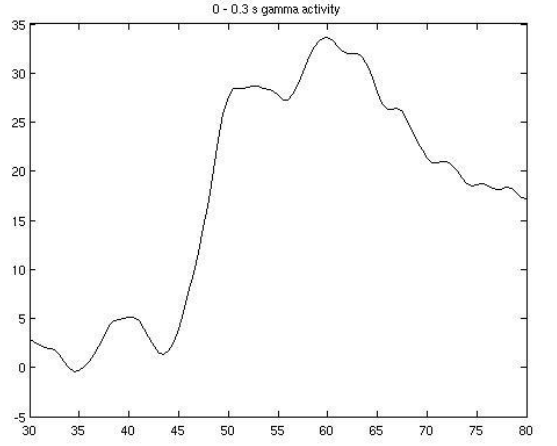 0 - 0.3 s gamma activity

8	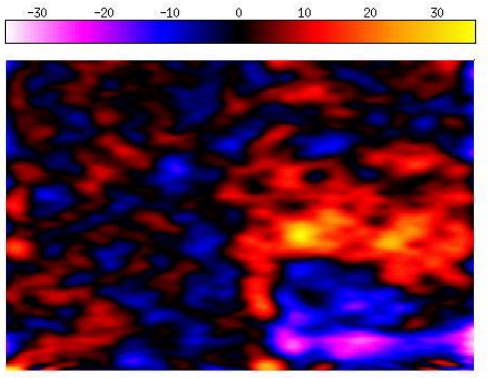 -30 -20 -10 0 10 20 30	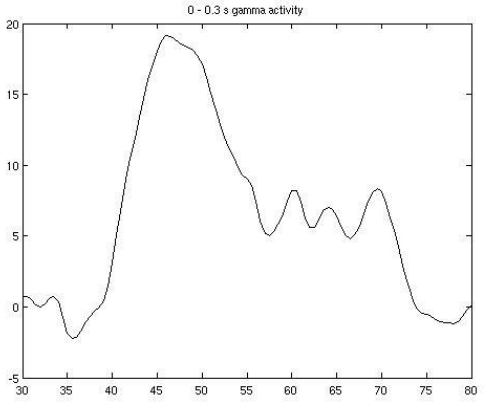 0 - 0.3 s gamma activity	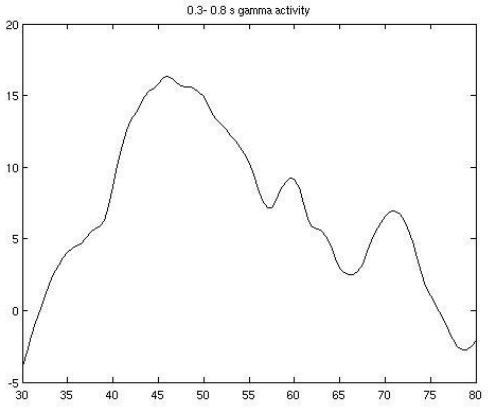 0.3- 0.8 s gamma activity
9	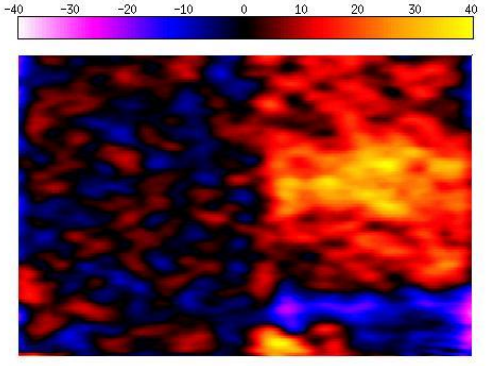 -40 -30 -20 -10 0 10 20 30 40	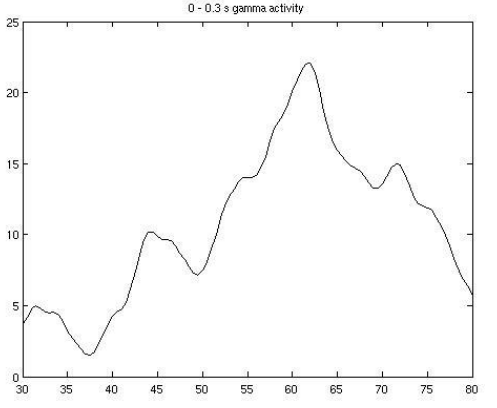 0 - 0.3 s gamma activity	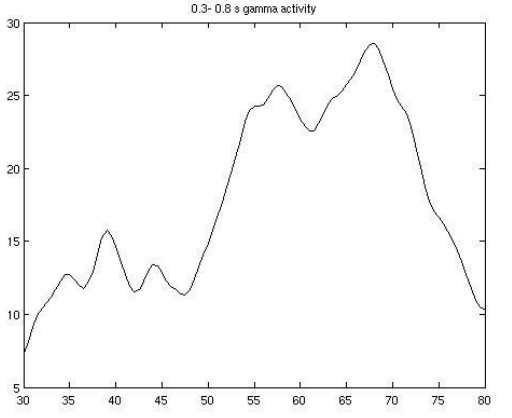 0.3- 0.8 s gamma activity

10	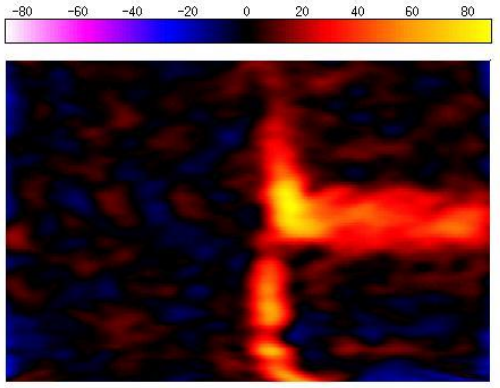 -80 -60 -40 -20 0 20 40 60 80	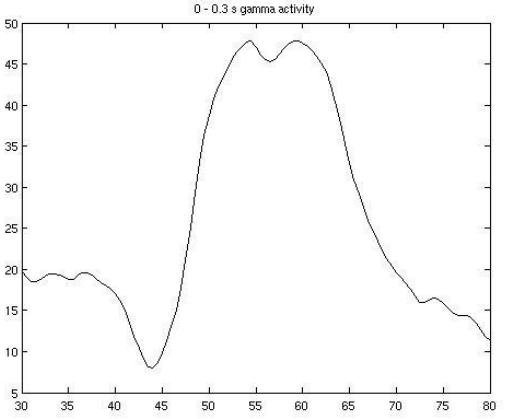 0 - 0.3 s gamma activity	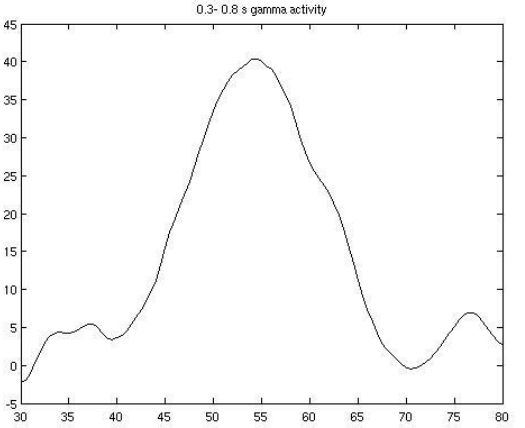 0.3- 0.8 s gamma activity
11	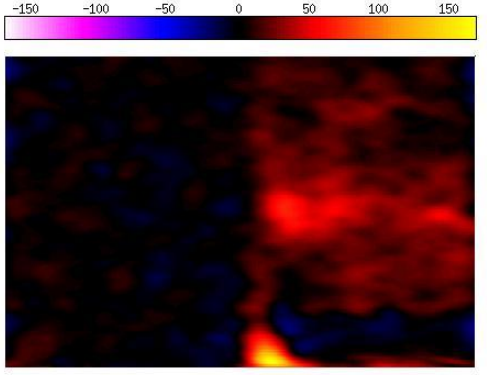 -150 -100 -50 0 50 100 150	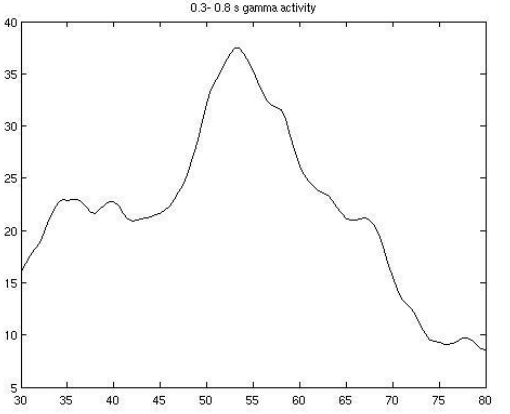 0.3- 0.8 s gamma activity	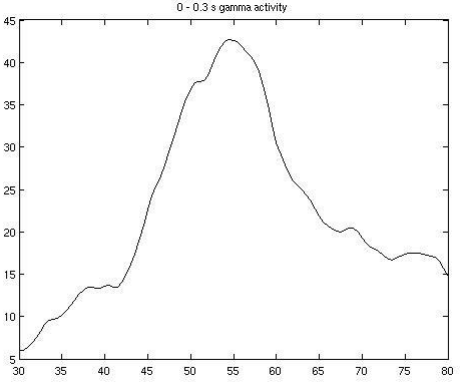 0 - 0.3 s gamma activity

12	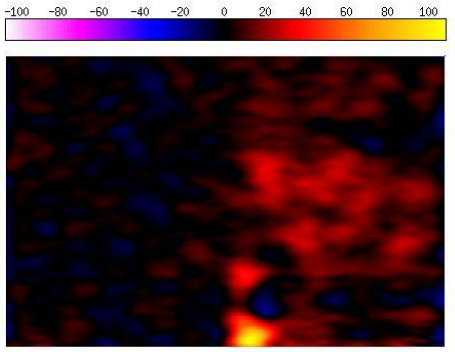 -100 -80 -60 -40 -20 0 20 40 60 80 100	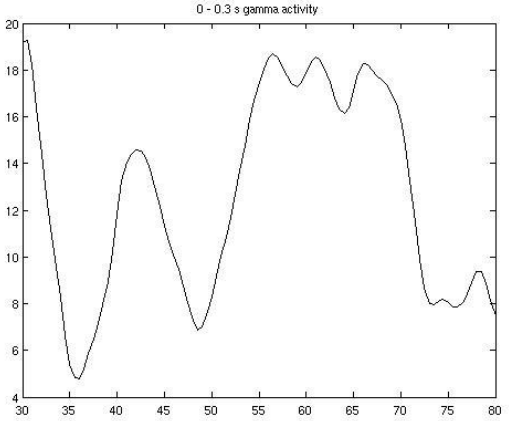 0 - 0.3 s gamma activity	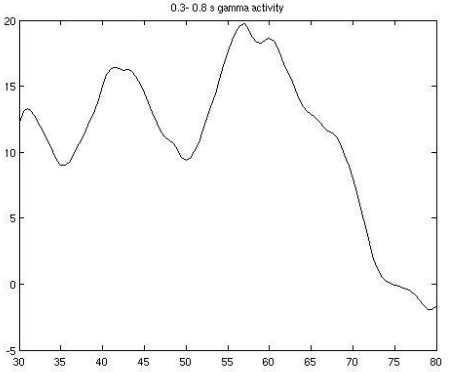 0.3- 0.8 s gamma activity
13	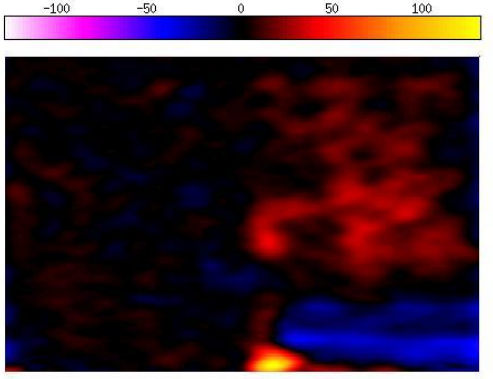 -100 -50 0 50 100	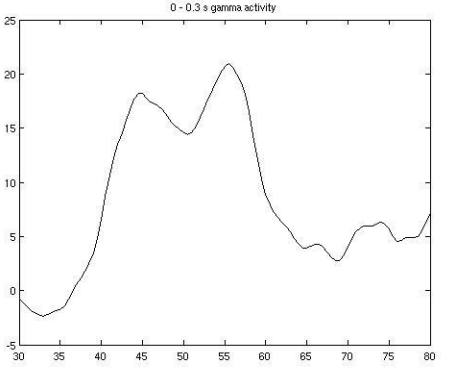 0 - 0.3 s gamma activity	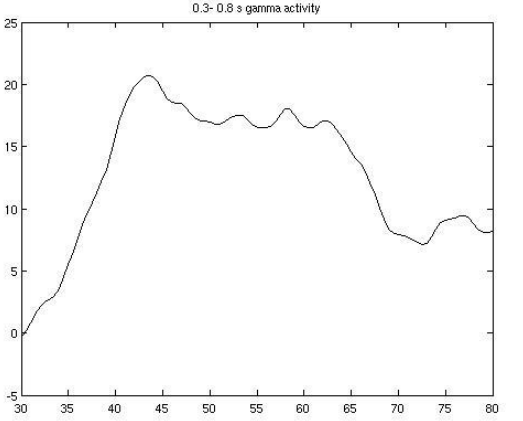 0.3- 0.8 s gamma activity

14	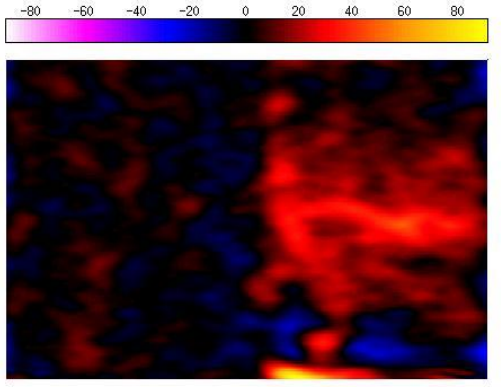 −80 −60 −40 −20 0 20 40 60 80	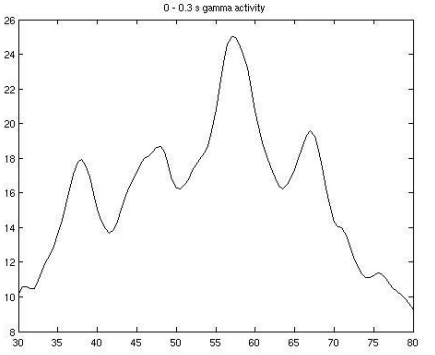 0 - 0.3 s gamma activity	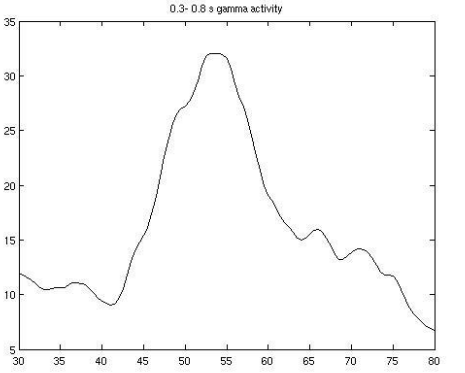 0.3- 0.8 s gamma activity
15	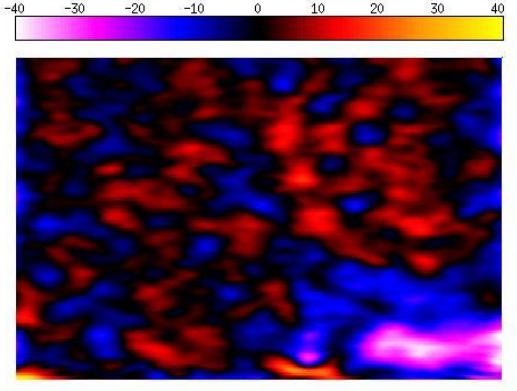 −40 −30 −20 −10 0 10 20 30 40	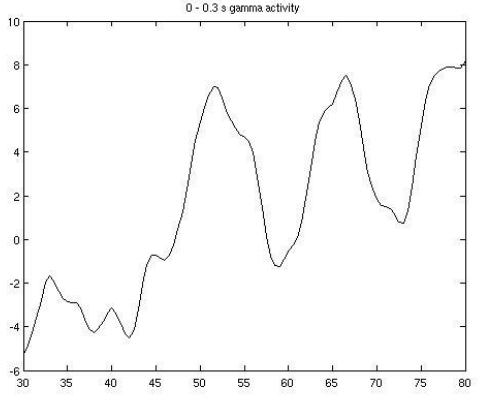 0 - 0.3 s gamma activity	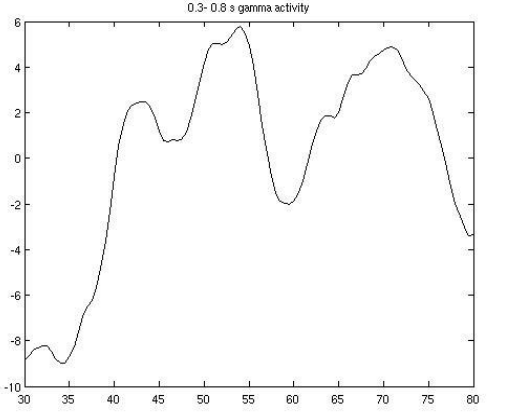 0.3- 0.8 s gamma activity

16	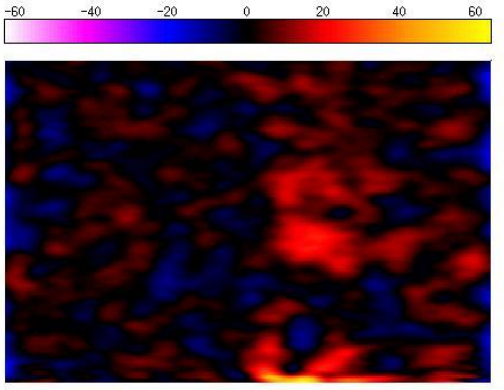 -60 -40 -20 0 20 40 60	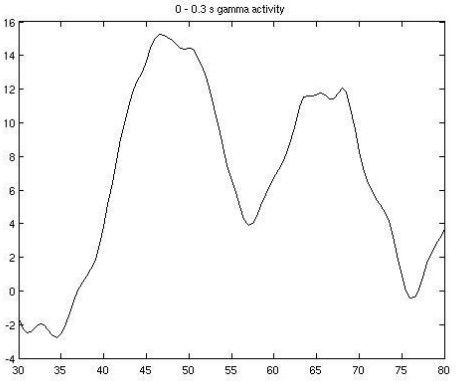 0 - 0.3 s gamma activity	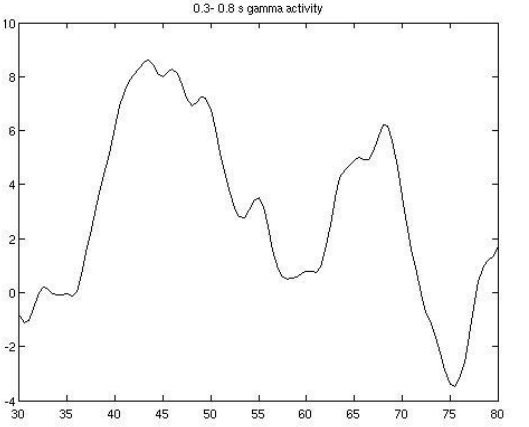 0.3- 0.8 s gamma activity
17	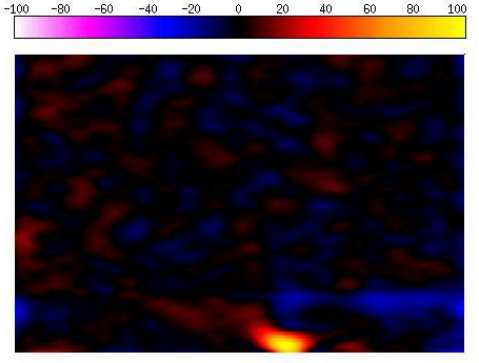 -100 -80 -60 -40 -20 0 20 40 60 80 100	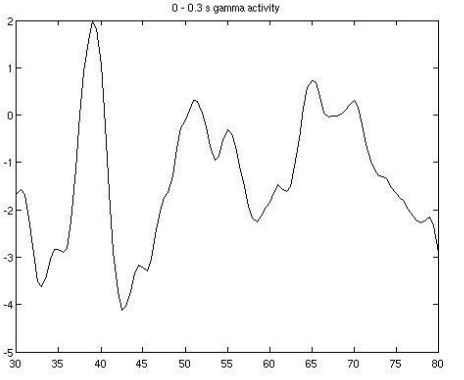 0 - 0.3 s gamma activity	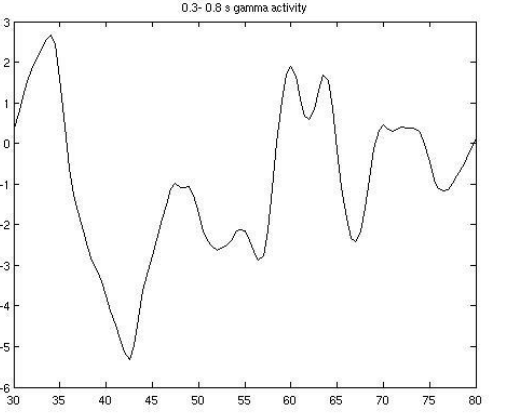 0.3- 0.8 s gamma activity

18	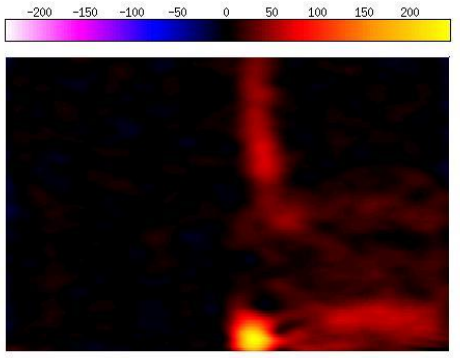 -200 -150 -100 -50 0 50 100 150 200	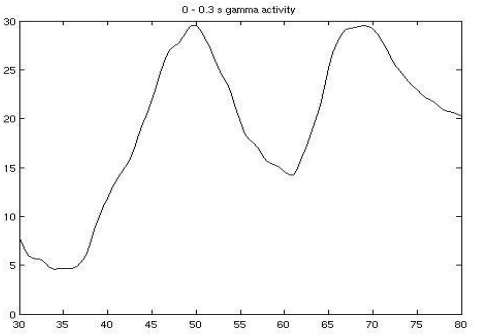 0 - 0.3 s gamma activity	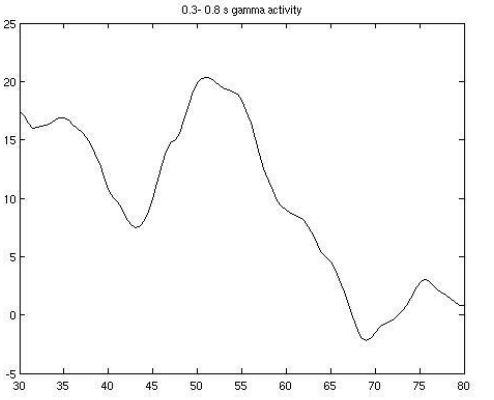 0.3- 0.8 s gamma activity
1	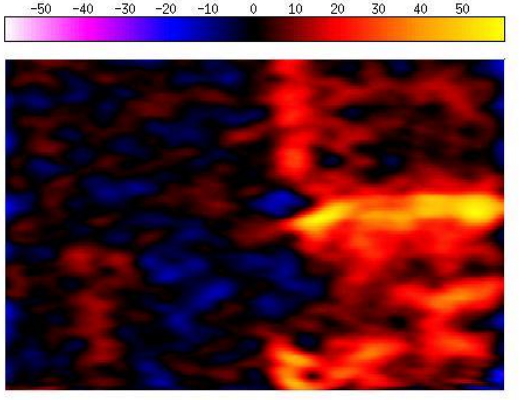 -50 -40 -30 -20 -10 0 10 20 30 40 50	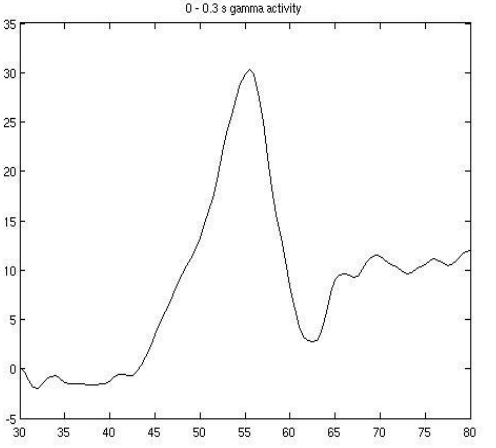 0 - 0.3 s gamma activity	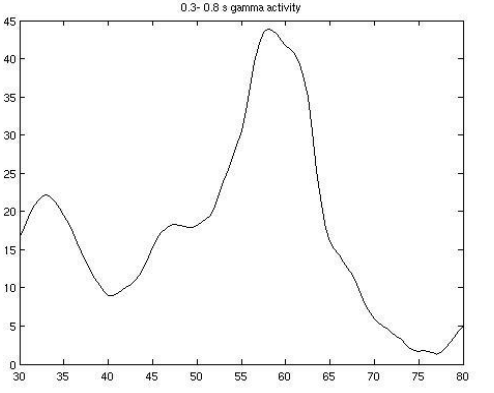 0.3- 0.8 s gamma activity

2

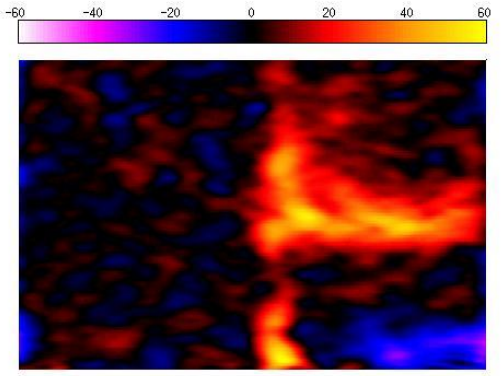
-60 -40 -20 0 20 40 60

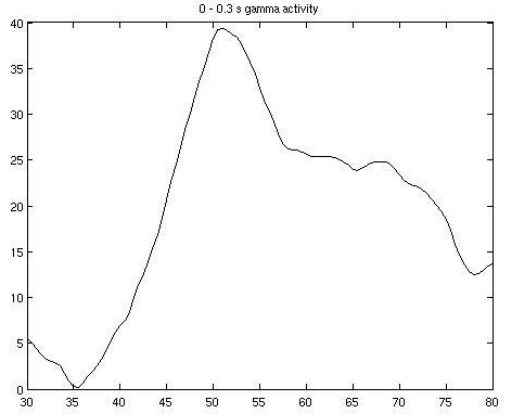
0 - 0.3 s gamma activity

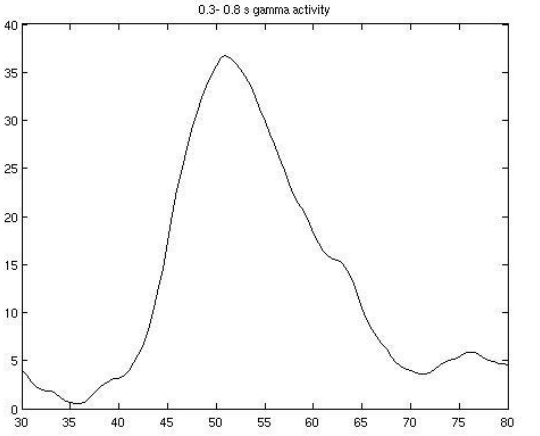
0.3- 0.8 s gamma activity

3

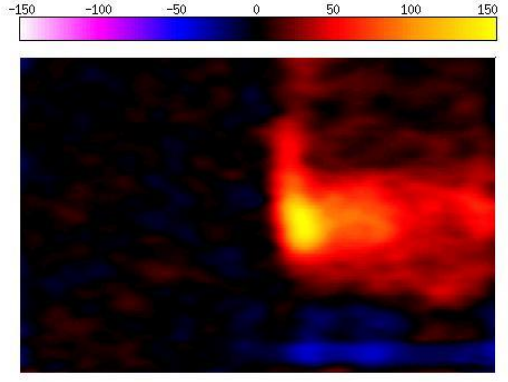
-150 -100 -50 0 50 100 150

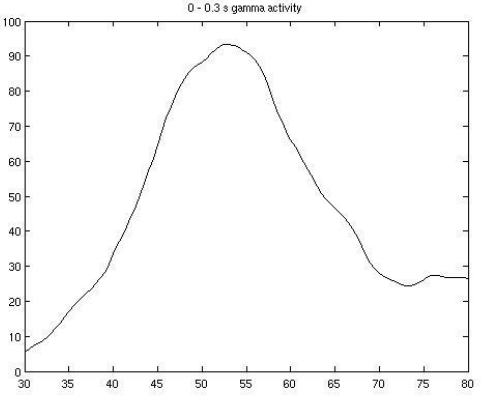
0 - 0.3 s gamma activity

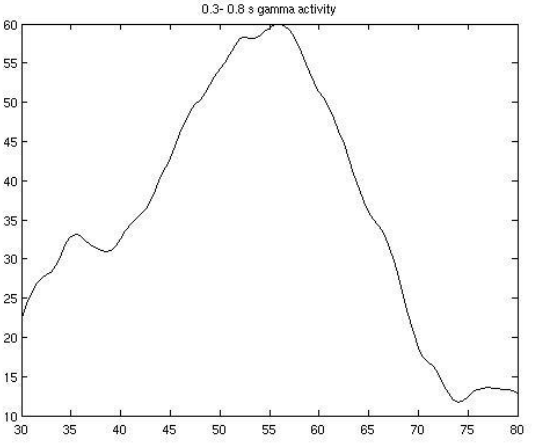
0.3- 0.8 s gamma activity

4	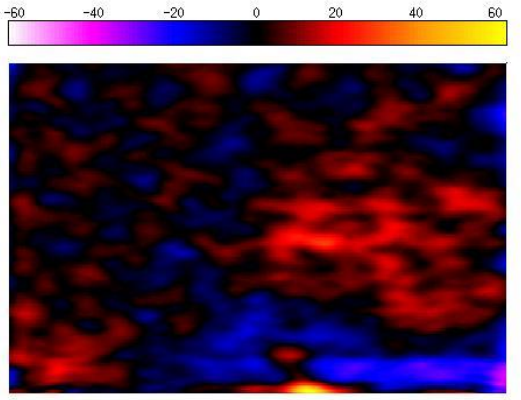 -60 -40 -20 0 20 40 60	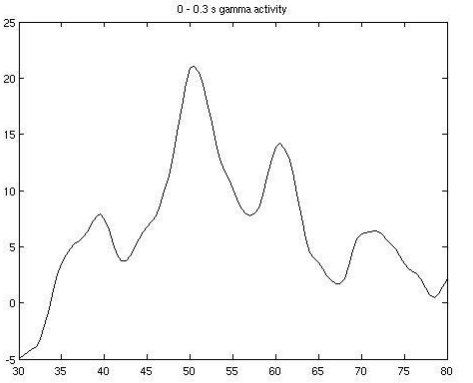 0 - 0.3 s gamma activity	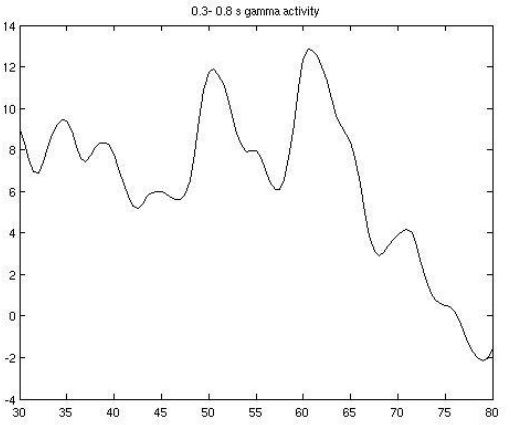 0.3- 0.8 s gamma activity
5	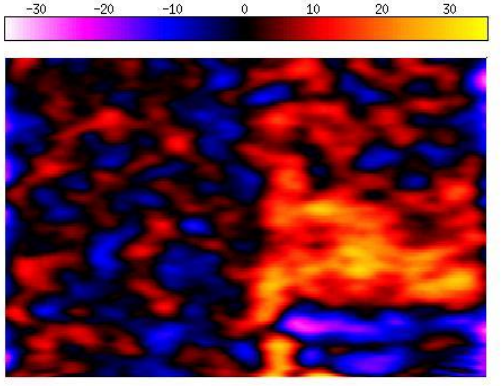 -30 -20 -10 0 10 20 30	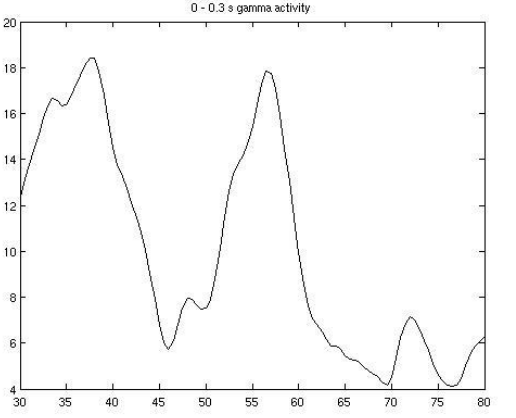 0 - 0.3 s gamma activity	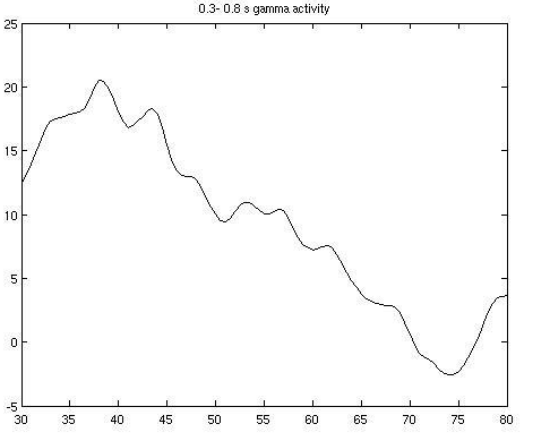 0.3- 0.8 s gamma activity

6	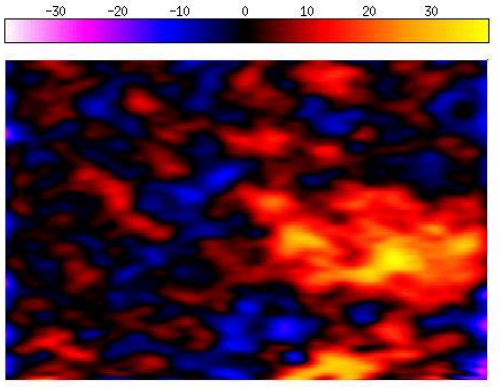 -30 -20 -10 0 10 20 30	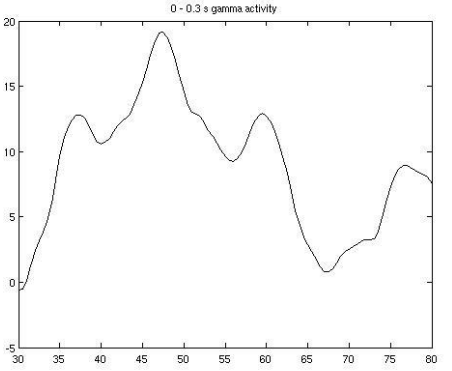 0 - 0.3 s gamma activity	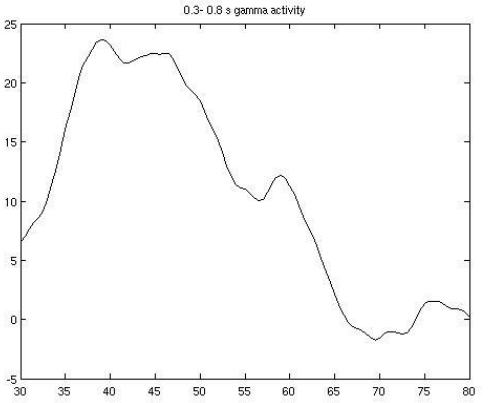 0.3- 0.8 s gamma activity
7	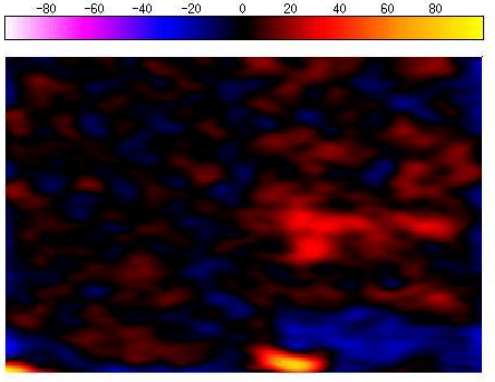 -80 -60 -40 -20 0 20 40 60 80	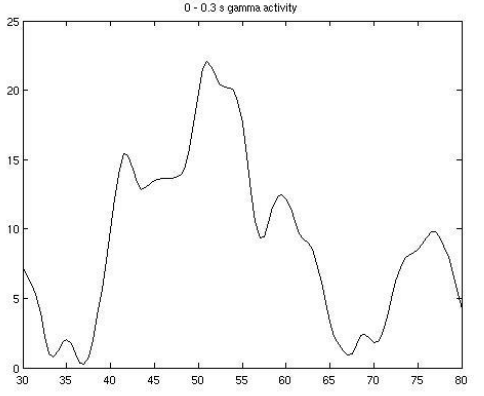 0 - 0.3 s gamma activity	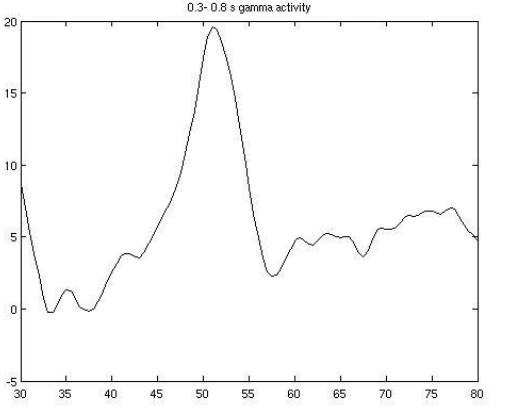 0.3- 0.8 s gamma activity

8	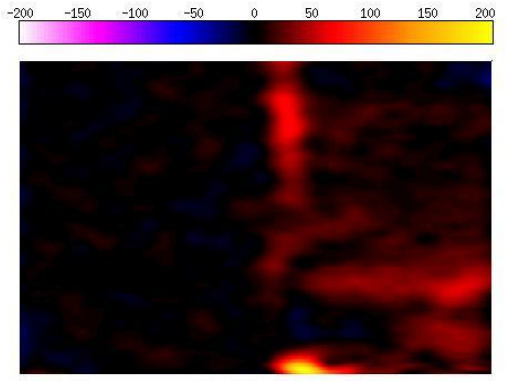 −200 −150 −100 −50 0 50 100 150 200	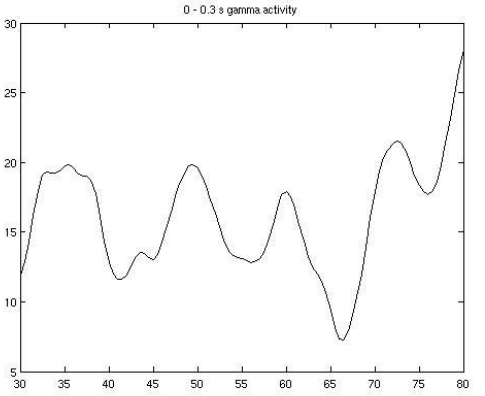 0 - 0.3 s gamma activity	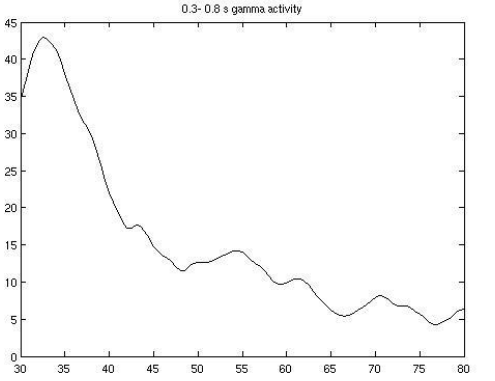 0.3- 0.8 s gamma activity
9	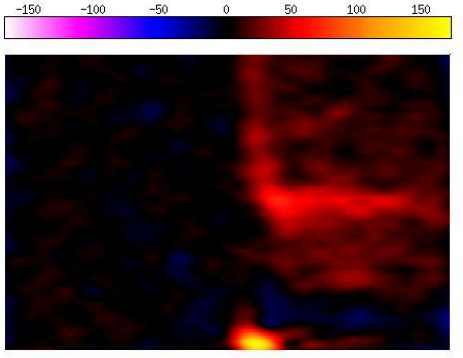 −150 −100 −50 0 50 100 150	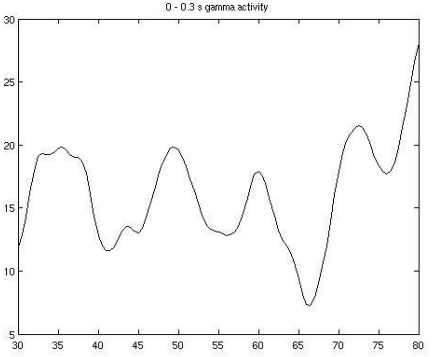 0 - 0.3 s gamma activity	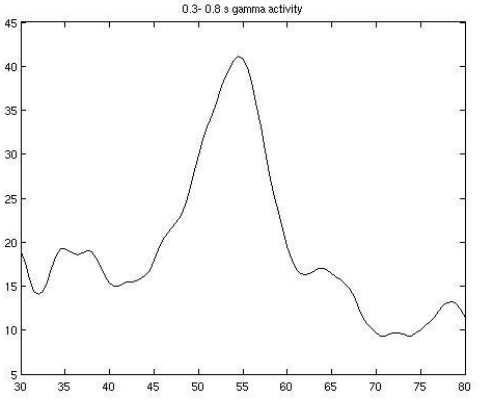 0.3- 0.8 s gamma activity

10	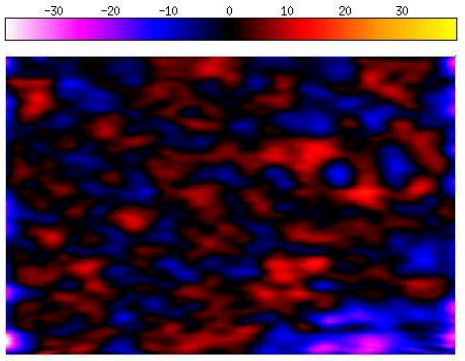 −30 −20 −10 0 10 20 30	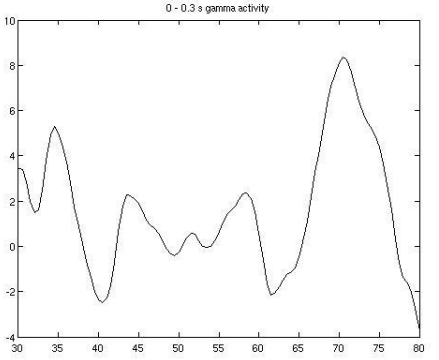 0 - 0.3 s gamma activity	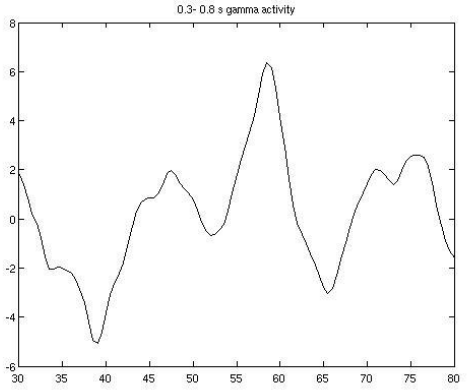 0.3- 0.8 s gamma activity
11	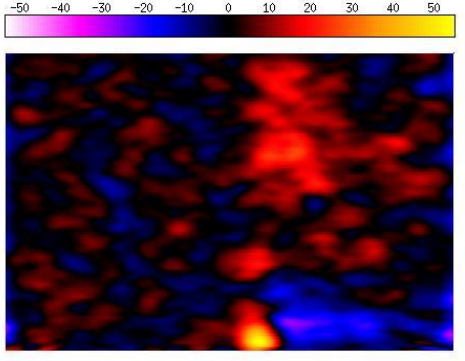 −50 −40 −30 −20 −10 0 10 20 30 40 50	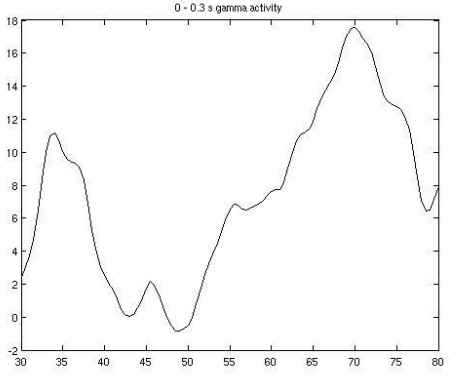 0 - 0.3 s gamma activity	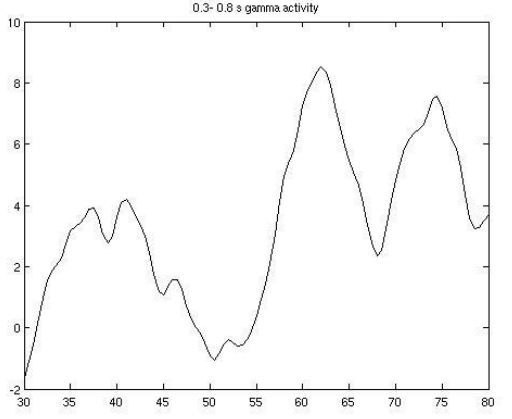 0.3- 0.8 s gamma activity

12	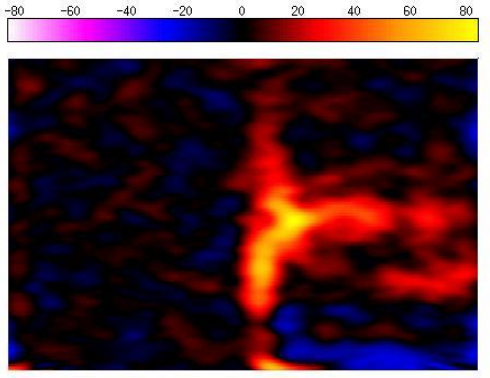 -80 -60 -40 -20 0 20 40 60 80	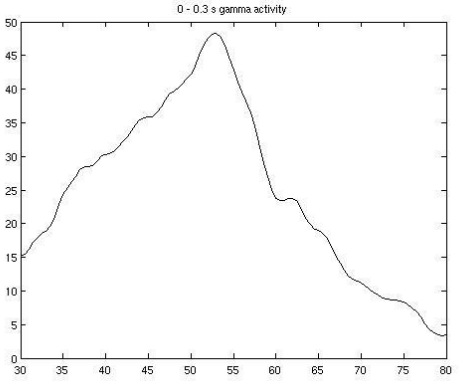 0 - 0.3 s gamma activity	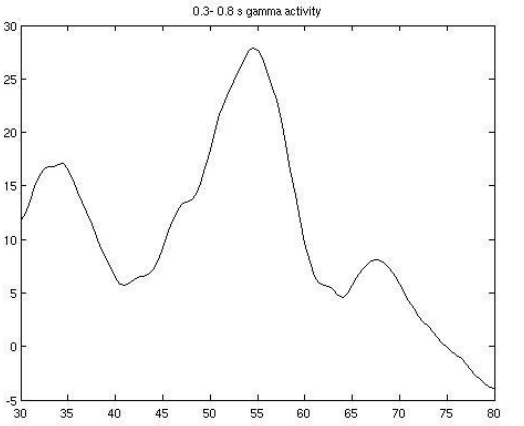 0.3- 0.8 s gamma activity
13	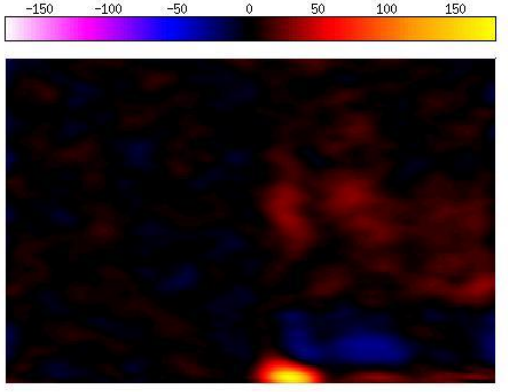 -150 -100 -50 0 50 100 150	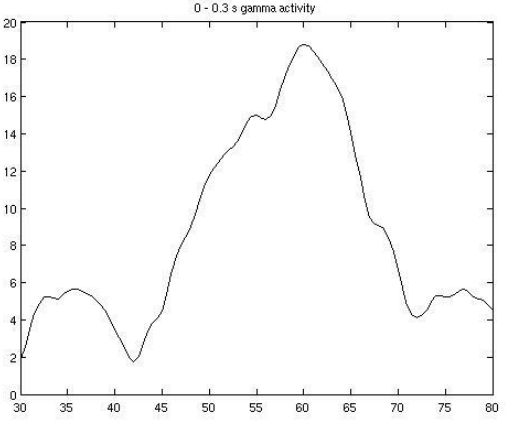 0 - 0.3 s gamma activity	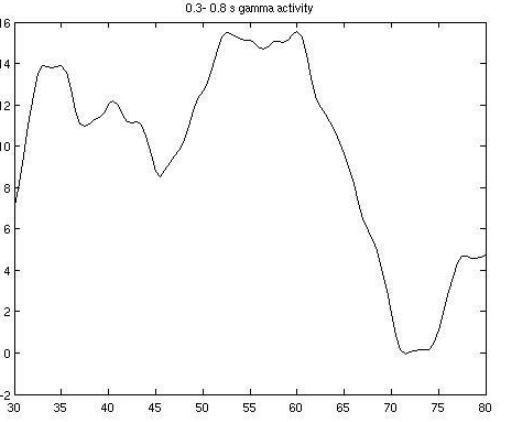 0.3- 0.8 s gamma activity

14	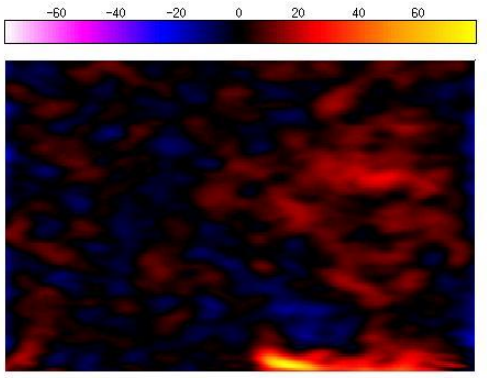 −60 −40 −20 0 20 40 60	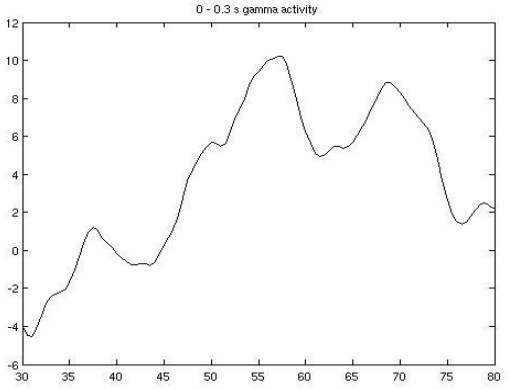 0 - 0.3 s gamma activity	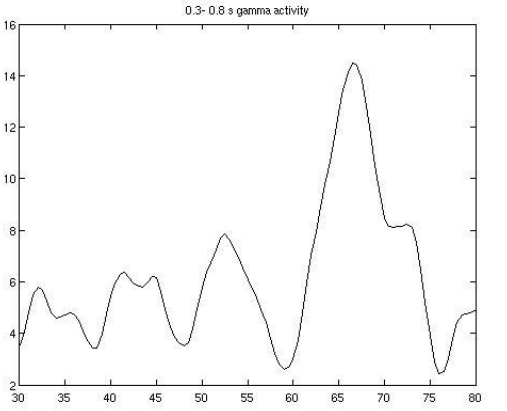 0.3- 0.8 s gamma activity
15	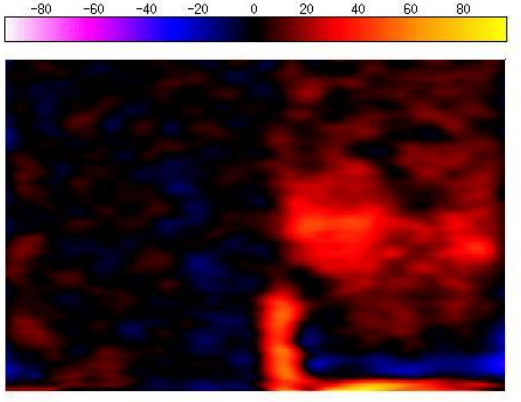 −80 −60 −40 −20 0 20 40 60 80	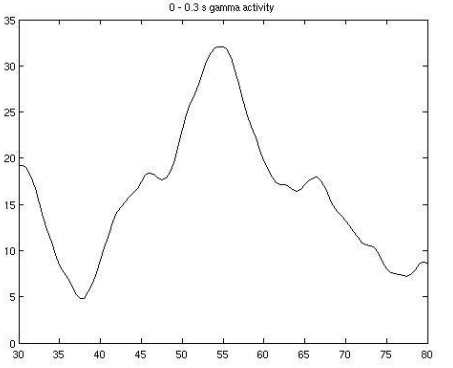 0 - 0.3 s gamma activity	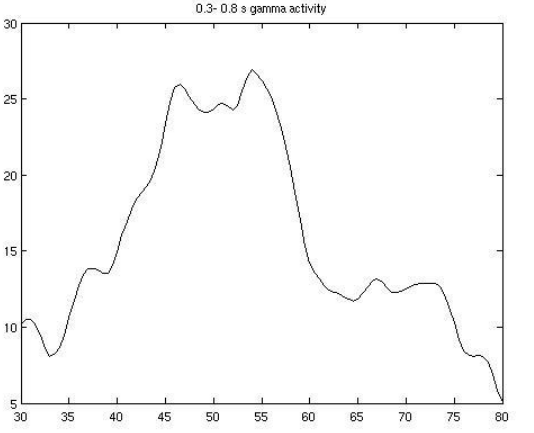 0.3- 0.8 s gamma activity

16	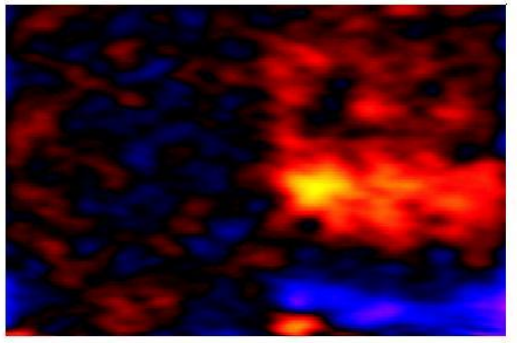	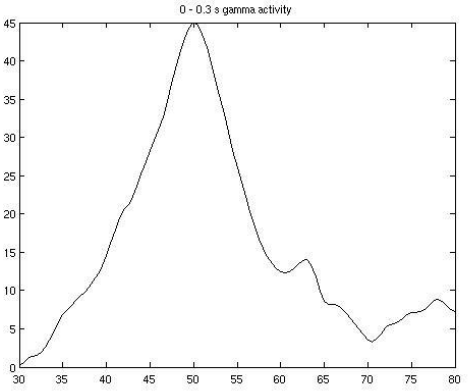	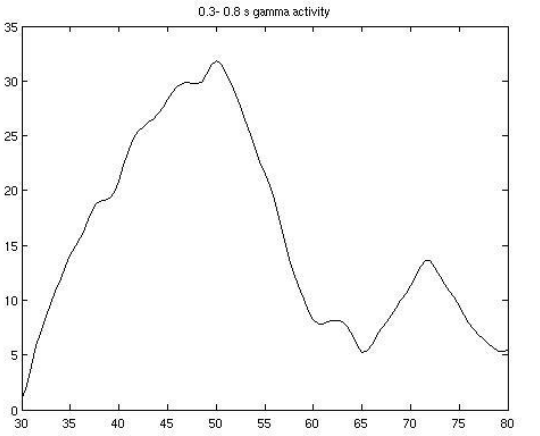

Appendix 2.

Individual level (error bars) data for the face-processing experiment in chapter 4.

Explicit task event related field data:

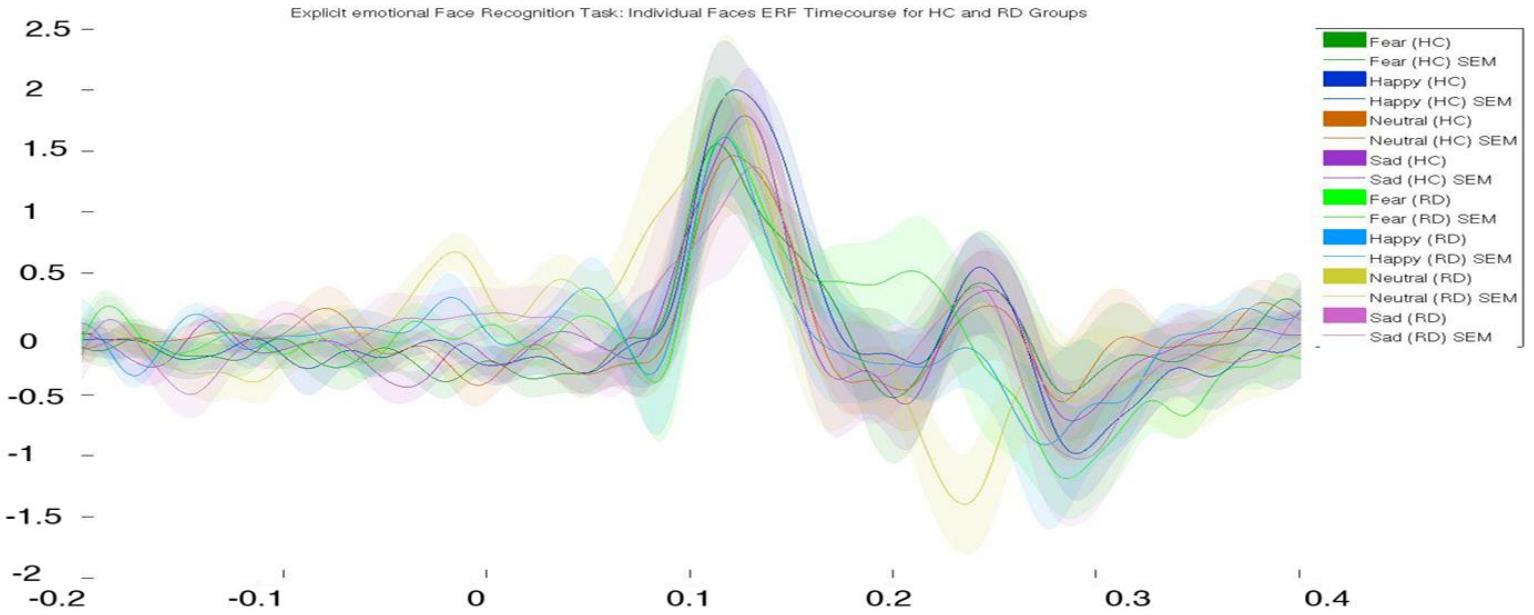

Implicit task event related field data (top: fear, bottom: sad):

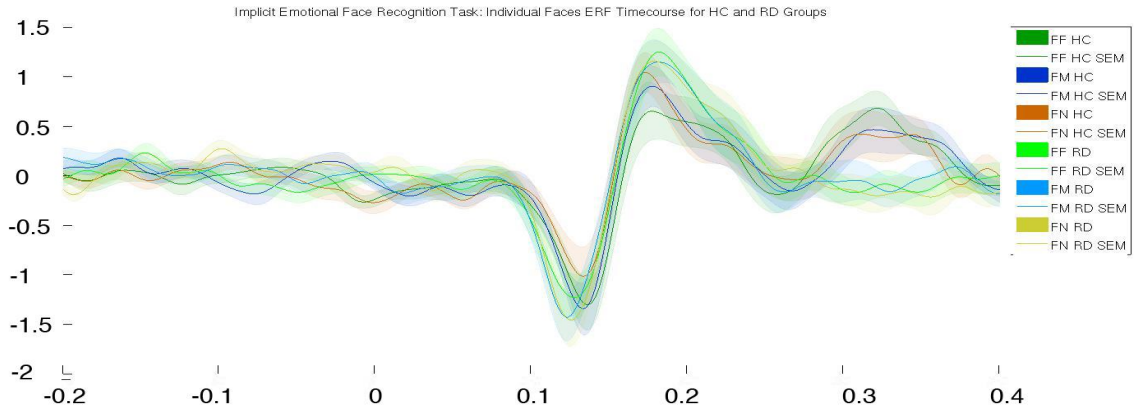

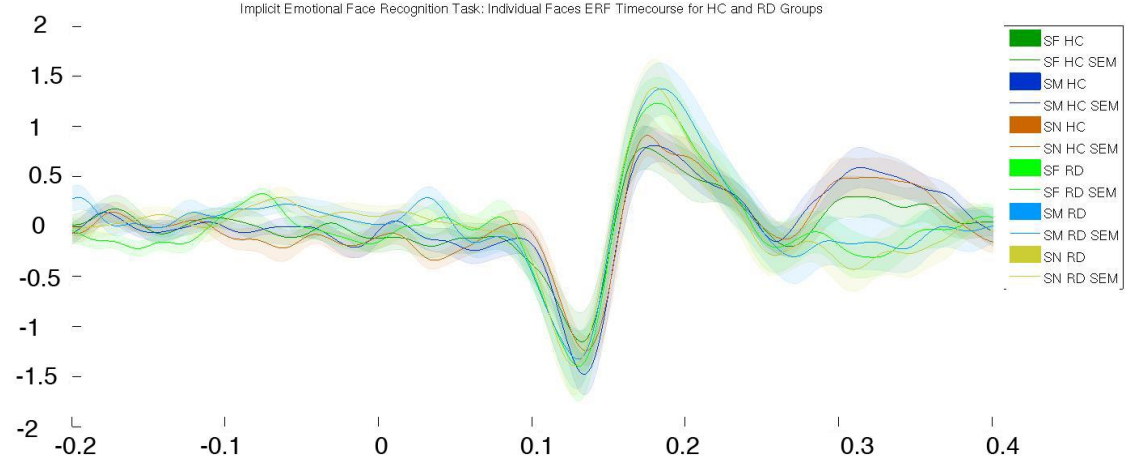

Spectrogram data for the explicit task data at group level (averaged by face type). Left: neutral, Middle: fear, Right: sad.

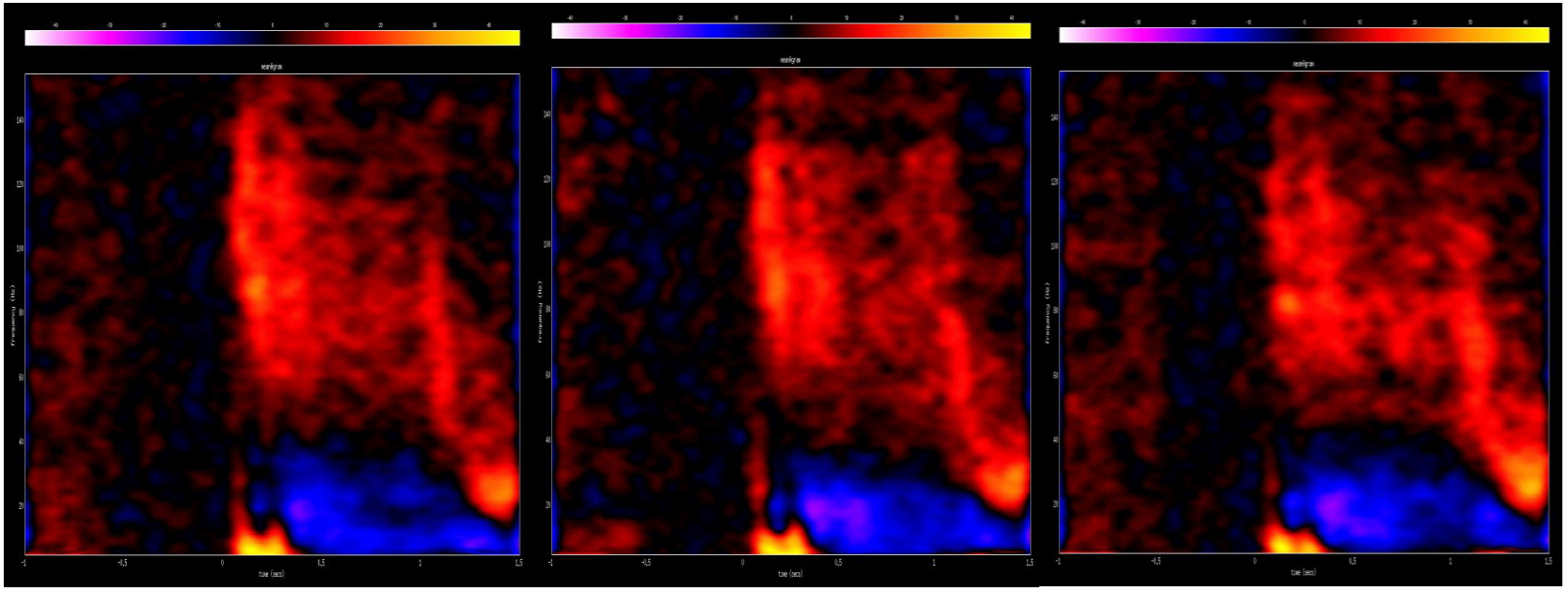

Representation of the group difference in the amplitude of gamma-frequency responses between groups. PH = Personal History of Depression.

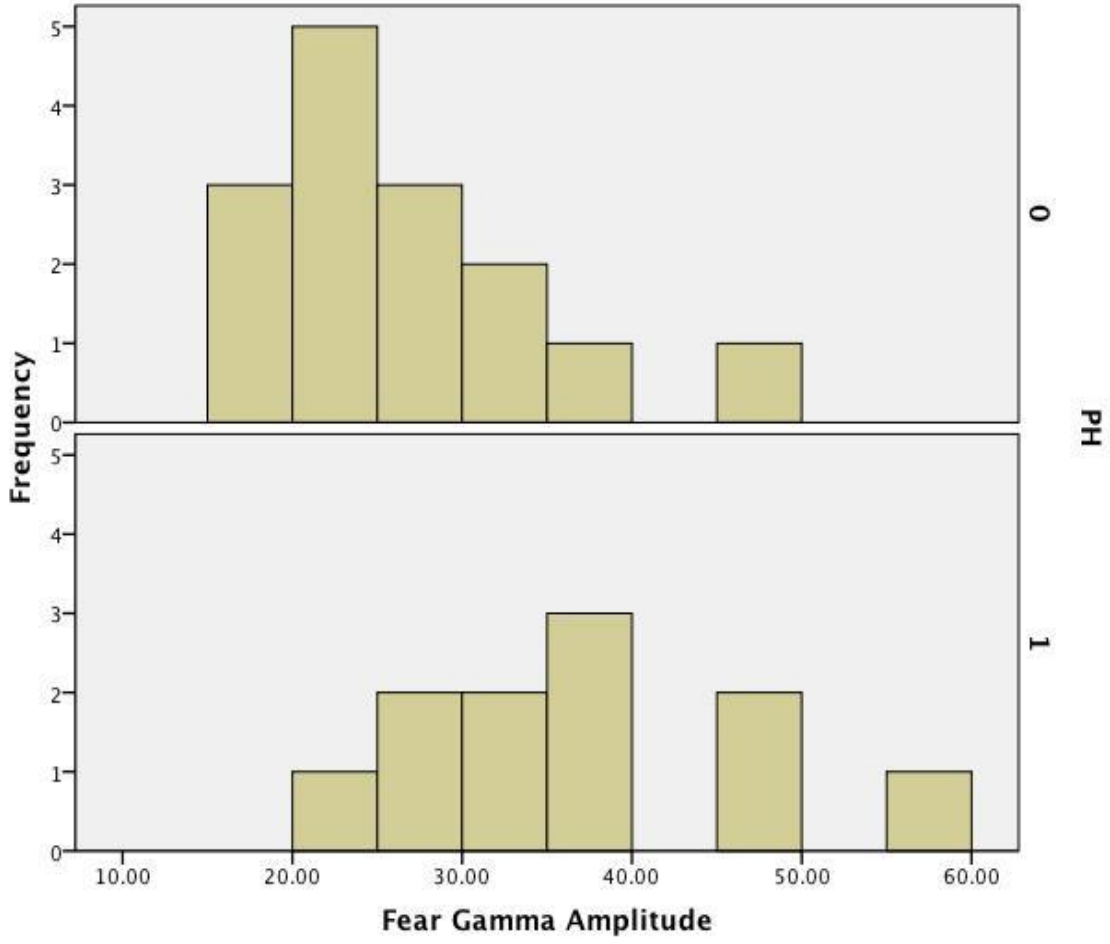

Peak difference (t-statistic above 3) maps for the explicit face task for remitted depression group > than healthy control group for data in the gamma range.

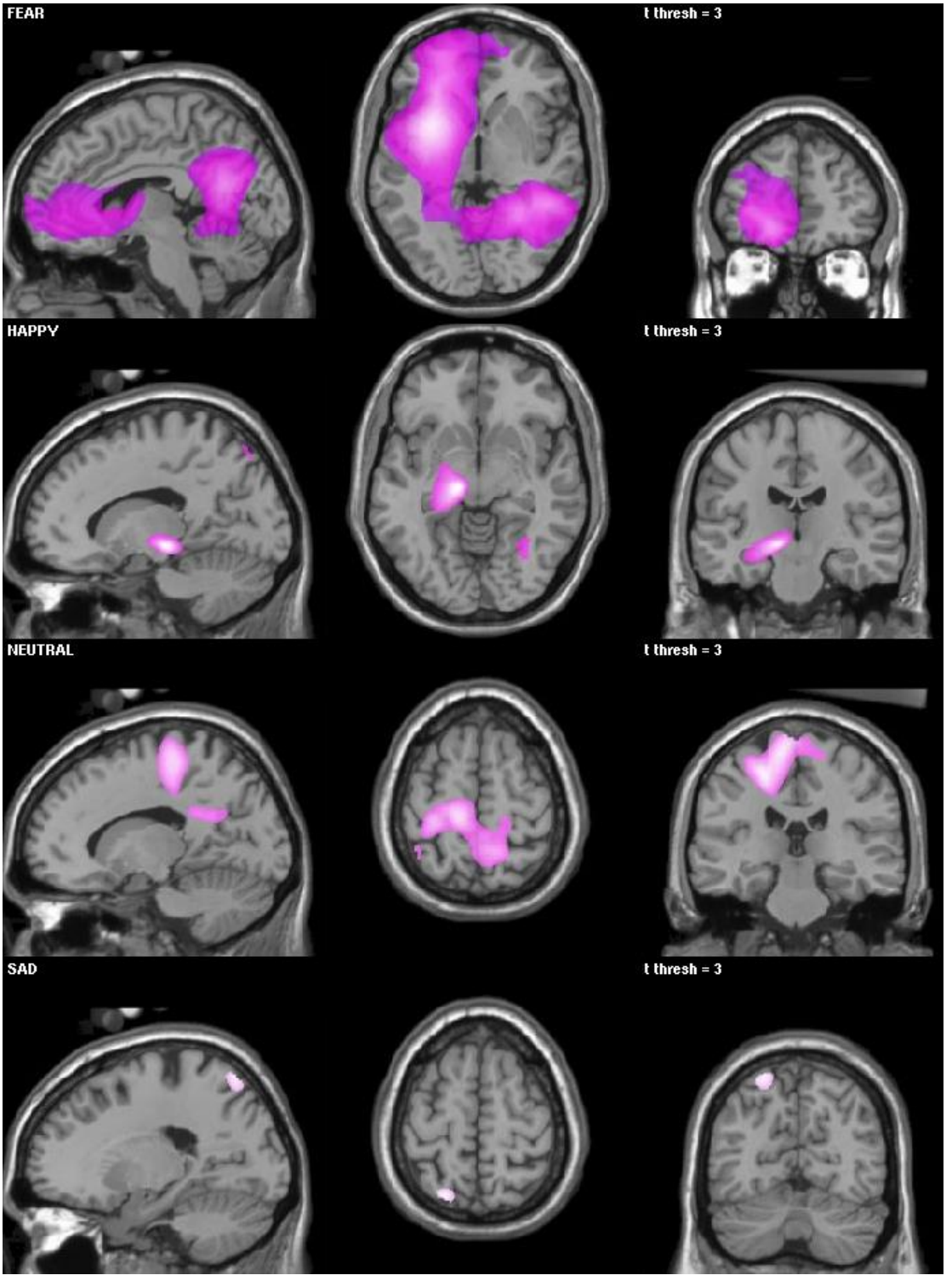

Appendix 3.

Individuals' spectrogram data for the groups not presented in appendix 1: individuals with a current episode of depression (n=1:13) and those with a family history of depression (n=1:18).

N	Spectrogram
1	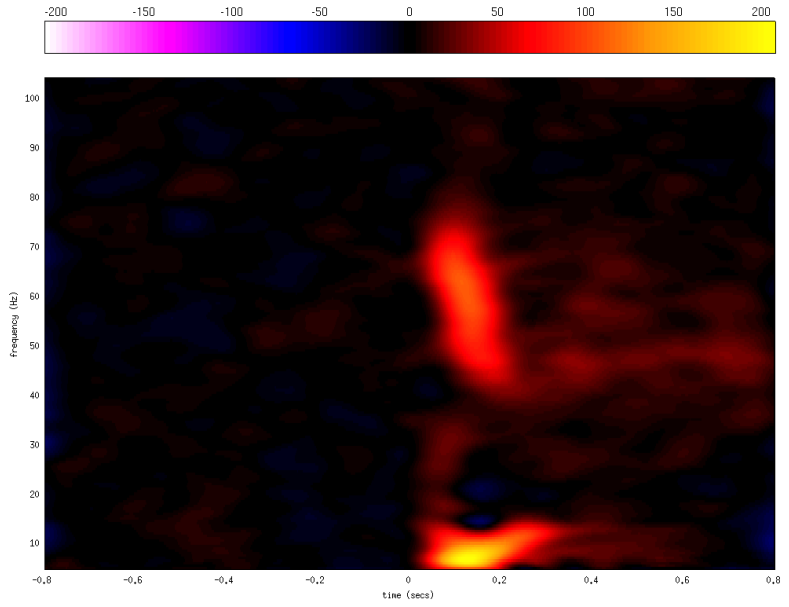

2	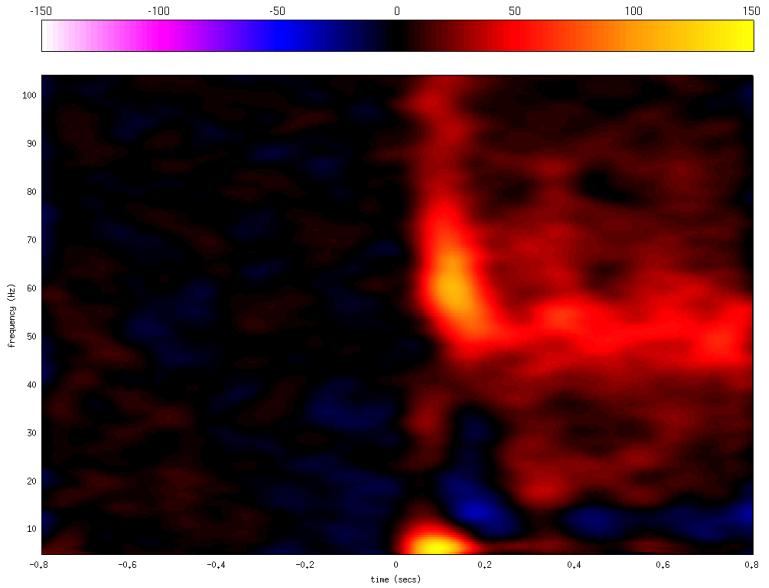 -150 -100 -50 0 50 100 150 100 90 80 70 60 50 40 30 20 10 frequency (Hz) -0.8 -0.6 -0.4 -0.2 0 0.2 0.4 0.6 0.8 time (secs)
3	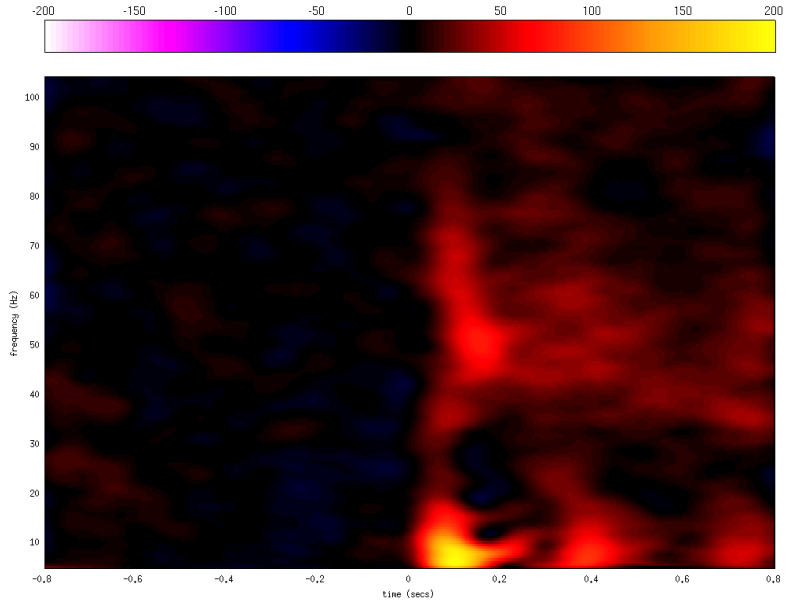 -200 -150 -100 -50 0 50 100 150 200 100 90 80 70 60 50 40 30 20 10 frequency (Hz) -0.8 -0.6 -0.4 -0.2 0 0.2 0.4 0.6 0.8 time (secs)

4	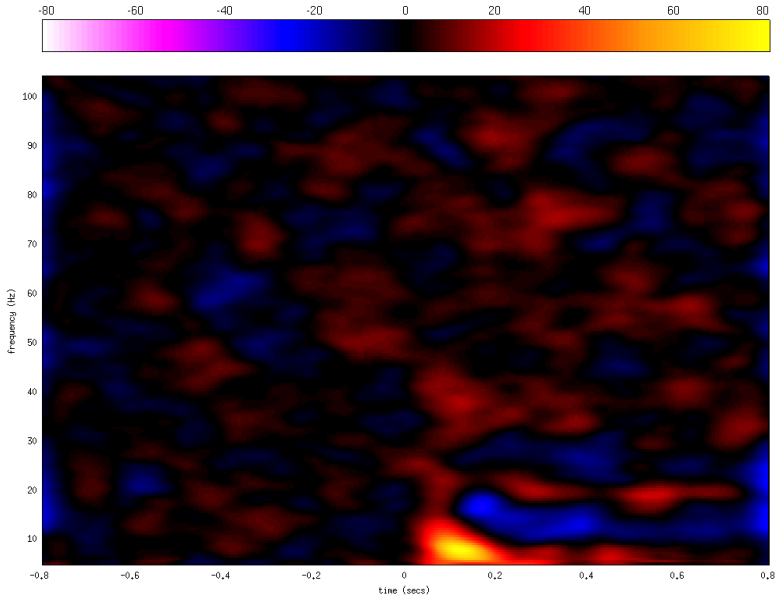 -80 -60 -40 -20 0 20 40 60 80 100 90 80 70 60 50 40 30 20 10 frequency (Hz) -0.8 -0.6 -0.4 -0.2 0 0.2 0.4 0.6 0.8 time (secs)
5	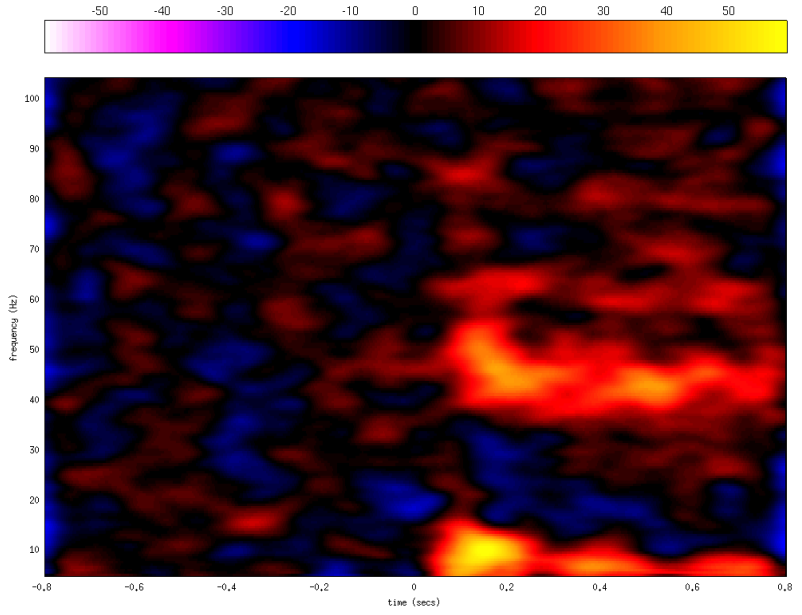 -50 -40 -30 -20 -10 0 10 20 30 40 50 100 90 80 70 60 50 40 30 20 10 frequency (Hz) -0.8 -0.6 -0.4 -0.2 0 0.2 0.4 0.6 0.8 time (secs)

6

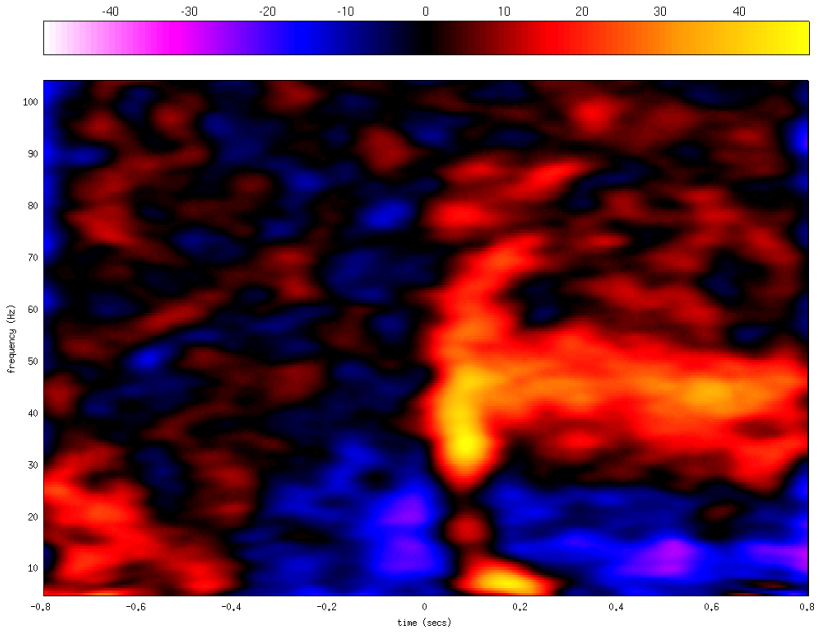
-40 -30 -20 -10 0 10 20 30 40
Frequency (Hz)
100 90 80 70 60 50 40 30 20 10
-0.8 -0.6 -0.4 -0.2 0 0.2 0.4 0.6 0.8
time (secs)

7

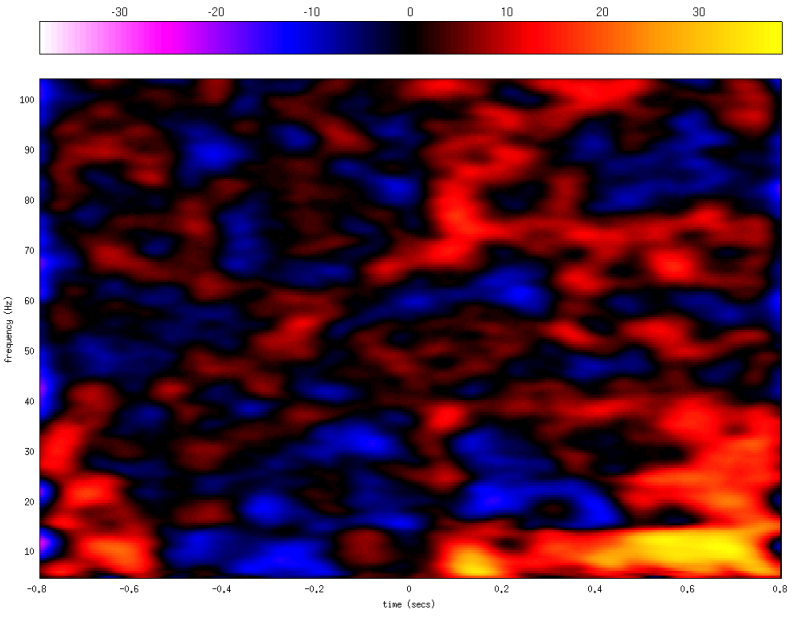
-30 -20 -10 0 10 20 30
Frequency (Hz)
100 90 80 70 60 50 40 30 20 10
-0.8 -0.6 -0.4 -0.2 0 0.2 0.4 0.6 0.8
time (secs)

8	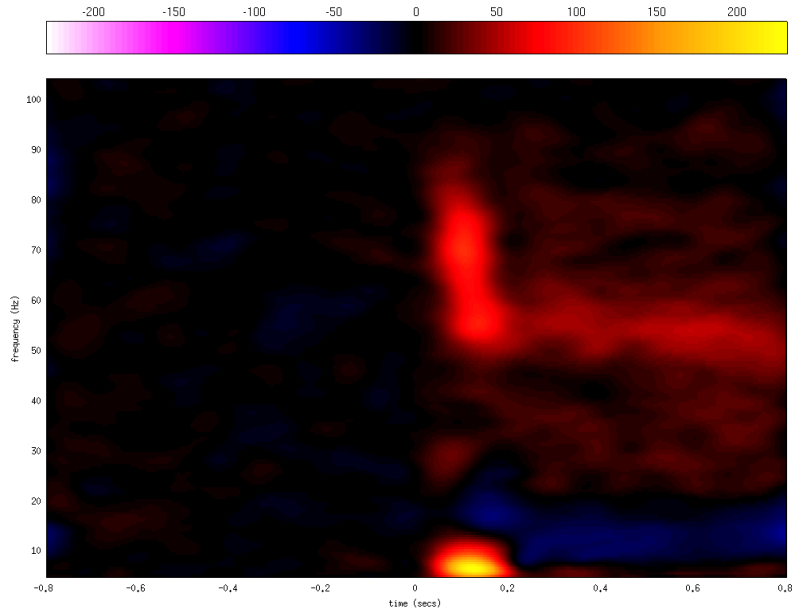 -200 -150 -100 -50 0 50 100 150 200 frequency (Hz) time (secs)
9	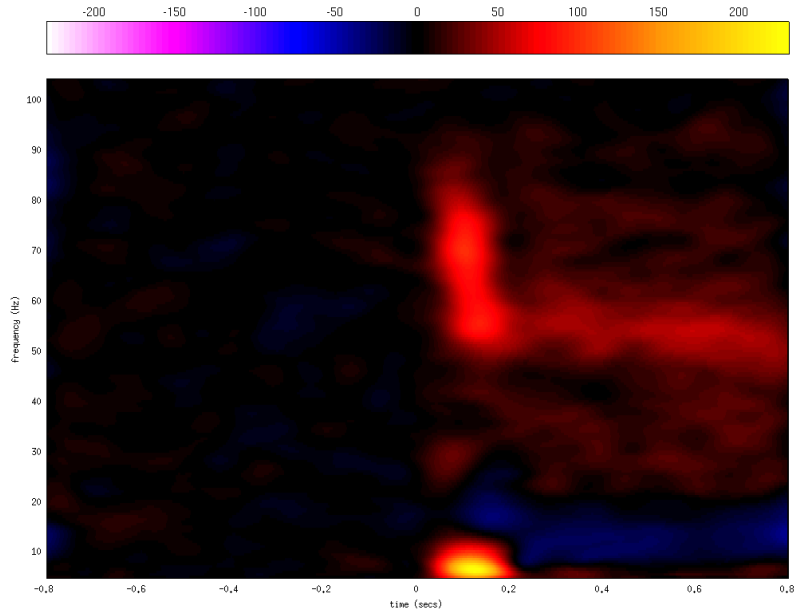 -200 -150 -100 -50 0 50 100 150 200 frequency (Hz) time (secs)

10	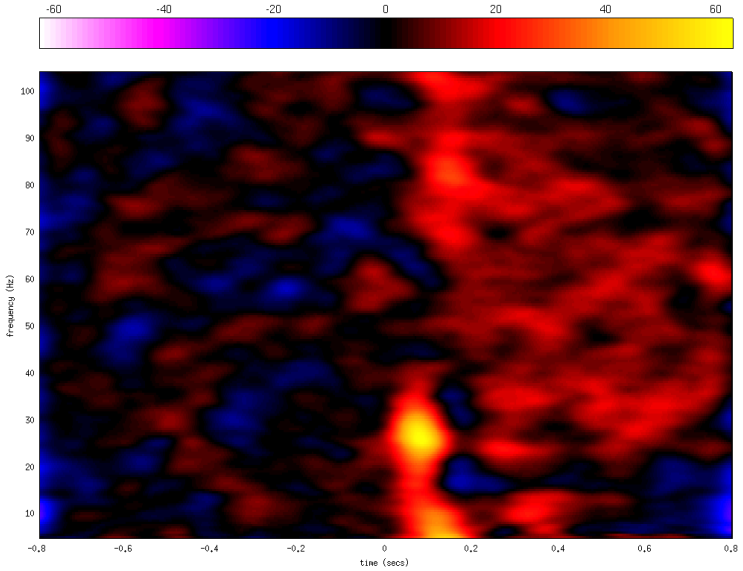 -60 -40 -20 0 20 40 60 frequency (Hz) time (secs)
11	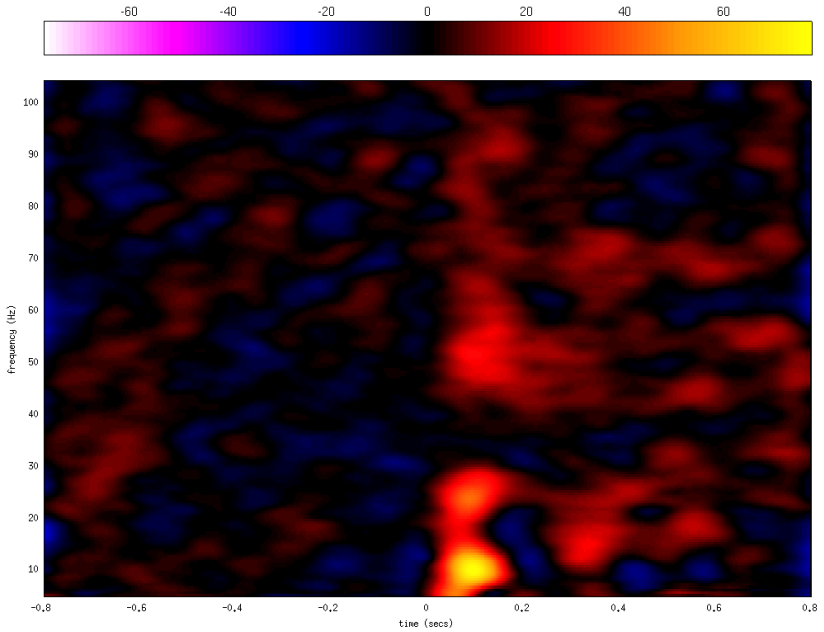 -60 -40 -20 0 20 40 60 frequency (Hz) time (secs)

12	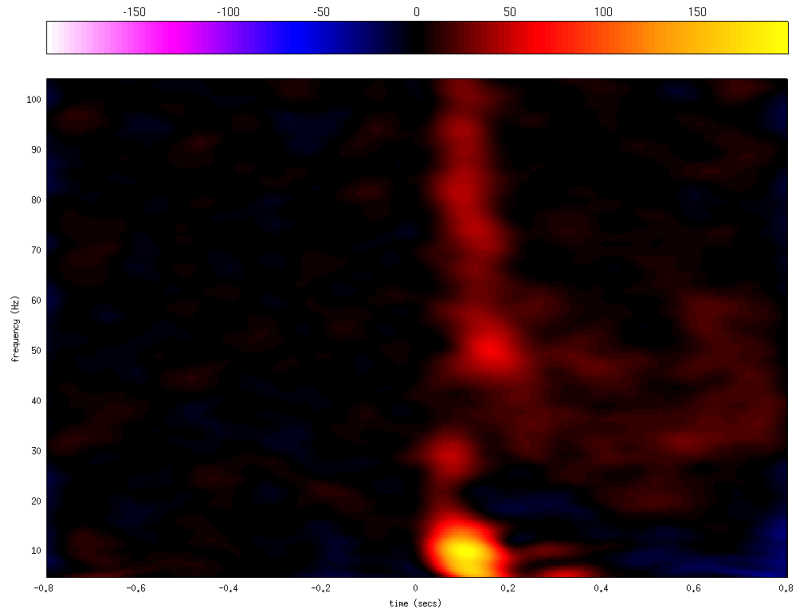 -150 -100 -50 0 50 100 150 frequency (Hz) time (secs)
13	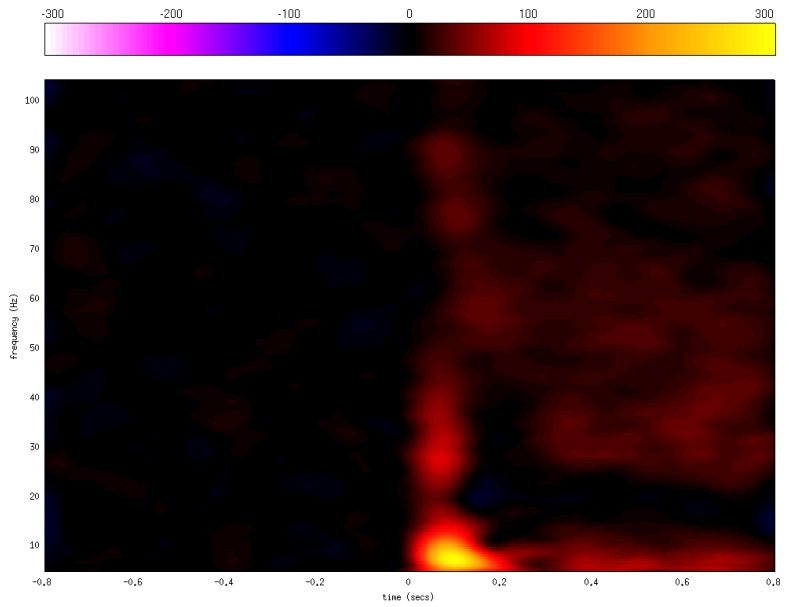 -300 -200 -100 0 100 200 300 frequency (Hz) time (secs)

1

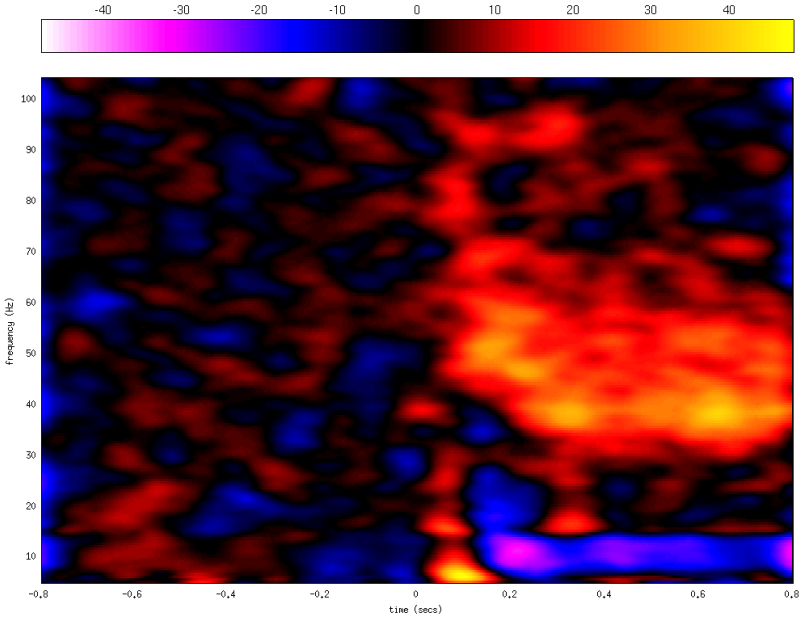
-40 -30 -20 -10 0 10 20 30 40
frequency (Hz)
time (secs)

2

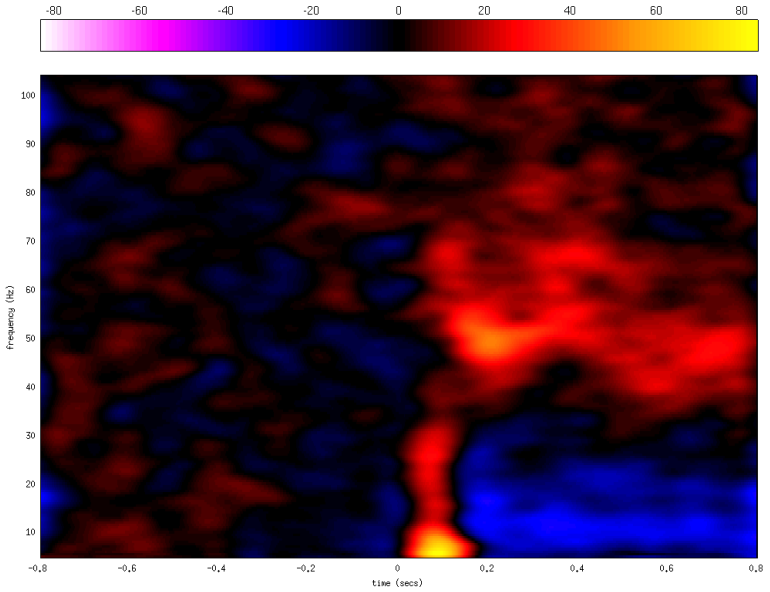
-80 -60 -40 -20 0 20 40 60 80
frequency (Hz)
time (secs)

3	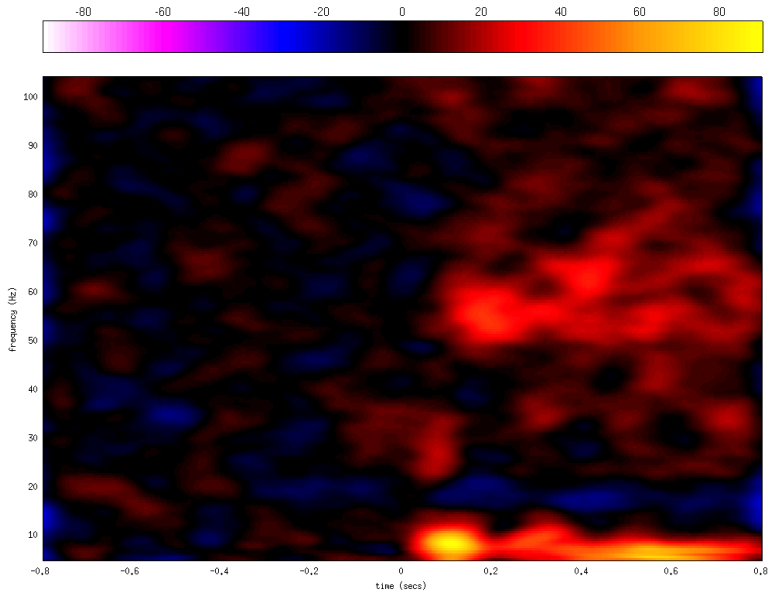 -80 -60 -40 -20 0 20 40 60 80 frequency (Hz) time (secs)
4	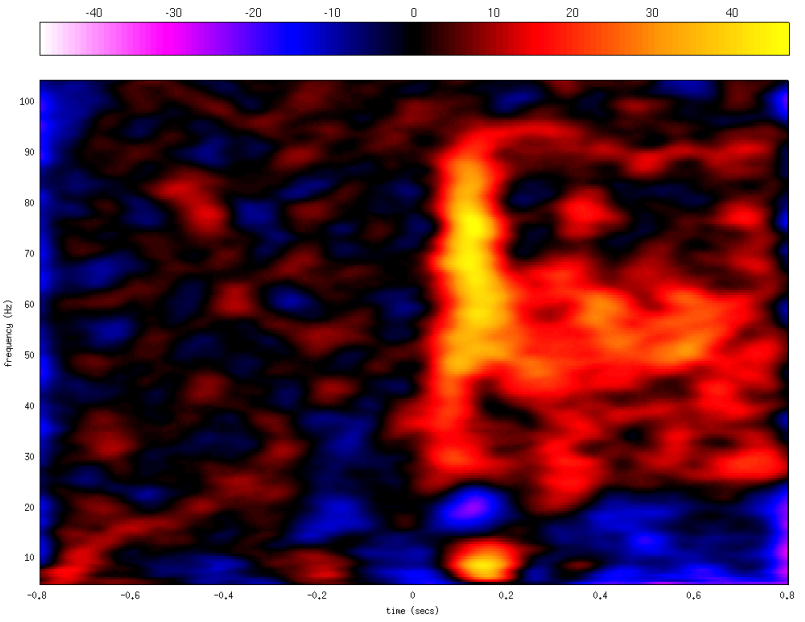 -40 -30 -20 -10 0 10 20 30 40 frequency (Hz) time (secs)

5	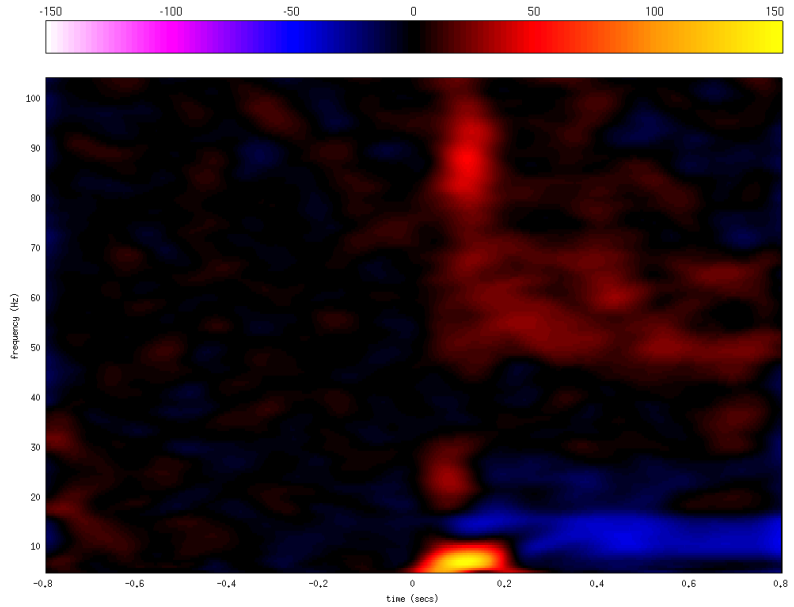 -150 -100 -50 0 50 100 150 Frequency (Hz) 100 90 80 70 60 50 40 30 20 10 -0.8 -0.6 -0.4 -0.2 0 0.2 0.4 0.6 0.8 time (secs)
6	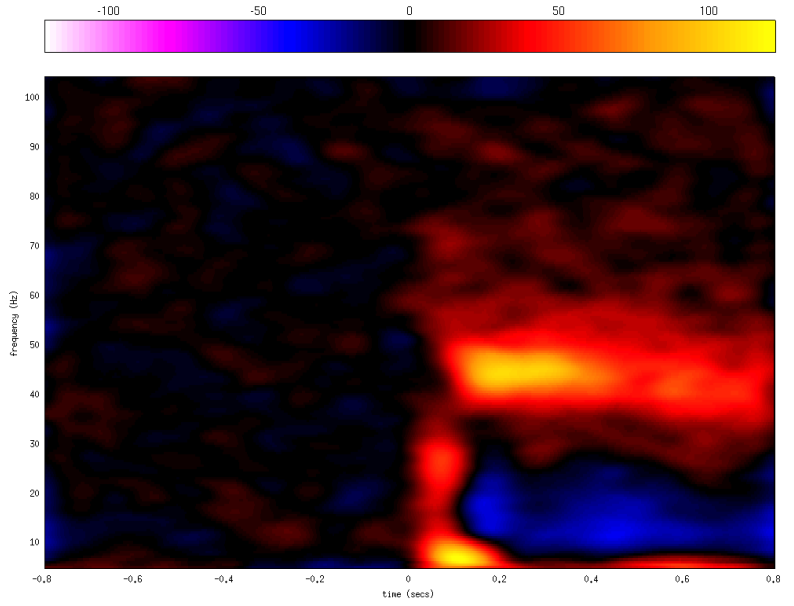 -100 -50 0 50 100 Frequency (Hz) 100 90 80 70 60 50 40 30 20 10 -0.8 -0.6 -0.4 -0.2 0 0.2 0.4 0.6 0.8 time (secs)

7	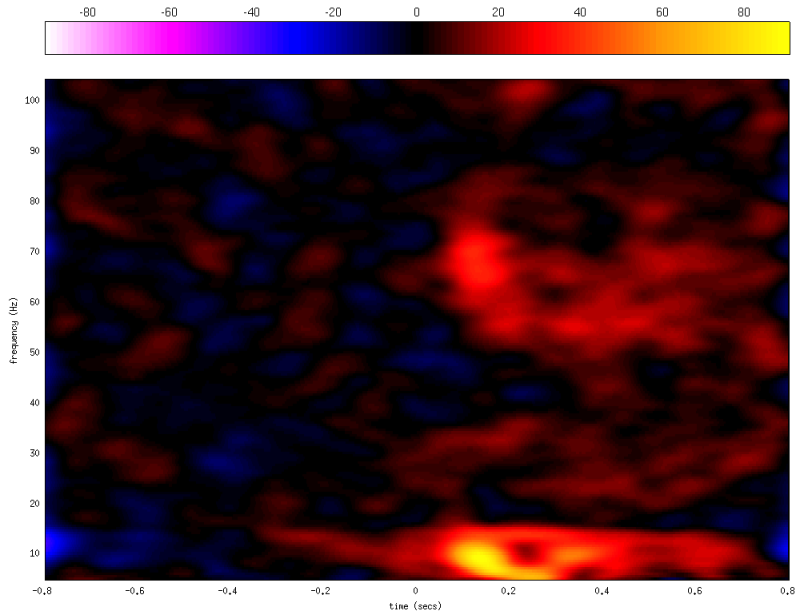 -80 -60 -40 -20 0 20 40 60 80 100 90 80 70 60 50 40 30 20 10 Frequency (Hz) -0.8 -0.6 -0.4 -0.2 0 0.2 0.4 0.6 0.8 time (secs)
8	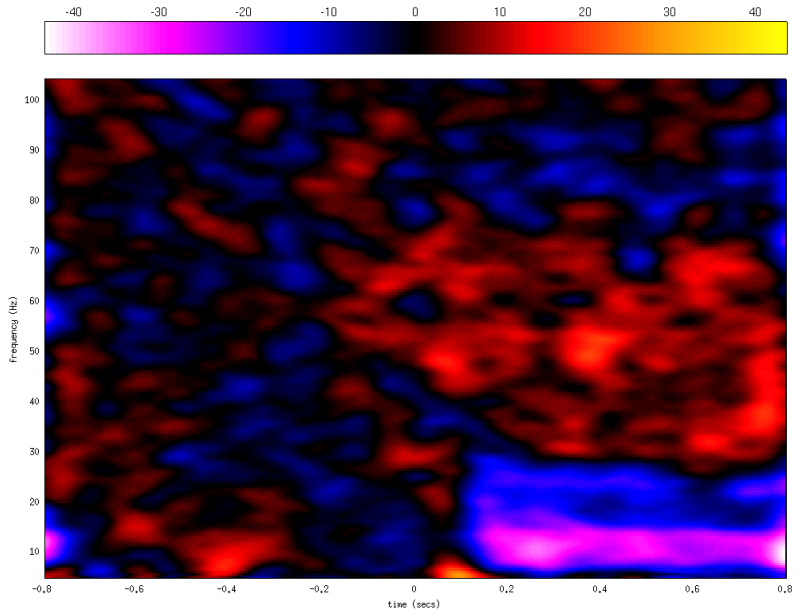 -40 -30 -20 -10 0 10 20 30 40 100 90 80 70 60 50 40 30 20 10 Frequency (Hz) -0.8 -0.6 -0.4 -0.2 0 0.2 0.4 0.6 0.8 time (secs)

9	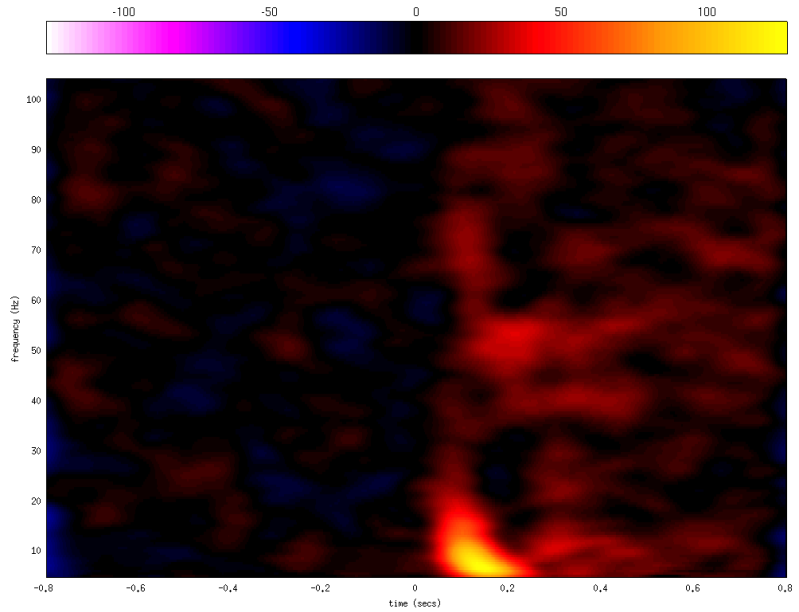 -100 -50 0 50 100 Frequency (Hz) time (secs)
10	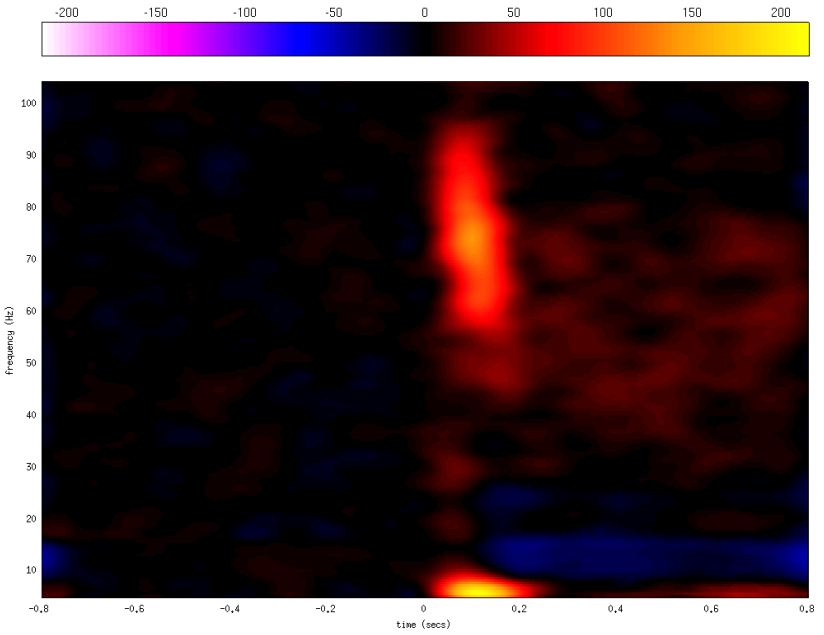 -200 -150 -100 -50 0 50 100 150 200 Frequency (Hz) time (secs)

11	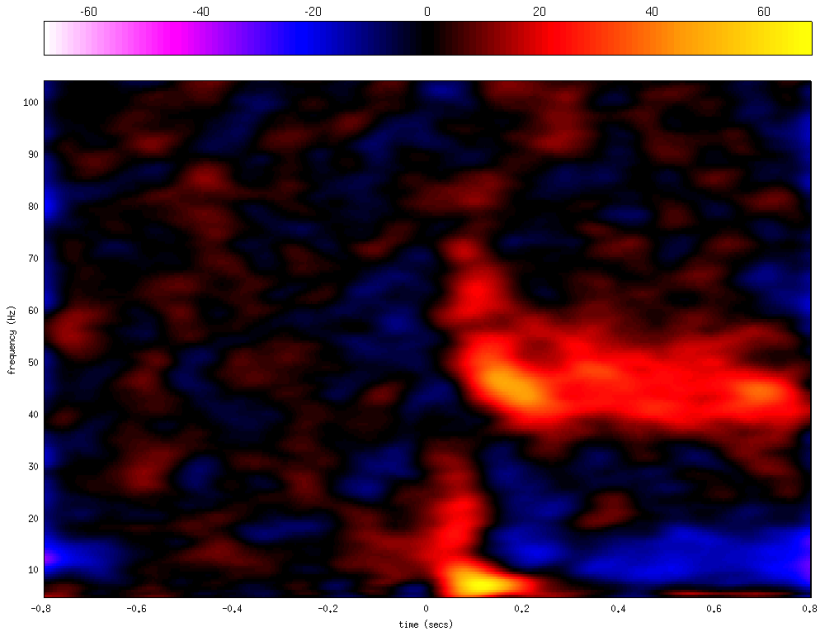 -60 -40 -20 0 20 40 60 100 90 80 70 60 50 40 30 20 10 frequency (Hz) -0.8 -0.6 -0.4 -0.2 0 0.2 0.4 0.6 0.8 time (secs)
12	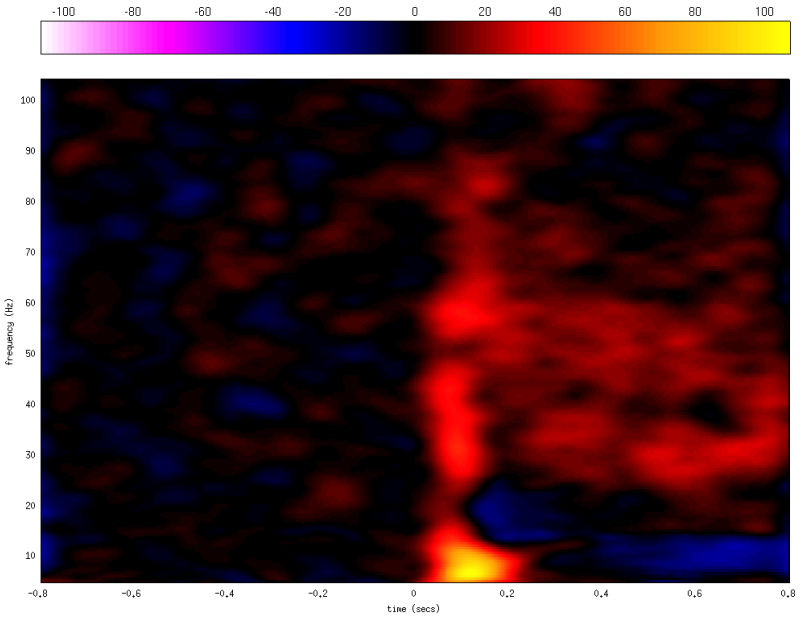 -100 -80 -60 -40 -20 0 20 40 60 80 100 100 90 80 70 60 50 40 30 20 10 frequency (Hz) -0.8 -0.6 -0.4 -0.2 0 0.2 0.4 0.6 0.8 time (secs)

13	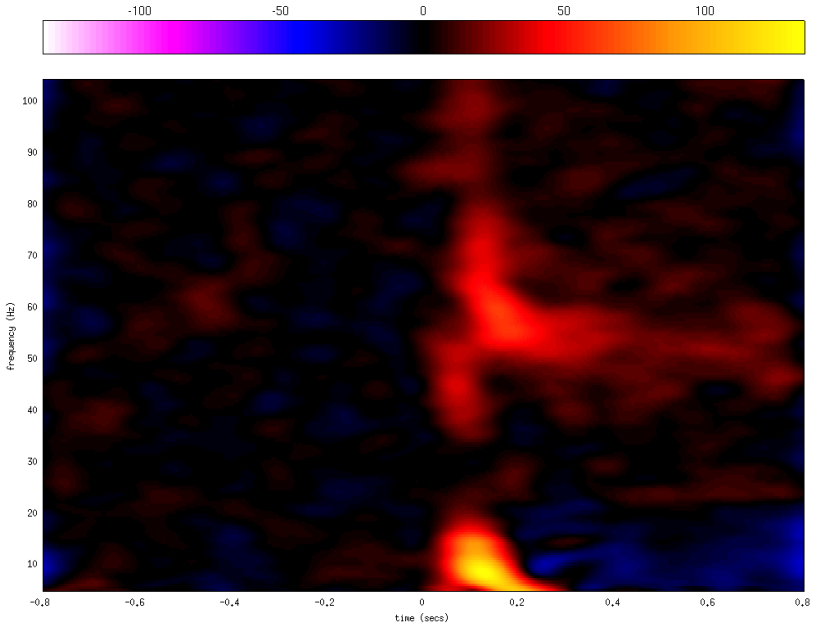 -100 -50 0 50 100 frequency (Hz) time (secs)
14	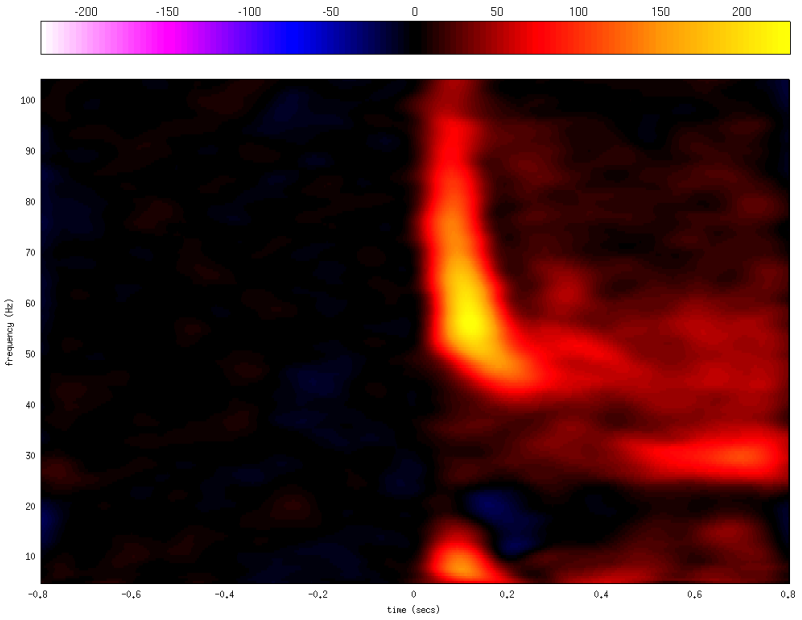 -200 -150 -100 -50 0 50 100 150 200 frequency (Hz) time (secs)

15	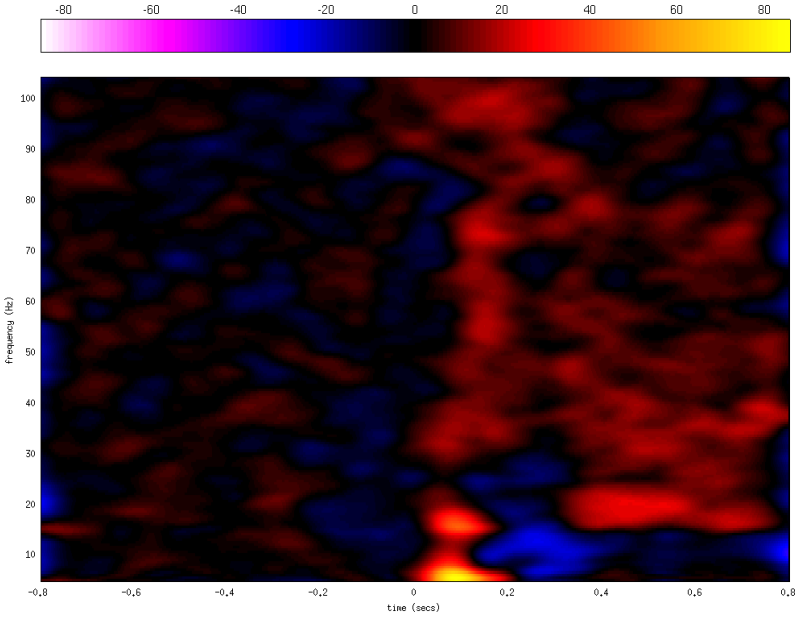 -80 -60 -40 -20 0 20 40 60 80 frequency (Hz) time (secs)
16	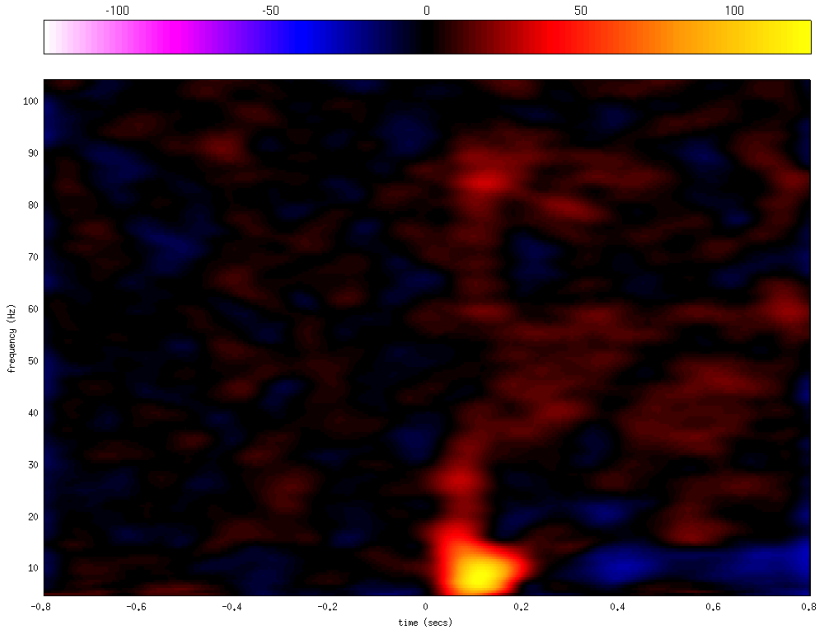 -100 -50 0 50 100 frequency (Hz) time (secs)

17	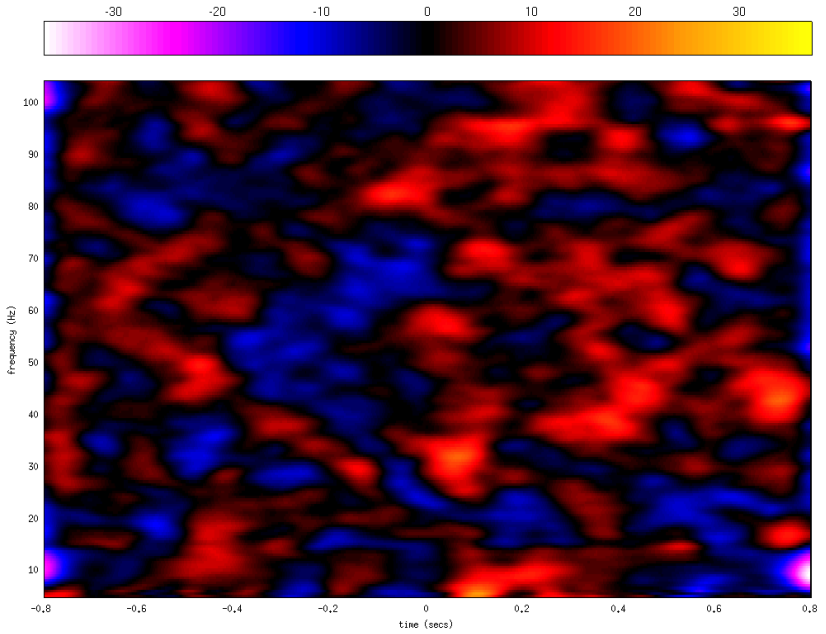 -30 -20 -10 0 10 20 30 frequency (Hz) 100 90 80 70 60 50 40 30 20 10 -0.8 -0.6 -0.4 -0.2 0 0.2 0.4 0.6 0.8 time (secs)
18	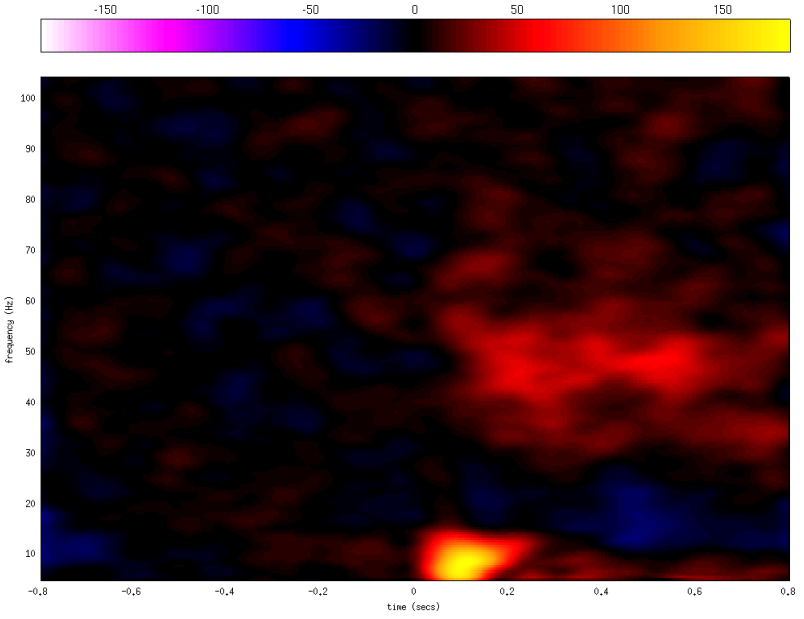 -150 -100 -50 0 50 100 150 frequency (Hz) 100 90 80 70 60 50 40 30 20 10 -0.8 -0.6 -0.4 -0.2 0 0.2 0.4 0.6 0.8 time (secs)